Boron determination in biological samples - Intercomparison of three analytical methods to assist development of a treatment protocol for neoplastic diseases of the liver with Boron Neutron Capture Therapy

Dissertation
zur Erlangung des akademischen Grades

„Doktor der Naturwissenschaften“

im Promotionsfach Chemie
am Fachbereich Chemie, Pharmazie und Geowissenschaften
der Johannes Gutenberg-Universität in Mainz

Christian L. Schütz

geboren in Mainz

Mainz, Januar 2012

Dekan: [redacted]

1. Berichterstatter: [redacted]
2. Berichterstatter: [redacted]
3. Berichterstatter: [redacted]

Datum der mündlichen Prüfung: 24.02.2012

Die vorliegende Arbeit wurde in der Zeit von Mai 2008 bis Januar 2012 am Institut für Kernchemie der Johannes Gutenberg-Universität Mainz unter der Anleitung von [redacted] erstellt.

Ich versichere gemäß § 10 Abs. 3d der Promotionsordnung vom 24.07.2007 des Fachbereichs 09 der Johannes Gutenberg-Universität Mainz, die vorliegende Arbeit selbst angefertigt und als Hilfsmittel ausschließlich die im Literaturverzeichnis und die in den Anhängen genannten Quellen verwendet zu haben.

_____

Mainz, den 11.01.2012

Πάντες ἄνθρωποι τοῦ εἰδέναι ὀρέγονται φύσει

(All men by nature desire to know)

Aristotle (384 BC - 322 BC),
Metaphysics

Table of Contents

List of figures

List of tables

Abstract

Boron Neutron Capture Therapy (BNCT) is a biologically targeted, indirect form of radiation therapy, relying on the release of densely ionising radiation to destroy tumour cells selectively. The released ions are the fragments of a nuclear reaction upon capture of a low-energy neutron (thermal neutron) by a boron isotope (^{10}B). The ^{10}B is placed selectively in tumour cells by using a specially designed boron compound, which itself is not radioactive.

Research at the Johannes Gutenberg-University of Mainz was initiated on a treatment protocol for neoplastic diseases of the liver protocol, stirred by two curative treatment attempts for patients with colorectal liver metastases (CRLM) at the University of Pavia, Italy, during which the liver was irradiated outside the body in a research reactor. As a first step, a clinical study was started in cooperation between different deparments of the University of Mainz to investigate clinically relevant parameters like the boron distribution in different kinds of tissue and pharmacokinetic behaviour of the administered boron compound in more detail.

The boron concentration in tissue was analysed with respect to the spatial distribution among different cell types, in order to know more about the uptake behaviour of the boron carrier *p*-boronophenylalanine (BPA) in correlation to the biological characteristics of tissue. Blood and tissue analysis was carried out by Quantitative Neutron Capture Radiography, Prompt Gamma Activation Analysis and Inductively Coupled Plasma Mass Spectroscopy combined with histological analysis. It could be demonstrated for both cancerous and non-cancerous samples that a very heterogeneous boron uptake in tissue areas of different morphology took place. The results of the blood samples contribute to the creation of a pharmacokinetical prediction model for the blood-boron kinetics in a future treatment and are in accordance with pharmacokinetic models published by other research groups. Furthermore, the analytical methods chosen were validated against each other by using specially made reference samples. The data obtained from all methods are in good agreement and standard protocols for the analysis of blood and tissue samples have been created.

So far, from the clinical point of view, the results were promising, but due to the small number of patients enrolled so far, a conclusion about the effectiveness of BNCT for neoplastic diseases of the liver cannot be drawn yet.

Zusammenfassung

Die Bor-Neuroneneinfang-Therapie (engl.: Boron Neutron Capture Therapy, BNCT) ist eine indirekte Strahlentherapie, welche durch die gezielte Freisetzung von dicht ionisierender Strahlung Tumorzellen zerstört. Die freigesetzten Ionen sind Spaltfragmente einer Kernreaktion, bei welcher das Isotop ^{10}B ein niederenergetisches (thermisches) Neutron einfängt. Das ^{10}B wird durch ein spezielles Borpräparat in den Tumorzellen angereichert, welches selbst nicht radioaktiv ist.

An der Johannes Gutenberg-Universität Mainz wurde die Forschung für die Anwendung eines klinischen Behandlungsprotokolls durch zwei Heilversuche bei Patienten mit kolorektalen Lebermetastasen an der Universität Pavia, Italien, angeregt, bei denen die Leber außerhalb des Körpers in einem Forschungsreaktor bestrahlt wurde. Als erster Schritt wurde in Kooperation verschiedener universitärer Institute eine klinische Studie zur Bestimmung klinisch relevanter Parameter wie der Borverteilung in verschiedenen Geweben und dem pharmakokinetischen Aufnahmeverhalten des Borpräparates initiiert.

Die Borkonzentration in den Gewebeproben wurde hinsichtlich ihrer räumlichen Verteilung in verschiedenen Zellarealen bestimmt, um mehr über das Aufnahmeverhalten der Zellen für das BPA im Hinblick auf ihre biologischen Charakteristika zu erfahren. Die Borbestimung wurde per Quantitative Neutron Capture Radiography, Prompt Gamma Activation Analysis und Inductively Coupled Plasma Mass Spectroscopy parallel zur histologischen Analyse des Gewebes durchgeführt. Es war möglich zu zeigen, dass in Proben aus Tumorgewebe und aus tumorfreiem Gewebe mit unterschiedlichen morphologischen Eigenschaften eine sehr heterogene Borverteilung vorliegt. Die Ergebnisse der Blutproben werden für die Erstellung eines pharmakokinetischen Modells verwendet und sind in Übereinstimmung mit existierenden pharmakokinetische Modellen. Zusätzlich wurden die Methoden zur Borbestimmung über speziell hergestellte Referenzstandards untereinander verglichen. Dabei wurde eine gute Übereinstimmung der Ergebnisse festgestellt, ferner wurde für alle biologischen Proben Standardanalyseprotokolle erstellt.

Die bisher erhaltenen Ergebnisse der klinischen Studie sind vielversprechend, lassen aber noch keine endgültigen Schlussfolgerungen hinsichtlich der Wirksamkeit von BNCT für maligne Lebererkrankungen zu.

1. Introduction

1.1 Radiotherapy as therapeutic option for the treatment of cancer

Cancer ranks very high among the primary causes of death in industrialised countries. Whereas until today, for several forms of cancer, therapies have been developed which may be curative for the patient, the diagnosis of cancer remains shocking as many forms of cancer are fatal no matter what therapy applied.
Cancer is the expression for a class of diseases characterised by the growth and subsequent clinical implications of malign tumours and metastases. Tumours are benign or malign formations of tissue caused by wrongly regulated growth behaviour of cells. The reasons for the creation of tumours are not fully known, as it is influenced by a series of environmental and genetic factors.

Benign tumours show usually few clinical symptoms, as they do not infiltrate into adjacent tissue, they do not create systemic secondary tumour entities (metastases) and they show no recurrence after removal. They consist of homogeneous tissue, are spatially clearly separated from the surrounding tissue (pseudo-capsula), well differentiated and usually grow very slowly. Nevertheless, their growth may be problematic for a patient, as they can displace other structures or can cause obstructions in vessels or other hollow spaces of the body, which is often the reason for their eventual treatment.

Malign tumours are characterised by destructive, infiltrating growth into adjacent structures, and, after removal, tend to recur at the same location. They consist of heterogenic tissue, often show atypical cell changes, and have a higher mitotic activity and cell number (hyperplasia) than benign tumours. Furthermore, they often come with clinical symptoms. However, the most striking argument for their categorisation as “malignant” is their tendency to form metastases: the spread of the tumour to regional or distant sites in the body, via the lymphatic system or the blood vessels. Therefore, the morphology and biology of metastatic tissue is characterised by their primary tumour and not by the host tissue in which they are growing. As a result, growth and further development can be fatal for the patient, if they are not taken care of accordingly.

The work presented in this thesis is focused on the treatment of cancer, therefore all aspects mentioned for tumours consider *malign* tumours if not explicitly mentioned otherwise.

Curative and palliative therapeutic attempts usually rely on a variety of different approaches like chemotherapy, surgical resection, immunotherapy, specialised antibody-therapy and radiotherapy. The choice of therapy is determined by age, physical condition, cancer type and progression of the disease.

In many cases, oncologists choose to treat patients with a combination of the forms of treatment available in order to optimise the clinical outcome. In the following, ionising radiation as treatment option will be closer looked at.

Characteristics of ionising radiation used for therapeutic purposes

Ionising radiation used for therapeutic purposes is commonly divided into radiation with a high linear energy transfer (high LET radiation) and radiation with a low linear energy transfer (low LET radiation). Linear energy transfer is defined as the energy loss of a particle per distance travelled in a certain medium. Therefore, it is a parameter to assess the biological efficacy of a type of radiation (several examples for high and low LET radiation used for therapeutic purposes are given in Table 1).

Tab. 1: Examples for different high and low LET radiation used in radiotherapy [1]

High LET	approx. energy (MeV)	LET (keV / µm)
α-particles	5	90
fast neutrons	6.2	21
protons	2	17
carbon ions	10 - 400	15-200
Low LET		
x-rays	0.2	2.5
γ-rays	1.25	0.3
electrons	2	0.2

As a result, there are particles which travel in tissue only for a limited distance, which may be more favourable for therapy of certain types of cancer. The energy is lost either by collision with other particles or by their ionisation. As a

consequence, the greater mass and charge of a particle, the more energy is released in tissue. Ionisation is caused by a number of interactions of particles with matter (photoelectric effect, Compton scattering, pair production and nuclear reactions). All of these interactions are particle and energy dependent. High LET radiation is characterised by its ability to directly ionise matter, whereas ionisation by low LET radiation is achieved mostly by indirect effects.

This difference is decisive when choosing a particular type of particle radiation for therapeutic application, as also biological effects, like the production of radicals (mainly H_2O^+), the damage dealt to the cell (single / double strand breaks in the DNA) are particle dependent. For example, particle radiation induces different effects in cells, if certain parameters are varying, e.g., cells with low oxygen content are more radio-resistant towards gamma rays (as less radicals are produced and therefore less damage is caused to neighbouring structures), whereas high LET radiation directly damages cell structures, therefore no significant difference between anoxic cells and cells well-supplied with oxygen can be observed.

Especially charged particles, such as protons or carbon ions have a high LET and are used for therapeutic purposes in Proton Therapy and Heavy Ion Therapy. In addition to their high LET, ions deposit most of their energy at the end of their penetration path, which makes the irradiation of tissue located several centimetres below the body surface possible (Fig.1). By varying the ^{12}C kinetic energy and by rastering the beam in x and y direction, the Bragg peak can “illuminate” the whole volume of the tumour without causing much damage to the surrounding tumour-free tissue because before the Bragg peak is reached, the particles are “minimum ionising”.

Application of ionising radiation in radiotherapy

In conventional radiotherapy (CRT), gamma radiation is the radiation of choice. Due to the physical properties, gamma radiation highly penetrates tissue and consequently damages all types of tissue along the penetration path and does not

physically discriminate between cancerous and healthy tissue. Neutrons have similar properties, which are used for therapy as well. Neutron radiation is indirectly ionising radiation and has a higher penetration depth than ion radiation, especially fast neutrons. Fast neutron therapy has been mostly applied for the treatment of carcinomas of the head and neck, salivary gland, paranasal sinus and breast; soft tissue, bone and uterine sarcomas and malignant melanomas [2]. However, Fast Neutron Therapy is available only at a few centres worldwide. To overcome the difficulty of irradiating tissues unspecifically, other forms of radiation are used for therapy.

Electrons can be used for external irradiation via accelerator systems [3], in this case discrimination in dose delivery is better possible, since electrons (depending on their energy) are charged particles and therefore loose their energy in tissue faster than uncharged neutrons and γ-rays. Another option is Heavy Ion or Proton Therapy, which can deliver much higher doses to tumour tissue without compromising the surrounding tumour free tissue due to their unique energy deposition in tissue (see Fig. 1) [4].

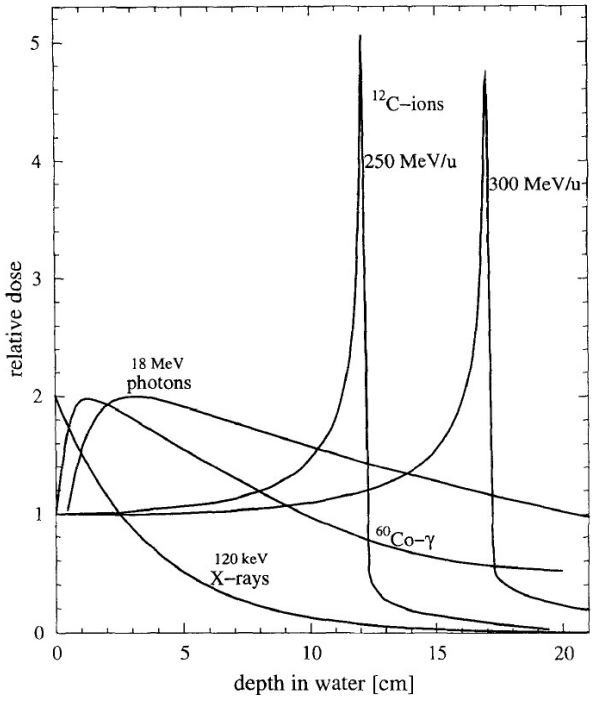

Fig. 1: Dose deposition of x-rays, Röntgen-Bremsstrahlung, ^{60}Co-γ-rays and ^{12}C ions of two different energies in water (figure taken from [4])

All of the above mentioned radiation techniques are applied from outside the body (external beam radiation therapy, EBRT), whilst it is feasible to generate radiation also *inside* the body. The volume irradiated when generated *in situ* depends of the particles chosen for irradiation and their respective energy. A possibility to irradiate very small volumes directly without irradiating too much surrounding tissue is, e.g., either using a so-called gamma knife during surgery [5] or brachytherapy. In brachytherapy, very small rods containing γ- or β^--emitters are place adjacent to the tumour or directly into the tumour to minimise travelling paths of the emitted radiation to the tumour. Prostate cancer [6, 7] and breast cancer [8] are frequently treated using brachytherapy. The isotopes commonly used for irradiation are ^{60}Co, ^{137}Cs, ^{106}Ru, ^{103}Pd, ^{125}I, and ^{193}Ir.

Irradiation using β^- emitters is an option, which combines a penetration depth of up to several centimetres, depending on the radioisotope in use, with biologically selective delivery of such radioisotopes by attachment of the latter to a tracer molecule, often by formation of a chemical complex. The major difference to externally applied radiation is that, for external radiation, the exact location and dimension of the lesions have to be known, while for the treatment by internally released radiation the tracer molecules enrich in all tumour cells selectively following a predefined parameter.

Treatment concepts include a variety of cancers, such as lymphoma [9, 10], liver cancer [11], bone metastases [12], or the maybe best known example: radioiodine therapy for thyroid cancer [13]. The generation of particles with a limited penetration depth makes it possible to irradiate single organs, vessels or small tissue compounds, while the surrounding tissue may be spared or would suffer only from very low doses. The β-emitters available have ranges from about 400 µm (^{199}Au; E_β-= 82 keV) to 5000 µm (^{76}As; E_β- = 1000 keV) [14] with respective emission energies between 80 and 1000 keV. If for dose application more than one carrier molecule is needed, therapy may be carried out also with a combination of β-emitters, because the location of the tissue, which is to be irradiated, may not correlate exactly with the spatial uptake of only one specific β-emitter. Therapeutic options are not limited to cancer, in radio-immunotherapy β-emitters are also used to treat chronic illnesses of the joints [15].

Another way to localise the site of irradiation and thus limit the spatial extent of the irradiated tissue are low-energy α-particles (< 5 MeV). In tissue, α-particles have a maximum path length of less than 30 µm. Internal irradiation requires either the administration of already radioactive tracer molecules, as it is done in β-therapy, or the administration of carrier molecules, which are activated by nuclear reactions caused by external irradiation. For example, isotopes like ^{213}Bi, ^{211}At and ^{225}Ac may be bound to monoclonal antibodies to selectively deliver α-emitters into the tumour cells [16].

Depending on the energies of the α-rays emitted, the range of such particles is usually limited to 50 µm, which is equal to two to three cell diameters. Dose estimation in α-therapy is not a trivial issue, as many α-ray emitting isotopes produce daughter isotopes, which may have different chemical properties. On the other hand, α-therapy poses like therapy with β-emitters the possibility of combining the ranges and energies of several α-emitters.

The use of α-emitters is not without risk for the patient for various reasons, e.g.,due to kinetic recoil, radioactive α-decay may destroy the complex of the α-ray emitter and its ligands. This means that the originally complexed isotope might engage in new chemical reactions and therefore alter its “original” biochemical behaviour radically. Thus, the prediction of the pharmacokinetic pathways in the body becomes very complicated. Not only their radioactive properties, like the generation of radioactive daughter isotopes which can behave chemically very different compared to the original isotope, would be a risk for a patient’s health, but also their chemical toxicity is problematic, as most of them are heavy metals.

To avoid such problems there is also the possibility to generate α-particles inside the body by external triggering, i.e., by irradiation with other particles inducing nuclear reactions. Ideally, the compound used for this purpose should not produce extensive or “leftovers”, such as radioactive daughter isotopes or fragmented isotope carrier molecules, which can react or metabolise in an unpredictable way. Also, the compound must have targeting abilities to enrich selectively in tumour cells to spare surrounding tumour free tissue from radiation damage. Such a triggered technique, which uses the advantage of internally generated α-particles by external neutron radiation, is boron neutron capture therapy (BNCT).

1.2 Principles of Boron Neutron Capture Therapy

Boron Neutron Capture Therapy (BNCT) is a biologically targeted form of radiotherapy using the effect of secondary particle radiation released inside tumour cells. The Isotope B-10, which is found with an abundance of around 20 % in natural boron, has a very high tendency to interact with thermal neutrons (E_n < 1 eV) in a fission reaction ($^{10}B(n,\alpha)^{7}Li$). In 94 % of all reactions, a 478 keV gamma photon is emitted, too (Fig. 2).

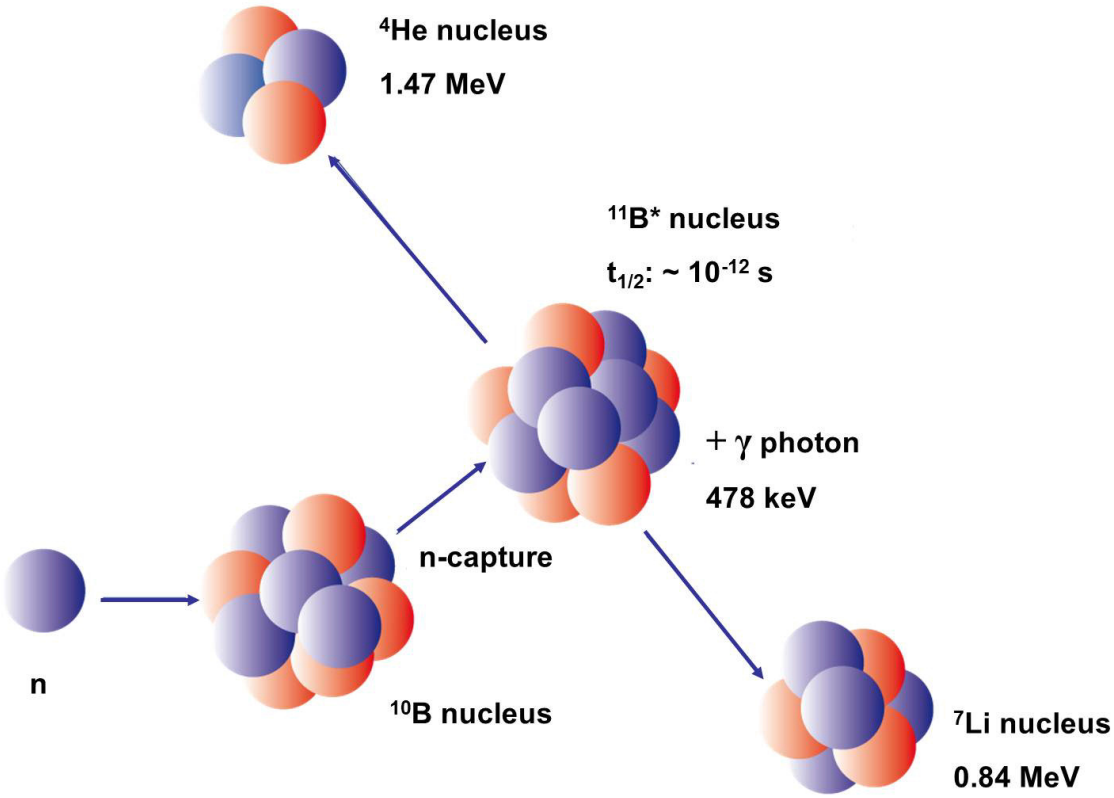

Fig. 2: The schematic of the $^{10}B(n,\alpha)^{7}Li$ reaction

The cross section for neutron capture is very high (3837 barn). The fragments produced in this reaction are characterised by their high linear energy transfer (LET) properties and a high relative biological effectiveness (RBE) in comparison to photon irradiation. If this reaction takes place in a cell, the cell may be severely damaged and die thereafter [17].

The major difference to conventional α-radiation therapy is the non-radioactive molecule carrying the ^{10}B isotope which, by externally delivered neutron radiation, makes it possible to generate relevant doses in predefined tissue volumes only, whereas α-emitting radioisotopes also irradiate healthy tissue along their metabolic transport paths. Moreover, the fragments of the neutron capture reaction do not leave any radioactive daughter isotopes and are not toxic.

Prerequisite for the lethal effect is the number of boron atoms inside each irradiated cell. The boron is transported using a molecule containing the isotope ^{10}B, which ideally enriches only in tumour cells and not in tumour-free cells. The released radiation dose in the respective cells is proportional to the number of neutron capture reactions and, hence, to the number of boron atoms found there. Usually 99.9 % ^{10}B-enriched compounds are used for clinical trials in order to minimise the amount of the boron carrier needed to 1/5 compared to a boron carrier with a natural isotopic composition of boron. In clinical trials worldwide mostly two substances are in use: *p*-boronophenylalanine (BPA, $C_9H_{12}{}^{10}BNO_4$) bound to fructose (BPA-fructose, Fig. 3a) or to mannitol (BPA-mannitol) and Sodium-borocaptat (BSH, $Na_2{}^{10}B_{12}H_{11}SH$, Fig. 3b) of which the latter has been used almost exclusively in brain tumour studies. Another compound structurally similar to BSH is GB-10 ($Na_2{}^{10}B_{10}H_{10}$), which up to this date has frequently been used in animal studies.

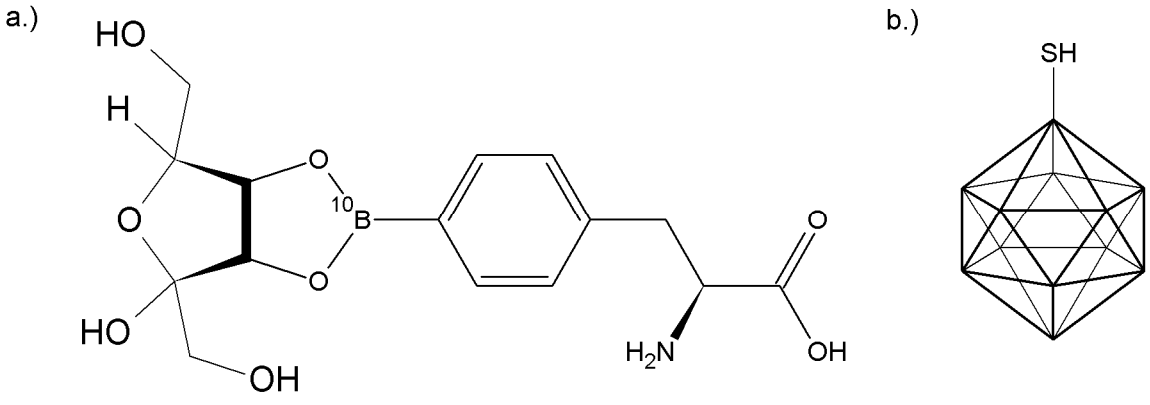

Fig. 3: a.) Structure of the BPA-fructose complex b.) Structure of BSH.

After infusion application of a boron carrier with a suitable concentration over a certain interval of time, BNCT requires irradiation of the targeted tissue volume in a specially designed neutron field.

The applied neutron dose is as low as possible to minimise additional risks for the patients' health (as always a certain background dose will be delivered to the tissue where the neutron beam or neutron field is applied) and is restricted to the area, where tumours or metastases have been detected before. Following this general concept, patients are usually treated one to three times.

1.3 Clinical application of BNCT

The idea to use thermal neutrons in combination with boron for cancer therapy was first proposed in 1936 by G. Locher [18]. First trials in the 1950s und 1960s at the Massachussetts General Hospital in Boston and the Brookhaven National Laboratory (both USA) were not successful, which was due to the poor targeting abilities of the boron carrier, the lack of precise dose planning tools and the wrong composition of the neutron beam [19].

BNCT research underwent significant progress with the development of two boron drugs, which are still the only ones used in clinical application [20]. Also, the design of mixed beams consisting of fast, epithermal, and thermal neutrons tailored for each application individually, the use of PET for treatment planning [21, 22] and improved dose simulation programmes [23] were reasons to give rise to the assumption, BNCT may be much more efficient than the trials had proved so far. Two major fields of application will be presented in the following.

BNCT for brain tumours

Most data in the last 20 years have been published for neoplastic diseases of the brain. In most BNCT related studies, patients suffering from tumours with unfavourable prognosis (WHO grade III and IV) like glioblastoma multiforme (GBM) or anaplastic astrocytoma (AA) have been enrolled. Median survival time (MST) for this kind of tumours is several months, if the disease remains untreated, depending on stage of the disease upon diagnosis. Standard treatment like chemotherapy, conventional radiotherapy, or surgical resection (single or combined) results in MST of 1 – 2 years, however this includes also tumours in stages with better prognosis.

Most patients participating in clinical studies have already received oncological treatment or have recurred malignancies, only a few studies patients with newly diagnosed tumours have been carried out. Moreover, BNCT has been selected only in single cases as first treatment against cancer. An overview over several recent studies related to the treatment of brain cancer is given in Table 2. These tumours are currently considered to be curable only for a very small number of

incidences. Kankaanranta et al. and Joensuu et al. reported treatment of 22 patients in Helsinki, Finland, who underwent surgery prior to BNCT. The protocol included a BPA infusion between 290 and 450 mg / kg body weight over two hours, the resulting median survival time was 7 M [24, 25]. Diaz et al. and Busse et al. reported results of 53 patients suffering from GBM treated with BNCT at the Brookhaven Medical Research Reactor, USA, with a similar BPA dose, with MST of 11 - 14 months in dependence of the dose [26, 27]. The dosage protocol was similar to the one presented by Joensuu et al., also the patients were enrolled after prior surgical treatment. A slightly higher MST (9.9 - 17.6 M) was achieved during a BNCT trial in Studsvik, Sweden. All 29 patients treated suffered from GBM, although BPA dose and infusion time were greatly increased compared to other studies (900 mg / kg over 6 hours) [28, 29]. The higher mean survival time was most deemed to be a result of the largely increased infusion time and dose.

In Japan, a greater variety of treatment protocols has been applied. Results from trials carried out from 1978 to 1997 have been reviewed by Nakagawa et al., including 105 patients treated at 6 different reactor institutions [30]. The results were found to be highly dependent on the dose planning strategy and the irradiation technique. The combined use of BPA and BSH was part of many studies in Japan to optimise the boron concentration ratio in tumour to healthy tissue. Amongst others, Miyatake et al. applied combinations of BPA and BSH in different concentrations (250 mg / kg body weight and 5 g per patient, respectively) to 13 patients in total, resulting in 30.3 - 87.6% reduction of the tumour volume [31].

Kageji et al. compared the outcome of a group of long-term BNCT survivors (more than three years) against a group of non-long-term survivors (less than three years). They found significant histopathological differences in tissue samples from both groups, indicating that tumour re-growth in the first group was significantly impaired. Though both groups were treated by intra-operative BNCT (IO-BNCT), in the first group, the BNCT radiation dose was 1.1-1.3 times higher.

Tab. 2: Selection of recent publications on BNCT trials for brain cancer
(MST – median survival time, M - months, XRT - X-ray therpy, GBM - Glioblastoma multiforme, GS - Gliosarcoma, AA - Anaplastic astrocytoma, AO - anaplastic oligoastrocytoma, KURRI - Kyoto University Research Reactor Institute, JAERI - Japan Atomic Energy Research Institute, BMRR - Brookhaven Medical Research Reactor, Helsinki - Finnish Research Reactor TRIGA Mark II, Helsinki; Studsvik - Studsvik Medical Reactor, Sweden

Author	Year	Facility	No. of cohorts / patients	Tumour type	B-compound(s) / dosage	Clinical outcome
Kankaanranta et al., Joensuu et al. [24, 25]	2003 / 2011	Helsinki	4 / 22	GBM	BPA: dose escalation; 290/350/400/450 mg / kg // 2h	MST: 7 M
Diaz et al. [26, 27]	2003	BMRR	3 / 53	GBM	BPA: dose escalation; 250/290/330 mg / kg // 2h	MST: 11 -14 M
Nakagawa et al. [30]	2003	KURRI / JAERI	* / 105	mostly GBM / AA	*	*
Miyatake et al. [31]	2006	KURRI	1 / 13	GBM (10) AA (1) AO (1) GS (1)	BPA: 250 mg / kg // 1h; BSH: 5g // 12 h	30.3–87.6% reduction of tumour volume
Yamamoto et al. [32]	2009	KURRI	2 / 15	GBM, newly diagnosed	BPA: 250 mg / kg // 1h; BSH: 5g // 12 h *OR* BSH: 5g // 12 h	MST: 25.7 M
Matsuda et al. [33]	2009	KURRI	1 / 8	GBM, newly diagnosed	BPA: 250 mg / kg // 1h; BSH: 5g // 12 h	MST: 27.9 M
Miyatake et al. [34]	2009	KURRI	2 / 22	GBM (11) AA (9) AO (2), recurred	BPA: 250 mg / kg // 1h; BSH: 100 mg / kg // 12 h *OR* BPA: 700 mg / kg // 6h; BSH: 100 mg / kg // 12 h	MST: 10.8 M
Kawabata et al. [35]	2009	KURRI	2 / 21	GBM	(2^{nd} cohort + 20-30 Gy XRT, single boost)	MST XRT cohort: 23.5 M; mean MST: 15.6
Sköld et al. [28, 29].	2010	Studsvik	1 / 29	GBM	BPA: 900 mg / kg // 6h	MST: 9.9 - 17.6 M
Kageji et al. [36]	2011	KURRI	2 / 23	GBM	BPA: 250 mg / kg // 1h; BSH: 100 mg / kg // 12 h OR BSH: 100 mg / kg // 12 h	MST: 19.5 M

* not given here, as patients from various studies with various treatment protocols were reviewed

However, BNCT in all of these cases was applied intra-operatively, which means that patients were irradiated under general anesthesia undergoing craniotomy to enable the direct irradiation of the targeted lesion (IO-BNCT). This is much more

complicated and stressful for patients than non-operative BNCT (NO-BNCT), though it proved to result in longer survival times [36].

Other studies combined the treatment outcome of recurring GBM versus newly diagnosed GBM. Yamamoto et al., Matsuda et al., and Kawabata et al. achieved in smaller groups of 8, 15, and 21 patients, respectively MST of 27.9, 25.7, and 23.5 M [32, 33, 37] for similar treatment protocols as in [31]. In the study of Kawabata et al. patients additionally received a 20-30 Gy X-ray boost, which increased the MST [35], in the study presented by Yamamoto et al. [32] the patients were treated with IO- or NO-BNCT. The treatment of 22 patients exclusively with recurred GBM reported by Miyatake et al. resulted in shorter MST (10.8 M) [34], illustrating the difficulty of treating lesions which obviously could not be destroyed in previous attempts.

Comparing survival times of recurred and newly diagnosed glioma to those found after conventional therapy, it becomes clear that, for subgroups, significantly higher MST can be achieved.

So far, no data on an entirely randomised trial of BNCT against other “standard therapies” have been published, e.g., conventional radiotherapy. However, Hopewell et al. [38] recently published a statistical evaluation of two different cohorts of patients from three different studies who received conventional radiotherapy with and without adjuvant temozolomide treatment against a cohort of 29 patients treated in Sweden [39]. In this comparison, patients with similar therapeutic background, age, and performance status were selected. Differences and uncertainties were assessed via the Cox Proportional Hazards Model [40] and recursive partitioning analysis (RPA) [41, 42]. Although in the BNCT cohort patients with higher RPA classes and worse prognosis were enrolled, BNCT appeared to be the more promising therapeutic option, because longer MST and a higher percentage for the one-year-survival were achieved.

BNCT for other neoplastic diseases

Another field of application of BNCT are malignancies of skin, head, and neck. An overview over several recent studies is given in Table 3. Patient enrolment in these studies was similar to BNCT studies on brain tumours: Usually, patients with bad prognosis and advanced disease were enrolled, partly after multiple surgical

or chemotherapeutical treatment or conventional radiotherapy. However, for several studies on head and neck cancer, patients with inoperable tumours were selected.

Tab. 3: Recent publications on BNCT trials for other tumour entities
(KURRI - Kyoto University Research Reactor Institute, JRR-4 - Japan Research Reactor 4, RA-6 - Argentine Research Reactor 6, Bariloche, Argentina; Helsinki - Finnish Research Reactor TRIGA Mark II, Helsinki; MST – median survival time, M - months, CR – complete response, PR – partial response, OR - overall response, MM - Malign melanoma, AdCC - adenocystic carcinoma, UCC - urothelial cell carcinoma, MFS -myofibroblastic sarcoma, MC - mucoepidermoid carcinoma, SGC - salivary gland carcinoma, SCC – squamous cell carcinoma)

Author	Year	Facility	No. of cohorts / patients	Tumour type	B-compound(s) / dosage	Clinical outcome
Fukuda et al. [43]	2003	KURRI	3 / 22	MM	BPA: 85 mg / kg // 3-5h *OR* BPA: 170 mg / kg // 3-5h *OR* BPA: 210 mg / kg // 3-5h	CR: 73%, PR: 23%
Menendéz et al. [44]	2009	RA-6	1 / 7	MM	BPA: 14 g / m² (skin) // 1.5h	OR: 69 %
Kankaanranta et al. [45],[46]	2007 / 2011	Helsinki	1 / 29	SCC (24) AdCC (4) UCC (1) MFS (1)	BPA: 400 mg / kg // 2h	CR: 45%, PR: 31% MST: 13 M
Kimura et al. [47]	2009	KURRI	1 / 6	SCC (2) MM (1) AdCC (2) MC (1)	BPA: 500 mg / kg // 2-3h OR BPA: 500 mg / kg // 2-3h; BSH: 2 g // 12 h	CR: 16%, PR: 67% MST: 26 M
Kato et al. [48]	2009	KURRI	3 / 26	SCC (19) SC (3) SGC (4)	BPA: 250 mg / kg // 1h; BSH: 5 g // 12 h *OR* BPA: 250 mg / kg // 1h *OR* BPA: 500 mg / kg // 1h	CR: 46%, PR: 38%, MST: 13.6 M
Morita et al. [49]	2006	JRR-4	1 / 4	MM	BPA: 200 mg / kg // 1h OR BPA: 500 mg / kg // 2h	CR: 75%, PR: 25%

Fukuda et al. treated at the Kyoto University Research Reactor (KUR), Japan, 21 patients after BPA-infusion of 200 mg / kg body weight over three to five hours. Out of 21 patients, 16 showed full response, 5 patients showed partial response [43]. Menendéz et al. reported results of 7 patients suffering of malign melanoma, of which 5 showed full reponse, 2 patients were found to respond partially [44]. Very good results were reported by Morita et al. for a small group of four patients treated at the KUR at the Japan Research Reactor 4 (JRR-4). The BPA infusions

were applied at concentrations of 250 and 500 mg / kg body weight. Three of four patients showed complete response (in two cases the treatment was considered curative), in the case of the fourth patient partial response was found [49].

In Europe the most BNCT trials have been carried out in Helsinki, Finland. The local TRIGA reactor has been modified and now serves most of the time for therapeutic application of BNCT, isotope production and basic research [50]. In a study with 12 patients suffering from head and neck cancer, Kankaanranta et al. reported complete response in 7 cases, partial response in 3 cases and stable disease for several months in 2 cases. The BPA-infusion administered had a concentration on 400 g / kg body weight, one year survival was 58 % [45], and overall response to the treatment was 83 %. After these encouraging results, the study was extended to a number of 29 patients. After final evaluation, 22 patients responded to BNCT. Two-year progression free survival and overall survival were 20% and 30%, respectively, and 27% of the patients survived for 2 years without locoregional recurrence [46]. Good response was also observed in a study on 6 patients by Kimura et al. [47], of whom four responded partially and one completely, MST was 26 M. In a larger study with 26 patients carried out by Kato et al. [48], a similar treatment protocol was applied as in the study presented by Kimura et al., BPA-infusions between 250 -500 mg / kg body weight, partly with additional application of BSH. In this study, a 6-year-survival of 24 % was reported.

In most studies considerable improvement of the quality of life of the patients was reported after a limited number of treatments (1-3). The treatment by BNCT in the aforementioned studies usually involves only the infusion of the boron carrier solution and the irradiation of the patient without any particular follow-up treatment after a certain post-irradiation supervision time. Therefore, the physical and mental stress for the patients is usually much lower compared to other oncological therapies such as conventional radiation therapy, chemotherapy, or surgery, which may require weeks or months for treatment and recuperation.

Generally, with respect to the gain in MST and quality of life, the efficiency appears to be higher in head and neck cancer and skin cancer compared to brain

cancer, though it is very difficult to deduce directly the general effectiveness of BNCT from studies like those presented above:

1.) In several studies, selected patients were enrolled, e.g., with a certain Karnofsky performance score [51] or excluding patients without (or with) prior surgical treatment, chemotherapy et cetera.

2.) BNCT was partly applied in studies along with surgery, X-ray irradiation, or as IO- or NO-BNCT.

3.) Also, the rather small number of patients (usually between 5 - 30 patients) enrolled in each trial make a reliable prediction and statistical evaluation of the efficiency of BNCT difficult.

4.) Furthermore, many of the studies carried out so far, were carried out with varying treatment protocols, which includes also a variation of the boron compounds and the dosage protocols. In addition, each facility provides a very individual irradiation field.

1.4 Neoplastic diseases of the liver

The liver is the largest gland and the largest internal organ of the human body. It plays a key role in digestion, protein synthesis, glycogen storage, bilirubin metabolism, hormone production and detoxification. The liver is located in the upper right abdomen, below the diaphragm and overlays the gallbladder, weighing around 1.5 kg. It is supplied by two large blood vessels: the hepatic artery, carrying blood from the aorta, and the portal vein carrying blood coming from the gastrointestinal tract, the spleen, and the pancreas. The site where the blood vessels (and also the bile ducts) enter the organ is called hilum or porta hepatis. As the liver has a right and a left liver lobe, both artery and vein divide into right and left branches after entering the organ. The liver is the only human organ with the ability to regenerate completely, even if up to 75% of its mass are removed. However, only the functional completeness is restored, not the original shape of the organ.

The two liver lobes consist of eight segments, which itself consist of a number of lobules with a diameter of 1 – 2 mm each. These smaller subunits are hexagonally shaped and made up of liver cells arranged in one-cell thick plate-like layers. In the centre of a lobule, the central vein is located. From there, rod-like structures of liver cells are arranged radiating to the edges of the lobule. Between these rows of liver cells, small blood vessels are placed carrying venous and arterial blood from the hepatic portal vein and the artery to the central vein. These portal vessels are located at each corner of the lobule, where they are joined by a bile duct. Between liver cells, frequently small granules of oxidised lipid and protein clusters can be found, which are called lipofuscin.

Around 80 % of the liver cells are hepatocytes, which carry out most of the different liver functions. This includes protein synthesis and detoxification (inactivation of exogenous compounds and toxins, also the production of urea from ammonia for subsequent excretion), also, several steps of the lipid metabolism (cholesterol synthesis and synthesis of bile salts) and the carbohydrate metabolism (production of fatty acids, lipoproteins, triglycerides, and gluconeogenesis). Hepatocytes have a life span of around 150 days, they are of round shape and have frequently more than one nucleus. In Fig. 4, a histological image of healthy liver tissue is displayed.

Neoplastic diseases of the liver

The research carried out for this thesis was focused on the application of BNCT for different forms of malignancies of the liver. Primary and secondary malignancies of the liver are very common. Worldwide, the World Health Organisation registered around 610,000 patients who died from colorectal liver metastases (CRLM), another 700,000 whose cause of death was hepatocellular carcinoma (HCC) [52], making them the 3rd and 4th most common types of cancer in the world. Less frequent, but unfortunately increasing are intra-hepatic cholangiocarcinoma (IHCC). For example, incidence in the USA is about 3,000 per annum [53].

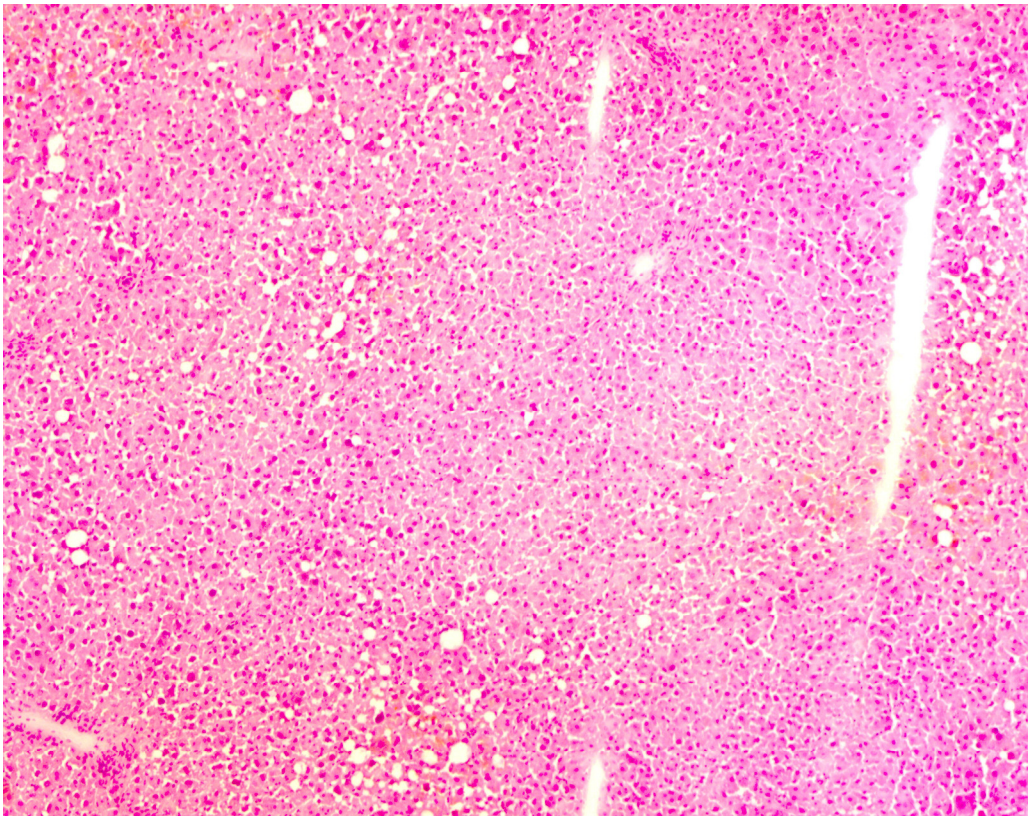

Fig. 4: Hematoxylin and eosin stained tissue section of a human liver (4.10 x 3.25 mm²)

HCC, IHCC, and the primary tumour responsible for the creation of CLRM, the colorectal carcinoma, spawn from epithelial tissue. Epithelial tissue forms glands and covers surfaces and cavities of a variety of structures in the human body. Malign tumours originating in epithelial tissue or neuroendocrine tissue are called carcinoma.

Hepatocellular carcinomas are primary liver tumours. They are often a result of liver cirrhosis, the consequence of a chronic disease during which large areas of functional hepatocytes (liver parenchyma) are destroyed by different forms of necrosis (externally caused premature cell death), which are then replaced by connective tissue (fibrosis) or regenerative nodules. Both cirrhosis and HCC can be triggered by hepatitis B and C, pesticides or natural toxins, anabolic steroids or by diseases of the metabolism.

Intrahepatic-cholangiocarcinomas are also primary liver tumours originating in the bile ducts inside the liver. It is morphologically distinct from HCC and does not occur as a result of cirrhosis or any of the other influences causing HCC. It is therefore not accompanied by cirrhotic reconstruction of the liver.

Colorectal carcinomas are tumours of the colon epithelium, which can be caused by adenoma (benign tumours of the colon) or by colitis ulcerosa. More than 50 % of all patients develop metastases in the liver, in many cases the liver is the first site where metastases are found.

Due to cancer and other diseases, the histology of parts of the liver is changed characteristically. For that reason, it is a standard clinical procedure to send tissue samples to a pathologist for further identification if cancer or other illnesses are suspected in a patient.

For example, during liver cirrhosis, large areas of connective tissue appear where hepatocytes and other liver cells would normally have been. Another example for a morphological change of tumour-free liver tissue is steatosis. Hepatocytes may retain lipids due to an impairment of the triglyceride metabolism, such cells are called steatotic.

Several features in tumour growth, which are very characteristic have already been mentioned: They are characterised by destructive, infiltrating growth into neighbouring tissue, often displaying atypical cell changes, e.g.,the occurrence of several nuclei per cell, and a higher cell number (hyperplasia) than other tissues. When growing, they develop their own blood supply. As the new blood vessels supply mostly the tumour rim, the inner parts of a tumour undergo necrosis, if the tumour reaches a sufficiently large size. However, even though the centre of a tumour may be necrotic, live functional cells can still be found. Also, fibroblastic tissue is present to a large extent in tumours, but it is particularly prominent in

carcinomas, where it is called desmoplastic stroma reaction. Triggered by the effect of growth factors liberated by tumour cells, this reaction guarantees the development of the tumour vascularisation and stromal support for the tumour growth. Hence, many tumours consist also of a component of fibrotic tissue. The very heterogeneous tissue morphology is illustrated in Figure 5.

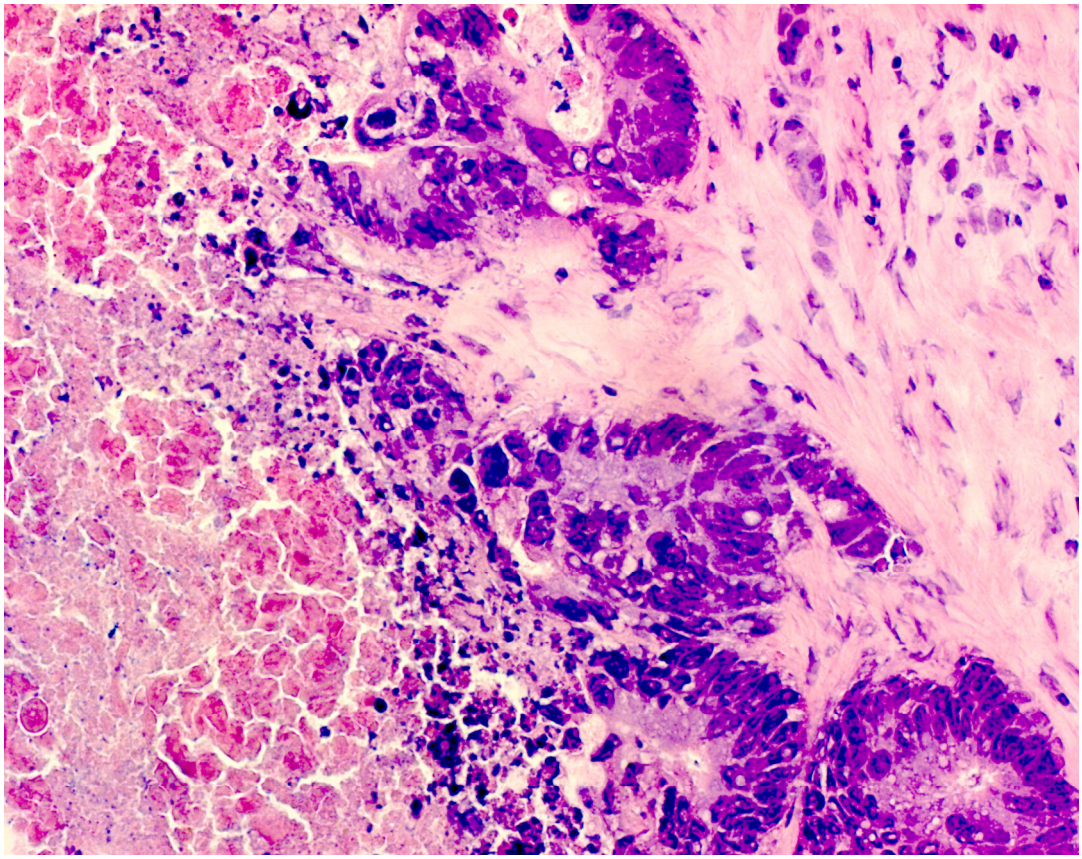

Fig. 5: Hematoxylin and eosin stained tissue section of a colorectal liver metastasis (410 x 325 µm²). It is visible how polynucleous tumour cells (adenocarcinoma) separate fibrotic cells (right half) and necrosis (left half)

Treatment options for neoplastic diseases of the liver

Treatment options for lesions caused by HCC, IHCC, and CRLM are similar due to their common location in the liver, however as they vary in size, position, number, and dissemination, there are considerable differences.

Due to number and specific location of the lesions, only in a minority of all cases, surgical or locally-ablative treatment is applicable, such as radiofrequency ablation [54, 55] or hepatic resection [56, 57]. If not amenable to resection, other options

are therapy by radiofrequency thermal ablation [58], chemotherapy [59–63], different forms of radiotherapy [64], and endoradiotherapy (ERT), for example by ^{90}Y-containing microspheres [65] or ^{166}Ho-containing microspheres [66]. Liver transplantation is an option which is rarely chosen, as in most countries there are not enough donor organs available, though it offers high survival probabilities [67]. Of the patients suffering from HCC or IHCC, about 75 % do not have any systemic metastases upon first diagnosis. However, one third of the lesions found cannot be removed by resection. Therefore, treatment options apart from resection are similar to those of liver metastases. Sadly, as of today, for a large number of patients diagnosed with any type of liver cancer, all therapeutic attempts in the end are only palliative.

Conventional radiotherapy for liver malignancies is a somewhat limited option due to high radioresistance of several tumours occurring in the liver and by the position of the organ in the body, where it is surrounded by too many radiosensitive structures which would be damaged if irradiated entirely. The success of endoradiotherapeutical approaches show that the biologically targeted application of high radiation doses offers a great therapeutic potential. Application of BNCT could offer another possibility of delivering very high doses exclusively to tumour tissue while sparing surrounding tumour free liver tissue and adjacent radiosensitive structures. About the issue of applying BNCT to the liver more will be said in section 1.5.3.

1.5 Treatment planning in BNCT

1.5.1 Pharmacokinetics and cellular uptake of boron compounds

The information about the pharmacokinetic behaviour of a boron compound is essential for an application of BNCT to patients in clinical trials. The knowledge of the different steps from the administration of the boron carrier, over its uptake in cells, until the clearing of the carrier molecule or its metabolic products from the body, is needed for the determination of the correct point in time and the interval of the neutron irradiation. The different stages from the moment of administration to the excretion can be described in a general action schematic in Figure 6, based on a schematic by T. Probst [68].

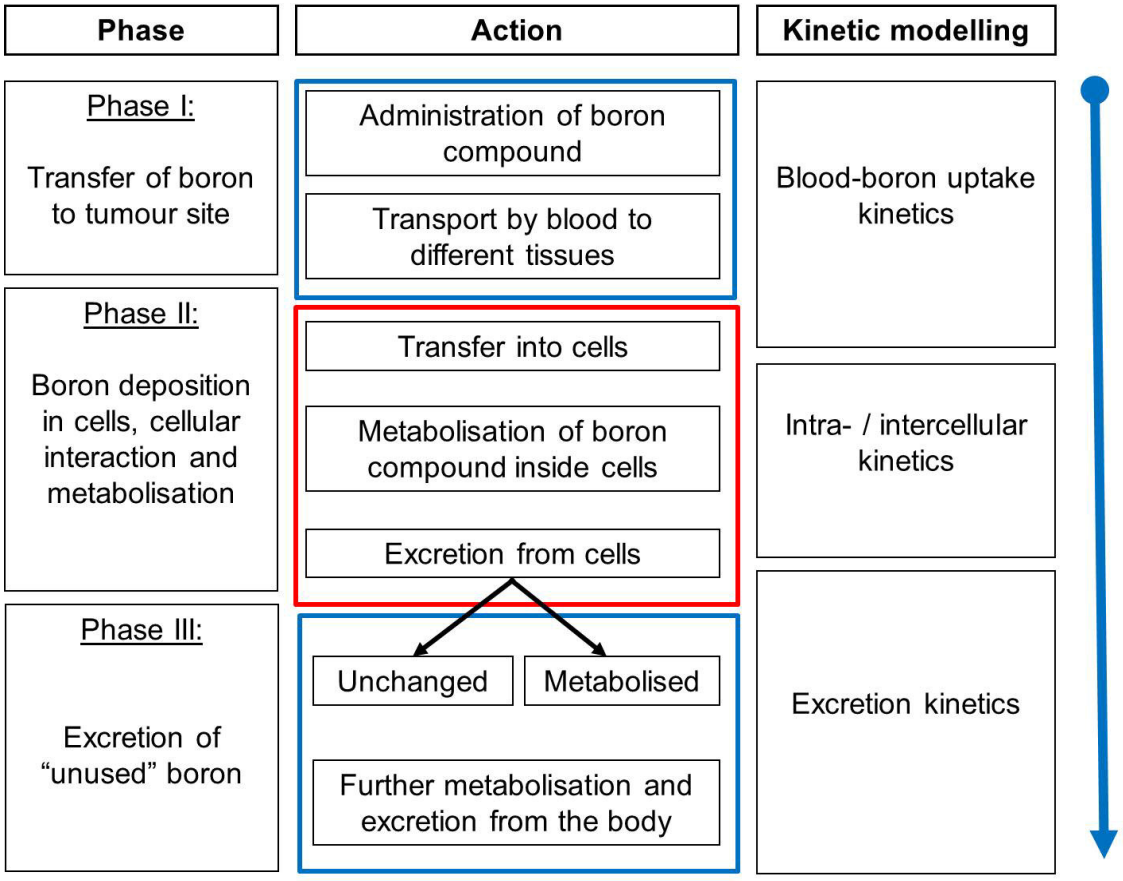

Fig. 6: A simplified representation of the pathways required to bring a boron-containing species from the moment of injection to the patient and then to excretion. The arrow denotes the chronological course of action. Blue boxes are assigned to actions taking place on a macroscopically traceable scale, the red box is assigned to all microscopic actions.

The schematic does not include therapeutic steps, which do not influence the kinetic processes directly, like neutron irradiation. The work presented in this thesis is closely linked to several of the steps shown in Figure 6, which is why the schematic is used to clarify the chronological context of the single steps and to stress the importance of pharmacokinetic modelling and quantitative boron analysis for treatment planning in BNCT. For some of these steps, qualitative confirmation of a boron compound acting in a certain way is not sufficient, the presence (or the action) of the compound has to be determined quantitatively.

It should be noted, however, that the schematic depicts a model situation and omits several factors and parameters, which have to be considered in a clinical situation as well. Most notably, these are biological and radiobiological effects concerning intra- and intercellular processes like DNA-repair mechanisms.
The different actions presented in Figure 6 can be roughly categorised in macroscopic and microscopic actions taking place. At the time of writing, most data available in literature have been published for macroscopic steps. Furthermore, there are three different phases in time, which can be regarded independently, when describing pharmacokinetics in BNCT. In the following paragraphs, the different phases and actions will be characterised more in detail:

Administration of the boron compound

As mentioned further above, there are two boron compounds which are the most frequently used in clinical trials. BSH was introduced by Hatanaka in 1968 as new boron carrier, which potentially might cross the blood brain barrier [69], and since then has been used in trials for brain tumour. BPA was originally designed by Y. Mishima for the application for melanoma treatments, as it is structurally similar to L-tyrosine, which is a precursor for the production of melanine [70]. Today BPA-fructose (BPA-f), BPA-mannitol (BPA-m) and BSH are the most commonly applied boron carriers in clinical trials.
The most frequent administration route for boron carriers is an intravenous infusion, often through a central vein catheter (CVC), or into another vein. However, other possibilities in administration for boron carriers, such as intra-

arterial injection, at times with the additional use of blood-brain-disrupting agents, have been tried in *in vivo* studies [71, 72], and in clinical trials ([73] for BPA [74], for BSH).

For the treatment of brain tumours, BPA-f and BSH have frequently been applied simultaneously for the treatment of selected brain tumours ([31, 33, 37, 75], among others). In this case, it is necessary to administer both boron compounds in different infusions at different points in time. The effectiveness of the simultaneous application appears to be higher for the chosen tumour entities than the application of only one boron compound for the respective tumours, which is probably due to better and more homogeneous boron enrichment in the different tumour compartments, as both compounds are subjected to different biochemical transport mechanisms [76].

Transport by blood to different tissues

Pharmacokinetic models for the blood-boron uptake kinetics are created according to experimental data. Several studies with a pharmacokinetic focus have been carried out in the past, mostly trying to characterise the transport of the boron carriers in blood with the aim to define the most favourable moment for neutron irradiation. To this avail, either *in vivo* models, which were subsequently adapted for humans or samples from clinical studies were used. Commonly, the course of the boron concentration in blood is recorded over the whole infusion period to obtain the wash-in kinetics and also for a certain period in time after the stop of the infusion to retrieve information about the excretion kinetics.

Additionally, tissue samples of the regions of interest are taken at different points in time to retrieve information about the boron uptake in tissue. Very often, tumour samples are taken in the same intervals to monitor the tumour-to-blood (T/B) and the tumour-to-tumour-free tissue (T/H) ratio. Blood-boron kinetics have been assessed in a number of studies for BPA-f, BPA-m and BSH. Ideally, the T/H ratio of the boron uptake is highest at the moment of irradiation. However, at the same time, the absolute boron concentration in the tumour cells must still be high enough to reach therapeutic dose levels, and it must be certain that due to a

probably too high boron concentration in the blood no damage is dealt to the blood vessels. Furthermore, boron accumulation in cells may also take some time.

For BSH, a rapid clearance from the blood has been found in various studies [74, 77–79], can be expressed exponentially. Also, in these studies, T/B and T/H ratios were determined, sometimes together with calculated theoretical dose ratios. All studies agree in the recommendation for an optimal effectiveness of the treatment to irradiate 12 to 20 hours *post*-infusion. Indeed, in most clinical trials involving the application of BSH patients are irradiated 12 hours after start of the infusion ([31, 33, 37, 75], among others). All of the pharmacokinetic features of BSH stated in this paragraph were outlined for intra-venous infusion. Intra-arterial infusion of BSH was discussed by Kageji et al. with the conclusion that the intra-venous infusion route should be preferred during treatment, as it provides less risks for the patient: BSH after intra-arterial infusion was found to move into the peripheral organs more easily than after intra-venous infusion [74].

So far, very few data about the kinetics of BPA-m are available, but which appear to phenomenologically agree with those published for BPA-f [73]. Most clinically applied BPA-f infusions last between 1 and 2.5 hours ([24–26, 44, 46, 48, 80], among others), but also significantly longer infusion times have been chosen for therapy [28]. The course of the BPA concentration curve in blood is characterised by a steep increase which leads into saturation. After the stop of infusion, rapid, exponentially expressible clearance from the body was found, although the clearance does not proceed as quickly as in the case of BSH. In most clinical studies, for various kinds of cancer, an interval of 2-3 hours for BPA-infusion is considered to be optimum for the enrichment of boron in tumour compared to surrounding tumour free tissue. An example curve for the typical course of the boron concentration in blood is presented further below in Figure 8, section 1.5.2. However, this should not be seen as general rule and might be different for each kind of tumour tissue [81].

Transfer of the boron compound into cells

Cellular uptake of BSH

The cellular uptake mechanism for BSH has not been investigated in detail and remains largely unclear, proposed mechanism hints at endocytosis [82]. However, it has been confirmed that cellular uptake definitely takes place in different brain cancer cells.

Ceberg et al. [83] measured boron in subcellular fractions of BSH-infused astrocytoma tissue from patients. After tissue homogenization and centrifugation, they found 21% of boron in nuclei, 18% sedimented with the fraction consisting of mitochondria and other cell organelles and 61% of boron was found in the soluble fraction, consisting of cytosol and extracellular fluid.

Similarly, Otersen et al. could show by immunohistochemical staining that there is an uptake of BSH into cell nuclei and cytoplasm. Partly, the BSH coincided with the expression of Ki-67 proliferation markers. Though the fraction of cells both proliferating and showing BSH uptake was not quantified, it appeared that only a minority included both features, hence a correlation of linking BSH-uptake to proliferative activity of cells could not be drawn [84]. Additionally, Neumann et al. found high BSH concentrations along the cell membrane examining tumour samples of patients suffering from glioma. Therefore, as mentioned further above, it was proposed that the BSH uptake could be carried out by endocytosis.

Cellular uptake of BPA

Compared to BSH, BPA has been used for the treatment of more types of cancer and its properties have been identified in more detail. Particularly, the transport mechanism for BPA has been identified with relative certainty. Bulky amino acids like phenylalanine, tyrosine, valine, and leucine, are transported via the L-system into cells. The L-system consists of four transporters (large amino acid transporters LAT-1, LAT-2, LAT-3, and LAT-4). Two are hetero(di)mers composed of a catalytic subunit (LAT-1 or LAT-2, as light-chain glycoprotein-associated amino acid transporter) linked covalently with the glycoprotein 4F2hc/CD98 (heavy

chain) [85]. The other ones, LAT-3 and LAT-4, are distinct in there structure, for both a monomeric structure has been proposed. They share many functional characteristics like sodium, chloride, and pH independence, narrow substrate specificity, a two-component kinetics, lack of *trans*-stimulation, stereospecificity, and sensitivity to the presence of the amino acid analogue BCH [86, 87].

The transporter with the seemingly greatest responsibility for BPA is LAT-1 [88, 89], which is most probably due to the structural similarity of BPA to phenylalanine. The efficiency of BPA as boron carrier in BNCT might be explained with the high expression of LAT-1 in various tumour entities [90–94]. For this reason, LAT-1 is being used as marker for prostate cancer [95] and is being considered, in combination with ^{18}F-fluorated L-DOPA, as tracking substance for tumour visualisation [96]. In addition, it seems to be possible to increase the LAT-1 expression by *trans*-stimulation, i.e.,the intake of BPA can be stimulated by offering structurally similar metabolites to the cell, which are transported by LAT-1 as well (Fig. 7).

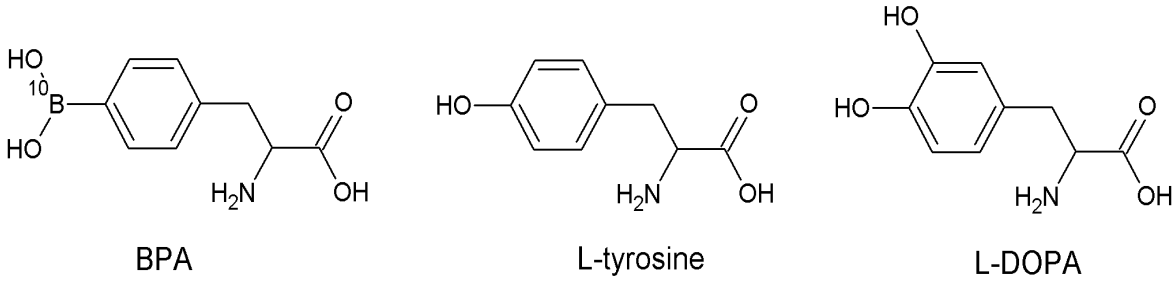

Fig. 7: Structures of BPA, L-tyrosine and L-DOPA

Papaspyrou et al. could show that trans-stimulation of BPA is possible by prior administration of L-tyrosine in an *in vivo* melanoma model (also-called “preloading”) [97]. Capuani et al. could show similar results for an in vivo glioma model after preloading with L-DOPA [98, 99]. However, though the structural resemblance of BPA, L-DOPA, and L-tyrosine is very high, even smaller changes greatly influence the uptake behaviour. Hiratsuka et al. found during *in vitro* studies with the structural isomers of BPA (*ortho*-, *meta*-, and *para*-BPA) that enrichment in the respective cells was highest for *para*-BPA. This could point to a

certain steric hindrance of the uptake of BPA in case of *ortho*-, and *meta*-BPA [100].
As also the A-System is responsible for transport of neutral amino acids like alanine to a certain extent [88], there is the assumption that the transport of BPA into a cell might be a two-step process of first using unidirectional A-system transporters for the intake of a similar metabolite, like L-tyrosine, and then exchanging this metabolite via the L-system [85].

An actual accumulation of boron after BPA-infusion inside tumour cells was demonstrated for glioma cells using secondary ion mass spectroscopy (SIMS) [101–103] and for melanoma cells using electron energy loss spectroscopy (EELS) [104]. More than that, Chandra et al. could demonstrate that in T98G human glioblastoma cells there is an elevated ^{10}B concentration in mitochondria-rich cell regions compared to other cell regions [103].
For a long time, uptake of BPA was believed to be mostly subjected to the proliferative activity of tumour cells, which was not unsurprising, as LAT-1 expression was found to be correlated with cell proliferation indicated by Ki-67 expression, e.g.,in non-small cell lung cancer [92]. However, contrary to these results, in studies by Detta et al. [89] and Wittig et al. [88], no significant correlation between immunohistochemical analysis using proliferation markers like Ki-67 or PCNA in squamous cell carcinoma, colorectal liver metastases, or glioblastoma could be found. Both groups concluded that the activity of LAT-1 therefore seems to be upregulated in these tumour cells regardless of their proliferative status.

The difference of such results clearly indicates the need for further research on this matter. Up until today, only few works have been published on assessing the tracing abilities of the boron compounds in clinical use so far. Also, only scarce information about the coincidence of tumour- and radiobiological parameters between boron compounds and the tumour entities, which are subject of clinical trials, is available.

Excretion from cells and from the body

The elimination of BPA from the body is most probably managed by the kidneys [105]. During metabolisation and following clearance from the body, a large fraction of the BPA-f is split into fructose and BPA. This process appears to start shortly after administration and proceeds within several hours [106]. Unfortunately, the implications of this structural fragmentation of the BPA-f molecule have not been assessed yet. Fortunately, the fragments of BPA-f are non toxic and can be excreted from the body without further difficulties. They therefore pose no threat to the patient's health.

In the case of BSH, the consequences of metabolisation and elimination from the body are at least partly known. Though most of the BSH is excreted unchanged (around 80%) [107], it partly aggregates to a dimeric form $Cs_4B_{24}H_{22}S_2$ (BSSB) [106], for which it is known to be taken up in higher levels in 9L rat gliosarcoma cells [108] and which has longer retention times in C6 rat glioma cells and M2R mouse melanoma cells [109]. However, it is very difficult to consider such structural changes in dose planning models, as there might be different kinetic constants be found for different kinds of tumour cells. It is very important to stress that cellular uptake of either of the two boron compounds (BPA and BSH) is cell and tissue type dependent.

Although many works have been published about cellular enrichment and pharmacokinetic issues of BPA and BSH, it is still very little known about the microscopic pharmacokinetic behaviour, e.g., the intake and excretion kinetics on the cellular level of either of the boron compounds. Kinetic modelling so far must rely on data available for the blood-boron kinetics and the linked boron-in-tissue / boron-in-tumour ratios. As all of these processes can be highly individual for each tumour, for each tumour entity, existing models should be verified or new ones should be established.

1.5.2 The relevance of boron concentration monitoring for treatment planning

Prediction of the boron concentration in blood

The numerical modelling for pharmacokinetic behaviour typically includes a multi-parameter fit for the transition of the boron from blood to tissue and out of tissue. This is commonly expressed by oligo-compartment models (with usually two or three compartments), e.g., a model that assumes transport of boron in single steps from one compartment to the other, which can be reversible. Such steps would include transfer of the boron from the infusion to blood, from blood to tissue or from extracellular to intracellular space. With such models, dose prediction for neutron irradiation after the stop of the infusions containing the boron compounds is made possible.

The pharmacokinetic behaviour of BPA is commonly described by an open two-compartment model [105, 110, 111]. The course of boron concentration during infusion is characterised by a steep increase which reaches slowly a level of saturation, if the infusion persisted for a longer time. After stopping the infusion, the boron concentration decreases exponentially within several hours. In Figure 8, the simulated pharmacokinetic behaviour of the boron concentration according to an open two-compartment model during and after BPA-f infusion is shown. In this example, three irradiations of the same patient are part of the treatment planning.

For BSH, the clearance from the blood also has been described by two-compartment models proposing a biexponential decline (Fig. 9) of the boron concentration after stop of the infusion [74, 77]. From the pharmacokinetic data collected, Kageji et al. drew the conclusion that BSH moved relatively quickly from the blood to other organs, where is was retained and slowly released over a period of several days [74]. The major part of the boron accumulated in tumour tissue was cleared 24 hours after stop of the BSH-infusion. Interestingly, the kinetic parameters found for BSH are similar to those for Carbamazepine, Clonazepam, Lorazepam, and Nitrazepam [112], which are all drugs targeting the nervous system.

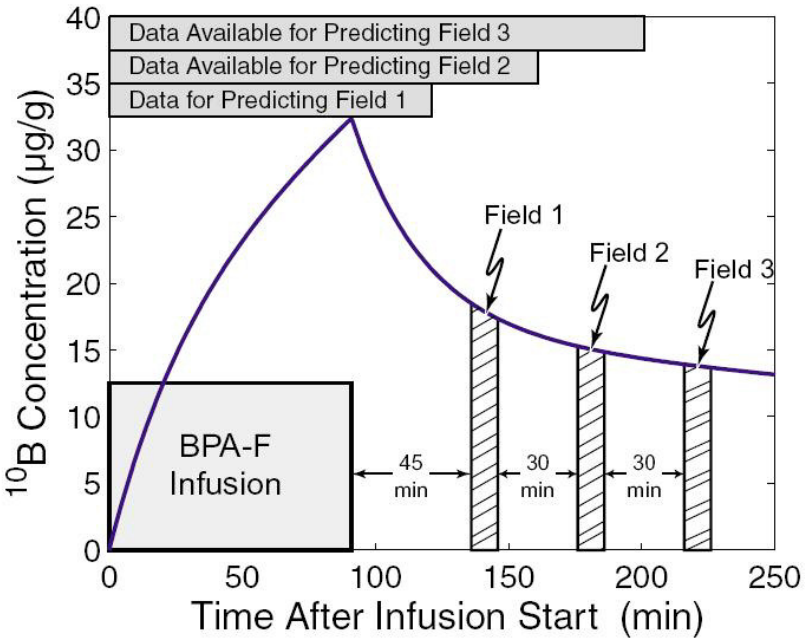

Fig. 8: Course of a simulated BNCT treatment involving a 90 min BPA-f infusion followed by irradiation of the patient with three irradiation fields. The horizontal bars above the course of the boron concentration denote the intervals of which boron concentrations in blood are available for calculation, field 1-3 are the intervals in which irradiation would take place (image taken from [105])

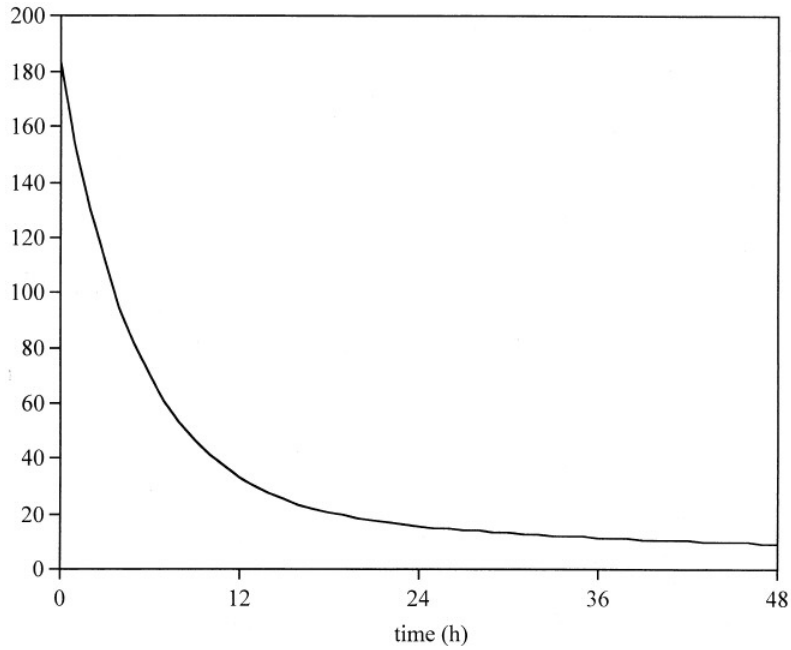

Fig. 9: Calculated concentration of boron in blood after a 100 mg/kg BSH infusion (figure taken from [79])

Description of the total dose

The boron dose in blood and different tissue compartments and cells is a key parameter for treatment planning in BNCT. The dose applied during BNCT treatment is commonly described by a sum of four major dose contributions, defined by the nuclear reactions that occur when neutrons pass through tissue and by additional radiation emitted from the irradiation facility. Of the four dose contributions, only one, the boron dose (D_B), is of therapeutic interest. *The boron dose* is the dose from the heavy charged particles generated during the $^{10}B(n,\alpha)^{7}Li$ reaction with a total energy release of 2.79 MeV (described in more detail in section 1.2). The other three dose contributions are:

1. *The nitrogen or thermal neutron dose* (D_N), caused by 580 keV protons released upon the capture of thermal neutrons by nitrogen atoms in tissue ($^{14}N(n,p)^{14}C$).

2. *The proton dose or fast neutron dose* (D_P), which is a result of the interactions of fast neutrons with hydrogen atoms in tissue ($^{1}H(n,n')^{1}H$). Fast neutrons are a part of the neutron spectrum in almost all neutron beams available for BNCT.

3. *The γ-ray dose* (D_γ). This dose consists of γ-rays of different sources, one part are γ-rays emitted from hydrogen atoms in tissue after capturing thermal neutrons ($^{1}H(n,\gamma)^{2}H$), while the other part are γ-rays emitted by the neutron source itself.

Mathematically, the total radiation dose a patient receives during BNCT is usually described by the following equation (Eq.1):

Eq. 1: $$D_{tot} = D_B + D_N + D_P + D_\gamma$$

As very different particles are released in tissue due to neutron capture (protons, α-particles et cetera), it is not convenient to merely express the dose contributions

as physical dose (in Gy) due to the very different radiobiological effects caused by each kind of particle (see also section 1.1).
The total dose in BNCT is therefore commonly expressed as sum of photon-equivalent doses. This is achieved using weighting factors (*w*) which are determined experimentally and which are then multiplied with each dose contribution. As a result, the weighed total BNCT dose is expressed like this (Eq. 2):

Eq. 2: $$D_{tot,w} = w_B D_B + w_N D_N + w_P D_P + w_\gamma D_\gamma$$

To distinguish weighed dose from physical dose, it is often given in units of Gy_w instead of Gy. The determination of such weighting factors is carried out by comparison of radiobiological effects caused by photon irradiation assessed in *in vitro* and *in vivo* models to the effects in the same models caused by radiation with a higher LET. More information about importance and determination of weighting factors may be found elsewhere [113–117].

The three latter dose components, apart from the gamma-ray contamination of the neutron beam, cannot be avoided during therapy. All of them are unwanted dose contributions as they cause unspecific dose deposition in the targeted tissue.
While γ-rays coming from an accelerator or a reactor core can be diminished by appropriate shielding, all other reactions occur due to the natural composition of tissue by interaction with incoming neutrons. Therefore, these dose contributions might be called *indirect* dose contributions, as their radiobiological effect can only be influenced by the intensity and the energy spectrum of the irradiation field.

The boron dose however is a *direct* dose contribution, its radiobiological effect can theoretically be controlled by the enrichment of boron in the tissues and cells which are irradiated during treatment. **The prediction of the boron dose is also the most difficult task, as it is usually not possible to predict the exact boron distribution in every patient individually, whereas the indirect dose components can be simulated very well using reference values for human tissue and by the precise characterisation of the irradiation field.**

Monitoring and determination of the boron dose is therefore usually accomplished in two steps:

First, the blood-boron kinetics have to be determined by a suitable pharmacokinetic model. With such models, a prediction of the kinetic boron curve is possible, if in different time intervals sufficient data about the boron concentration in the blood is provided. To do this, during infusion of the boron carrier, blood samples are taken regularly which have to be analysed in a very short time. With the analytical methods in use for routine boron determination in blood, such data can be produced within several minutes, a short geographical distance between operation theatre and analytical laboratory provided. The methods routinely used for rapid boron analysis during BNCT treatment are inductively coupled plasma mass spectrometry (ICP-MS), inductively coupled plasma optical emission spectroscopy (ICP-OES), and prompt gamma activation analysis (PGAA) (for further details about methods for boron analysis see section 1.6.3) [118–120].

Second, the boron enrichment in tumour tissue has to be predicted. This task is more difficult to deal with, as it is not possible to take tissue samples from the tumour and the surrounding tissue during BNCT treatment. Therefore, models for the prediction of the enrichment are created relying on data obtained during preclinical studies. Additionally, it is possible to assist such models by determining enrichment factors during or shortly before treatment by non-invasive methods like positron emission tomography (PET) [34, 46, 120]. In this case, a small quantity of a structurally similar radiotracer is injected in order to retrieve values reflecting the uptake behaviour in the moment of the treatment itself as realistic as possible.
Preclinical studies to determine enrichment factors of boron may be carried out using animal models, whose data are either later extrapolated for patients [121]. Similarly, data from such trials are used to explore the general possibility of a favourable enrichment in a specific tumour entity, thus determining if it is at all possible to treat this entity by BNCT ([122–125], among others).

If this is confirmed, studies involving patients have to be carried out including administration of the boron carrier during surgery, e.g., indicated resection of

tumours or metastases independently of the BNCT related questions. Often this includes also sampling of the relevant tissues during the infusion and/or at the moment when an irradiation should take place ([73, 79, 126–128], among others).

The obvious conclusion can be drawn that the exact prediction of the boron dose is a task requiring much work prior to a clinical application of BNCT. Ideally, not only the integral boron concentration in tissue is determined. The detailed knowledge of the boron concentration and distribution in a targeted tissue (down to the subcellular level) allows inclusion of more parameters for safe and successful treatment planning. Especially, the characterisation of dose weighing factors can be greatly improved. In many reports published by several groups concerning the spatial boron distribution in tissue compartments or inside cells, the results strongly indicate the need for differentiated boron analysis of tissue samples to improve treatment planning [126, 127, 129]. Moreover, not only precise boron determination, but also the accompanying analysis of morphological and biological properties of the tissue will provide further refined treatment planning. Other approaches suggest higher precision for dose calculation, if microdosimetrical models are used [130]. However, for most tumour entities and boron carriers, too few information is available to realise such approaches at present.
At this point, it should be stressed again that the possible radiobiological consequences of the metabolisation of a boron compound have to be taken into account for treatment planning as well. Also the correlation of the spatial boron concentration in tumour tissue to its biological features is particularly useful. However, only a few publications on this topic have been issued so far [88, 89].

1.5.3 Treatment planning for an application of BNCT to the liver

The application of BNCT to treat liver malignancies has been limited to three cases world wide so far. The general interest of the BNCT research community was stirred by the TAOrMINA programme initiated in the late 1980s in a cooperative project of several institutions of the University of Pavia, Italy [131], with the aim to treat patients suffering from inoperable colorectal liver metastases

(CRLM). *Intra-corporeal* irradiation of the liver was considered not to be feasible due to location of the liver inside the abdomen, where it is surrounded by several organs which would suffer irradiation as well. After a series of *in vitro* and *in vivo* studies with BPA as boron carrier confirming the theoretical feasibility of BNCT for CRLM, it was decided to explore the possibility of an *extra-corporeal* liver irradiation. For this kind of treatment, the irradiation facility, the TRIGA Mark II research reactor at the laboratory for applied nuclear energy (L.E.N.A.) in Pavia had to be structurally modified. This included most notably the enlargement of the irradiation channel in the thermal column and the installation of two bismuth shields to reduce the gamma-rays emitted from the reactor core [132, 133]. More detailed information about clinical outcome and treatment planning of the trials can be found elsewhere [134, 135], therefore, only a brief summary of the trials will be given here:

Extra-corporeal liver irradiation

In 2001 and 2003 one patient each was treated. The first patient died 44 months after BNCT due to systemic metastases, the second patient died 33 days after BNCT from a preoperatively existing dilatative cardiomyopathy. Upon autopsy, remnants of vital tumour tissue were found in the liver of the second patient [135]. Both patients received a BPA-f infusion of 300 mg / kg body weight over two hours prior to complete removal of the liver from the body. After removal, the liver was washed, chilled, packed in sterile, hydrogen-free plastic bags and a polytetrafluoroethylen (PTFE, Teflon) box for irradiation and then transferred to the TRIGA Pavia reactor for irradiation, and biopsies from both tumour and tumour-free liver were taken to determine the enrichment factor of the boron in tumour tissue, which were 5.9 : 1 and 5.6 : 1, respectively. Subsequent irradiation lasted about 10 min. The whole treatment including surgery for explantation, transport and preparation of the organ, irradiation, and re-implantation took 21 and 18.4 h, respectively.

Intra-corporeal liver irradiation

Intra-corporeal BNCT for hepatocellular carcinoma was tried in Japan by Suzuki et al. [136] in one case. Two infusions with both BPA and BSH along with a vessel embolising agent were administered. About 6h after infusion, irradiation with two different irradiation fields took place at the Kyoto university research reactor institute. The moments for irradiation were chosen following the boron concentration in the patient's blood, the monitoring of the boron level was carried out by prompt gamma activation analysis. Tumour growth was stable for one month post BNCT, the patient died 10 months after the treatment. The trial confirmed the technical feasibility of in situ BNCT for liver malignancies, however many questions, most of all concerning the boron concentration and distribution in the different irradiated tissues remain.

Advantages of extra-corporeal liver irradiation compared to the intra-corporeal approach

The irradiation of an explanted organ comes with certain therapeutic advantages and difficulties for both the patient and the physicians, who are responsible for a successful therapy. A treatment protocol following the TAOrMINA-approach includes extensive and complicated surgery (auto-transplantation) which greatly increases the risk for the patient. Also, the number of patients eligible for such a procedure is limited, as only patients with a "structurally stress-resistant" liver can be chosen, because the organ has to be mobilised, resected, and transported. Therefore, patients with cirrhotic livers (not uncommon in case of HCC) would not be amenable for therapy.

Moreover, the idea of irradiating the organ *ex-situ* enables the radio-oncologist to expose the organ to a (theoretically) ideal irradiation field. In BNCT, patients are mostly irradiated in front of a beam aperture, which means that all neutrons for irradiation are coming from the same direction. This may require extensive beam shaping and/or a particular neutron spectrum to ensure the presence of sufficient thermal neutrons also after a certain penetration of tissue. In case of the irradiation

of the explanted liver inside the thermal column of a reactor, the liver is placed in an irradiation field where a significant part of the neutrons reach the liver from all sides (Fig. 10).

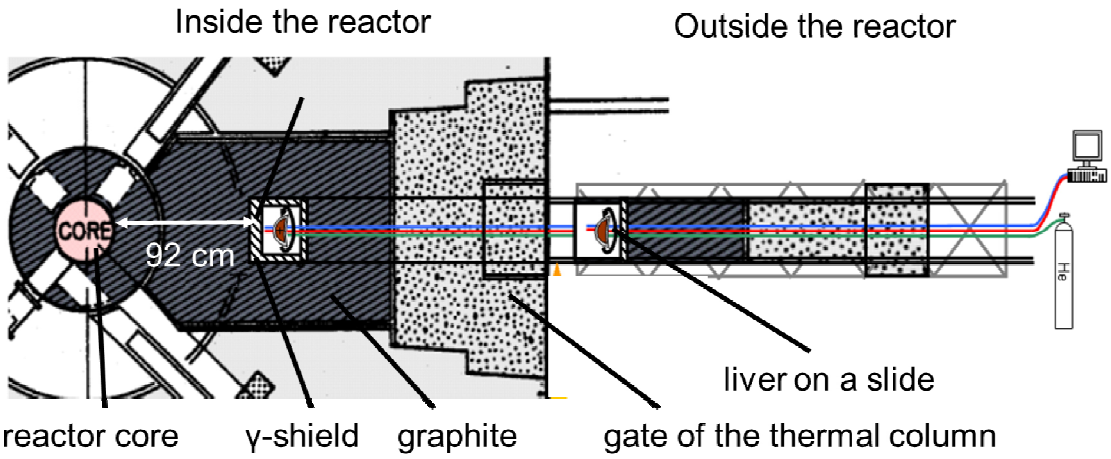

Fig. 10: Example for a possible structural modification of the thermal column of the TRIGA Mainz. Figure re-used from [137].

Therefore, it is possible to choose the location in the thermal column with the most suitable irradiation field, thus providing a more homogeneous dose for the whole organ. Also, the liver can be repositioned, e.g., by rotation, during irradiation if needed for an optimal irradiation, and it can be carefully put into a specific container to change its three-dimensional shape, e.g., by using a spherical container to irradiate a more “ball-shaped” organ [138]. Additionally, especially if the organ has to endure longer irradiation times, a cooling system for the organ has to be installed.

If kept outside the body and separated from their natural vasculature, organs have to be perfused with preservation solution in order to clear the blood from all the blood vessels, since coagulation would cause serious damage during the time they spend outside the body. If cooled after perfusion, there are little metabolical influences on boron distribution inside the organ (and the tumour) to be expected. This simplifies pharmacokinetic modelling, as far as the possible consequences of the perfusion of the organ are known, because the model only has to consider the time interval of the boron infusion, after which the blood vessels to the liver will be clamped and resection will begin.

In several studies, the irradiation field inside the thermal column of the TRIGA Mainz research reactor was characterised and it was successfully shown that the facility, after some structural modification, would be adequate to serve as neutron source for a BNCT trial involving extra-corporeal irradiation of a human liver [137, 139].

However, the patient has to undergo surgery involving auto-transplantation, which is a very complicated operation with the risk of a fatal outcome. Therefore, the reasons for and against extra-corporeal BNCT treatment must be carefully considered and weighed. To be able to do this, a number of crucial parameters must be assessed. The work presented in this thesis is mainly focused on one of these parameters: the boron distribution and concentration and their correct determination in cancerous and tumour free liver tissue.

1.6 Boron imaging and boron analysis

1.6.1 Characteristics of boron

Boron is a low-abundance, metalloid element. Of the two stable isotopes ^{10}B and ^{11}B, ^{10}B is used frequently in the nuclear sciences due to its ability to capture neutrons, e.g., as neutron stopping shielding material. Boron cannot be found chemically unbound in nature, most commonly, it is found as borate in minerals like Kernite ($Na_2B_4O_7 \cdot 4\ H_2O$), Borax ($Na_2B_4O_7 \cdot 10\ H_2O$), Borocalcite ($CaB_4O_7 \cdot 4\ H_2O$) and Colemanite ($Ca_2B_6O_{11} \cdot 4\ H_2O$). Elemental boron has to be produced industrially. Crystalline boron can be extremely hard and exists in five allotropic forms. The formation of crystalline boron structures and their properties highly depend on different parameters like external pressure [140].
The chemistry of boron is very complex and unique, as it has three valence electrons and four valence orbitals; it forms preferably strong, covalent bonds. The characteristic electron deficiency is the reason for the variety of boron compounds trying to complete their electron octet by π-bonds or three-centric bonds containing two electrons. It may form complex, three-dimensional structures, especially when combined with other elements like carbon, nitrogen or different transition metals [141].

Boron is essential to life and has a very low toxicity in mammals. While the nutritional essentiality for higher plants was confirmed decades ago [142], it remained to be somewhat debated if this accounted for humans, too. However, this seems to be confirmed now as well [143].
Boron plays also a role in life sciences, though its biological and physiological potential has not been fully explored yet. For example, in animal models, boron was found to ameliorate fulminant hepatic failure by counteracting the changes associated with the oxidative stress [144].
In cancer therapy, boron is mostly associated with BNCT, though more recently, the use of polyhedral boron compounds was proposed as carriers for radionuclide therapy and diagnostics [145].

1.6.2 The importance and application of boron analysis

The need for precise analysis of boron concentrations arose as early as it was considered as essential for life and when its application in nuclear sciences became of interest. Due to potential toxicity, the analysis of boron in drinking and groundwater has become a routine task, there are threshold limits established by the World Health Organization (WHO) and the European Union (EU) [146, 147]. Partly linked to boron analysis in water, trace analysis of boron is also of interest for nuclear power plants using water as cooling agent and moderator, which might contain traces of boron [148].
Considering the importance of boron in life sciences and oncology, the need for boron analysis in biological materials such as tissue, blood, and cells is evident.

Boron may be quantitatively analysed using a variety of methods. Each analytical protocol allows boron determination at a certain spatial resolution. The resolution automatically determines the biological relevance of the data which are gained during analysis. Whilst macroscopic analysis may give information about rough boron distributions in larger tissue compartments (of a volume of several cm^3), e.g., boron concentration in a whole tumour, with increasing resolution down to the cellular and subcellular level, it is possible to derive information on microscopic parameters such as cellular uptake, cellular transport behaviour, or metabolisation of the boron carrier molecule. Though some of this information may be obtained by cell culture studies, the analysis of actual tissue and blood samples from either *in vivo* or clinical studies is required to investigate for a detailed knowledge of the true biological situation.

The resolution is defined differently for destructive and non-destructive methods. For destructive methods, often only an integral (or bulk) determination of boron is possible. Therefore, the spatial extent of a sample automatically sets the limit of the resolution. Non-destructive methods may be limited as they analyse only the surface of a sample. Radiospectroscopic methods, which are frequently non-destrucitve as well, are limited by the spatial efficiency and resolution of their detector array. Also, the applicability of a method for either bulk or differential boron analysis is restricted by its respective upper and lower limits of quantification.

If boron analysis of a living organism is required, one will tend to choose a non-invasive method in order to not compromise health or physical integrity of the organism. In this case, mostly radioanalytical methods are chosen.

Furthermore, time-resolved analysis may be an issue when regarding samples for dynamic systems. While boron content in water samples is usually not subjected to major fluctuation, this might be completely different in a living organism. For example, sampling time is a key parameter in cell analysis, as the uptake of a boron containing metabolite might be linked to one of the steps in the cellular reproduction cycle. Sampling time can also be decisive, if the boron carrier is metabolised or cleared from the system, e.g., through excretion by the kidneys. In this case, not the originally administered substance, but rather its subsequent metabolic products could be detected.
Moreover, sample throughput of a method can be an issue. If either the method itself or sample preparation for the measurement requires too much time, it might not be chosen for a given task (e.g., because it would not be possible to obtain statistically reliable data within a certain period of time).
Additionally, though from an entirely scientific point of view not always an issue, time and cost efficiency also determine the kind of analysis chosen for a set of samples.

Particularly for biological samples, simply the imaging of the boron, i.e., obtaining qualitative information about the boron distribution can be sufficient for resolving a task. Whilst there are methods which exclusively yield qualitative information, others are applicable for both qualitative and quantitative analysis. Of course, the combination of several methods to reach the desired end-point of an analytical task is an option as well.
Different methods are presented with respect to their possible field of application in the following section (see also Figure 11 at the end of section 1.6.3).

1.6.3 Methods for boron analysis

As sampling and work-up of biological material is an issue in the thesis presented as well, these matters will be briefly addressed together with advantages and drawbacks of different quantitative and qualitative analytical methods to give a short overview of possibilities for boron analysis. On the issue of boron analysis, especially if required for BNCT, several reviews have been published focussing on applicability, boron imaging [149], and the limits of detection and quantification [68, 150, 151]. It is not the intention in this introduction to give a comprehensive overview of analytical methods, but rather a short presentation to explain the most common methods to provide a context of the experimental work carried out for this thesis. The methods most relevant for the thesis will be presented in more detail in chapter 3.

Sample preparation

To analyse a sample, it might be necessary to carry out sample preparation for the respective method chosen for this task. The preparation must be planned carefully as boron is ubiquitous in nature and environment, therefore, the possibilities for boron loss and contamination are manifold and the analysis may be greatly influenced. Every step of sample preparation must be carefully planned with respect to each source of potential boron contamination [152]. Generally, sample preparation serves the purpose to allow or to ease boron analysis in a given sample. This might include extraction or separation of the boron from the sample matrix or the decomposition of the sample matrix. The latter is the case when, e.g., an originally solid sample is to be analysed by a method requiring liquid samples. Possibilities for sample decomposition might require the addition of further substances to assist sample preparation. Among the options frequently chosen are wet open vessel digestion in mineralic acids [153–155] or under basic conditions [156], dry ashing [153], wet ashing [118], fusion [157], combustion in oxygen atmosphere [158], liquid extraction with hot water [159] or nitric acid [160], and microwave digestion [159, 161–164]. Especially for tissue samples, microwave digestion has been found to be more effective and more reliable than other methods [153].

However, all mentioned possibilities for sample preparation have the side effect of altering the original properties of the sample, in which the boron is to be analysed. If the spatial distribution of boron inside tissue is not of principal interest of the analysis of a given sample, a bulk or integral technique will be chosen. More “traditional” methods are titrimetry, ion chromatography [165], spectrophotometry [166], and potentiometry [167], which require time-consuming separation of the boron species from the sample matrix. This may include particularly distillation of borate species or the use of ion exchangers in combination with addition of various substances facilitating the separation. Such techniques can be practical for cases of isotope dilution analysis (IDA) or flow injection analysis (FIA) [168].

Less complex sample preparation is usually required for atomic absorption spectroscopy (AAS), flame atomic absorption spectroscopy (FAAS), or graphite furnace atomic absorption spectroscopy (GFAAS) measurements [169, 170], though these techniques are only of limited efficacy for analysis of biological samples due to boron carbide formation.

From the field of atomic spectroscopy emerged three other methods, which are the most commonly used methods for boron analysis: Direct current plasma and inductively coupled plasma optical emission spectroscopy (DCP-OES and ICP-OES, also-called DCP-AES and ICP-AES) [118, 153, 164, 171–174], and inductively coupled plasma mass spectrometry (ICP-MS) [173, 175–179]. All of these methods combine important characteristics such as the possibility of a high throughput of samples, low quantification limits, and reasonable sample preparation prerequisites. Sample introduction for these methods usually requires liquid samples, which after passing through a nebulizer eventually are injected as aerosols. Samples which are not liquid in the first place, therefore, have to undergo digestion or a comparable process of liquification. Alternatively, injection of solid samples can be achieved after electrothermal vaporisation (ETV) for either of OES or MS (ETV-ICP-OES and ETV-ICP-MS [180]) or, for ICP-MS, by laser ablation (LA-ICP-MS) [181, 182]. LA-ICP-MS is a very versatile method, as it does not require much sample preparation and very few material, it offers furthermore the possibility of either performing bulk analysis, two dimensional surface analysis,

or the analysis up to a certain depth when focussing the laser to one spot, thus searing through the analysed material.
Very common for boron analysis in geological samples is negative or positive thermal ionisation spectroscopy (NTIMS/PTIMS), which is frequently combined with chromatographic methods for boron purification. Furthermore, it is possible to perform isotope specific analysis [183, 184].

Radioanalytical boron analysis

If the analysis of boron containing materials can be carried out at a facility equipped with a high-flux neutron source such as a nuclear reactor or an accelerator, radioanalytical techniques are an option. The most obvious advantage of such techniques over other techniques is that they are non-destructive.
Several of these techniques are based on the on the high probability of ^{10}B for neutron capture reactions, as the isotope has a cross section for thermal neutrons of 3837 barn. The $^{10}B(n,\alpha)^{7}Li$ reaction provides the possibility to detect two different kinds of fission products.
Prompt-gamma activation analysis (PGAA, also PGNAA, PGRA or PGRS) is a form of gamma spectroscopy, which detects gamma rays emitted by short-lived isotopes created by neutron capture. As stated above (see section 1.2), neutron activation of the ^{10}B istotope to $^{11}B^*$ is followed by fragmentation of the latter and by emission of a 478 keV gamma photon in 94 % of neutron capture reactions by the ^{7}Li-nucleus. The spectroscopic recording of the gamma spectrum provides an indirect method to measure the integral boron content in a sample [185, 186]. Another possibility related to this kind of measurement is indirect determination of the boron content by measuring the attenuation of a neutron beam after passing through a given material [187]. Since only the energy of a gamma photon, but not its origin can be determined, PGAA can only be carried out for bulk analysis, unless two-dimensional detector systems are used with the ability to discriminate between the single gamma emitters in a given volume.
Two methods detecting the fragments of the $^{10}B(n,\alpha)^{7}Li$ reaction are neutron activation mass spectrometry (NA-MS) [188] and quantitative neutron capture radiography (QNCR) [189, 190]. In NA-MS the He-nuclei emitted after neutron

capture are detected directly by a mass spectrometer. Measurements may be carried out with very low quantification limits, however, there may be a considerable contribution to the background signal by other isotopes emitting α-particles after neutron capture.

QNCR is a quantitative application of neutron capture radiography (NCR), which is used for the qualitative analysis of materials which emit charged particles upon neutron capture [191, 192]. Contrary to NA-MS, analysis with QNCR is carried out using solid state nuclear track detectors (SSNTDs) enabling the user to spatially analyse the boron concentration in a sample by visualisation of tracks created by the impact of ^{4}He and ^{7}Li onto the STNTD's surface. Closely related to QNCR is spatially selective α-spectrometry, using a different detector system [193].

The possibility of non-invasive analysis of boron in the metabolism of animals or humans after administration can be achieved indirectly by use of suitable isotope marked boron carrier molecules, which can be detected by positron emission tomography (PET) or single photon emission computer tomography (SPECT). Both methods are used for qualitative analysis and quantitative analysis. Especially PET has been established in several BNCT centres as a semiquantitative technique for treatment and dose planning by determination of the uptake coefficient between tumour and tumour-free tissue for each patient individually before irradiation [46, 194]. Either ^{11}C or ^{18}F can be used as tracer isotopes. Whereas ^{11}C would be preferred, as it does not change the chemical properties of the carrier molecule [195], it is not conveniently used due to its short half life. The more commonly used tracer is, therefore, ^{18}F-BPA [22, 196–198]. Also, PET in combination with computed tomography (PET/CT) is a possible application [199]. For the application of SPECT, the use of ^{99m}Tc, ^{123}I, and ^{128}I as tracers was proposed [200], though never thoroughly pursued. A very interesting approach is the use of SPECT for tomographic imaging in BNCT. In first experiments it was possible to depict the neutron capture rate in a model phantom [201].

Boron imaging is a discipline of analysis of almost exclusive importance for BNCT, though in material science, e.g., for analysis of silicon used for production of photovoltaic cells, and environmental science, some application has been noted

[202]. The importance of boron imaging is easily explained by the questions arising in treatment planning. For the different stages of treatment planning, different information is required, therefore, macroscopic and microscopic imaging is an issue to be addressed during analysis. It exist a number of methods which are applicable for these tasks, some of them being suitable only for qualitative analysis, others also for quantitative analysis.

Of the radioanalytical methods presented, neutron capture radiography is frequently used for the determination of the boron distribution in biological samples in combination with histological staining techniques to facilitate the analysis of tissue morphology. With NCR it is possible to analyse larger samples like whole body-sections of small animals [203], but also of tissue slices of small diameters [204]. With some effort and use of particular SSNTDs, it is possible to create radiographic images of very high resolution (high-resolution alpha-track autoradiography (HRQAR)) [205–207].

Qualitative boron analysis and boron imaging

Any quantitative method can also be used to prove the mere presence of boron in a given sample. However, there are possibilities to conduct qualitative analysis which yield much more information than just confirming the presence of boron.

An entirely qualitative technique for cellular imaging is electron energy loss spectroscopy (EELS), which is able to create images of the morphological properties of a tissue sample and of the boron distribution on a cellular scale [104].

As a non invasive technique, nuclear magnetic resonance spectroscopy (NMR), for local analysis, or magnetic resonance imaging (MRI) for boron imaging in either patients or animals, can be chosen [208–210].

A very powerful tool for subcellular boron imaging is secondary ion mass spectrometry (SIMS). SIMS pictures image the boron distribution with a resolution of several nanometres, thus enabling the analyst to assess, whether the boron is found inside the cell nucleus, in the cytoplasm or in extracellular spaces [101, 211, 212]. With the data derived from such analysis, the exact deposition of the fragments of the NCT reaction of the ^{10}B isotope can be further used for

microdosimetric calculations [130]. Images of comparable resolutions may also be gained by sputter initiated resonance ionization microprobe (SIRIMP) or laser atomization resonance ionization microprobe (LARIMP) [213], however both methods are not commonly used in BNCT at the moment, even though it is possible to perform precise quantitative analysis as well.

Quantitative, integral boron determination	
titrimetry	ion chromatography
potentiometry	spectrophotometry
FIA	AAS
FAAS	GFAAS
DCP-OES	DCP-MS
(ETV)-ICP-OES	(ETV)-ICP-MS
NA-MS	NTIMS
PGAA	PTIMS

Qualitative analysis and boron imaging	
PET / PET-CT	SIMS
SPECT	NMR / MRI
NCR	SIRIMP
EELS	LARIMP

Quantitative, spatially selective boron determination	
QNCR / HRQAR (PET)	LA-ICP-MS

Fig. 11: Overview over the analytical techniques for boron analysis introduced in section 1.6

1.7 Statistical data evaluation

In this section, the 'tools' used for statistical data evaluation in chapters 3 and 4 will be briefly presented:

Mean values

Arithmetic mean: $\bar{x}_A = \frac{\sum_{i=1}^{n} x_i}{n}$; for a number of *n* values

Geometric mean: $\bar{x}_G = \sqrt[n]{\prod_{i=1}^{n} x_i}$; for a number of *n* values

Regression analysis

Linear regression of measurement values was carried out via the *least squares method,* by which the coefficients of the best fitting regression curve for a set of data is determined. For two linear parameters, a first order polynomial is chosen as fit function:

$\min_{a_0, a_1}! \sum_{i=1}^{n} r_i^2$, with $r_n = a_0 + a_1 x_n - y_n$

The coefficients a_0 and a_1 are defined as: $a_1 = \frac{\sum_{i=1}^{n} (x_i - \bar{x})(y_i - \bar{y})}{\sum_{i=1}^{n} (x_i - \bar{x})^2}$ and

$a_0 = \bar{y} - a_1 \bar{x}$, with $\bar{x}$ and $\bar{y}$ being the arithmetic means of x and y.

The correlation between two linear datasets for simple linear regression of a model can be predicted by the *coefficient of determination R²*, which in this case ranges form 0 to 1, with 1 indicating full predictability:

$$R^2 = \frac{SS_{xy}{}^2}{SS_{xx} \cdot SS_{yy}} = \frac{\left(\sum_{i=1}^{n}(x_i - \bar{x})(y_i - \bar{y})\right)^2}{\sum_{i=1}^{n}(x_i - \bar{x})^2 \cdot \sum_{i=1}^{n}(y_i - \bar{y})^2}$$, with $\bar{x}$ and $\bar{y}$ being the arithmetic means of x and y.

Standard deviation

In a probability distribution or a set of normally distributed values, the *variance* is used to describe how far the numbers lie from the mean (expected value). The parameter describing how much variation exists from the mean is the *standard deviation σ*, which is defined as the square root of the variance. Obviously, during repeated measurement of a sample low standard deviation is desired.

$$\sigma^2 = \frac{\sum_{i=1}^{n}(x_i - \bar{x})^2}{n}$$, with $\bar{x}$ being the arithmetic means of x.

Uncertainty and propagation of uncertainty

Usually, measurement of a certain parameter depends on more than just one factor. Therefore, for determination of the total uncertainty of a measured value, the different contributing factors must be known. Furthermore, their connection between each other must be assessed, i.e., whether they are independent or influence each other. Uncertainties can either be systematic or arbitrary. Assuming that the analyst works flawlessly, systematic uncertainties are method or instrument specific or, e.g., a pipette or an analytical balance cannot be operated without intrinsic uncertainty. While intrinsic uncertainty of a method can be determined and corrected by control measurements, intrinsic instrumental uncertainties have to be mathematically integrated in data evaluation. Arbitrarily occurring uncertainties can be minimised by repeated measurement, but never be

ruled out completely. Consequently, both kinds of uncertainties have to be considered when determining the total uncertainty via *propagation of uncertainty*. Since they cannot be avoided and are independent from each other, systematic uncertainties are accounted for in *linear propagation of uncertainty* by addition of their respective highest possible uncertainties. The total uncertainty T_L is therefore:

$T_L = |r_a \Delta a| + |r_b \Delta b| + |r_c \Delta c| + ...$, with Δa, Δb, Δc as highest possible uncertainties of the parameters a, b, c… and r as parameter specific factors.

In case uncertainties may counteract each other, total uncertainty is calculated by Gaussian propagation of uncertainty using either total absolute uncertainty of the involved parameters or their standard deviation:

$T_G = \sqrt{(r_a a)^2 + (r_b b)^2 + (r_c c)^2 + ...}$, with a, b, c… as highest possible uncertainties or the standard deviation of the involved parameters and r as parameter specific factors.

Conformity of two values

With respect to their uncertainty, two values can be checked for conformity following a criterion based on Bayes statistics:

$$|x - y| \leq \gamma \cdot \sqrt{u_x^2 + u_y^2}$$

According to Weise et Wöger $\gamma = \sqrt{2}$ is a sufficient constraint [214].

2. Motivation

The potential clinical advantage of BNCT lies in selectively delivering a minimum radiation dose to healthy tissue and a suitable therapeutic dose to cancerous tissue by a controlled, selective uptake of ^{10}B into tumour cells. Dose planning, however, is not an easy task, as a very complex combination of biological and technical parameters has to be considered. The determination of the ^{10}B distribution in targeted cells or tissues is a crucial issue in this context.
Dose planning involves dose modelling from a larger scale down to the microscopic scale. As modern computing allows the simulation and prediction of dose deposition in a very small volume (< 1 μm^3), this offers theoretically the possibility to calculate the exact dose to be delivered in each cellular compartment during therapy. The subcellular boron distribution must be known, to ensure the ionising radiation created in the $^{10}B(n,\alpha)^7Li$ reaction damages crucial cell function and that this radiation is not generated too far away from the respective cellular structures. However, such calculations are still limited by the fact that the boron distribution at the time of irradiation in most tissues is not yet known on a microscopic scale.

Most published data from clinical studies focus on the difference of “tumour” and “healthy” tissue. Usually, a number of samples were retrieved from the tumour site and tissue around the tumour; the morphology was confirmed by histological and patho-morphological analysis and the samples were analysed by a number of analytical methods, mostly with respect to their boron concentration.
However, tumour entities may be very heterogenic in morphology, with metabolically active and inactive cell groups, necrotic areas, or areas rich in desmoplastic stroma cells. In present clinical application of BNCT, these features are responsible for an uncertainty about the resulting spatial distribution of the boron carrier and, thus, make the exact prediction of an effective therapy of tumour malignancies in a targeted tumour entity very difficult. In case there was more emphasis on the morphological or biological relation to the boron distribution, usually great differences in the boron concentrations were found, most prominently where necrotic tissue was analysed. Also tumour free tissue can be very heterogenic, however, there are even less data available in literature addressing

the issue of a correlation between the boron concentration and cellular characteristics.
Therefore, the mere classification of a sample as “tumour” or “healthy” can be misleading, as it does not fully describe the biological environment in which the generated radiation comes into effect. Consequently, the interpretation of the boron concentration found in such samples does not necessarily lead to the correct conclusion.

In addition, in many works, integral analytical methods have been used for boron determination, which are unable to distinguish between different tissue or cell compartments. With the given heterogeneity, such methods can only be used to determine the boron concentration correctly, if prior to boron analysis, the homogeneity of the boron distribution in the samples has been proven.
Also, in most research groups, very different analytical techniques are chosen for boron analysis. Though boron determination in biological samples can be a very complex task, few publications have been issued so far addressing standardisation of boron determination (especially in BNCT) and standardisation of reference materials, which could serve for intercomparison of the methods used by different research groups.

Most clinical BNCT trials in the past have been focused on the treatment of neoplastic diseases of brain, head, and neck, and the skin. Regarding the present structure of the TRIGA research reactor, similar treatments for cancer patients are not possible at the University of Mainz. However, researchers of the University of Pavia, Italy, reported an intriguing concept for extra-corporeal irradiation of auto-transplanted livers, thus enabling application of BNCT for cancer treatment without irradiating the patient inside the reactor facility [131].
Until today, one patient with hepatocellular carcinoma [136] and two patients with colorectal liver metastases have been treated by intra-corporeal BNCT or extra-corporeal BNCT [134, 135]. Though boron analysis in tissue was performed during the trials in Pavia, Italy, scarce clinical data concerning boron uptake in different cell types of the targeted tissue, such as necrotic, fibrotic, or steatotic cells are available so far. Stirred by this pioneering work, several feasibility studies in Germany, the Netherlands, and Argentina were initiated to explore the applicability

of such a procedure in other research centres. Cardoso et al. [126] and Wittig et al. [127] reported the uptake behaviour of BPA in human liver tissue from two clinical studies. Both groups indicated the need for a correlation of histological analyses with the analysis of the boron concentration, as different areas within the same tumour had different uptake behaviour depending on biological tumour characteristics. Their results also indicated that the boron-uptake was dependent on the biological activity of cancerous tissue.

To conduct research on BNCT for liver cancer in Mainz, animal trials were not considered to serve as promising model. Thus, the necessary data had to be obtained from a clinical trial with the involvement of patients. Such a trial [EudraCT number 2006-002796-40] was started in 2008 in collaboration with the Department of Hepatobiliary, Pancreatic and Transplantation Surgery, the Institute of Pathology of the University of Mainz with assistance of the Department of Theoretical and Nuclear Physics of the University of Pavia. As tumour model, patients suffering from colorectal metastases in the liver were chosen, as there were data already available for this malignancy in literature. Patients with colorectal liver metastases served as clinical model, as surgery (hemihepatectomy), is carried out many ways similarly to an autotransplantation.

The enrolled patients received an infusion of *p*-boronophenlyalanine (BPA) over a certain period of time during which blood samples were taken continuously. After that, the liver lobe with the metastases was resected and perfused with preservation solution to simulate the same course of action during transplant surgery. Before and after perfusion, tissue samples from tumour and tumour free liver tissue were retrieved.

The aims of this thesis are closely linked to the realisation of this clinical study:

1. A standard protocol for retrieval and storage of tissue biopsies and blood samples had to be created.

2. For further treatment planning, which would include pharmacokinetic modelling and the determination of the therapeutic boron dose, routine analytical protocols for boron determination in blood and tissue samples had to be created.

3. Homogeneous tissue samples and blood samples were to be analysed by Inductively Coupled Plasma Mass Spectroscopy (ICP-MS) and Prompt Gamma Activation Analysis (PGAA).

4. In tumour tissue, the boron distribution on the smallest scale possible was to be determined and analysed in correlation to morphological tissue characteristics. For spatially selective boron determination. Quantitative Neutron Capture Radiography was chosen, as there had been preliminary works already been carried out on this topic [215].

5. QNCR, ICP-MS, and PGAA were to be compared according to their suitability, precision, and upper and lower limit of detection for boron analysis in both blood and tissue samples. To enable the analyst to perform an intercomparison study, a suitable reference system to verify the results obtained from three methods had to be created.

3. Experimental and Results

In this part, the planning and conduction of all experimental work for this thesis will be laid out in detail. This includes sample retrieval and sample preparation for the measurements. Also, the analytical methods used for boron determination for the results presented in this thesis will be introduced in more detail. A part of what is written down in this section has already been published in peer-reviewed journals [137, 139, 216, 217]. However, compared to the publications, especially the methodical development of the analytical protocols will be looked at more closely.
A more detailed discussion of the clinical implications of the results presented in this chapter can be found in chapter 4.
For a complete list of all publications related to this thesis, please see Appendix A.

3.1 Clinical study on pharmacokinetic behaviour and boron uptake in colorectal liver metastases

As explained in more detail further above (see section 2), the need for additional research on uptake behaviour and pharmacokinetics of BPA for the application of BNCT for liver malignancies was given, as no detailed information about these issues was available in the literature. Furthermore, in case of an irradiation of an explanted organ, perfusion would be necessary. However, there was no information available about how the boron concentration in tumour-free and cancerous liver tissue would be affected by this procedure.
The aforementioned clinical trial (registered under EudraCT number 2006-002796-40: *"Konzentrationsmessungen von Bor-Phenylalanin (BPA) in Leber- und Tumorgewebe bei Patienten mit Lebermetastasen kolorektaler Karzinome"*) was designed in a collaboration with the Department of Hepatobiliary, Pancreatic and Transplantation Surgery, the Institute of Pathology of the University of Mainz with assistance of the Department of Theoretical and Nuclear Physics of the University of Pavia. It started November 2008 with admission of the first patient.
Study protocol, including drug administration, surgical procedures, retrieval of samples, and consecutive scientific work-up of samples, was performed with

permission of the German Federal Institute for Drugs and Medical Devices (Bundesinstitut für Arzneimittel und Medizinprodukte, BfArM) and with permission of the Ethics Commission of the Board of Physicians of the State of Rheinland-Pfalz (*Ethikkomission der Landesärztekammer Rheinland-Pfalz*).

3.1.1 Study protocol for surgery

The protocol includes the following steps: Adult patients undergoing typical hemihepatectomy [218] for CRLM were included in this pilot study, i.e. one liver lobe (Fig. 12) with confirmed metastases was removed by surgical resection. Patients with renal dysfunction and phenylketourenia were excluded. The patients' consent was to be given one week prior to surgery. More details about the patients who participated in the study can be found in Table 4.

Tab. 4: Patient and tumour characteristics and number of samples retrieved in four patients with colorectal liver metastases.

	Patient 1	Patient 2	Patient 3	Patient 4
Age (years) and gender	61 / male	70 / male	69 / female	49 / female
Performed surgery	right hemihepatectomy	right hemihepatectomy	right hemihepatectomy	left hemihepatectomy
Number of metastases	1	1	1	3
Diameter of metastases (cm)	3	10	4.5	3.5 / 3.5 / 2
Grading	G2	G2	G2	G2
Interval between primary and hepatic surgery (months)	64	27	25	16
No. of biopsies used for boron determ-ination (tumour / tumour free	3 / 5	6 / 5	5 / 8	6 / 9

After resection, an ex-situ perfusion using histidine-tryptophan-ketoglutarate (HTK) solution was immediately started in two steps: 2.0 L HTK-solution via the portal

vein and 0.5 L via the hepatic artery were used (Fig. 13 & 14). This protocol was chosen in order to reach a degree of resemblance to the approach required for future clinical use with total hepatectomy, ex-situ BNCT, and re-implantation of the liver after neutron irradiation as performed in Pavia [134, 135].

After perfusion, tissue samples from the tumour and the tumour free areas of the liver specimen were taken for further radiochemical and pathomorphological analysis. The remainder of the specimen was used for dosimetric experiments in the thermal column of the TRIGA Mainz research reactor.

So far, four patients undergoing resective surgery for CRLM were included in study. During surgery, ^{10}B was administered to each patient by an intravenous infusion of 200 mg / kg body weight of a p-borono-phenylalanine–fructose (BPA-f) complex for two hours. The ^{10}B was enriched to 99.9 % and purchased from Hammercap, Sweden. During this time, the hilar structures were isolated, the liver was mobilised and parenchymal transsection was performed using a clamp fracture technique without hilar occlusion. As last step before surgical removal of the liver specimen, 50 ml of heparin were infused via the portal vein to counteract blood-coagulation.

Fig. 12: Liver specimen after resection. The area of the cut is visible on the right

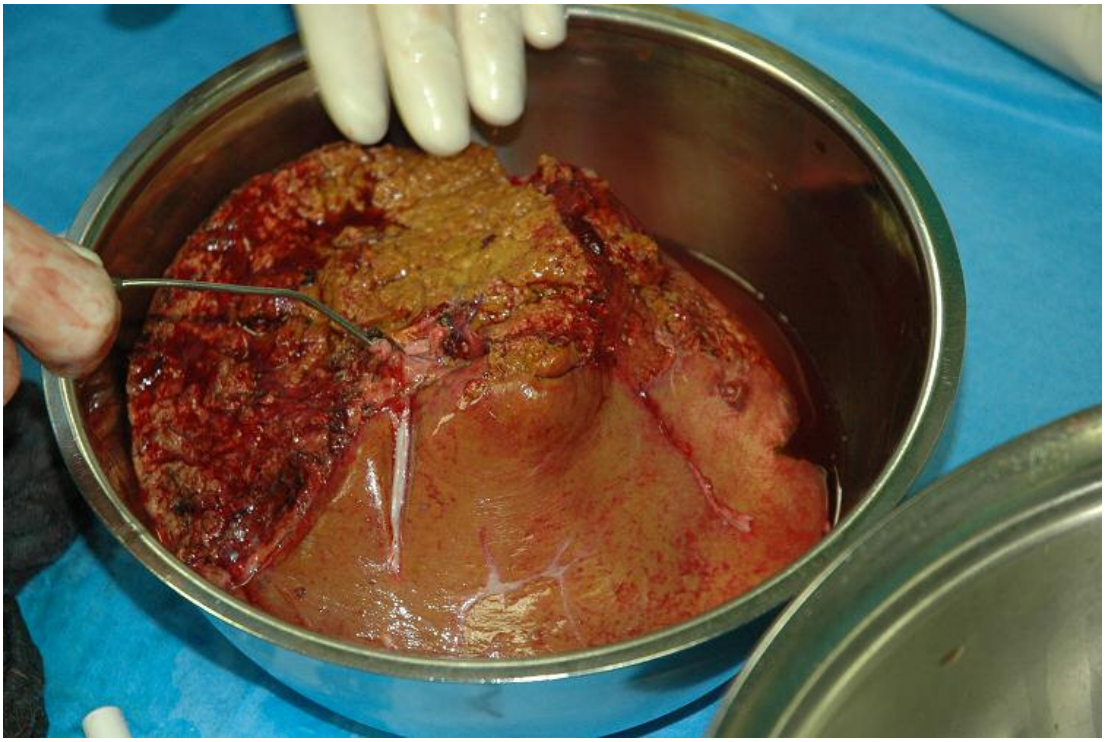

Fig. 13: Perfusion of the liver specimen via the hepatic artery

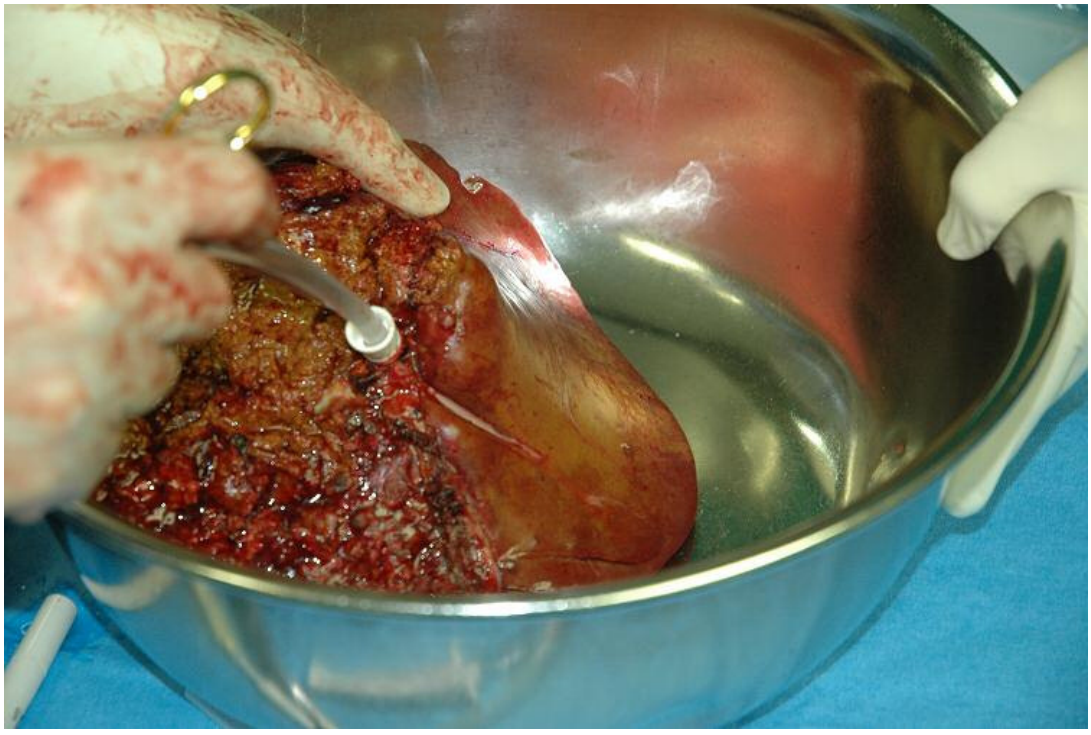

Fig. 14: Perfusion of the liver specimen via the portal vein

3.1.2 Sample retrieval

Samples of metastatic tissue were taken from the surface and at different depths of the metastases to analyse the microscopic two-dimensional ^{10}B distribution in the investigated specimens (Fig. 15). Tumour-free liver tissue samples were obtained similarly from different locations in the liver to permit a macroscopic, three-dimensional analysis of the boron concentration distribution in the whole resected liver specimen (Fig. 16).

The samples were retrieved in the following way: The liver specimen was vertically cut in 4-5 lamellas without separating them completely. This means that they shared a common baseline and could be opened like the pages of a book. This was done in order to preserve the shape of the specimen as intact as possible for subsequent dosimetric experiments, for which the lamellas could be folded back together. The dosimetric experiments were not part of this thesis.

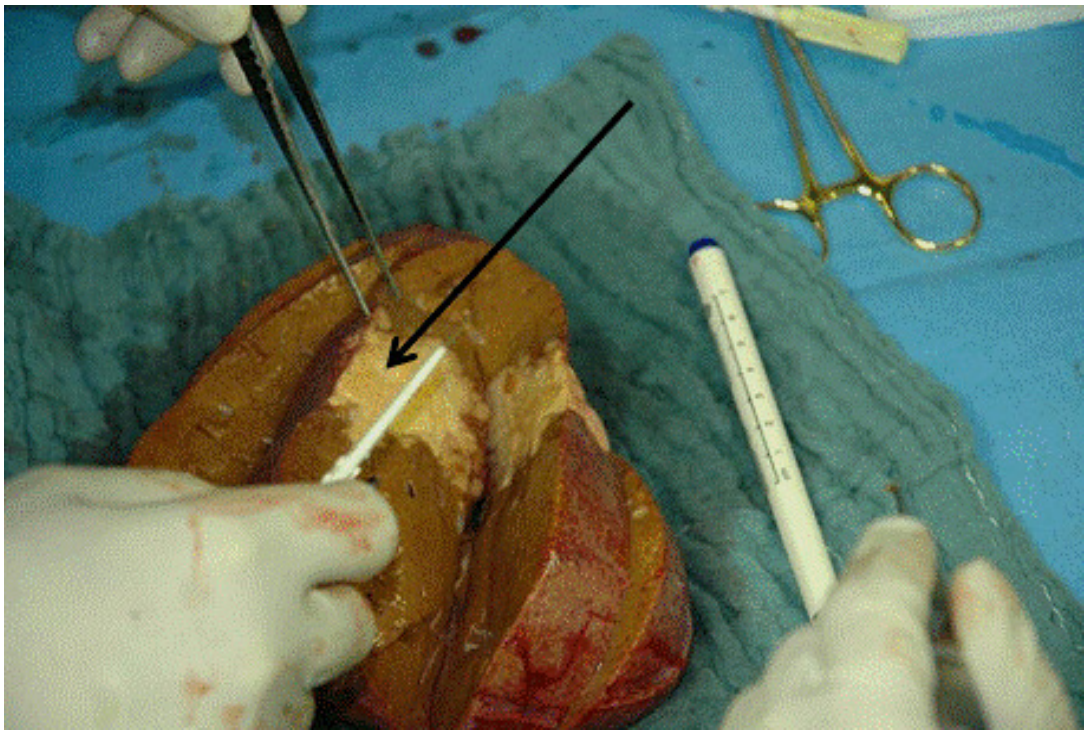

Fig. 15: Retrieval of biopsies from a metastasis. Four of five lamellas are visible in this case. The tumour (dark white) is marked by an arrow

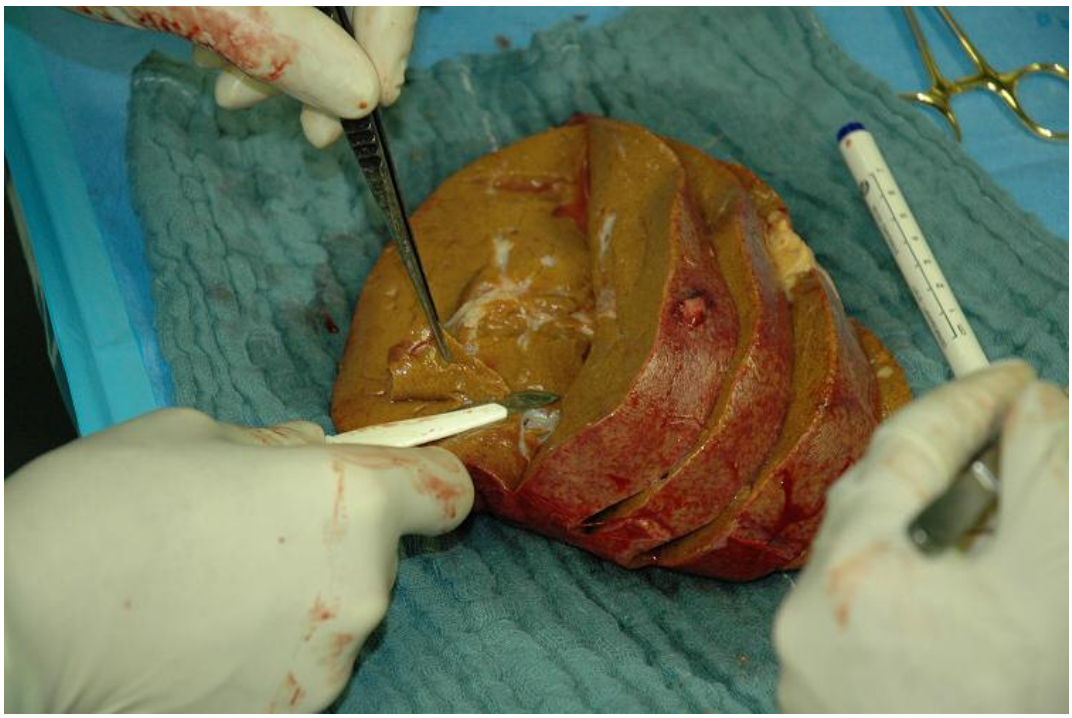

Fig. 16: Retrieval of samples from tumour-free liver tissue. Five of five lamellas are visible in this case.

From each patient, samples of about 1 cm³ each in size were obtained. The number of tumour samples was limited by the dimensions of the lesions (Table 4). One sample of tumour free and tumour tissue each were taken before perfusion with HTK-solution, all other samples were taken immediately after the end of the perfusion. Regarding all patients, no general rule was followed whilst retrieving the biopsies, because the resected specimens were very different in size, shape, and weight. It was therefore tried to take tissue from widely spread positions inside the specimen.

It took five to ten minutes to perfuse the specimen and another five to ten minutes to retrieve the biopsies. Perfusion and sample retrieval were carried out as quickly as possible in order not to allow for any redistribution of the BPA. After retrieval, the samples were transferred in polypropylene (PP) vials and stored in liquid nitrogen until they were transferred to a freezer where they were stored at - 80°C.

Parallely, blood samples were taken after five time intervals for the first three patients and after nine intervals for the fourth patient during surgery. Data evaluation after three patients showed that pharmacokinetic estimations would be more detailed if more detailed time-dependent blood-boron curves were available.

Therefore, it was decided to take blood samples every 15 min instead of every 30 min for all following patients.
The time of the first sample taken in each surgery slightly differed. For the first, second, and the fourth patient, the first sample was taken shortly before the infusion started. For patient 3, it was taken 2 min after the start of infusion. The other four samples were taken every 30 / 15 min during the two-hour surgery, except for patient 2, where the last two samples had to be taken earlier than planned because surgery already finished after 1.5 h.

Each sample was sub-divided into five small cryo-tubes made of polypropylene (Nunc, Roskilde, Denmark), which were stored at - 80°C in a freezer until the moment of sample preparation for boron analysis.
The weight of each blood sample was between 500 and 1500 mg, in total around 8 ml of blood were taken at each time point. No further processing of the blood samples was carried out, and all samples measured were whole-blood samples.

Various experiences made when working with these samples suggest to strictly follow this protocol, as even brief thawing can either alter the boron distribution in tissue (by diffusion) or have the effect that a sample cannot be used any more for production of croysections.

3.2 Quantitative Neutron Capture Radiography

3.2.1 Principles of Quantitative Neutron Capture Radiography for BNCT

As neutral particles, neutrons are detected due to their interaction with atomic nuclei. The consequences of such interaction are defined by the kinetic energy of the neutron and by the nature of the targeted atomic nucleus. An elastic collision can result in: (A) a recoiling atomic nucleus, which is how the neutron was originally detected by Chadwick in 1932 [219], or in a (B) nuclear reaction between neutron and atomic nucleus (also-called neutron capture). The so-formed compound nucleus can now release the excess energy by transferring it into motion, e.g., vibration, by emission of particles or electromagnetic radiation, e.g., γ-rays, or by fragmentation.
Use of the phenomenon “neutron capture” is therefore the physical basis to detect neutrons indirectly by using specific nuclei as beam converter after neutron bombardment or to analyse the content of specific isotopes in solid materials according to their emitted γ-spectra.

A method relying on neutron capture of different isotopes and their detection is neutron capture radiography. Since radiography is an imaging method, solid state nuclear track detectors (SSNTD) are used which enable the analyst to determine the spatial distribution (qualitative analysis) and the quantitative distribution of the isotope looked for. In both cases, the spatial resolution can vary with respect to the SSNTDs in use, sample preparation, work-up et cetera. The SSNTDs are usually polymer films, in which trespassing radiation damages the molecular structure of the film. This can occur with structural changes so large that an image is immediately created. In other cases, the damages (also-called “latent tracks”) have to be deliberately enlarged by chemical etching to obtain a visible image.
A very important feature of SSNTDs is that they do not have equal sensitivities towards ionising radiation, i.e. there SSNTDs have different detection thresholds with respect to the atomic number (Z). Therefore, the analyst may choose a suitable SSNTD for the detection of each targeted isotope. In nuclear sciences, most SSNTDs are used for the detection of charged particle radiation, but also for neutrons and gamma rays (radiography for diagnostic reasons). This was of

significant importance for cluster radioactivity research, where SSNTDs are used to detect emitted ^{14}C without registering lighter fragments, e.g., α-particles [220].
The recording of charged particles produced as fragments after neutron capture is called *indirect* neutron radiography, whereas the recording of the neutrons themselves is called *direct* neutron radiography.

In BNCT, the beam converters are the ^{10}B isotopes. The reaction, during which the detectable particles are generated is therefore the same neutron capture reaction, which is used for therapeutic purpose ($^{10}B(n,\alpha)^{7}Li$). If also other neutron capture reactions in tissue (for those with the largest contribution see section 1.5.2) are considered, the detectable solid fragments are, for the major part, α-particles, ^{7}Li-nuclei and protons.
Though protons are not exclusively generated during the $^{14}N(n,p)^{14}C$ and $^{1}H(n,n')^{1}H$ reaction, these protons are by far the largest share due to the combination of natural abundance in tissue and their cross sections for incoming neutrons of different energies. Also neutrons themselves and γ-rays generated in the sample or emitted by the neutron source itself could be detected. To exclude the latter, in BNCT only SSNTDs are used, which are sensitive only towards charged particles. Such films often require subsequent work-up, as holes produced after neutron bombardment and fragmentation of the targeted nuclei are too small to be seen with the naked eye or a microscope. The enlargement of these latent tracks can be achieved by chemical etching, usually performed under basic conditions, often including heating of the etching solution. After that, number and size of the resulting tracks determine the spatial resolution and, hence, the efficacy of a radiographic method.

The protocol for neutron capture radiography in BNCT usually includes fixation of a piece of tissue on a SSNTD film, as the major objective of radiographic analysis is to image the boron distribution, therefore, any space left (or any “obstacle”) between detector and sample would lead to a distorted picture. This is followed by irradiation of the film in a neutron beam or neutron field, etching of the film, and evaluation of the result. As the films can be theoretically cut to any size and shape, the irradiation of very small tissue slices or of entire animal sections is possible, if there are microtomes available, which facilitate the cutting of samples.

As it is a non-destructive, both quantitatively and qualitatively applicable method, neutron capture radiography was considered and used very early for tissue analysis in BNCT [221, 222]. If stored appropriately, analysis of the same sample can be carried out repeatedly, enabling the analyst to ensure the quality of the measurements.

Analysis of liquids is theoretically possible, however difficult to achieve in the laboratory. While solid samples keep their shape, thickness, and position during irradiation, liquids have to be prepared with considerable efforts [223], if mere immersion of the SSNTD film is not desired. Though feasible, radiography has been seldom used for boron determination in, e.g., blood samples. Until today, most applications of neutron capture radiography have been carried out for imaging of boron distributions in smaller tissue sections and whole body sections of small animals [191, 203, 224–226] and less frequent for quantitative analysis. Also, different approaches for quantitative analysis using neutron capture radiography were developed over the years [189, 190, 206, 227, 228], though there is no “standardised” method, neither for irradiation and etching, nor for image evaluation.

All radiographic images for the work presented were produced using a polyallyl-diglycol-carbonate film purchased from TASTRAK (Track Analysis Systems Ltd., Bristol, United Kingdom) (Fig. 17). TASTRAK films are sensitive only towards irradiation of charged particle energies and fast neutrons.

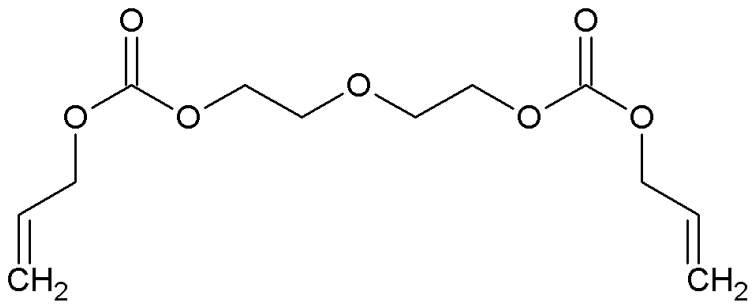

Fig. 17: The polyallyl-diglycol-carbonate monomer

3.2.2 Neutron sources for Neutron Capture Radiography

For neutron capture radiography, of course, a suitable neutron source has to be provided. These can be smaller, not necessarily stationary sources, relying on spontaneous fission of atomic nuclei, e.g., a ^{252}Cf-neutron source, on the emission of neutrons after nuclear reaction of α-particles with surrounding nuclei, e.g., in an Am-Be source, or relying on high-energy gamma photons, which can cause ejection of neutrons from a nucleus, if the latter is irradiated with gamma rays exceeding the binding energy of the targeted nucleus.
Such neutron sources commonly produce neutron fluxes between 10^4 – 10^8 n / cm² · s. For experiments requiring higher neutron fluxes, as it was the case for the work described in this thesis, the use of accelerator facilities or reactor facilities has to be considered. In BNCT, mostly reactor facilities are used for clinical research and therapy, as they often provide better irradiation fields, which is due to their initial construction design. Accelerator facilities have been modified, too, or are currently being modified for both clinical research and therapeutic application [229, 230].
Since the neutron capture reaction depends on the neutron energy, a source has to produce not only a sufficient flux, the neutrons may have to be moderated to generate a sufficiently thermal neutron spectrum.

The neutron source for all radiographic analyses presented in this thesis was the TRIGA Mark II research reactor of the University of Mainz. In Figures 18 and 19, a horizontal and vertical cut through the whole TRIGA Mainz can be seen. The reactor is a swimming pool reactor with a maximum thermal neutron flux of $1.6 \cdot 10^{12}$ n / cm² · s at the maximum power of 100 kW_{th} (steady state operation). The core comprises of 75 fuel elements containing 20% enriched U-235, encased in either aluminium or steel. The uranium is bound as uranium-zirconium-hydride, which is a combination of uranium hydride and zirconium(II)hydride. The fuel is characterised by its prompt negative thermal coefficient of reactivity, which makes it possible to operate the reactor as well in pulsed mode. This is achieved by a hydraulic system that ejects one of the control rods from the reactor core, the power of the reactor then rises to a maximum of 250 MW_{th} for about 30 ms, after which neutron production ceases completely.

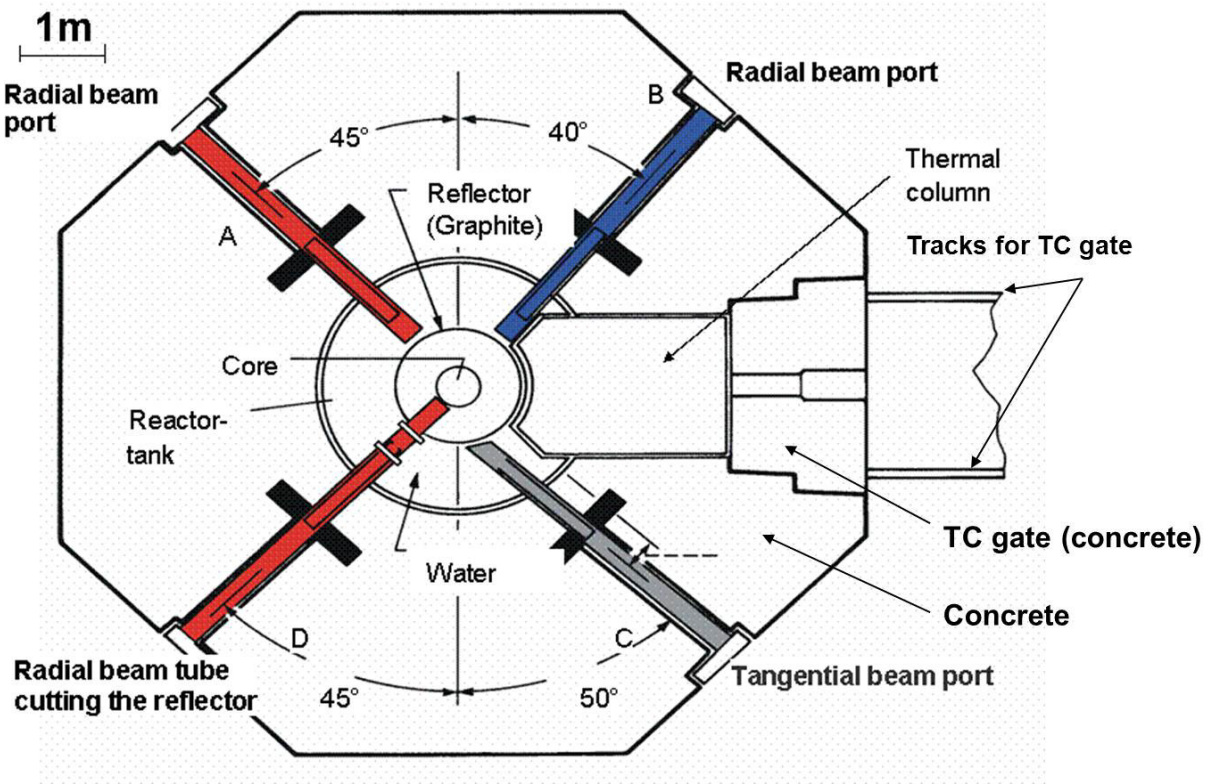

Fig. 18: Horizontal cut through the TRIGA Mainz research reactor

For irradiations the TRIGA Mainz offers four horizontal beam tubes, one central vertical irradiation tube, three pneumatic transfer systems (with sample transport times < 1s), a carousel for up to 40 samples and a thermal column. The thermal column is made of graphite blocks, which can be extracted individually to provide different irradiation channels for samples of different sizes.

For all irradiation radiographic experiments, a channel in the so-called thermal column was used (for more details see Fig. 20).

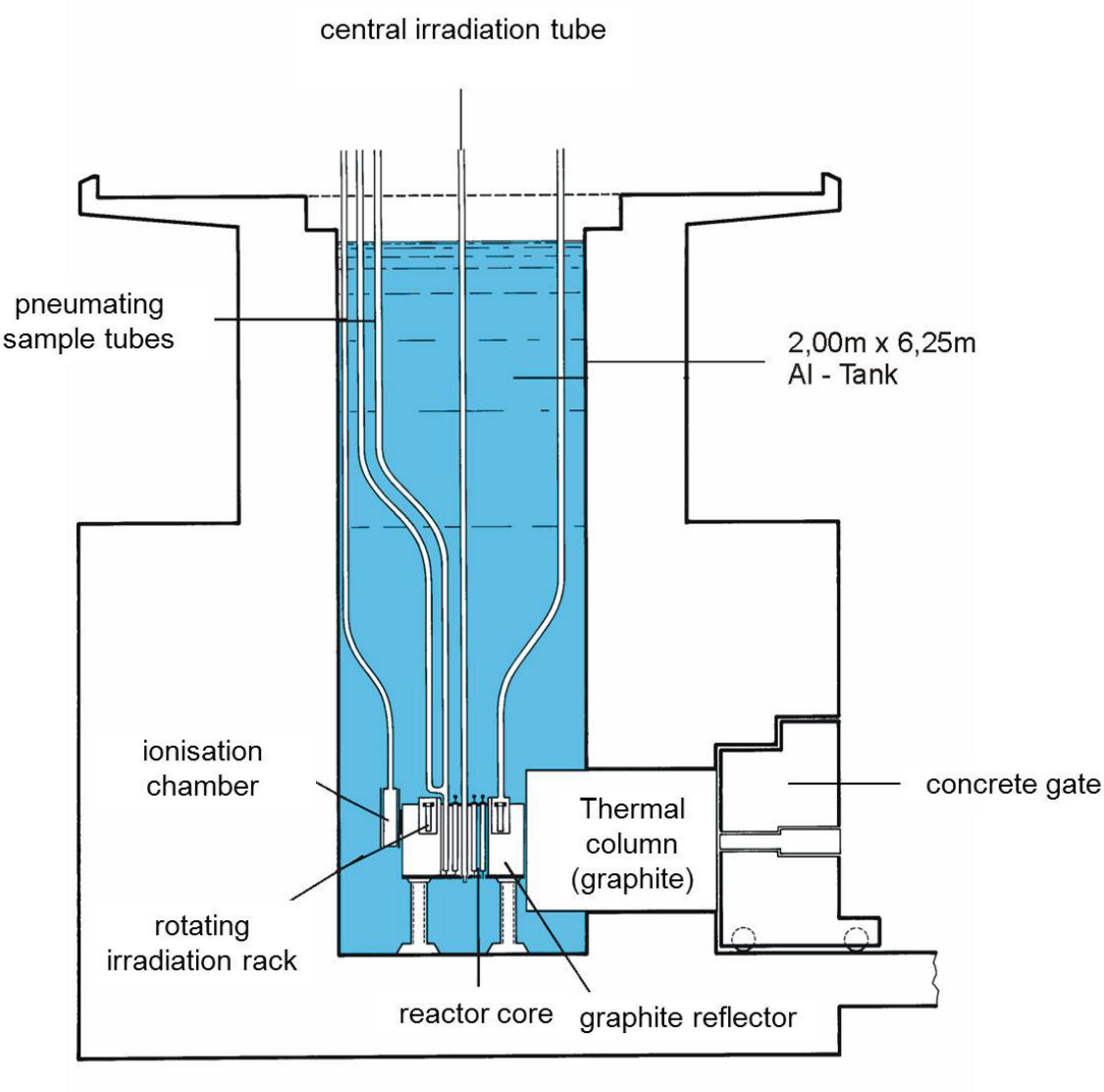

Fig. 19: Vertical cut through the TRIGA Mainz research reactor

3.2.3 Characterisation of the irradiation field of the TRIGA Mainz reactor

Irradiation positions in the thermal column

The correct imaging of the boron content is only possible, if the neutron field used for irradiation is homogeneous for the whole area of the irradiated sample and the exact thermal neutron flux is known. Samples irradiated anywhere *inside* the thermal column will be irradiated by an isotropic field and not by a neutron beam, which is maybe the case in other facilities, though the majority of the neutrons will still hit SSNT films coming straight from of the reactor core.

For the work presented in this thesis, it was made sure that the variation of the neutron flux inside the irradiation channel of the thermal column of the TRIGA Mainz was indeed very low. In Figure 20, the irradiation channels in the thermal column are shown.

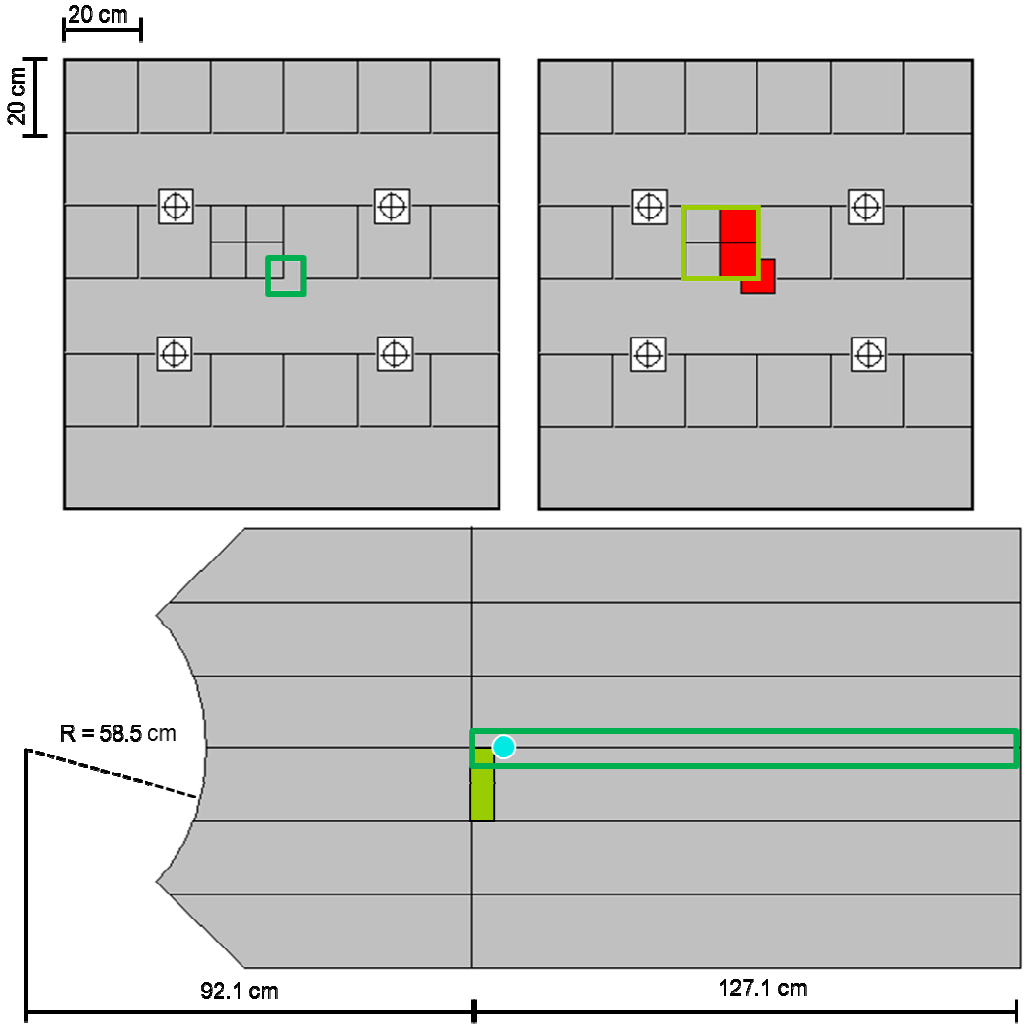

Fig. 20: Back view (upper left and right) of the thermal column and top view of the thermal column (below). The irradiation channel is marked in green (upper left and below), the irradiation position is marked by a light-blue spot (below). The distances in the top view image are measured from the centre of the reactor core. The graphite bars which have to be extracted to enable radiography are marked in red (upper right). The bismuth shield is marked leaf-green.

For the experiments, an irradiation channel (marked in green) of 10 x 10 cm² is created by extraction of some of the graphite bars (shown in red (upper right)). The thermal column is also used for irradiations during *in vivo* and *in vitro* studies, which are not part of this thesis; for such irradiations a larger channel is needed.

For this purpose, the red marked three graphite bars and the two adjacent 10 x 10 cm² bars in Figure 20 are extracted as well to create a 20 x 20 cm² channel for irradiation.
For reasons of radiation protection during *in vivo* and *in vitro* experiments, a bismuth shield (20 x 20 x 8 cm³) was inserted at the end of the channel, which was closer to the reactor core (also-called “hot end”; consequently the end further away from the reactor core is called “cold end”). As a result, one corner of this shield looms into the central irradiation channel used for neutron radiography.

Characterisation of the thermal neutron field at two possible irradiation positions

After extraction of the graphite bars to create the central channel, there is no longer a homogeneous environment for the neutrons passing through the thermal column, as their moderation is different in air, bismuth, and graphite. Any graphite block removed or material inserted into the thermal column (like the bismuth shield) will additionally modify the known energy spectrum [231, 232] of the neutrons at the irradiation position.

The thermal column had already been used for radiographic experiments [215], however, due to reconstruction, the irradiation channel and the different graphite bars, which had to be extracted for the introduction of samples, working conditions had changed for the works presented in this thesis. As mentioned further above, when performing quantitative neutron capture radiography, the neutron flux must be constant for the whole area of the irradiated sample. To ensure this, the homogeneity of the neutron flux had to be characterised for the irradiation position. This was done experimentally and confirmed by particle transport simulations.

Experimental characterisation of the neutron field

The experimental characterisation was carried out indirectly via the $^{197}Au(n,\gamma)^{198}Au$ reaction using a Ge-semiconductor detector for the recording of the gamma spectrum. The evaluation software used was Genie2000 (Canberra Eurisystems /

Areva, France). For efficiency calibration, a multi-isotope standard was used (QCY48, UKAS calibration, Amersham, United Kingdom). The gold-foil measurements were carried out using a specially made phantom, which was inserted into the irradiation channel of the thermal column. The same phantom was used for all radiographic measurements. It is made of PTFE and consists of a rod with a quadratic pan at one end (Fig. 21).

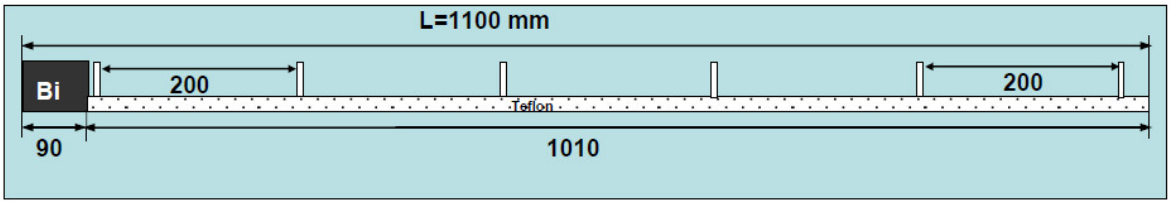

Fig. 21: Schematic design of the phantom for radiography. The pan with the bismuth blocks is on the left side

Small bismuth blocks are placed into the pan to lower the gamma background for radiation protection of the analyst inserting and extracting the phantom from the thermal column (Fig. 22), as the bismuth shield already built into the thermal column does not cover the total area of the channel. Between the bismuth blocks, cavities are left to insert up to eight SSNTD detectors for irradiation. The whole phantom was left in the thermal column during the experiments.

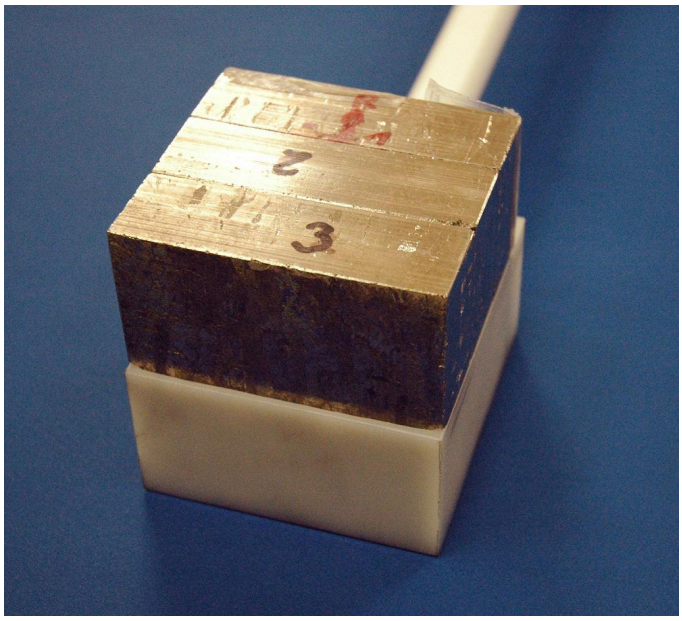

Fig. 22: Image of the sample holder of the irradiation phantom with blocks of bismuth inserted

The homogeneity of the neutron flux for the irradiation position of the SSNTDs for radiography was confirmed by irradiation of two SSNTD films (508 x 676 mm² each) equipped with 16 and 20 gold foils of 5 x 5 mm², respectively. One was irradiated at the spot where irradiation for radiography originally was to take place, the other one was irradiated at a spot considered being an alternative in case the originally location aimed for would be unsuitable due to two-dimensional heterogeneity of the flux. The alternative spot considered was the hot end of the channel created by extraction of the topmost graphite bar (marked red in Fig. 20).

The gold foils on the films were distributed in a way that the area of the respective channels was representatively covered. The flux measured with each gold foil was determined using the following equation (Eq. 3):

Eq. 3: $$\Phi_n = \frac{A_0}{N \cdot \sigma_{th} \cdot \left[1 - \exp(-\lambda \cdot T_B)\right]};\ N = \frac{m \cdot N_A}{M_{Au}}$$

Φ_n = neutron flux; A_0 = starting activity in becquerel (Bq); N = number of gold atoms; σ_{th} = cross-section for thermal neutrons of the targeted isotope in barn (1 / 10^{-24} cm²); λ = decay constant (1 / t); T_B = time of irradiation; M_{Au} = molar mass of gold; m = mass; N_A = Avogadro constant

The irradiations took place at a reactor power of 1 kW for 15 min. The results are shown in Fig. 23 and 24. The mean flux ($3.44 \cdot 10^5$ n / cm²·s per W) of the central channel is higher than in the alternative channel ($2.24 \cdot 10^5$ n / cm²·s per W). This is because the channel is closer (on the vertical axis) to the reactor core.
One measurement in the central irradiation channel (topmost peak on the right in Figure 24) yielded a surprisingly low result of only $1.967 \cdot 10^5$ n / cm²·s, however it remains unclear, why only at this point a considerably deviation from the other values was found. For further considerations, this value was excluded. Apart from that, in both positions, a homogeneous neutron flux was measured. The standard deviation of the flux for the central and the alternative irradiation channel is 2.64 % and 2.18 %, respectively.

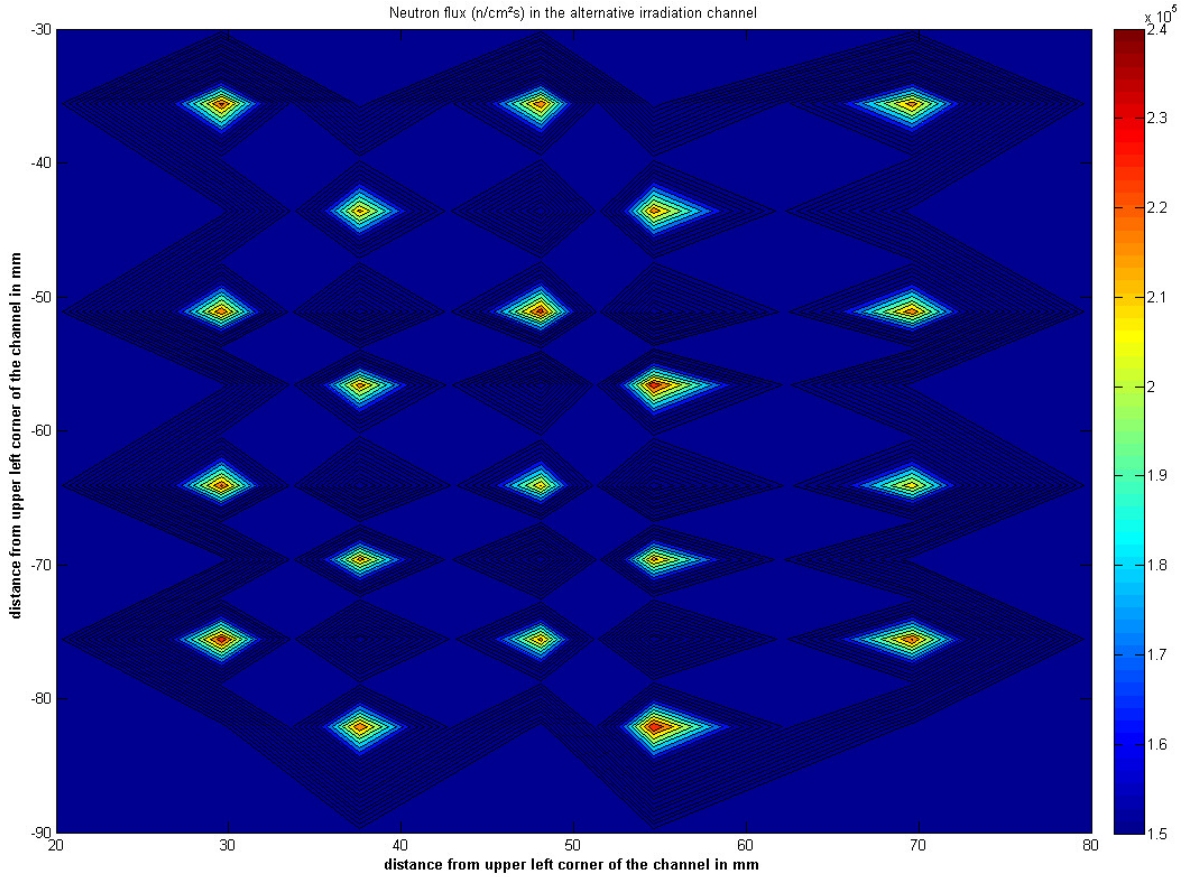

Fig. 23: Two-dimensional plot of the neutron flux distribution at the hot end of the alternative irradiation channel. Each peak represents one gold foil measurement. The tip of the peak accounts for the whole gold foil

Characterisation of the neutron field by FLUKA simulations

For both positions, the homogeneity of the neutron flux was also assessed by FLUKA simulations, a multipurpose Monte Carlo transport code [233]. The calculations were kindly carried out by [redacted] at the Institute for Nuclear Chemistry in Mainz. For the calculations, only a part of the thermal column and not the reactor as a whole was simulated. As neutron source, a source plane, located 75 cm versus the cold end of the thermal column from the reactor core was chosen. The same source plane used other findings related to the BNCT project in Mainz [137, 139, 232, 234]. In Figure 25, a graphic representation of the neutron flux is shown for the whole thermal column (top view), in Figures 26 and 27, a graphic representation of the two-dimensional flux distribution at both positions examined experimentally.

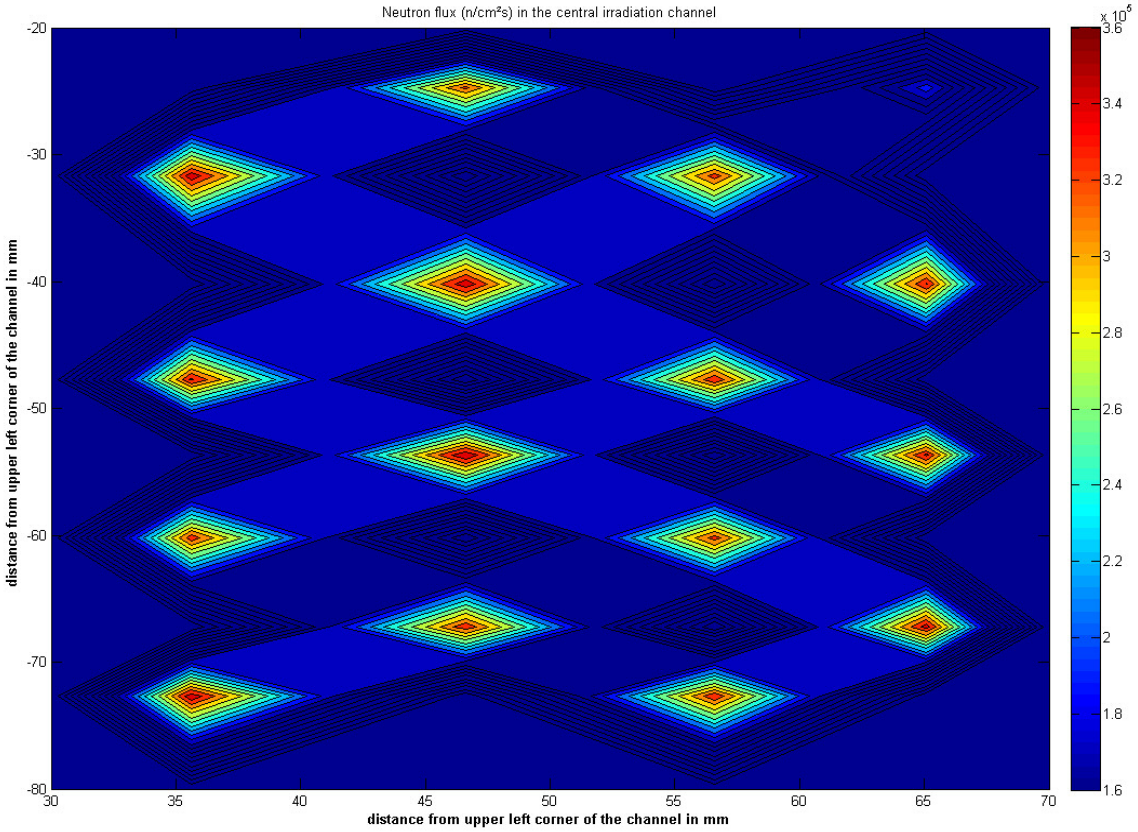

Fig. 24: Two-dimensional plot of the neutron flux distribution at the hot end of the central irradiation channel. Each peak represents one gold foil measurement The tip of the peak accounts for the whole gold foil

In both figures the fraction of particles (in this case: neutrons) which pass trough the simulated volume elements at the given position are shown, however the energy of the neutrons in the respective volume elements is not calculated. It can be seen that in both cases, a uniform amount of neutrons passes through the area of the simulated SSNTD plate. This is in accordance with the experimental results presented in Figures 23 and 24.

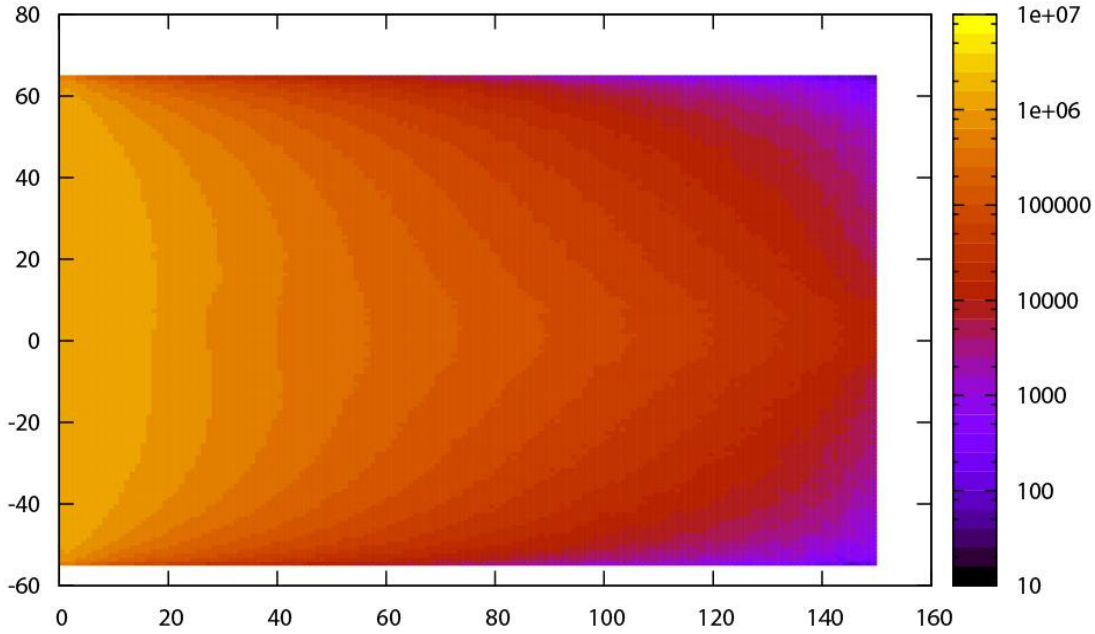

Fig. 25: FLUKA simulation of the two-dimensional neutron flux distribution (n/cm²s per W) in the whole thermal column, top view. Dimensions are given in cm.

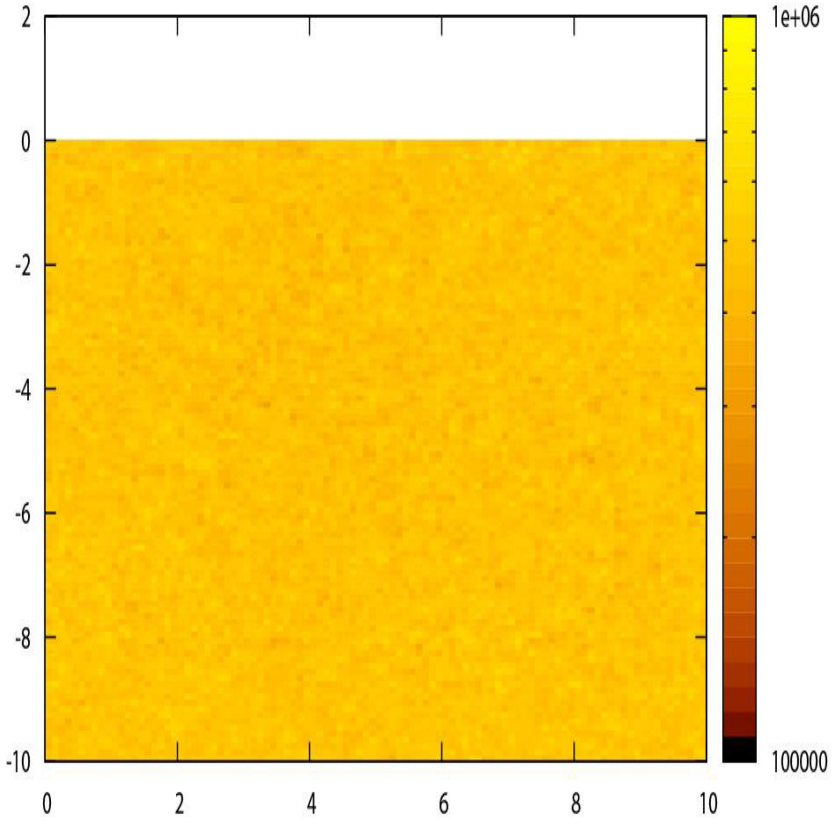

Fig. 26: FLUKA simulation of the two-dimensional neutron flux distribution at the cold end of the alternative irradiation channel (n/cm²s per W). All dimensions are given in cm. The position 0 cm / 0 cm is the upper left corner of the channel.

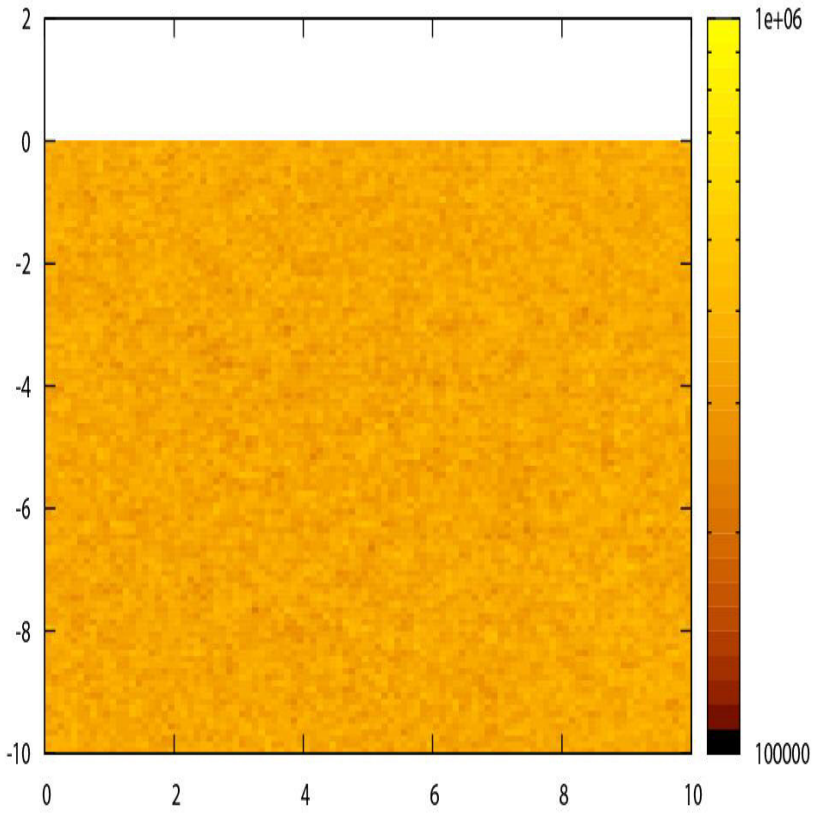

Fig. 27: FLUKA simulation of the two-dimensional neutron flux distribution (n/cm²s per W) at the cold end of the central irradiation channel. All dimensions are given in cm. The position 0 cm / 0 cm is the upper left corner of the channel.

As a result, the central channel was chosen for all irradiations concerning radiographic analysis, because the neutron flux was higher than in the upper irradiation channel considered as alternative, the quality of the position, i.e., the homogeneity of the two-dimensional distribution of the neutron flux, was deemed equally adequate.

3.2.4 Development of radiographic images

After irradiation, on most SSNTD films no changes can be observed, the films have to be developed (very much as a photographic image). Development of the radiographic images is achieved by chemical etching.
In this context, the etching process is a targeted damaging of the structure of the polymer film's surface. On a smooth, uniform surface of a homogeneous, solid material, during etching the damage is inflicted in layers, which means there is a constant abrasion of the material. This changes, if the surface of a material is not entirely smooth. A SSNTD irradiated with either charged particles or uncharged particles with higher energies receives considerable damage on its surface, which creates a situation for the etching process that now there is not a smooth surface. Therefore, abrasion of the material will now create a very heterogeneous surface, as the etching at sites, which have been damaged by irradiation, are made visible because there the etching speed is higher. This process, i.e., the production of visible tracks from latent tracks, is called track-etch radiography.

Etching dynamics

Since many parameters can influence the etching (material properties of the etched detector, choice of the etchant, temperature, etching time and ionisation damage of the etched material (= choice of the projectile)), several different mathematical approaches have been developed to describe the creation of the tracks during etching for both growth speed and shape [235–237].
The most important conclusion drawn from experimental observations and from all theoretical approaches is that the irradiation of a SSNTD with particles of different ionisation potentials inevitably leads to the formation of distinct tracks (Fig. 28). Ideally, a track "grows" in width and depth to the shape of a cone along the ionisation path of the particle created by the latent track. If extensive etching is carried out, the shape of the tracks change from conical to cylindrical with a round bottom (Fig. 28 and 29). Thus, the characteristic "pores" are created, which are visible in many radiographic images.

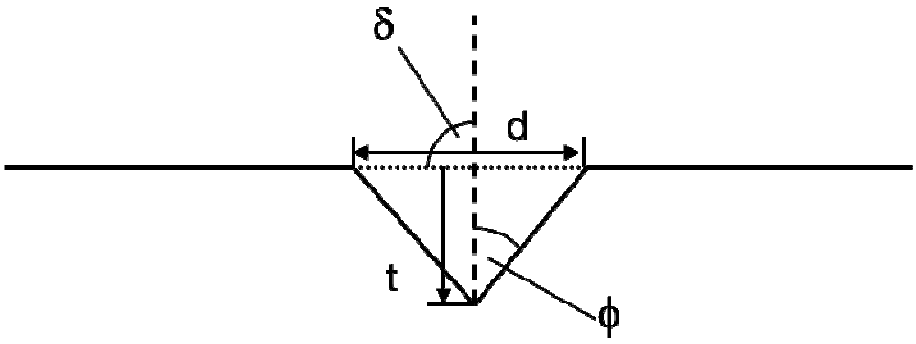

Fig. 28: Track growth after particle impact on a SSNTD. The width of a track is denoted by d, its depth by t; the impact angle of the particle is denoted as δ and the opening angle of the track as ϕ. For tracks produced after neutron impact with $\delta \neq 90°$, ϕ is the opening angle to one side, with its counterpart $\phi*$ for the other side

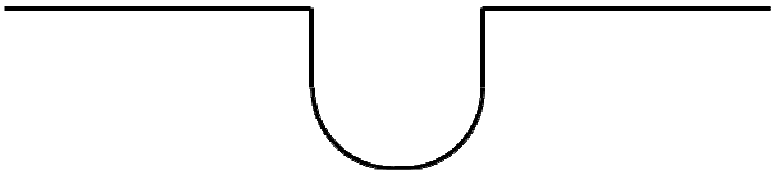

Fig. 29: Track shape after extensive etching ("over-etching")

The tracks illustrated in Figure 28 and 29 are the result of latent track production after perpendicular particle impact ($\delta = 90°$; $\phi = \phi*$). For all other angles, the growth behaviour (under the same etching conditions) leads to tracks of different geometrical shapes and different growth behaviours. Also in this case, the track grows initially pointedly downwards and then wide up to create an elliptically shaped track. A simulation of how track growth in this case proceeds is shown in Figure 30. Experimental examples for both cases tracks created after particle impact of $\delta = 90°$ and $\delta \neq 90°$ are given in Figure 31.

For equal etching conditions, track diameters and depths depend on the energy of the particles which produced the corresponding latent tracks. Particles with higher kinetic energy create tracks with small aperture angels (ϕ), i.e., small diameters but greater depths. The diameter will grow, if heavier and/or higher charged particles are chosen for detection.

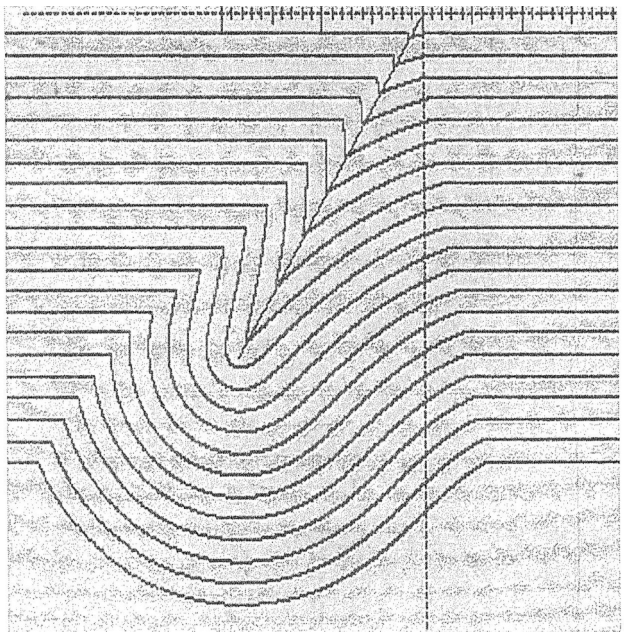

Fig. 30: Simulated track growth after extensive etching and for a neutron impact with $\delta \neq 90°$ (Image taken from [238])

Track shapes

Equally, heavy and higher charged particles will create flat tracks with greater diameters (For an example see Figure 31): The tracks created by protons (bottom left and right) have much smaller diameters than the alpha tracks in the image (arrows). This way, tracks can reveal their “origin”, if enough information about the etching parameters is available. Higher track densities therefore correspond to tissue regions with higher concentration of the isotopes which initially produced the charged particles responsible for the tracks.

For application of neutron radiography to analyse the boron content in tissue samples, tracks are almost exclusively produced by protons, ^{4}He- and ^{7}Li nuclei.

Though the image for analysis is created by chemical etching, the actual evaluation of the data especially for quantitative analysis has to take place using a microscope and special imaging software.

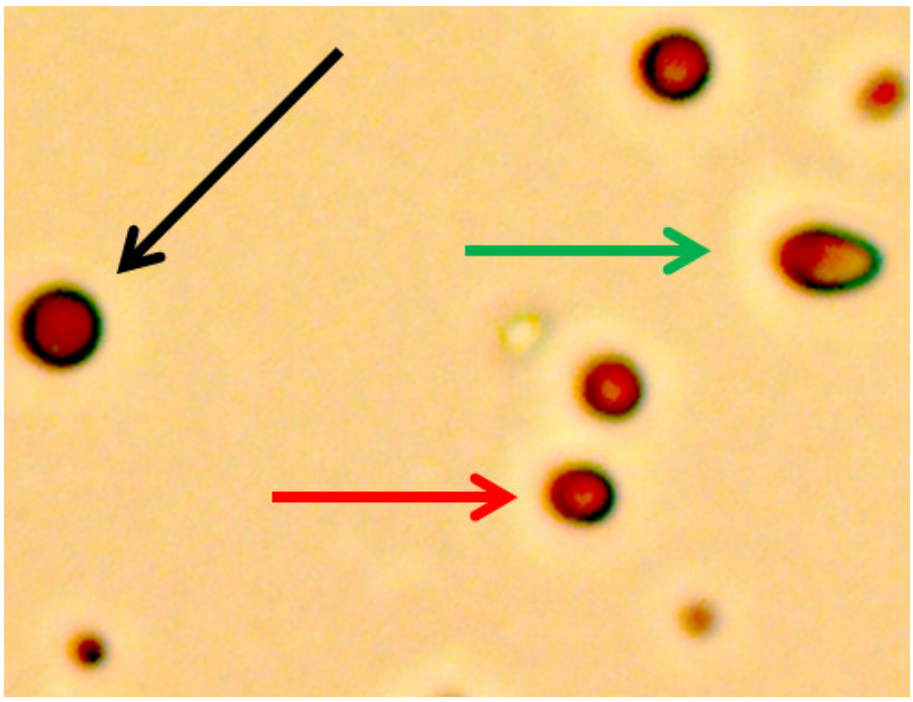

Fig. 31: Alpha- and proton tracks of a radiographic image after etching and image processing. The arrows all point to alpha tracks: there are examples given for track growth for $\delta = 90°$ (black) and $\delta \neq 90°$ (red and green; with δ(green) > δ(red)). The image is scaled 48 x 36 µm²

3.2.5 Suitable standard reference materials for QNCR

Properties of reference materials

For quantitative analysis, standard reference materials are required that mimic or match the characteristics of the sample matrix. When using a standard reference material, several characteristics have to be considered:

- The standard must produce charged particles creating tracks (after etching) that are suitable for corresponding sample calibration. For boron analysis, this would be α-particles and/or ^{7}Li-nuclei.

- The charged particles must have the same energy when hitting the surface of the SSNTD like the particles emitted during BNCT to produce equivalent tracks. This can be particularly difficult to determine, because particle energy

is diminished by absorption in the material in which the particles are generated before being “released” onto the film.

- It must be known, if there are other particles emitted, which would also create latent tracks on the SSNTD. If this is the case, a way must be found to deal with them for calibration.

An example is the standard reference sample used by the BNCT group in Pavia, Italy, which is a sample where a specific number of ^{10}B were implanted in a silicon support [132]. However, this is a standard reference sample used for α-spectrometry.

The choosing of a standard reference material was lead by prior experiences in image analysis, most notably with the problem of discrimination between tracks of similar geometry, but which were of different origin. Also, the change in particle energy by absorption in the material of origin was visible when analysing features of tracks produced in radiographic images (see section 3.2.7). This issue can be assessed by simulating the particle-matter interactions, if appropriate models and transport codes are used. This is a practical solution if samples of lower complexity have to be analysed, e.g., the boron content in a lead-shield used for radiation protection in reactor facilities. The radiographic analysis of boron in tissue samples is more complex, as tissue is characterised by its elemental and structural heterogeneity and therefore a series of different particles are emitted upon neutron irradiation. Furthermore, moderation can vary due to unequal content of water in different tissues. As a result, the material, in which the boron would be present has to be tissue equivalent.

In tissue, there are effectively two sets of signals emitted upon neutron capture of boron: the fragments of the ^{10}B capture reaction (the ^{4}He and ^{7}Li nuclei) and the particles producing a certain underground signal (those emitted due to other neutron capture reactions in tissue, e.g.,$^{14}N(n,p)^{14}C$, and fast neutrons coming from the reactor core. By choosing a suitable neutron source (= high and homogeneous flux, mostly thermal neutron spectrum), SSNTDs, etching parameters, and an appropriate type of image analysis, the desired signal can be isolated and evaluated.

Since the neutron source chosen for the radiographies produced for the work presented was the TRIGA research reactor, the possibility to irradiate samples in

the thermal column was given, where neutrons of a very favourable energy spectrum and flux can be used for experiments (see section 3.2.3). Due to the very small share of fast neutrons in the neutron spectrum [231], the particles taken into consideration for track generation are the charged particles named above.

Production of calibration standards for QNCR

As aforementioned, TASTRAK films are generally sensitive to charged particles, therefore all protons are recorded as well. Special attention was paid to the background problem of the radiographic images by using tissue equivalent standard reference materials. A first attempt was to use boric acid in membrane filters. The filters were drenched in boric acid with a filter syringe. The homogeneity of the boron distribution was assessed qualitatively by irradiation of the filters on TASTRAK films. However, the distribution within membrane filters of different thicknesses and pore sizes was never homogeneous enough to serve as unquestionable standard reference material, which is why this approach was abandoned.

A successful approach to cope with the problem of the boron homogeneity and tissue equivalency was eventually the production of standard reference samples with the kind assistance of [redacted] at the University of Bremen, Germany. The single steps of the production of the standard reference samples are illustrated in Figure 32.

A slurry of thoroughly homogenised chicken liver with boric acid (High Purity Standards, Charleston, SC, USA) as boron compound with concentrations of 0.1, 0.2, 0.5, 1, 2, 5, 10, 20, 50, 100, and 200 ppm ^{10}B was used as reference material. As support, carboxymethylcellulose solution produced from carboxymethylcellulose sodium salt with water was frozen by immersion in liquid nitrogen in a specially tailored, open box to form a solid, rectangular block. While the walls of the box were designed as flexible frame, which could be removed and attached independently, the bottom of the box was designed to serve also as holder of the block for the cutting with the microtome. This way, the carboxymethylcellulose did not have to be removed from its support for the cutting,

which decreased the risk of damaging or breaking the relatively brittle frozen cellulose.

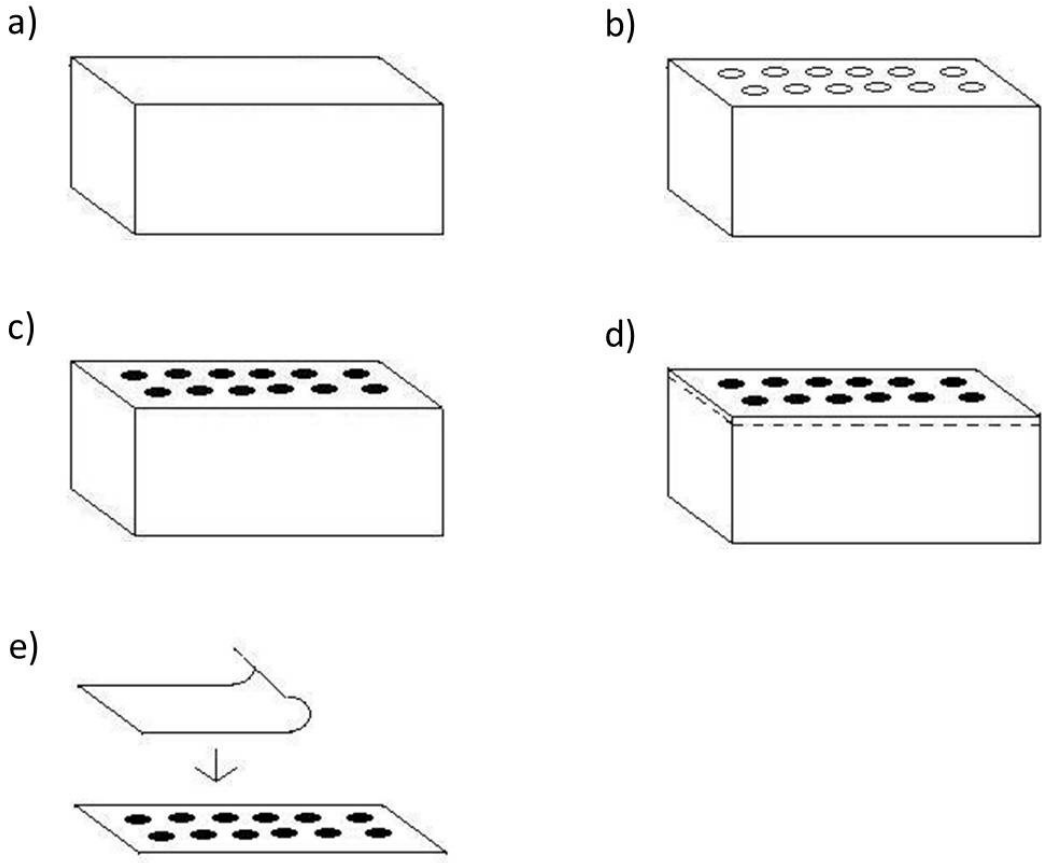

Fig. 32: Schematic overview of the standard reference material production for radiographic analysis. Steps a) – e) include the freezing of a block of carboxymethylcellulose, the drilling of holes into the block, filling the holes with the slurry used as reference solution, cutting of the single standard reference samples using a microtome and fixation of the slices on adhesive tape

The block was left over night at - 20 °C in a freezer to ensure that it solidified. The next day, a series of holes was drilled into the block, one for each boron concentration of the slurry. The slurry was then filled into the holes and left for freezing for two hours. After that, layers of the block were cut in a whole-body cryomicrotome (PVM, Stockholm, Sweden) from the surface of the block until the surface was completely smooth. Now single slices of 50 µm thickness were cut from the block using adhesive, polyvinylchloride tape (tesafilm® 4104, Tesa AG, Hamburg, Germany) to pick up the slice, and then freeze-dried over night. Each slice could be easily fixed and removed on a SSNTD film. After all, 40 slices with sets of standards on adhesive tape were produced.

The slices therefore contained a series of tissue-equivalent circular droplets with a diameter of about 6 mm and mostly uniform thickness. In some cases, the droplets crumbled during freeze-drying, which caused thin fissures to appear in the droplet or, in worse cases, parts of the droplet fell apart. Such standards were not used for calibration.

The standards were stored on plastic sheets in a folder. No particular sealing or storage under cooled conditions was considered necessary, as each droplet was automatically sealed between the plastic sheets and the adhesive tape, except for the moments when it was used for calibration.

After some time working with the standard reference samples, an effect of apparent diffusion was observed. When analysing radiographic images of over-etched SSNTD films qualitatively, especially the higher concentrated droplets (≥ 20 ppm) seemed to have a “halo” around the droplets in the image (Fig. 33).

This was apparently caused by the solubility of boric acid in carboxymethylcellulose, which was not considered to be significant for the production of the standard reference samples, as the whole process (including storage of the carboxymethylcellulose block during breaks) took place at temperatures below - 20 °C, therefore the tissue slurry was always in contact only with solid carboxymethylcellulose.

The observed halo in the standards was so large that obviously there was diffusion of the boric acid into neighbouring cavities in which the other liquid standard solutions were filled in. This was a considerable problem for establishing a calibration curve for a given measurement, as apparently not only a part of the boric acid from each cavity was not available when cutting the droplets from the block, but also there was a certain overlap between concentrations.

Therefore, it was necessary to produce a second series of standard reference samples, this time using BPA-f in human whole blood. The BPA was purchased from Syntagon / Hammercap, Sweden; the BPA-f was kindly prepared by the University Hospital’s Pharmacy. The whole blood was kindly provided by the blood bank of the University Hospital. As solubility of BPA-f in blood was not an issue for the desired concentrations, the solution was simply mixed with the whole blood. The most notable difference in the elemental composition between whole blood and tissue as matrix for the standards is the different carbon and water content,

which are the elements chiefly to be considered for the moderation of the emerging fragments from the $^{10}B(n,\alpha)^{7}Li$ reaction. This difference and all further consequences for the resulting calibration curve were assessed in a separate trial, which will be presented in section 3.2.7.

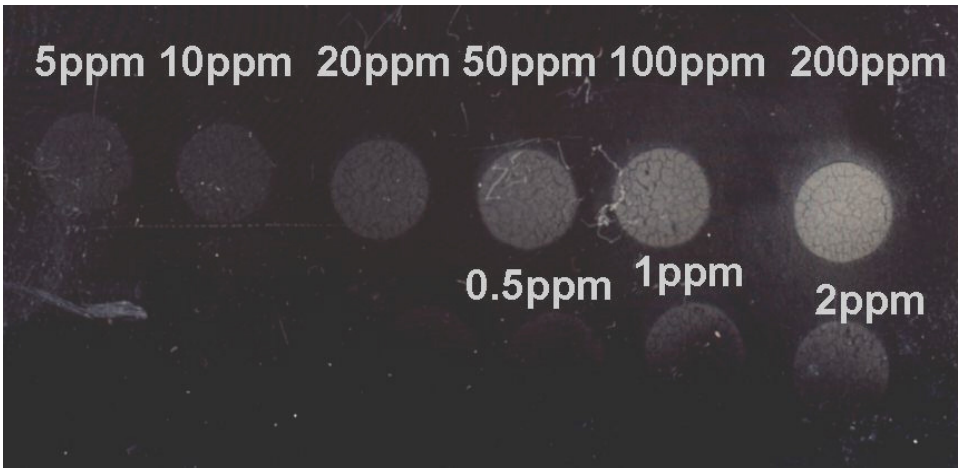

Fig. 33: Contrast and illumination altered image of a radiographic image of a set of standards for radiographic analysis after over-etching of the respective SSNTD film. Diffusion of boric acid from the cavities of 50, 100, and 200 ppm into the cavities of 0.5, 1, and 2 ppm is visible.

3.2.6 Histological analysis and sample preparation

After macroscopic inspection, representative samples from normal liver tissue and tumour tissue were snap frozen in liquid nitrogen, cut into 5 or 20 µm thick sections and finally stained with haematoxylin and eosin according to standard methods. After producing the cryosections for radiographic analysis, the remainder of the tumour free tissue biopsies were stored away for being measured using Prompt Gamma Activation Analysis (PGAA) at the Research Centre of the European Union in Petten, The Netherlands, and at the Technical University of Munich, Germany. However, of several samples all of the tissue was used up for the preparation of cryosections, therefore, not for all samples there are corresponding pairs of data of QNCR and PGAA. Details about sample preparation and the PGAA measurements themselves can be found in section 3.3.

The images from radiography and the histological analyses were made from consecutive slices of the tissue samples, thus stemming from directly neighbouring cryosections. After histological assessment, different areas in the sample were selected for radiographic examination, based on their different characteristics (Fig. 34).

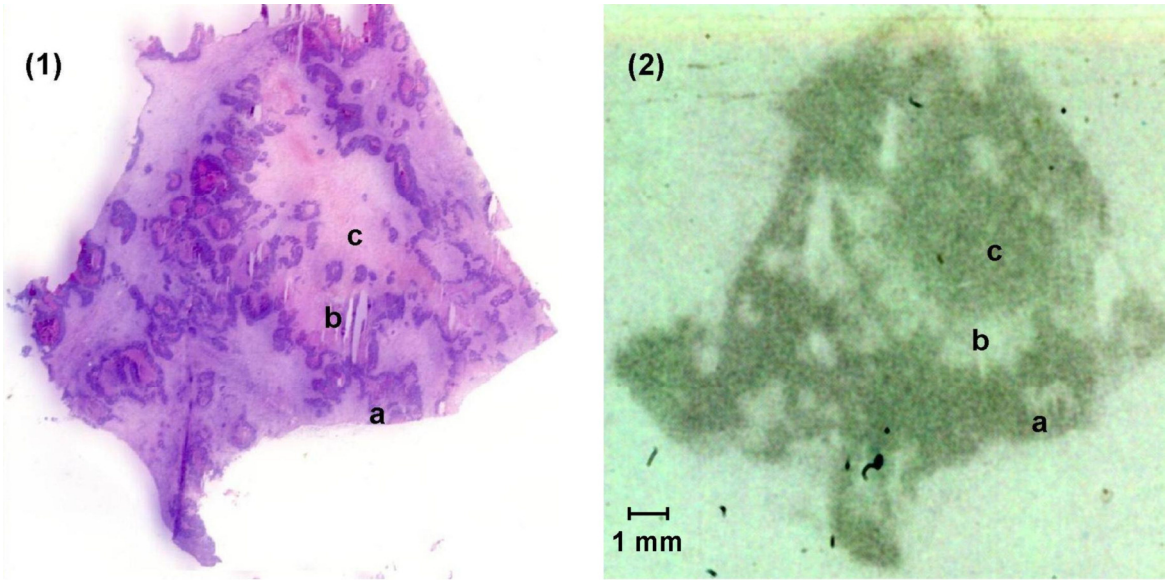

Fig. 34: (1) HE-stained image of a cryosection taken from cancerous liver tissue. (2) Contrast enhanced radiographic image of a cryosection from the same tissue sample. Areas of higher ^{10}B concentrations (= higher track densities) appear darker in the image. The black dots are errors from the scanning process. Detailed radiographic images of cell areas (a-c) are shown in section 3.2.8 (Fig. 46).

The specimens were analysed by light microscopy using an Olympus BX45 (Olympus, Hamburg, Germany) microscope. Areas of vital tumour tissue, necrosis, and normal liver tissue were identified. Special attention was paid to the tumour viability, which was determined morphologically by the cellular integrity of the tumour cells. Histological findings were documented with the help of a digital camera (Olympus Camedia C-7070). To correlate histomorphological areas to the boron concentration, one HE-stained image and one radiographic image of the consecutive slide with enhanced contrast properties were overlaid using Adobe Photoshop™.

For each cryosection, up to 15 areas of interest were located and analysed. The spatial resolution was limited by the characteristics of the camera and the

microscope; the dimensions of the digital images taken by the camera were at a maximum magnification of 410 x 325 µm². This magnification was chosen for all measurements presented in this thesis. For tissue characterisation in the radiographic images, only areas with a known histomorphological correlation were included.
All works concerning tissue characterisation according to its morphology and histology were carried out with the kind assistance of Dr. Christoph Brochhausen, Institute for Pathology, University of Mainz.

Etching protocol

The analytical protocol from previous works for development of the films by chemical etching foresaw placing the films in a stirred bath of 3 M NaOH solution (Merck, Darmstadt, Germany) for 70 min at 70 °C [215]. The approach for computed image analysis relied on counting the visible tracks after chemical etching. However, it was then decided not to stick to the previously determined etching protocol. The reasons to do this were two major problems:

After a series of irradiations of the standard reference samples it became clear that not all parts of a SSNTD film were developed homogeneously, which meant that there were visible changes in the track density of larger areas (> 5 mm in diameter), where the track density must be equal, as the neutron flux was known to be homogeneous (see section 3.2.3).
Even though this phenomenon of heterogeneity was not investigated quantitatively, it became clear that the deviation would influence image analysis too greatly. The heterogeneity was less prominent when stirring of the NaOH bath was avoided, though still unacceptable. It was therefore eventually decided to etch without heating the NaOH bath for 24 h. As this increased the development time for quantitative analysis greatly, as tracks now needed more time to grow, the etching was carried out in closed PE vessels to avoid changes of the pH of the solution due to interaction with CO_2.
The second problem revealed itself during data analysis. For various reasons more closely looked at in section 3.2.7, the relevant tracks produced under these

etching conditions were too small (< 1 µm in diameter). This was amended by applying longer etching times (8 days). Clearly analysis with 8 days waiting time would result in a very time consuming process, especially when considering that sample irradiation was not possible each given day. After more tests, etching time could be further reduced to 96 h if the SSNTD films were immersed in 7 M NaOH instead of 3 M NaOH. Additionally, the NaOH solution was changed after 48 h to provide a fresh etching potential.

Though this etching protocol is in contrast to the etching conditions reported in previous works found in literature [170, 223, 228, 239, 240](among others), the etching conditions were chosen parallely to the creation of the programme for image analysis and adapted accordingly. The final protocol for sample preparation is given below:

1. Cryosections were produced in the Institute for Pathology from each tissue sample by cutting them from tissue samples fixed with TissueTek fixation glue on metal stamps. Slices were cut from the blocks using a microtome (Leica, Germany) at -20 °C, any thawing was avoided. For technical reasons, the thickness of these slices varied between 5 and 50 µm.

2. The cryosections themselves were then put on glass microscope slides to which they stuck naturally (Fig. 35). The glass slides were free of boron, which was tested by irradiation and SSNTD analysis. After that, they were fixed with adhesive tape onto the TASTRAK films with the tissue facing towards the films surface. The films were 1 mm in thickness and were cut to match the measurements of the irradiation phantom. Prior to this, the films were cleaned with deionised water, isopropanol, and again deionised water to provide a clean and smooth surface for irradiation.

3. The samples were introduced into the channel of the thermal column using the irradiation phantom shown in Figure 21. The phantom remained in the channel during the whole period of irradiation. For irradiation, the films were sealed in small PE bags to prevent contamination with carbon by the surrounding graphite rods in the thermal column. After etching, the films were rinsed with deionised water and dried at open air.

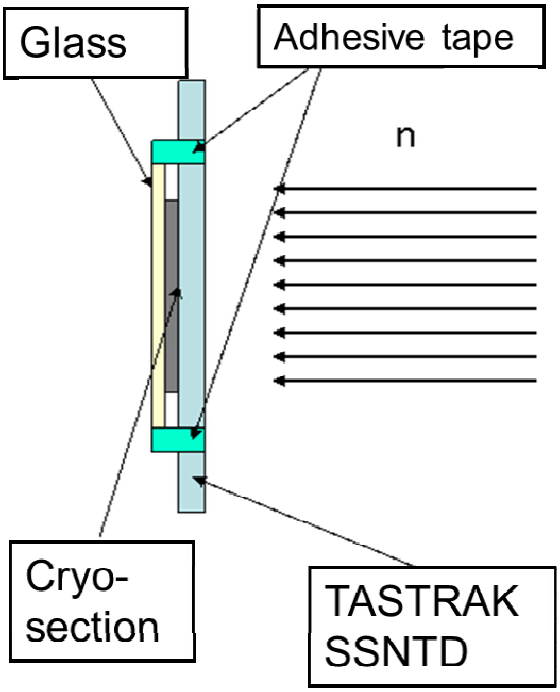

Fig. 35: Schematic of the set-up for neutron irradiation of the cryo-sections of tissue samples. The arrows represent the incoming neutrons.

Between measurements, the cryosections were stored in a freezer at -20 °C. If left at room temperature, after several weeks, a fading in the boron signal on the SSNTD films could be observed. The most likely reasons for that are evaporation effects of the boric acid group of the BPA, which could be separated from the aromatic ring, or diffusion effects within the tissue slice. This assumption is based on observations made in the weeks between July and September 2009, during which the mean environmental temperature rose considerably. A considerable number of cryosections of patients 1 – 3 were affected and were therefore not available any more for radiographic analysis, most of the samples had already been irradiated and were in the process of image analysis and data evaluation.
As mentioned further above, no such effect was observed for the standard reference samples. Due to sealed storage of the standards, any evaporation is unlikely. Whereas diffusion of the boric acid could have also occurred within the standards, such an effect would hardly be noticeable, as it was the intention in the first place to create reference samples from homogenised tissue.

3.2.7 Computed image analysis and data evaluation

For the computer assisted evaluation, images were taken using a Zeiss Axioplan microscope at a magnification of x200 and a Zeiss Axio Cam (Carl Zeiss, Oberkochen, Germany), a reflex camera equipped with a 8.2 Mio. CCD chip. Each picture used for analysis shows an area of 410 x 325 µm² and 2600 x 2060 pixels. All images were saved in the tagged image file format (TIF) to avoid graphic compression effects common in other formats. For the microscope and the digital camera parameters such as luminous exposure, brightness, or contrast correction were fixed for all images taken in one set. Image analysis for quantitative radiography proceeds in a series of steps, which are illustrated very generally in Figure 36.

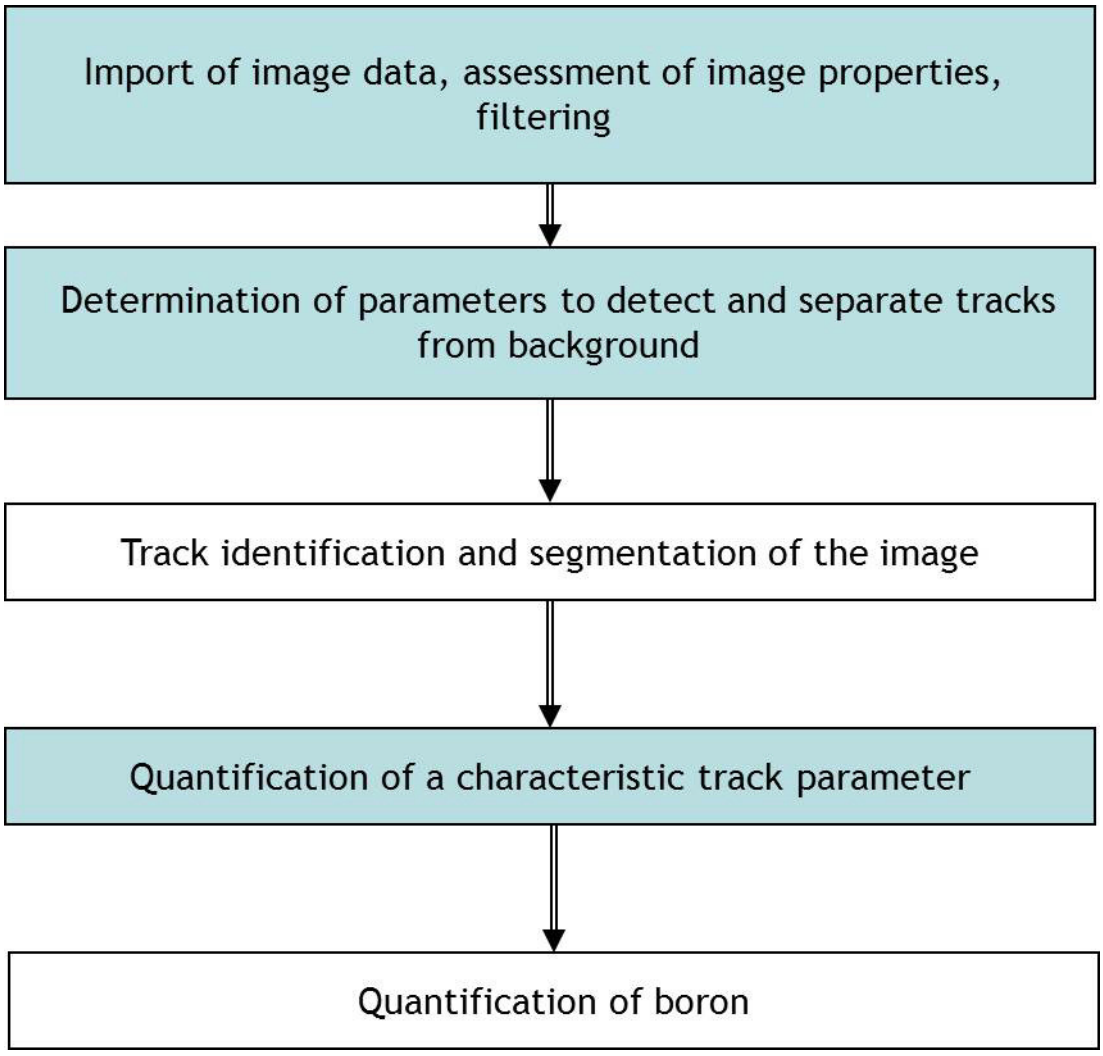

Fig. 36: Flowchart of the general steps required for image analysis of etched SSTND films

The programme to evaluate the digitised pictures of the samples was custom-made using MATLAB (The MathWorks, Version 7.5.0.338 (R2007b)) in cooperation with Dr. Frieder Enzmann at the Institute for Geo Sciences, University of Mainz. Most algorithms referred to in this section were already existent or in development. A comprehensive overview over these algorithms can be found elsewhere [215], therefore, in this work only entirely new algorithms relevant for the final analytical protocol will be mentioned. However, to provide the background information for the works presented in this thesis, a short introduction to the aforementioned work is given in the following.

Track characteristics in radiographic images of tissue samples containing boron

Most of the visible tracks in the images were those caused by the incidence of protons, α-particles, and ^{7}Li-nuclei. Especially the proton tracks are very distinct of the other two, as they cause rather sharp, round tracks after etching (see also Fig. 31). However, the attempt to analyse only the tracks produced by the neutron capture reaction was not successful, as though etching conditions were the same for each sample, the etching process proved to be more dynamic, which was most apparent in the variance of the peak shape, width, and tailing when plotting the minimum track diameters found in an image as histogram (for an example see Fig. 37).
Since the peaks lie close to each other it is obvious that separation by size exclusion of the tracks is difficult. This is mostly caused by the effect of self-absorption of the fission fragments emerging from neutron capture reaction deeper below the surface before reaching the SSNTD. As a result, it was decided to consider all tracks without further discrimination. This also meant that for correct quantification the standard reference material would have to produce proton tracks in the same way as tissue does (see section 3.2.6).

The first approach for quantification was then to determine the boron concentration via the number of all tracks in an image and to compare it to a standard reference curve. Therefore, the crucial parameter is to count the tracks correctly.

In previous works, a programme for image analysis had been already presented. It relied mainly on converting the digitised images into black and white images after subtraction of a background image, followed by segmentation of the tracks.

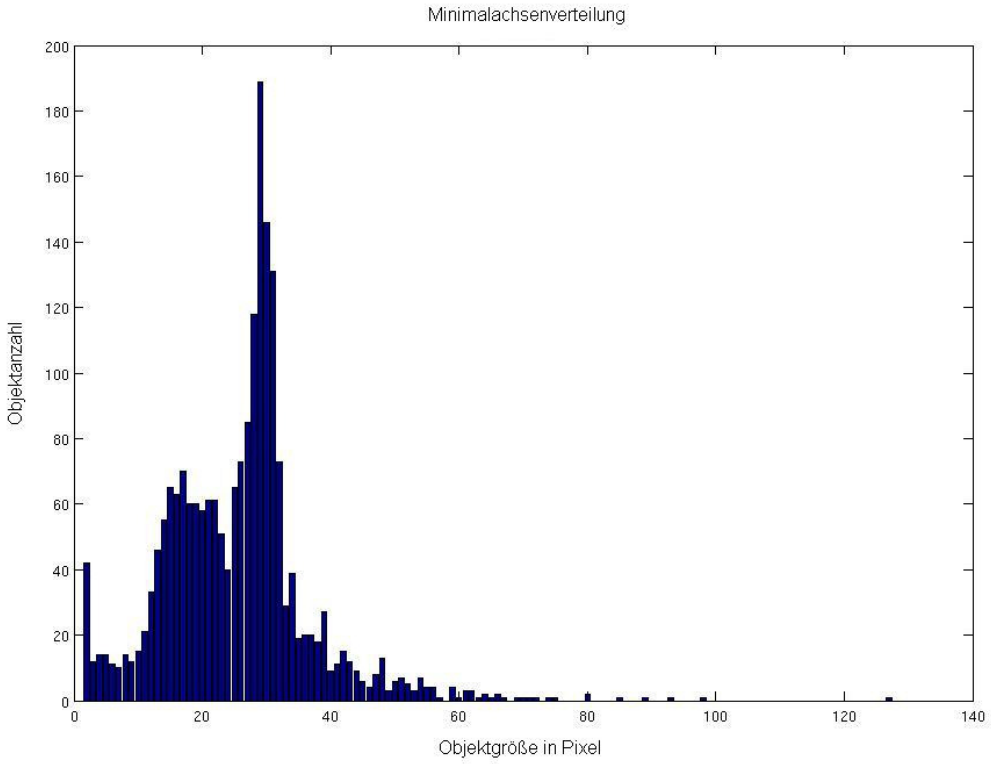

Fig. 37: Histogram of the distribution of the minimum axes of all tracks in a radiographic image of lower resolution (1300 x 1030 pixels) of a tumour-free liver tissue sample. The track size is given in pixel. The higher peak on the right and its tailing represent α- and ^{7}Li-tracks, the broader peak on the left represents the proton tracks. Figure re-used from [215])

Image segmentation

In this context, segmentation means that certain objects visible in the image are defined as a distinct group of objects − compared to the rest of the image, which is recognised as background. For quantitative analysis it has to be decided, what object group is to be segmented and how the programme should further process this information. Segmentation of a group of objects has to be carried out by categorisation of such objects via one (or more) characteristic parameters.

This can be achieved by different algorithms, of which several had already been tried before in this project. Two approaches were thought to be most promising: One included segmentation via the gradient of intensity in the images that rises

sharply at the border between background and track area, for which it can be used to define the borders of a track. The other included the kmeans-clustering algorithm [241], which allows categorisation of all geometric shapes in a pre-defined number of clusters, which can then be separately further processed.
Both are semi-automated approaches, as they require the manual input of at least one parameter (the threshold gradient or the number of clusters, respectively) when analysing an image.

With routine quantitative analysis of images, it soon became evident that the kmeans-clustering was not reliable enough and frequently yielded wrongly segmented images. Therefore, the approach was chosen which relied on the gradient approach for segmentation. As mentioned further above, the etching conditions were adjusted in correspondence with the development of the algorithm for image analysis. For the determination of the boron content, the approach of counting the tracks numerically was chosen, as this was a very common approach in QNCR [189, 190, 205] and also included in other codes for image analysis [242, 243]. Keeping the irradiation and etching conditions fixed for all standard reference samples, it should be possible to obtain a general calibration curve by plotting track number or track density versus the boron concentration. Therefore, after segmentation the number of tracks per image had to be determined.

Track characterisation during computation of the digital images

As tracks appear in the image either round or elliptical (see also Fig. 31), it is possible to count all segmented objects fulfilling certain geometric criteria, e.g., a specific circumference to area ratio. While this works well for single tracks, it is less simple for track-clusters. Track clusters appear, if two or more tracks are produced during etching in such close vicinity that they “melt” into a track cluster. This effect depends on the number of tracks created, i.e., on the number of particle incidences on the surface of the SSNTD, and on their size, i.e., on the etching conditions.

A solution to the problem seemed to be to choose irradiation conditions and etching conditions producing not too many tracks per image and to ensure they had small diameters. However, during the digitising of the images, it was also observed that a number of “graphical artefacts” was created when storing the images. Graphical artefact in this context means that a certain number of single or several pixels bound together in groups appeared in the image where previously no track had been. These had to be excluded for segmentation. Especially if the majority of the tracks visible in the image was rather small in diameter (around 20 pixles) the chance of confounding artefacts and tracks produced applying the initial analytical protocol was relatively high. It was therefore decided to produce tracks with larger diameters (≥ 100 pixels) sufficiently high, so they would not be confused with other graphical artefacts.

The inevitably emerging track-clusters in the images had to be considered for track number determination as well. As the concentration range of the standard reference material available was from 0.1 to 200 ppm (in 12 concentrations, including a blank sample), etching conditions had to be found that would produce a number of tracks sufficiently high for each concentration standard to be distinguished from the other standards, but without producing too many track-clusters at higher boron concentrations, which would lead to cluster production and far more complicated image analysis. Furthermore, the quantitative result would be very incorrect, as correct calibration at higher concentrations would be impossible.
After a series of irradiations, it became clear that a compromise between these two had to be found, as high fluences (up to 10^{13} n / cm²) combined with long etching times (up to 120 h at room temperature) lead to a good distinguishability of the lower concentrated standards (0.1 to 5.0 ppm), but also to a quick track saturation seen in images of the concentrations ≥ 10 ppm (A series of exemplary images is shown in Figure 38).

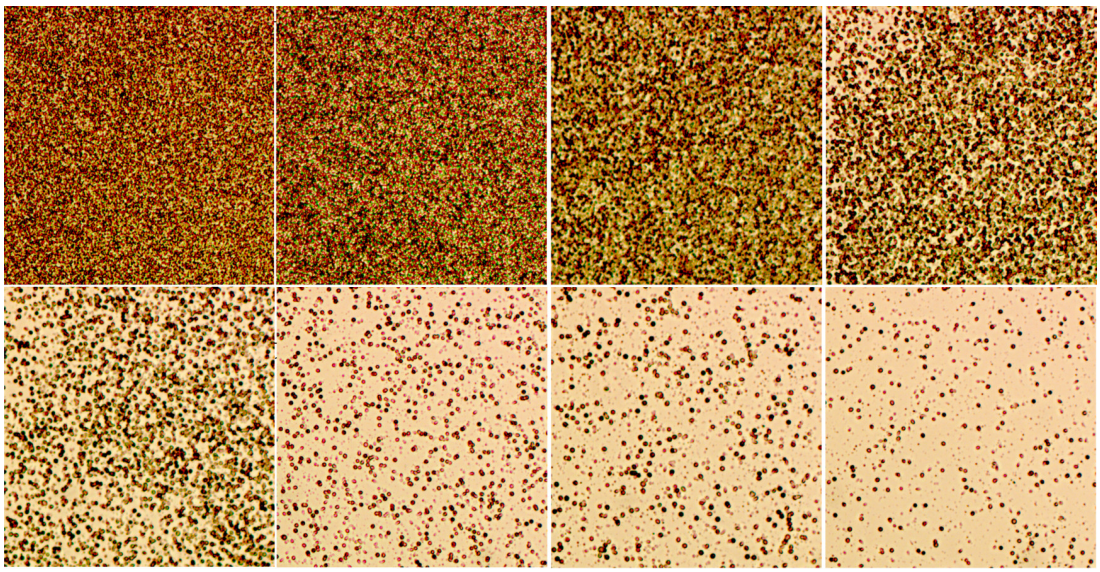

Fig. 38: Track densities of one set of radiographic standards irradiated at a fluence of $4.08 \cdot 10^{13}$ n / cm². Concentrations of 200, 100, 50, 20, 10, 5, 2, and 1 ppm boron are shown (upper left to lower right, captions are scaled 115 x 115 µm²)

Lower fluences (< 10^{11} n / cm²) and shorter etching times avoided saturated images at higher concentrations, but yielded also images, which did not allow good of distinction boron concentrations below 10 ppm. (A series of exemplary images is shown in Figure 39). For the etching conditions, after all tests, a compromise between these two outcomes mentioned above had to be chosen in order to obtain a calibration curve for the most relevant concentration range: the samples were irradiated 20 min at 1 kW (= $4.08 \cdot 10^{11}$ n / cm²) in the thermal column of the TRIGA research reactor and then developed by etching in 7 M NaOH for 96 h at room temperature in closed PE vessels. Corresponding radiographic images for this case are shown in Figure 40. It can be seen that there is a certain saturation of the track density at higher concentrations and also poor distinguishability of the track density at lower concentrations. However, the concentration range between 1 and 100 ppm appears now fit for calibration.

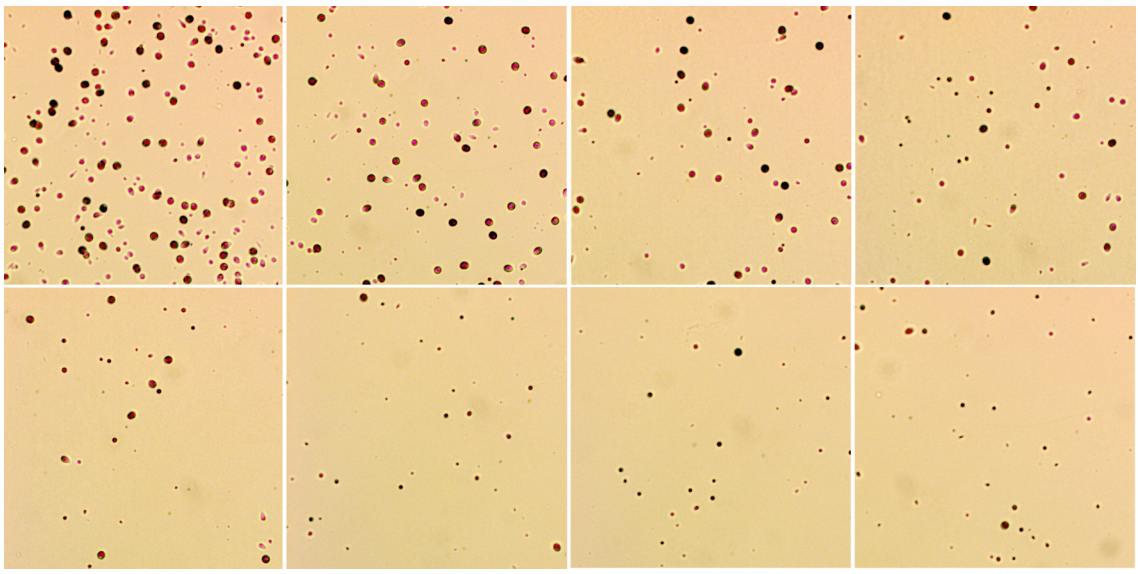

Fig. 39: Track densities of one set of radiographic standards irradiated at a fluence of $4.08 \cdot 10^{10}$ n / cm². Concentrations of 100, 50, 20, 10, 5, 2, 1 and 0.5 ppm boron are shown (upper left to lower right, captions are scaled 115 x 115 µm²)

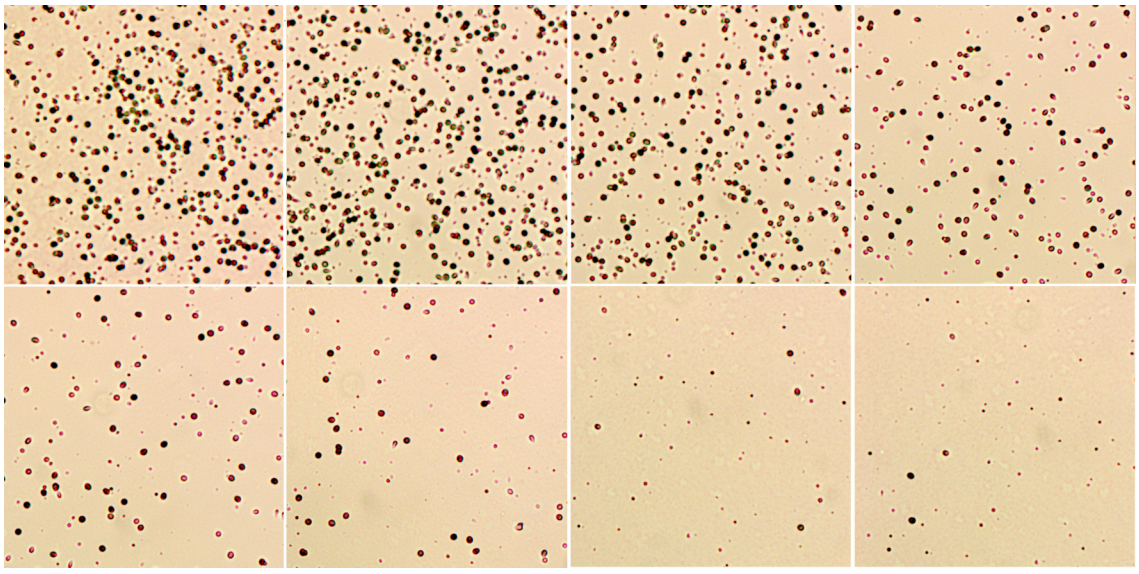

Fig. 40: Track densities of one set of radiographic standards irradiated at a fluence of $4.08 \cdot 10^{11}$ n / cm². Concentrations of 200, 100, 50, 20, 10, 5, 2, and 1 ppm boron are shown (upper left to lower right, captions are scaled 115 x 115 µm²)

A second attempt included the calculation of the number of tracks forming a cluster after determination of the circumference to area ratio. At first this approach seemed to be promising, therefore, a test that included counting of the tracks in 10

images by hand and by analysis of the programme was carried out. However, the difference between both approaches was between 5 and 20 %, and the difference was roughly proportional to the number of clusters visible in the image, which hinted at a poor ability of the algorithm to determine the correct track number in larger clusters.

Boron determination via the track area

As the correct analysis of inevitably formed track-clusters could eventually not be achieved, the concept of determining the track density was abandoned in favour of determination of the track area. The track area can be determined independently of the formation of track-clusters in the image by simple categorisation into “track” and “no-track pixels” and therefore easily used as characteristic parameter for boron quantification.
The route via area determination seemed uncritical, save for the problem of ellipticity of tracks that leads inevitable to an incorrect determination of the track area, as elliptical tracks appear larger than round tracks generated by the same particle. However, in previous works it was found that most tracks were found to be of almost round shape, so the error caused by ellipticity was deemed to be tolerable.

The final algorithm is illustrated in a flowchart diagram in Figure 41. It foresees that the digitised images were converted into black and white images, after which several filters were applied to smooth the image. This included subtraction of a background image, which was taken for each set of images taken for certain microscope parameters. Background subtraction was necessary to rule out errors created by certain hardware parameters of the microscope.
This was followed by median filtering and sharpening of the contours of the tracks to obtain sharper intensity differences between tracks and background, which helped to get a correct segmentation. After that, the segmentation was carried out as the algorithm differentiated the selected track and non-track area by evaluating the black-to-white gradients in the picture. The ‘track area’ is defined as a pixel cluster which is encompassed by a set of black-to white colour gradients.

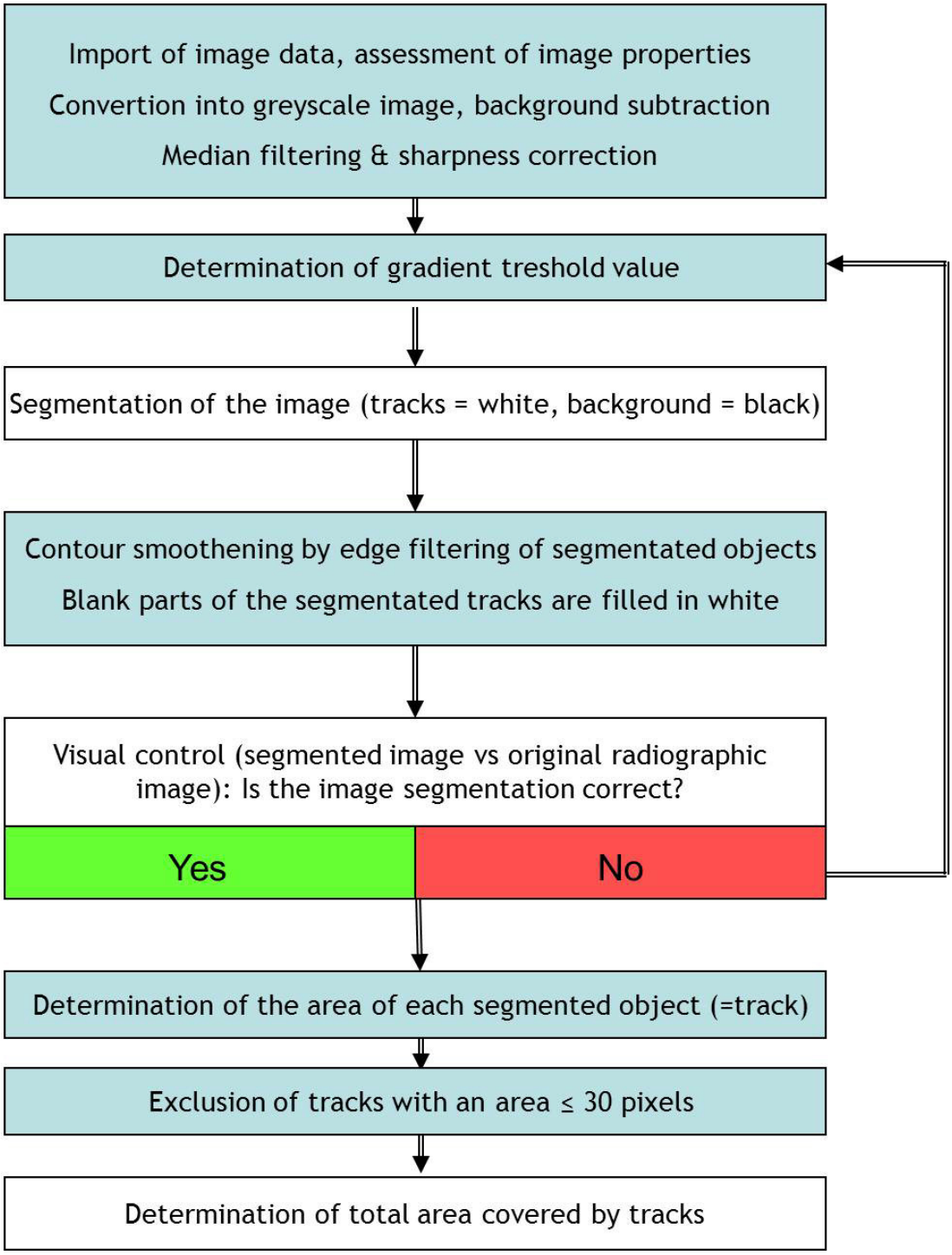

Fig. 41: Flowchart of the algorithm used to compute the digitised radiographic images

Such a cluster had to be sufficiently large in dimensions, thus eliminating the selection of single, pairs, or small sets of pixels, which are generated during the digitalisation process of an image by the photo-camera. Typically, a single α-track consisted of 200 ± 40 to 1500 ± 100 pixels, pixel formations if an area of less than

30 pixels were excluded from evaluation. The variance in size of a single α-track was radiographic images was not expected to be this large and caused problems for the calibration and quantification. This will be looked at more closely further below in this section.

As next step, a threshold value (a specific gradient value for each image) was set manually to distinguish between track and non-track areas. A gradient was determined for each pair of neighbouring pixels in the image. If equal or higher than the previously set threshold value, these pixels were set as white pixels, otherwise they were set as black pixels. The gradients were obtained by analysing the occurrence of each gradient in the image. Between 80 and 90 % of all gradients found are numerically small, as they represent the gradient between, e.g., two neighbouring background pixels. Therefore, the numerically larger gradients are the much smaller share in the image. The threshold value was effectively the gradient value that would “separate” these two shares of gradients, if they were plotted in a histogram. Consequently, the tracks were depicted as white rings on a black background. To create an exact black-and-white image of the radiographic image with tracks depicted white, the previously created rings were filled white and an edge filter was applied to the image.
To determine quantitatively the amount of boron in the samples, the programme determined the area of the film covered by the tracks. The result was compared to tissue equivalent standards (as described above) to deduce the boron concentration in the image.
Initially, it was tried to let the programme run with a fixed threshold value applied to every image. However, after analysing histograms of a series of images, it became clear that the gradient value was too sensitive towards several microscope parameters which could not be kept fixed for every image analysis carried out, e.g., the illumination could not be set following a scale, but only according to the user’s personal choice. Therefore, the threshold value had to be controlled for every set of images to be correct in segmentation of the tracks. This could easily be achieved by comparing the processed black / white image to the original image. The programme is therefore a semi-automated programme, since the input of the threshold values is required. To further ensure correct numerical performance of the programme to determine the correct track area, specifically written control

programmes which create a number of specified artificial tracks in a blank image were analysed with the final evaluation programme. The analysis of such artificially created images showed no errors in the evaluation programme.

Calibration for boron quantification

Mathematically, the course of the track area vs. boron concentration can be described by a sigmoid function. The curves obtained were best characterised with a five-parameter sigmoid function, which accounted for a signal offset, some tailing followed by a steep increase and (later) quick flattening of the curvature at critical points of the regression curve (Eq. 4).

Eq. 4:
$$x = y_0 + \frac{a}{\left(1 + \exp\left(-\left(\frac{x - x_0}{b}\right)\right)\right)^c}$$

The plot of such a calibration curve is shown in Figure 42. All fits were carried out using SigmaPlot (version 8.0). Regarding this calibration curve, the setting of the parameters for the production of radiographic images and their subsequent computed analysis should now enable the analyst to establish a general calibration curve. To do that, 30 sets of standard reference samples were irradiated for 20 min at 1 kW (= $4.08 \cdot 10^{11}$ n / cm²) in the thermal column of the TRIGA research reactor and then developed by chemical etching in 7 M NaOH for 96 h at room temperature in closed PE vessels.

For each boron concentration of a set of standards, five images were taken and the total area covered by the tracks was determined. The mean track area of these five images was plotted with all other mean track areas of the other 30 irradiated sets of standards versus the boron concentration. Though parameters were held fixed throughout the whole trial, the result was far from satisfying. A great variance of the mean track area was found for each image, as the mean track area found for proton tracks and α-tracks fluctuated from irradiation to irradiation. Thus, the standard deviation of the total track area alone (without respecting propagation of

error from the preparation of the standard reference samples et cetera) was 15 - 30 %, whereas standard deviation was greater for higher concentrations (Fig. 43).

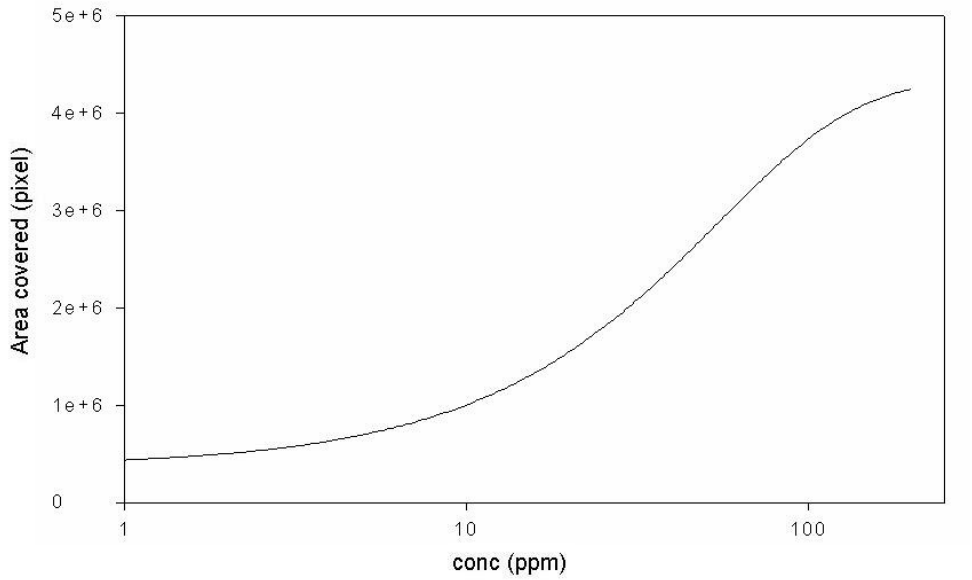

Fig. 42: Resulting calibration curve of a the track area plotted vs the boron concentration in a set of tissue equivalent standard reference samples, fitted with a 5 parameter sigmoid function (see Eq. 4).

This was most probably due to the fact that most tracks at lower concentrations are generated by background protons emitted from the neutron-tissue interaction upon irradiation.

However, subsequent data analysis revealed that between a series of images taken for the same concentration in one set of standards, the standard deviation of the track area was much smaller (1.5 – 7 %). Therefore, from one set of standards it was possible to obtain a reliable calibration curve.

As the SSNTD films were etched at equal conditions but in different vessels and different dates, the conclusion was drawn that though development conditions may be equal, this does not necessarily lead to equally developed tracks. The idea of establishing a generally valid calibration curve was therefore abandoned in favour of a more reliable approach: For each cryo-section from tissue, one set of standards would be irradiated on the same SSNTD film. This way it would be ensured that irradiation and etching conditions would be exactly the same for both sample and calibration standards, though this created a much more time-

consuming protocol, as now for each analysis a unique calibration curve had to be created.

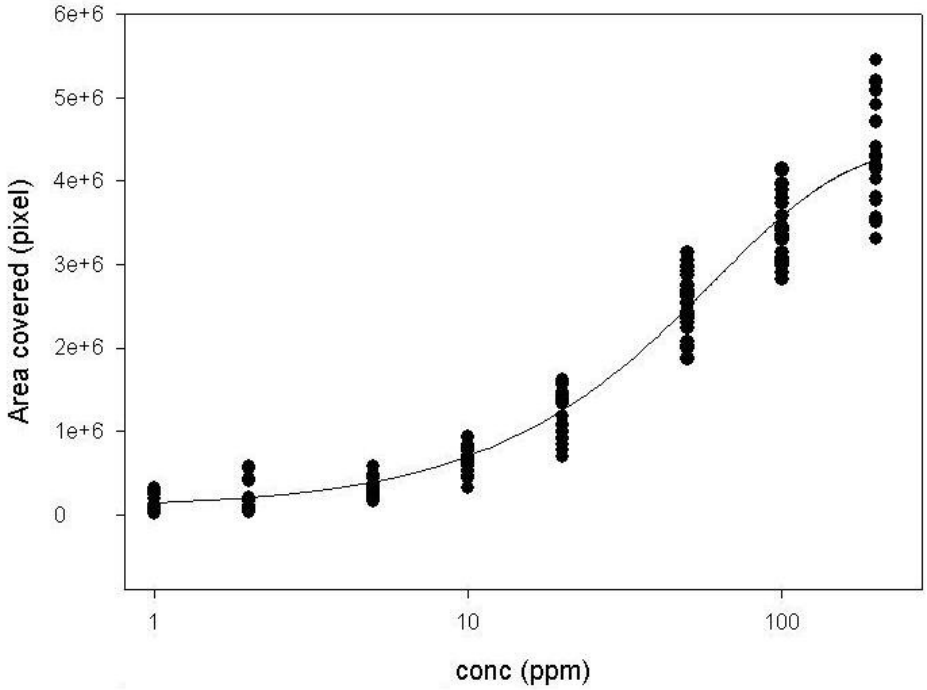

Fig. 43: Resulting general calibration curve of the track area plotted vs. the boron concentration for 30 sets of equally irradiated and developed tissue equivalent standard reference samples, fitted with a 5 parameter sigmoid function (see Eq.4).

Eventually, the protocol foresaw for each concentration five digital images to be taken and evaluated. For each of these sets of five, the mean area covered by tracks was determined and then used to plot an individual calibration curve for the samples irradiated on the same SSNTD film.
When the analysis of one image was carried out repeatedly to check reproducibility, the deviation of the determined pixel area of such computer-assisted measurements was lower than 0.1 %.

As mentioned further above (see section 3.2.5), a second series of standard reference samples made from BPA-f in whole blood was produced for analysis of cryosections. As a part of the samples were not available any more for new irradiation, a short trial was conducted to obtain a correction function which could be applied to the older data:

Sets of standards produced from boric acid in tissue and BPA-f in whole blood were irradiated together on the same SSNDT film and evaluated as described above. The set produced from BPA-f in whole blood was chosen as “reference set” for the plot of the other set. In Figure 44 an example is given for such a pair of two sets of standards, which illustrates the qualitative observation that the diffusion effect was more pronounced for boron concentrations ≥ 20 ppm.

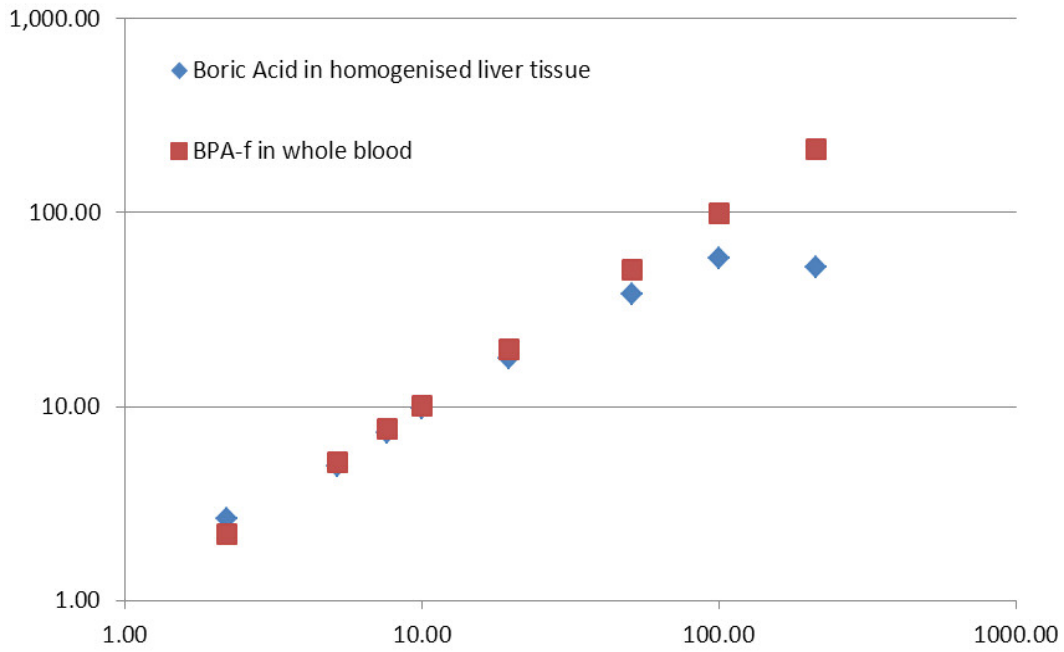

Fig. 44: Comparison of two different calibration curves from both series of standards, obtained after irradiation on the same SSNTD film

From these set pairs, a second order polynomial was deduced as correction function ($y = 0.012\ x^2 + 0.9706\ x + 0.13$), which was subsequently applied for all concentration values originally calculated from the data obtained using standards made from boric acid. The resulting correction of the concentration values in absolute numbers was 0.5 to 1.5 ppm for samples of tumour free tissue and 2.0 to 8.0 ppm for samples from vital tumour tissue.

At the time of publishing the results [216], the production of the second series of reference samples and the necessary numerical correction had not been carried out. Therefore, the values presented in section 3.2.8 vary slightly from the published numbers.

3.2.8 Results of tumour and tumour free tissue samples

Thickness correction

For technical reasons, there was variable thickness of the slices cut from the standard material and from the tissue samples retrieved. The minimum thickness for the standard material was 50 µm, this was due to the technical properties of the microtome in use at the University of Bremen. However, the cryosections from the samples were produced using a different microtome at the Institute for Pathology in Mainz. In order to achieve homogeneous cuts, the cryosections produced with this machine were at thicknesses of 20 µm (patients 1-3) and partly 5 µm (patient 4). During sample evaluation, a variation in the concentration between different sample thicknesses was observed. This was not entirely surprising, as the moderation of the fragments of the $^{10}B(n,\alpha)^{7}Li$ reaction is very different in tissue slices of different thicknesses. As a consequence, the dependence of the boron concentration on the thickness of cryosections was to be determined.
From one sample of tumour free tissue, three cryosections of 5, 8, 10, 20, and 50 µm each were cut and the boron concentration in all of them was determined. The mean concentrations were plotted vs. the thickness of the cryosections. The plot revealed a hyperbolic dependence between the thickness of the cryosections and the resulting boron concentration (Fig. 45). A similar dependence on thickness was found when measuring the concentration in areas of viable tumour cells. This dependence is significant for thicknesses below 20 µm. In tissue, the maximum range of α-particles and ^{7}Li nuclei does not exceed 10 µm, therefore for higher thicknesses the additional fragments produced in deeper regions of the cryosections are not detected due to self-absorption. All values given in this thesis have been normalised to a thickness before freeze-drying of 50 µm. By normalisation, the absolute change for results obtained from cryosections of a thickness of 20 µm was less than 1 ppm. For the cryosections of 5 µm in thickness, the normalisation caused a change of more than 2 ppm, but as stated above, this was only relevant in the case of patient 4.

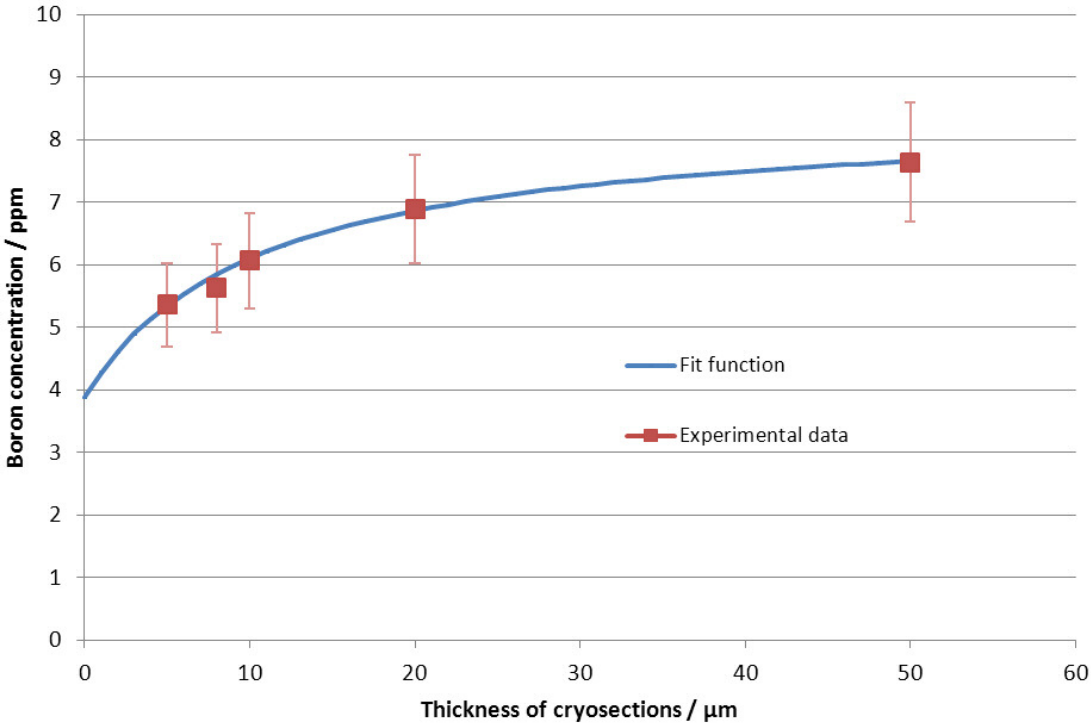

Fig. 45: Boron concentration in tumour-free tissue in dependence of the thickness of the respective cryosections. Experimental data are given as dots, the resulting correction function as solid line

Determination of measurement uncertainties

Determination of the propagation of uncertainty by the Gaussian formula (see section 1.7) was carried out according to the following relation:

$$\frac{c_{B,smpl}}{A_{B,smpl}} = \frac{c_{B,Std} \cdot D_{std}}{A_{B,std}}$$, with c_B as boron concentration in sample (*smpl*) and calibration standards (*std*), D_{std} as dilution factor of the calibration standards (during sample preparation) and A_B as track area of the boron recorded by the SSNTD films of samples (*smpl*) or calibration standards (*std*). For the samples no dilution factor has to be respected, since the tissue samples were only cut and not further treated.

The respective uncertainties of all factors (except $c_{B,smpl}$, obviously) have been obtained by the producer (in case of the boron standard), were calculated or obtained from measurement data.

As uncertainty of the boron concentration in samples the standard deviation of track area $A_{B,smpl}$ measured within samples of one type of tissue was chosen. Relative standard deviation (RSD) ranged from 2 – 10 %, in single cases up to 20 %. This is not surprising considering that the boron distribution in a very complex biological system had to be determined. For propagation of uncertainty, 10 % are chosen for calculations.

Track area of the standard reference samples was measured more homogeneously, RSD was between 1.5 % (for higher concentrations) and 7.5 % (lower concentrations). Since a sigmoidal fit function was used for evaluation of each irradiated and etched SSNTD film, uncertainty would have to be calculated for each curve separately. As uncertainty is not uniform for the whole range of concentration, an uncertainty function is needed to describe uncertainty at every concentration correctly. As suitable simplification the highest uncertainty (7.5 %) is set for all measured standards.

Uncertainties of the dilution factor D_{std} originate from the preparation of the calibration standards. These were entirely weighed, which is why only the uncertainty of the analytical balance has to be regarded. Total uncertainty (0.2 %) was obtained from linear propagation of uncertainty.

The total uncertainty calculated by Gaussian propagation of error is therefore 12.51 %

Results for the different cell types

For each patient, mean values for vital tumour tissue, tumour tissue intermingled with necrotic tissue, fibrotic tissue caused by desmoplastic stromal reaction, necrotic tissue, healthy hepatocytes, and steatotic hepatocytes were calculated. For this, the mean values of all measurements of one specific tissue or cell type of all cryosections produced from the different tissue samples taken were used for each patient. The standard deviations of such values were between 20 to 25 %. However, tissue consisting of healthy hepatocytes or of necrosis was more homogeneous. In these cases, a standard deviation of 15 % and 10 %, respectively, was found. Exceptions were observed for the necrotic tissue in the samples of patient 2, where the standard deviation was around 34 % and in the

healthy hepatocytes of patient 4, where the standard deviation was 29 %. The standard deviation between the results for healthy tissue obtained for all four patients is 19 %.

An overview for all measurements in the different tissue samples of all patients is given in Table 5. The mean values for all patients were determined with a median standard deviation of around 20 %, except for patient 2 and 4, where single values showed a standard deviation of up to 35 %.
The standard deviation between the values for healthy tissue obtained for all four patients is 19 %.

Tab. 5: Absolute ^{10}B-concentrations detected in tissue samples of the four patients participating in the clinical study.
When several values from the same tissue were measured, the range is given, and the mean ± standard deviation is given in parenthesis.

	^{10}B concentration in tissue, µg / g (ppm)			
	Patient 1	Patient 2	Patient 3	Patient 4
Hepatocytes	10*	13	8	8
Steatotic Hepatocytes	n.d.	n.d.	2 – 5 ** (3 ± 1)	4 – 7 ** (5 ± 1)
Necrotic tissue	4	3 - 9 *** (6 ± 1)	5	5
Tumour tissue intermingled with necrotic areas	15 - 24 *** (19 ± 3)	n.d.	10 - 21 *** (16 ± 3)	n.d.
Fibrosis	n.d.	25	n.d.	19
Tumour	n.d.	28	34	20

n.d. = not determined,* mean over hepatocytes and steatotic hepatocytes together, ** values varied according to dimension of steatosis, *** values varied according to dimension of necrosis

Tumour-free liver tissue specimens from patient 1 had a homogeneous uptake of 10 ppm ^{10}B in all tumour-free samples taken. In all of these samples, a homogeneous distribution of steatotic hepatocytes among healthy hepatocytes was found. Therefore, the given values represent the mean for normal and steatotic hepatocytes together. For this patient, it was not possible to determine concentrations for desmoplastic stroma cells due to very few, thin desmoplastic

fibre bands which could not be discriminated from the vital tumour. The tumour tissue showed a heterogenous ^{10}B concentration distribution, which ranges between 15 ppm in tumour tissue with large necrotic areas, with diameters of 1 to 2 mm, and 24 ppm in tumour tissue with small necrotic areas (diameters below 1 mm). Large necrotic areas in the centre of the tumour specimens without any vital tumour tissue had low boron concentrations of 4 ppm.

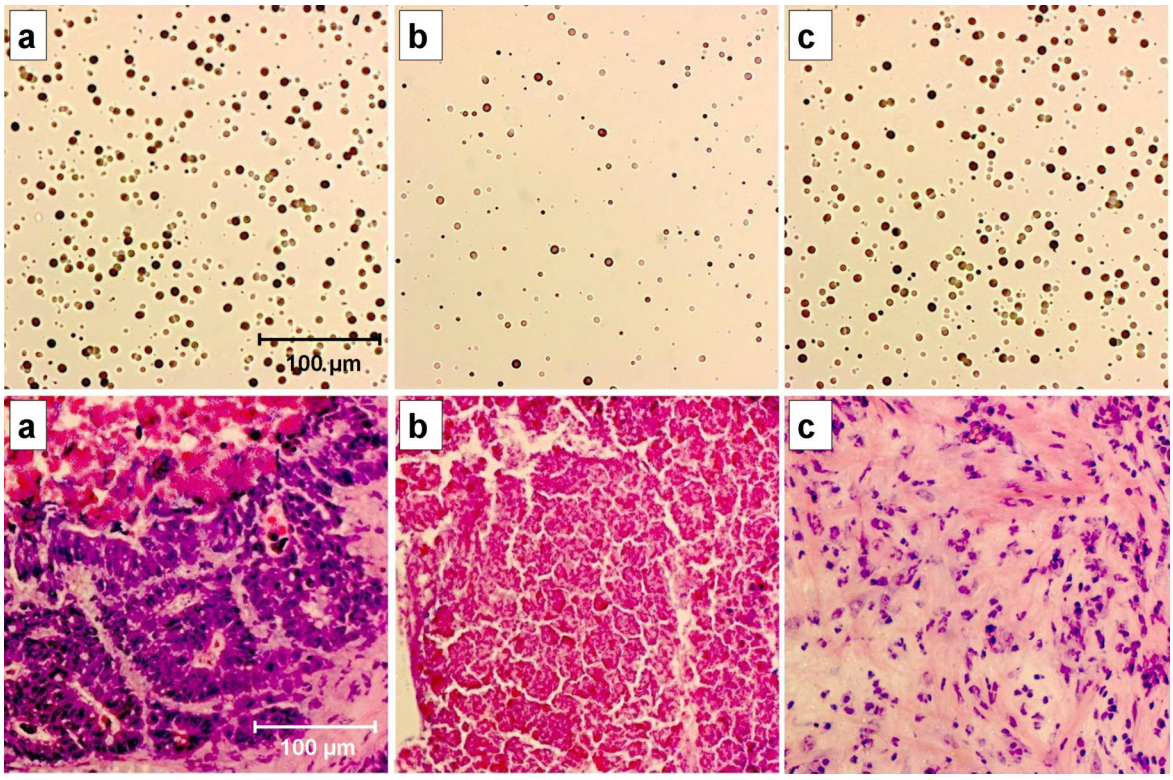

Fig. 46: Radiographic images (above) and the corresponding HE-stained images (below) of selected areas of the image shown in Figure 34 (section 3.2.6) are displayed, captions are scaled 325 µm x 325 µm. Viable tumour tissue (a) showed an uptake of 28 ppm. Areas of necrosis (b) showed an uptake of 4 ppm ^{10}B. Fibrotic areas generated by desmoplastic reaction showed concentrations comparable to tumour cells ((c), 24 ppm).

In the tumour-free samples of patient 2, hepatocytes had a concentration of 13 ppm ^{10}B. In this patient, no steatotic hepatocytes could be found. The tumor samples showed a mean uptake of 28 ppm ^{10}B. Within the tumor samples, larger areas of desmoplastic stromal reaction were observed (see Fig. 34 and 46). In these areas, boron concentrations of 25 ppm were detected. In necrotic tissue of this patient, boron concentrations between 3 and 9 ppm were found, depending on the dimensions of the necrotic area; in smaller necrotic areas, the boron

concentration was higher than in large ones. For patient 2, a higher variation of the boron concentration in necrotic tissue was observed compared to the other patients.

Samples of tumour-free tissue obtained from patient 3 showed large areas of macrovesicular steatosis (Fig. 47). Steatotic cells showed considerably less ^{10}B enrichment than neighbouring non-steatotic hepatocytes, with a range between 2 - 5 ppm and a mean value of 3 ppm. In areas without steatosis, a homogeneous boron concentration of 8 ppm was found.

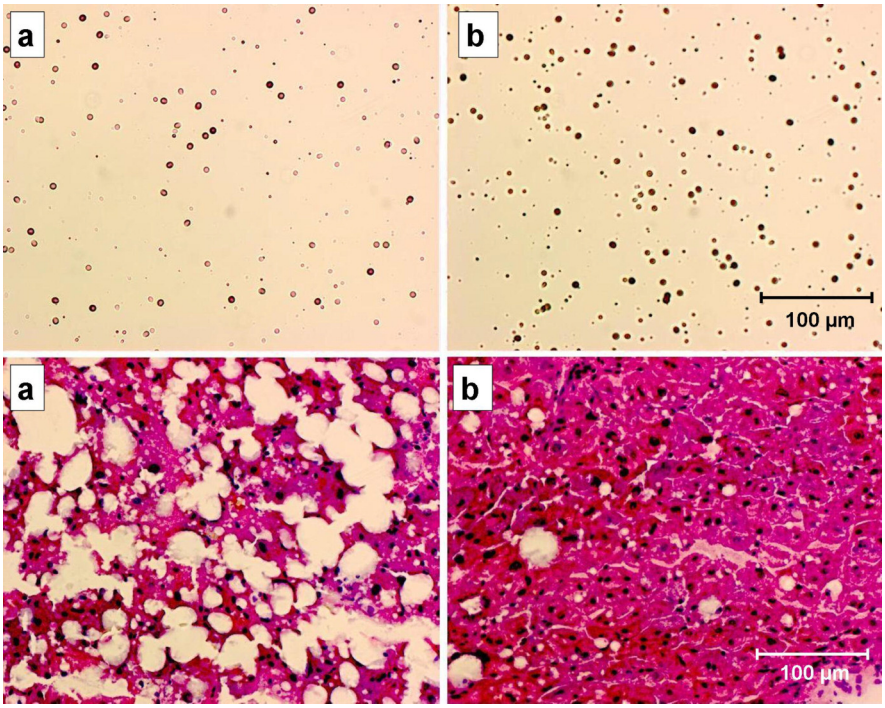

Fig. 47: Radiographic images (above) and the corresponding HE-stained images (below) of selected areas of a cryosection of tumour free liver tissue are displayed, captions are scaled 410 µm x 325 µm. Areas with macrovesicular steatosis (a) showed an uptake of 4 ppm ^{10}B; areas without steatosis (b) showed an uptake of 8 ppm ^{10}B.

Tumour samples obtained from patient 3 were very heterogenous. Due to their minor histomorphological manifestation, it was not possible to analyse fibrotic areas found in these samples, which is why no values for fibrotic tissue are reported for patient 3. The boron concentrations of 34 ppm found in vital tumour tissue without necrosis were higher than in areas with tumour tissue intermingled with necrotic areas. These specimens had a boron concentration of between 10 – 21 ppm, depending on the extent of necrosis.

In the tumour-free samples of patient 4, large areas of steatosis were also found as well, having a boron concentration ranging from 4 – 7 ppm, with a mean value of 5 ppm. Tissue areas without steatosis showed a concentration of 8 ppm. In desmoplastic stromal tissue, the boron concentration was 19 ppm and in vital tumour tissue 20 ppm. Also in this case, necrotic tissue showed low quantities of boron with a value of 5 ppm.
The mean boron concentration in tumour free tissue of all patients is 9.6 ppm.

Results for the samples retrieved before perfusion with preservation solution

It was the aim to determine whether the perfusion with HTK-solution would alter in any way the boron concentration in both tumour and tumour free tissue. Fortunately, in all cases it was possible to retrieve tumour tissue without cutting through the liver capsule, as in all cases there was either accessible tumour tissue at the surface of the liver specimen or very close to the cauterised resection plane. For both types of tissue only one small sample was taken in order to not to influence the structural integrity of the liver, because this could also influence the natural course of the perfusion.
In case of the first patient, both biopsies were taken using a hollow needle. Since only a very small strip of tissue was acquired in both cases (both lighter than 50 µg), it was not possible to prepare cryosections for radiographic analysis. The sample from tumour free tissue was kept for later analysis with Prompt Gamma Activation Analysis (see section 3.3). The biopsies of patients 2 – 4 were taken with a scalpel, from all biopsies cryosections were produced.
The radiographic analysis of the cryosections yielded similar results for patients 2 and 4. The sample taken from patient 3 proved to be largely necrotic and was therefore not analysed with respect to possible perfusion effects. For patient 2 in vital tumour tissue, a mean value of 27.7 ppm and for patient 4 a mean value of 17.9 ppm boron was found. If compared to the boron values found for vital tumour tissue after perfusion, it is evident that, with respect to the measurement uncertainty reported above, no apparent altering of the boron concentration took place (Fig. 48).

The results of the analysis of the cryosections of patients 2, 3, and 4 are depicted in Figure 49. Before perfusion, boron concentrations of 12.3, 10.9, and 9.1 ppm were found. The comparison of concentration values before and after perfusion do not lead to a consistent conclusion, as in patient 2 no alteration of the concentration was observed, whereas for patient 3 and 4 29.6 % and 8.8 % less boron was found, respectively. More analysis on that issue was performed with PGAA (see section 3.3.4)

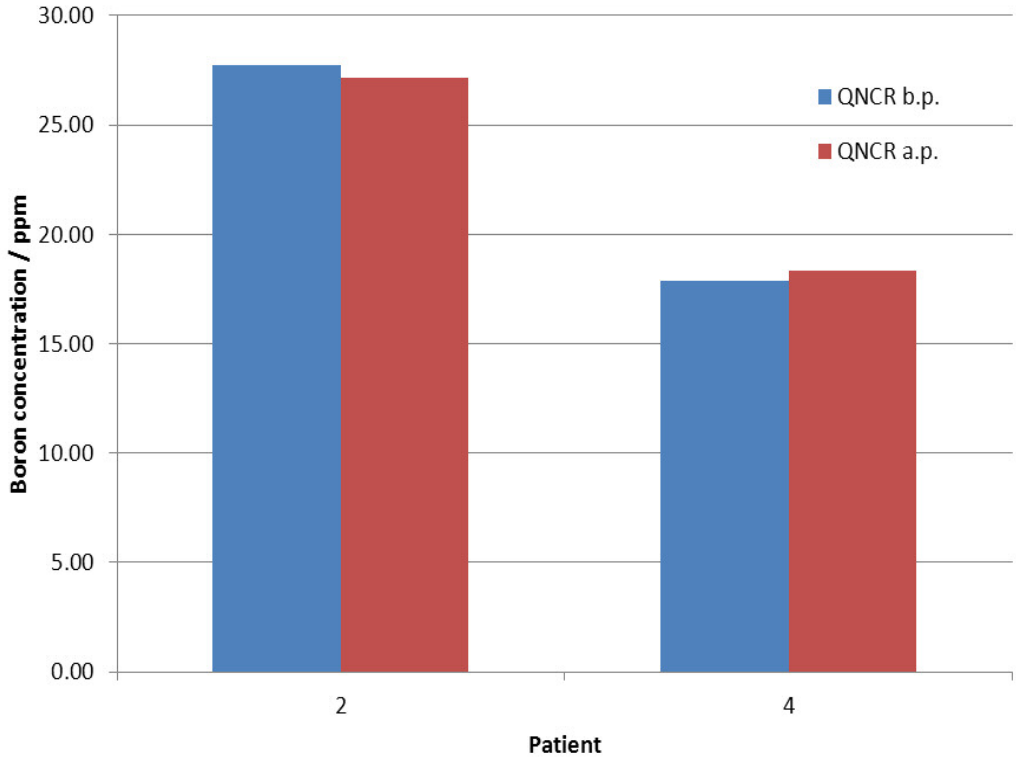

Fig. 48: Boron concentration found in tumour tissue taken before perfusion (b.p.) with HTK solution and after perfusion (a.p.)

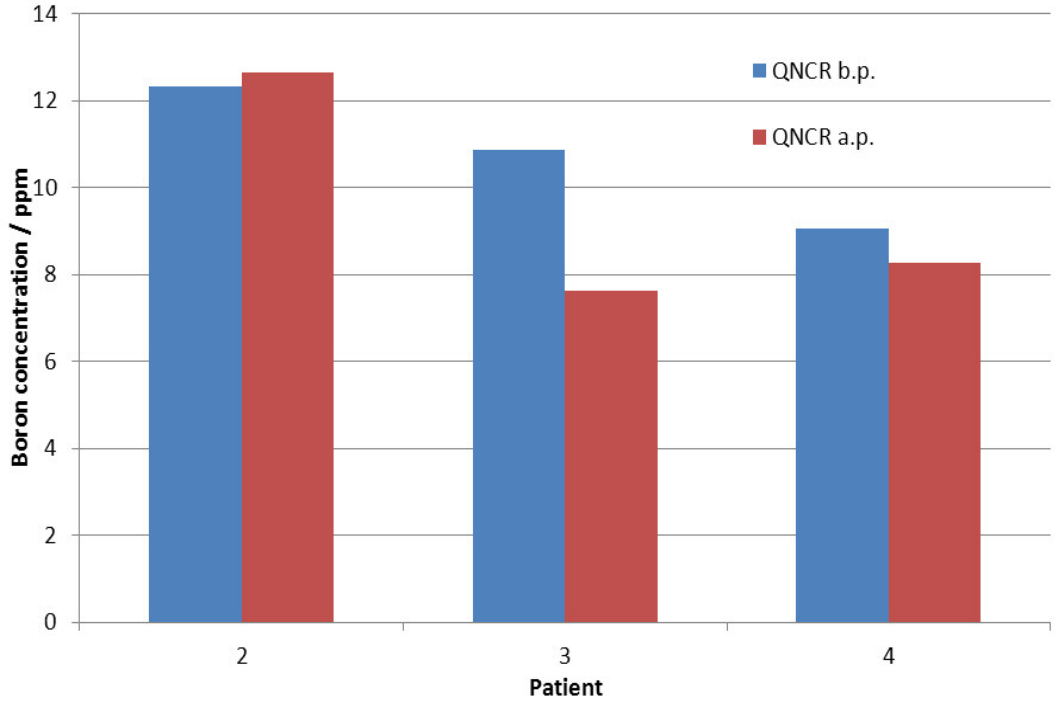

Fig. 49: Boron concentration found in tumour free tissue taken before perfusion (b.p.) with HTK solution and after perfusion (a.p.)

3.3 Prompt Gamma Activation Analysis

3.3.1 Principles of Neutron Activation Analysis and Prompt Gamma Activation Analysis in BNCT

Neutron Activation Analysis (NAA)

Every nucleus has a certain tendency to interact with neutrons in a way that an incoming neutron becomes integrated in the nucleus, which creates an excited compound nucleus. Such a compound nucleus has different possibilities to dispose of its excess energy, namely fragmentation, transformation into kinetic energy, interaction with other nuclei and emission of electromagnetic radiation or particles. In Neutron Activation Analysis (NAA), a sample is irradiated in a neutron field. As a result of the occurring (n,γ) reaction a β^--unstable product nucleus is formed. In its decay, excited energy levels of the daughter nucleus are populated which cause emission of characteristic γ-photons of the different isotopes in the sample. If recorded with an appropriate detector, NAA can be carried out at very low quantification limits (in the µg / g to ng / g range, depending on the element analysed) for a large variety of elements. For NAA no particular sample preparation is needed, unless the sample has to be cleaned to avoid interferences in the γ-spectrum from dirt particles also undergoing neutron activation. As the analysis proceeds without damaging the sample and (if necessary) with very small quantities (several µg), NAA is a very powerful tool for trace analysis.

Prompt Gamma Activation Analysis

Prompt Gamma Activation Analysis is a radioanalytical, non-invasive method based on the detection of prompt-emitted gamma rays upon neutron capture of ^{10}B. As explained in section 1.2, this occurs in 94 % of all ($^{10}B(n,\alpha)^7Li$) reactions. Due to its nature, the prompt γ-spectrum has to be recorded instantly after neutron capture and following fragmentation of the boron isotopes.

The usual procedure in neutron activation analysis includes neutron irradiation of a sample in a neutron field, which is followed by the transfer to a suitable detector or detector array for detection of the γ-spectrum. As there is no time for a transfer of an irradiated sample in PGAA for boron detection to the detector, the latter must be integrated in the irradiation facility. The conception and setup of the neutron beam and the detector is crucial for the quality of the γ-spectra obtained during measurements and, hence, also for the detection and quantification limit of this method. Since research reactor facilities often have initially not been equipped with a PGAA detector setup upon construction, most existing facilities were implemented later, which is why they are all uniquely designed for the facility where they are operated.

3.3.2 Irradiation facilities and detectors used for PGAA

The TRIGA Mainz is unfortunately not equipped with a PGAA setup, which is why the necessary measurements for the samples obtained during the clinical study were carried out at the High Flux Reactor of the Joint Research Centre of the European Union in Petten, and the Forschungsneutronenquelle Heinz-Meier-Leibniz of the FRM II reactor at the Technical University of Munich. As both facilities are very different in design and measurement characteristics, they will be presented shortly below:

The PGAA setup at the HFR Petten

The HFR is a light-water cooled, materials testing reactor of the tank-in-pooltype, operated at 45 MW_{th}. The PGAA facility (Fig. 50) is located at one of the 12 horizontal beam tubes, namely HB07, and was originally described by Raaijmakers et al. [186]. The PGAA setup was custom made for boron analysis in BNCT research. Neutrons coming from the reactor are thermalised by a mirror system made of a Fe-Co-alloy and focussed by a cone-shaped beam collimator to a neutron beam of 3 cm in diameter. At the sample position, the thermal neutron

fluence is of the order of 10^7 n / cm² · s. The space around the sample holder is confined by a shielding system made of three-layers for radiation protection. The first layer is made of PE to scatter incoming neutrons, which are then caught by a 0.6 cm LiF-foil encased in aluminium. Most of the LiF is ^{6}LiF (93 %), which reacts with neutrons in a fragmentation reaction (^{6}Li(n,t)^{4}He)

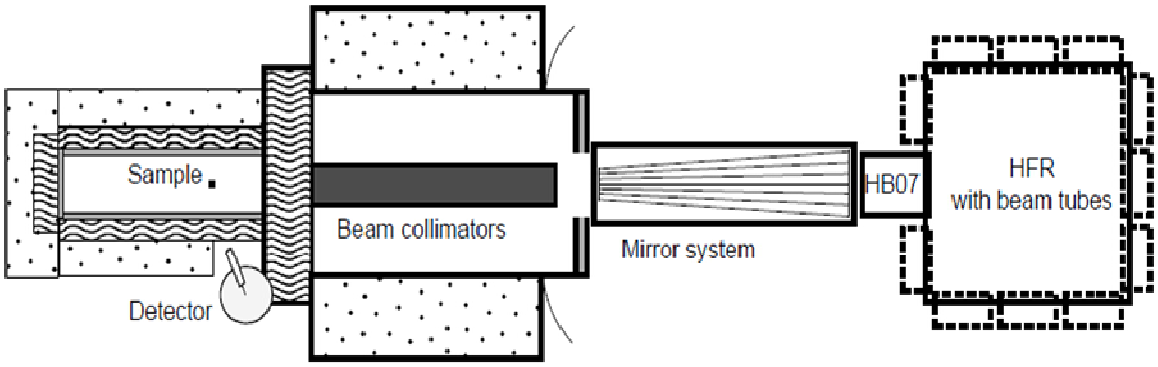

Fig. 50: Schematic image of the HFR reactor facility in Petten and of the PGAA measurement setup (waves: polyethylene; dots on white: Pb; light grey: ^{6}LiF)

The third layer is a lead shield of 10 cm thickness. As shown in Figure 50, the layers are interrupted at one spot to leave some space for the γ-ray detector. The detector is a semiconductor detector made of a cylindrical high-purity Ge-crystal, which is positioned at 60° to the neutron beam to minimise the background created by the γ-rays coming from the reactor core. The samples can be introduced automatically by an autosampling system offering spots for 24 samples.

The PGAA setup at the FRM II in Munich

The FRM II has a compact core with just one fuel element and is operated at 20 MW. The PGAA facility (see Fig. 51) is located at the neutron guide NL4b and has been described by Canella et al. [244]. At the end of the neutron guide, the maximum neutron flux is 6.1 · 10^{10} n / cm² · s. For irradiations the neutron beam can be further regulated with different collimators and moderators to obtain the desired shape and flux. Concerning the samples of the clinical study, the flux was reduced to 7.8 · 10^8 n / cm² · s for patients 1–3 and to 8.3 · 10^8 n / cm² · s for

patient 4. The main difference to the facility in Petten is that a cold neutron beam instead of a thermal neutron beam is used. Also, the background radiation is much lower, which is obtained by the characteristics of the neutron guide between the sample position and the reactor core. The neutron guide is more than 50 m long and curved. Also, there are two gamma detectors available, one high-purity Germanium detector and one NaI detector. All measurements concerning this work were carried out using the Ge-detector.

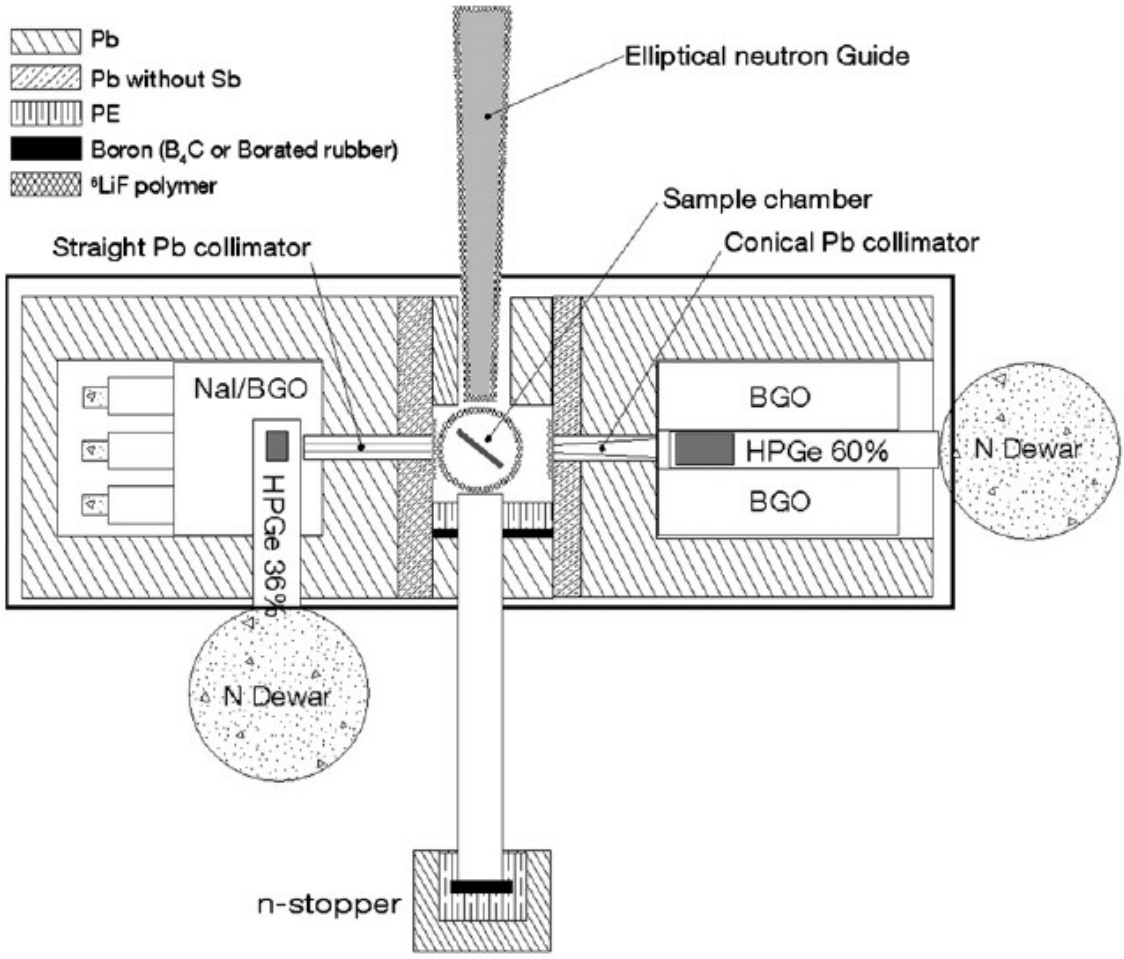

Fig. 51: Schematic image of the PGAA facility at the FRM II reactor in Munich (BGO: Bismuth Germanate) (figure taken from [244])

The quality of the signal spectrum is further improved by a Compton-suppressed spectrometer used for detection of the prompt γ-rays. This is accomplished by a coincidence measurement of all signals in the Ge-detector and in the bismuth germanate crystal (BGO), which surrounds the detector completely. If gamma photon is detected in both the Ge-detector and the BGO due to Compton-scattering of a photon in the detector, it is ignored. This way, the Compton-

continuum-background in the spectra at Munich is much lower compared to those recorded in Petten (Fig. 52).

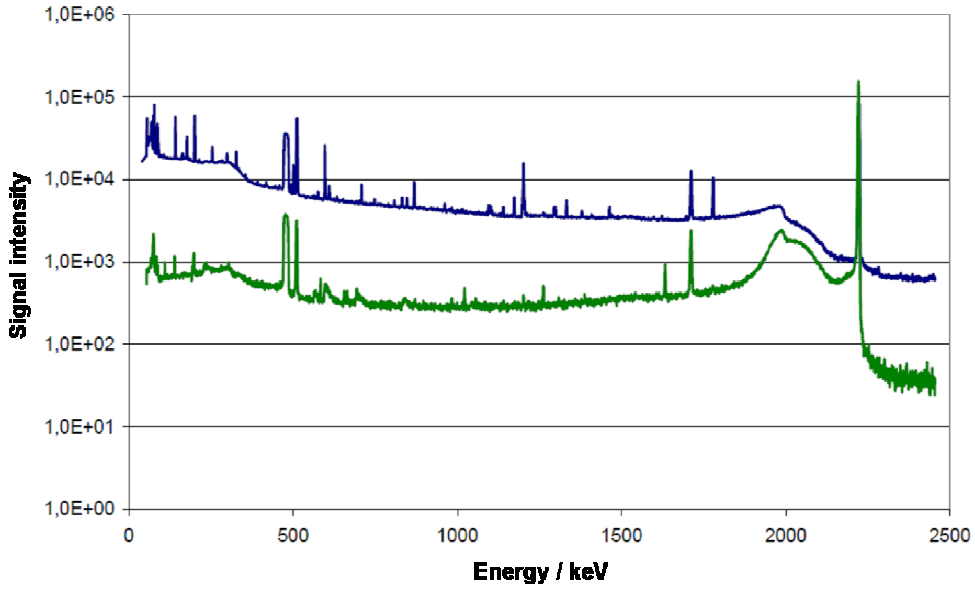

Fig. 52: Gamma spectra of a 40 ppm aqueous boric acid standard measured in Munich (green) and Petten (blue) (with courtesy of [redacted])

3.3.3 Sample preparation

The quality of the measurements depends also on the sample geometry. The blood samples have approximately the same geometry (cylindrical) in the vials as the reference samples, but the tissue geometry can be more different. For calibration at both facilities, freshly prepared aqueous boric acid standards were used.

The actual positioning of the tissue in the vial is very important. for example, for the depth of neutron penetration, especially in Munich, where cold neutrons are used. To overcome such possible problems, the tissue samples have been additionally weighted by the hydrogen signal (2223 keV) using the k_0-method [245]. The hydrogen content in liver tissue is known from literature (International Commission on Radiation Units (ICRU) report, 1992) and has been confirmed via

combustion analysis at the Department of Inorganic and Analytical Chemistry of the University of Mainz.
PE-vials, which were used for sample analysis, make a certain hydrogen background, which is just a small fraction of the hydrogen signal of vials containing blood, but which becomes disruptive for the tissue specimens, because their mass is partly much smaller. Therefore the tissue samples have been measured in PTFE vials which contain no hydrogen. Both blood samples and calibration samples were irradiated for 2500 s.

As mentioned in section 1.6.2, PGAA cannot be used for spatially selective boron quantification. Therefore, no samples from tumour tissue were chosen for determination by PGAA, because the results would not contain any useful information about the uptake characteristics of the different cell types in these very heterogenic samples. All samples were whole blood samples and tumour free tissue samples. Apart from transferring the samples from the cryotubes used for storage to vials with appropriate dimensions to fit into the sample holder at both PGAA facilities, no further processing was carried out. After the measurements, all samples were retrieved and kept for further analysis by ICP-MS (see section 3.4)

For the methodical comparison, two series of reference samples of BPA-f in human whole blood were prepared. One of the series was also used to prepare the second series of reference samples for measurements by QNCR. Both series were prepared for ^{10}B concentrations between 0 and 200 ppm. Details about the preparation of the reference samples can be found in section 3.2.5.

3.3.4 Results of tissue and blood samples

Results of samples taken during the clinical study

In this section, the results concerning the measurements with Prompt Gamma Activation Analysis (PGAA) are presented. A considerable part of the works described in this section has already been published [217]. The biopsies and blood samples of the four patients were measured by [redacted], whereas the measurements for the methodical comparison of PGAA with ICP-MS and QNCR were performed by the author himself. The latter were all carried out at the PGAA facility in Petten, whereas the samples from the clinical study were measured in Petten and at the PGAA facility in Munich.

In this chapter, therefore, also the results of the samples from the clinical study are given to able to provide a complete overview over all three methods used for boron determination (see section 3.5). More details about sample preparation, calibration, and data evaluation for the respective samples may be found elsewhere [217, 246].

Results of tissue samples

In Petten and Munich for patient 1 in tumour free tissue, boron concentrations of 9.3 and 9.0 ppm were found. The respective pairs of values for patients 2, 3, and 4 are 12.0 ppm / 12.0 ppm, 10.1 ppm / 9.8 ppm, and 8.3 ppm / 8.4 ppm. These values are mean values of all biopsies from the respective patient. The relative standard deviation found is ≤ 2.0 ppm and 2.5 ppm, respectively. The limit of detection for both PGAA facilities in Munich and Petten is reported as 1.8 ppm and 1.5 ppm, respectively [186, 244].
The values in tumour free tissue between the two PGAA measurements are in good agreement and are given in Table. 6. The mean boron concentration in tumour free tissue of all patients is 9.9 ppm.

Tab. 6: Results of the PGAA measurements of tissue and blood samples of all four patients. Concentrations are given in ppm				
Patient	Petten ^{10}B-tissue conc.	Munich ^{10}B-tissue conc.	Max. ^{10}B-blood conc.	blood : tissue ratio
1	9.3 ± 0.3	9.0 ± 0.1	23.4 ± 1.0	2.6 ± 0.1
2	12.0 ± 2.0	12.0 ± 2.4	20.8 ± 0.6	1.7 ± 0.2
3	10.1 ± 1.1	9.8 ± 2.5	20.1 ± 1.1	2.0 ± 0.3
4	8.3 ± 0.3	8.4 ± 0.4	15.1 ± 0.5	1.8 ± 0.1

PGAA was also used to assess the potential alteration of the boron concentration in tumour free tissue by preservation solution. As mentioned before, the samples taken before perfusion in the case of patient 1 were needle biopsies too small for the production of cryosections, therefore these biopsies were analysed only by PGAA. After the producing cryosections from the biopsies of patients 2 – 4, only in case of patient 4 enough tissue was left for PGAA analysis. The values found for patients 1 and 4 are shown in Figure 53.

For patient 1 and 4 a decrease of 29.6 % and 24.3 %, respectively, was found. These values are more consistent than those measured by QNCR (see section 3.2.8 or section 3.5. for a direct comparison).

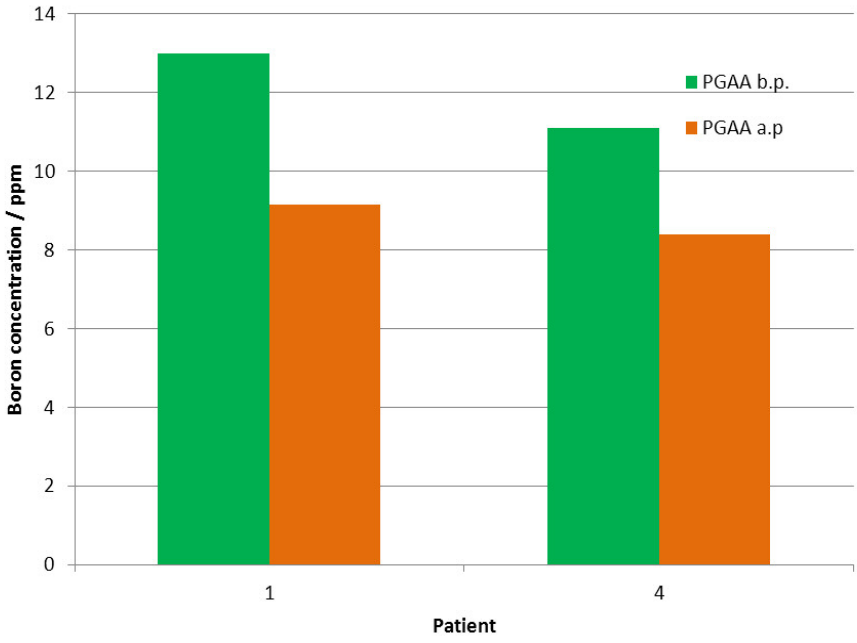

Fig. 53: Boron concentration found in tumour free tissue taken before perfusion (b.p.) with HTK solution and after perfusion (a.p.)

Results of blood samples

The blood samples were taken at 5 points in time (in case of patients 1-3) or at 9 points in time (patient 4). In case of patient 1 the infusomate responsible for the administration of the BPA had a malfunction. Therefore, the infusion was stopped after about 100 min for ten minutes and then re-started with a higher infusion rate in order to administer the whole amount of infusion solution until the scheduled end of the infusion after 120 min. In case of patient 2, surgery proceeded much quicker as anticipated, which is why also in this case the infusion rate was considerably increased after 60 min. Total application time in this case was 90 min. Administration of BPA for patients 3 and 4 proceeded as planned and lasted 120 min.

The time-dependent concentration curves for samples measured in Petten and Munich are shown in Figure 54 and 55. As it was the case for the tumour free tissue samples, the values differ within an error of ≤ 5 %. Standard deviation of the boron concentrations for each time interval is ≤ 2.0 ppm and 2.5 ppm, respectively.

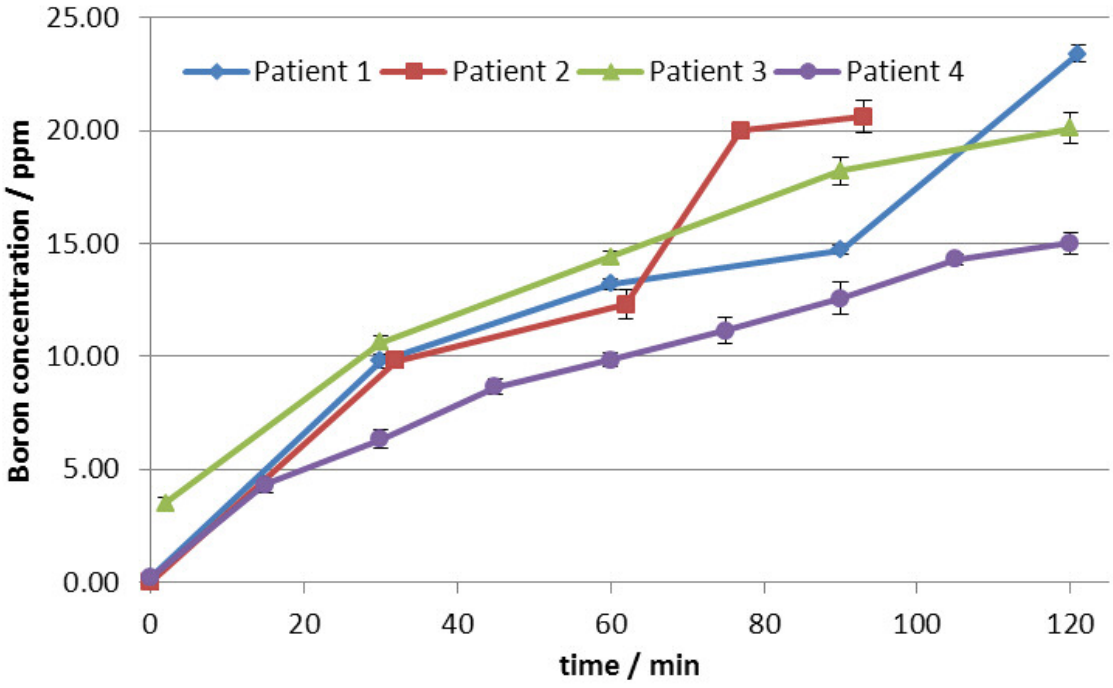

Fig. 54: Time-dependent boron concentration, including standard deviation, measured in Petten in the blood of each patient

The mean maximum concentration of the measurements in Petten and Munich reached for each patient is given above in Table 6. Maximum values for patients 1 - 3 were between 20.1 and 23.4 ppm, for patient 4 a maximum value of 15.1 ppm was reached. The resulting blood to tumour free tissue ratios are between 1.7 and 2.6 (Tab. 6).

In total, only 107 of the 120 blood samples taken during the study were analysed by PGAA (and ICP-MS). Thirteen blood samples were digested for test measurements by ICP-OES at the Technical University of Graz, Austria, which were not included in this thesis.

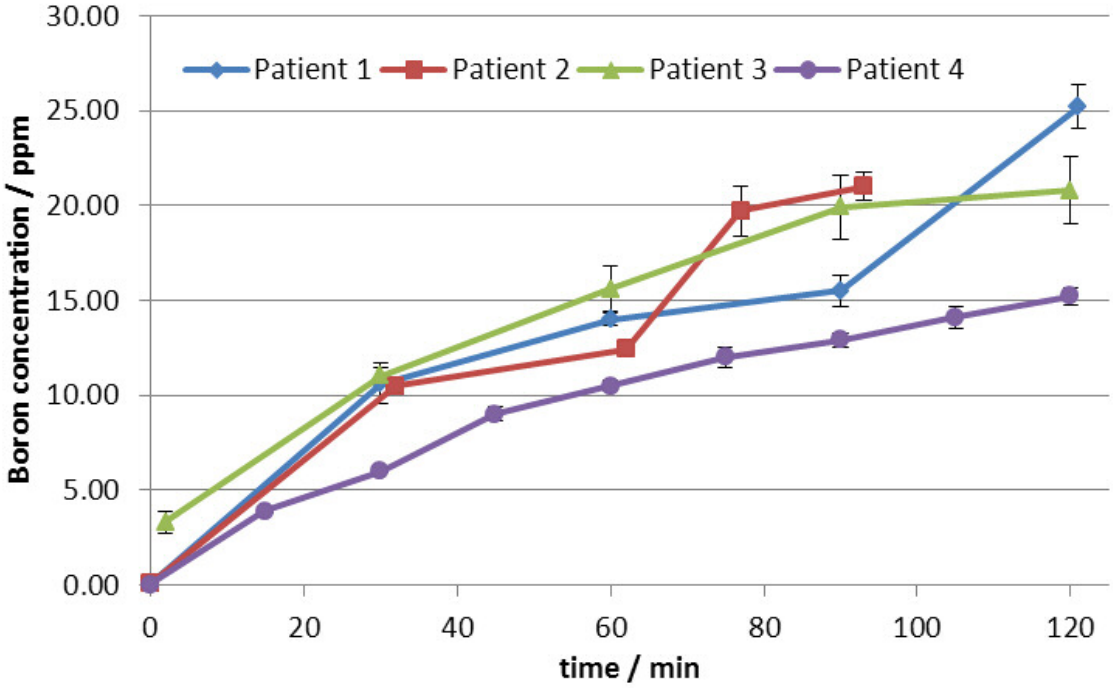

Fig. 55: Time-dependent boron concentration, including standard deviation, measured in Munich in the blood of each patient

Results of blood reference samples used for the production of standard calibration samples for QNCR

Both series of blood samples were evaluated using the same calibration. In Figures 56 and 57 the ^{10}B-recovery for both series is shown. The series in Figure 56 is the one used for the production of the QNCR reference samples. Mean recovery was 100.1 ± 6.9 %. While all samples have recovery values around

100 %, three samples show greater differences. If bearing in mind that the quality of the PGAA spectra recorded in Petten for boron are of not of good quality for samples below 5 ppm, only the sample with the highest boron concentration shows a considerable deviation from the ideal recovery value.

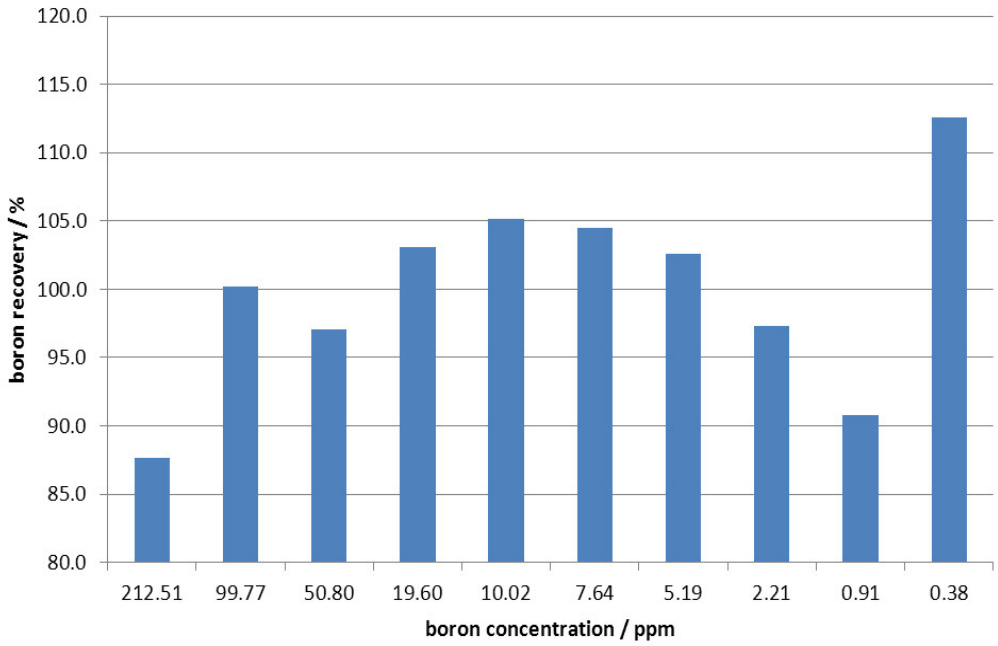

Fig. 56: ^{10}B-recovery for the first series of blood samples. The series was used for the production of reference samples for QNCR as well.

The second series showed recovery values comparable to those of the first series (mean recovery of 96.0 ± 8.7 %). Due to problems with the autosampler, two samples of this series were not measured correctly, therefore only the values of seven samples are reported here. Also in this case, one value varied considerably from the ideal recovery of 100 %. It was not possible to determine why single values varied so much from the desired 100 % recovery, the quality of the spectra did not show any qualitative changes within one series.

Total measurement uncertainty for the boron determination by PGAA in both facilities is known, being 3 % (Munich, [244]) and 5 % [247]. For calibration, certified standards (with an uncertainty of 0.1 % of the boron concentration) were used. The uncertainty during sample preparation (carried out completely by weighing the liquids) depended only on the analytical balance, therefore propagation of uncertainty was deemed negligible.

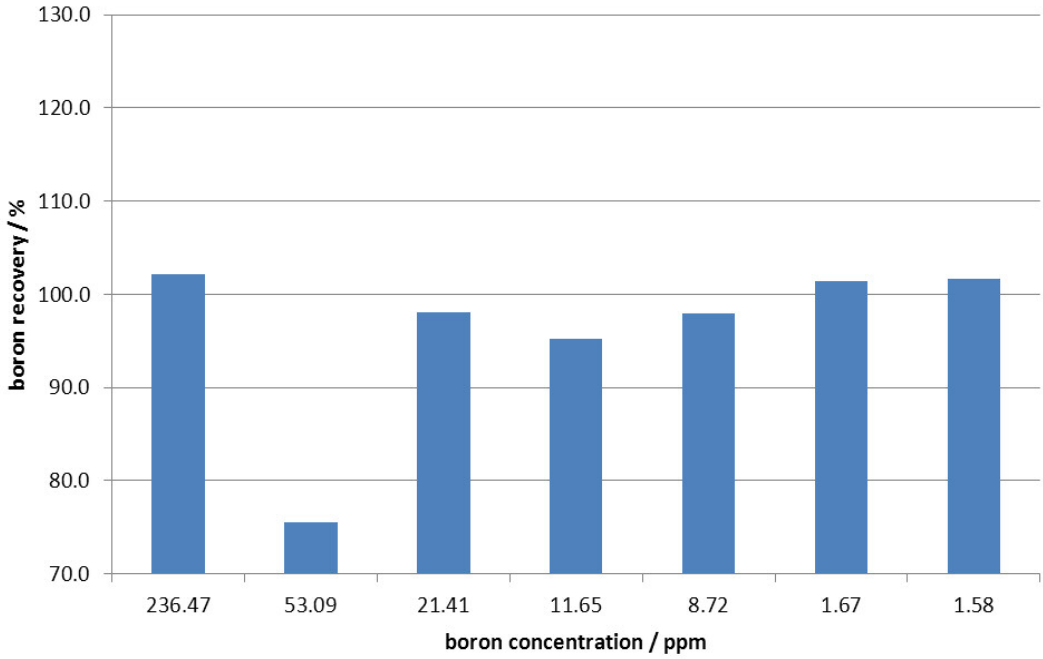

Fig. 57: ^{10}B-recovery for the second series of blood samples.

3.4 Inductively Coupled Plasma Mass Spectroscopy

3.4.1 Brief introduction to Inductively Coupled Plasma Mass Spectroscopy

The term ‘Inductively Coupled Plasma Spectroscopy’ describes two analytical techniques, which share several characteristics in their technical conception and their application: Inductively Coupled Plasma Optical Emission Spectroscopy (ICP-OES) (or Inductively Coupled Plasma Atomic Emission Spectroscopy, ICP-AES) and Inductively Coupled Plasma Mass Spectrometry (ICP-MS).
As the work related to this thesis was carried out using ICP-MS, ICP-OES will be not be presented in detail, however a short summary of the possibilities posed by Inductively Coupled Plasma Spectroscopy in BNCT can be found in section 3.4.2.
ICP-MS is a powerful method as it combines multi-element analysis with high resolutions with the possibility of speciation and isotope specific analysis.
A general schematic design of an ICP-MS is given in Figure 58. The most relevant components of ICP-MS instruments will be briefly presented in the following paragraphs.

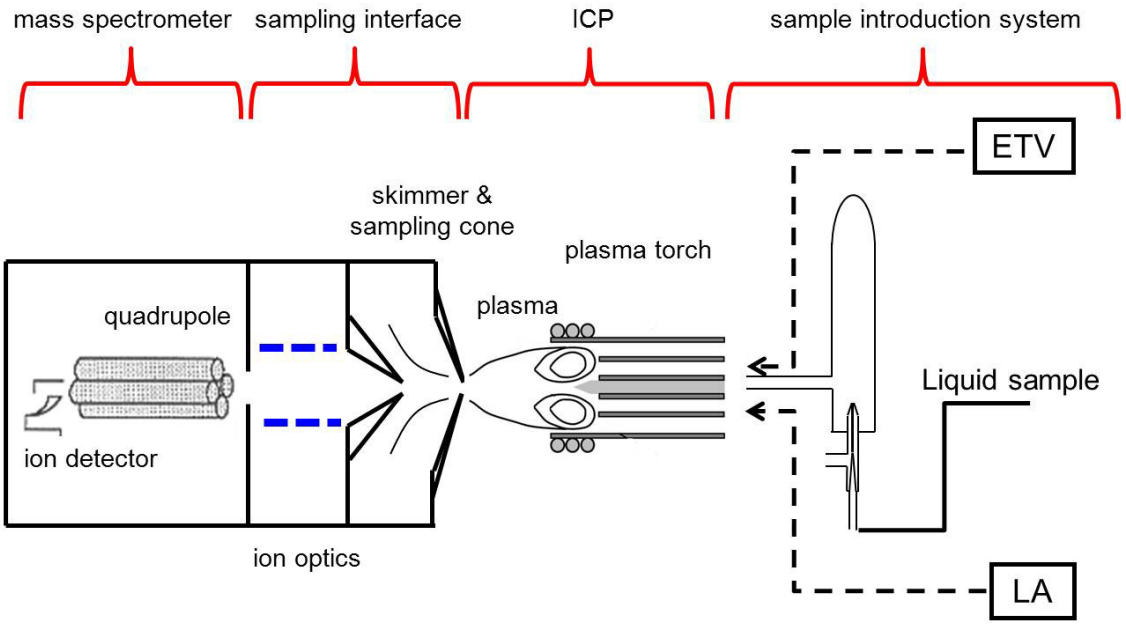

Fig. 58: Schematic design of the main components of an ICP-MS processing liquid samples

All measurements presented in this thesis were carried out with an ICP-MS system processing *liquid* samples. Therefore, all considerations regarding performance and comparability of ICP-MS measurements towards other methods are uttered for this type of sample introduction, if not mentioned explicitly otherwise.

Sample introduction

Most sample introduction systems for ICP-MS require the use of liquid samples. Liquids can be injected directly into the plasma (direct injection nebulisation, DIN), although this method allows only very small quantities (several µl / s) to be injected. The more common approach is the use of a self-aspirating, ultrasonic or pneumatic nebuliser, which permit larger quantities of liquid (up to several hundreds of µl / s).
If solid material has to be examined without liquification, it can be achieved either by electrothermal vaporisation (ETV-ICP-MS) or laser ablation (LA-ICP-MS). The latter enables the analyst additionally to perform locally selective analysis by ICP-MS.
To widen the analytical spectrum, ICP-MS can be furthermore combined with chromatographic and separation methods such as gas chromatography (GC), high-performance liquid chromatography (HPLC), liquid chromatography (LC), and capillary electrophoresis (CE).

Aerosol production

Nebulisers are made of glass or from an assortment of plastics. The choice of the nebuliser material is usually linked to the desired application. Furthermore, different designs are available, the most common being concentric (Fig. 59) and cross-flow nebulisers. For all works presented in this thesis glass concentric nebulisers were used.

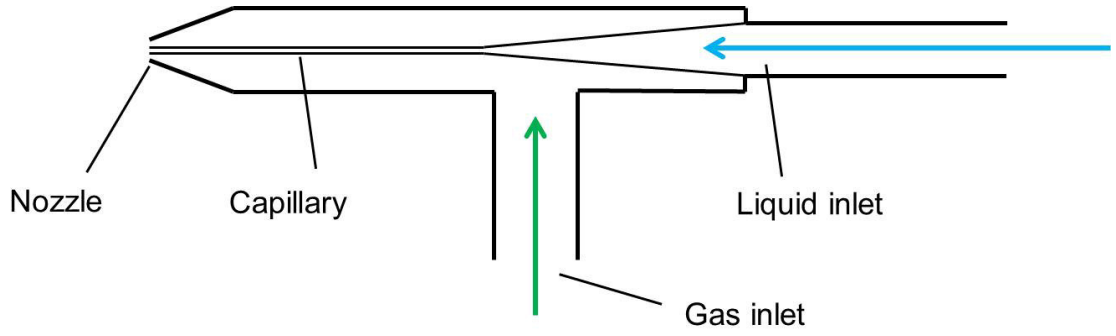

Fig. 59: Schematic design of a glass concentric nebuliser

Spray chambers

The mist of droplets of a large range of different sizes and shapes produced by the nebuliser is filtered by using a spray chamber. Spray chambers force the droplets to follow a certain flight path, which eventually separates aerosols by their aerodynamic properties. Larger drops exit the spray chamber via the drain directly or after hitting the surface and, thus, are lost for analysis. Like nebulisers, spray chambers can be manufactured using different materials (again, glass or plastics) and designs. The designs mainly used in ICP-MS application are conical, cyclonic, and Scott-type spray chambers. To reduce vapour loading in the aerosol, spray chambers can be additionally cooled. All works presented in this thesis were carried out using Scott-type spray chambers.

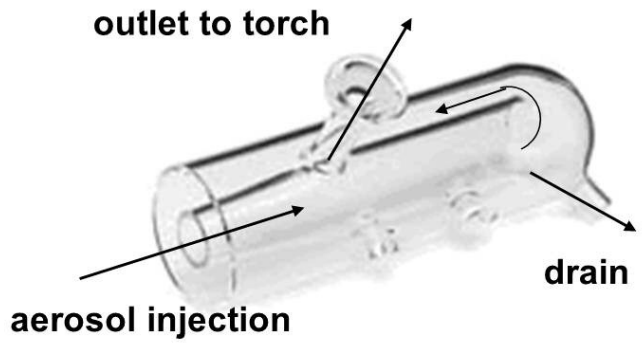

Fig. 60: Scott-type double-pass spray chamber made of quartz glass. Image taken from www.agilent.com (date of retrieval: 11/06/2011).

The inductively coupled plasma

As ultimately ions have to be detected, a number of steps occur from the moment of introduction of the aerosol until the registration of the analyte by the detector:

$$\text{Droplet} \xrightarrow{\text{Desolvation}} \text{Solid} \xrightarrow{\text{Vaporisation}} \text{Gas} \xrightarrow{\text{Atomisation}} \text{Atom} \xrightarrow{\text{Ionisation}} \text{Ion}$$

All these steps occur passing within milliseconds in the plasma. A plasma is a macroscopically neutral, ionised gas, consisting of the same number of positive particles (ions) and negative particles (electrons). Plasmas can be initiated and maintained by a number of methods, they can be classified according to the field by which they are created: direct current plasma (DCP), microwave induced plasma (MIP), and inductively coupled plasma (ICP). While MIPs are generated applying a microwave field to a cavity, DCPs are obtained by a direct current field across electrodes, and ICPs are generated when a high frequency field is applied through a coil. Such fields are created by radiofrequency (RF) generators that operate usually using piezo-electric crystals at a fixed frequency (usually multiples of 13.56 MHz).

As plasma gas in most cases, Argon is chosen. Argon is very abundant in air (~ 1%) and therefore the cheapest noble gas. Its first ionisation energy (15.759 eV) enables it to ionise all other elements except for F, Ne, and He, which have higher first ionisation energies. Being a noble gas, in the plasma it forms only very short lived compounds with other elements, thus minimising potential interferences. Dependent on the desired analysis, also other gases can be chosen or used in a mix together, each with different advances and drawbacks. The typical plasma power applied in ICP-MS is between 900 and 1600 W.
Dimension and shape of the plasma are influenced by the plasma torch and the gas flow. Torches are made of quartz glass and consist of three concentric tubes with different diameters. While there are micro-torches requiring less Argon, the design of a torch generally varies only in diameter of the tubes and position of the gas inlets. Most torches are manufactured in a way that they are one demountable piece, there are also torches consisting of a number of separable parts.

Each tube carries defined streams of gas which eventually meet at the end of the torch. The innermost tube carries the aerosol coming from the spray chamber (carrier or nebuliser gas). The second innermost tube carries the auxiliary gas stream with the function to “lift” the plasma away from the torch to prevent melting of the glassware. The outermost tube carries a coil-shaped stream of gas (plasma gas), gives the plasma its annular shape. Torch and plasma are shown in Figure 61.

In all works concerning this thesis, a Fassel-type torch additionally equipped with a torch shield made of platinum was used. Torch shields are grounded metal plates attached to the outlet of the torch to prevent the formation of polyatomic ions usually caused by capacitive coupling between plasma and the grounded sampling interface.

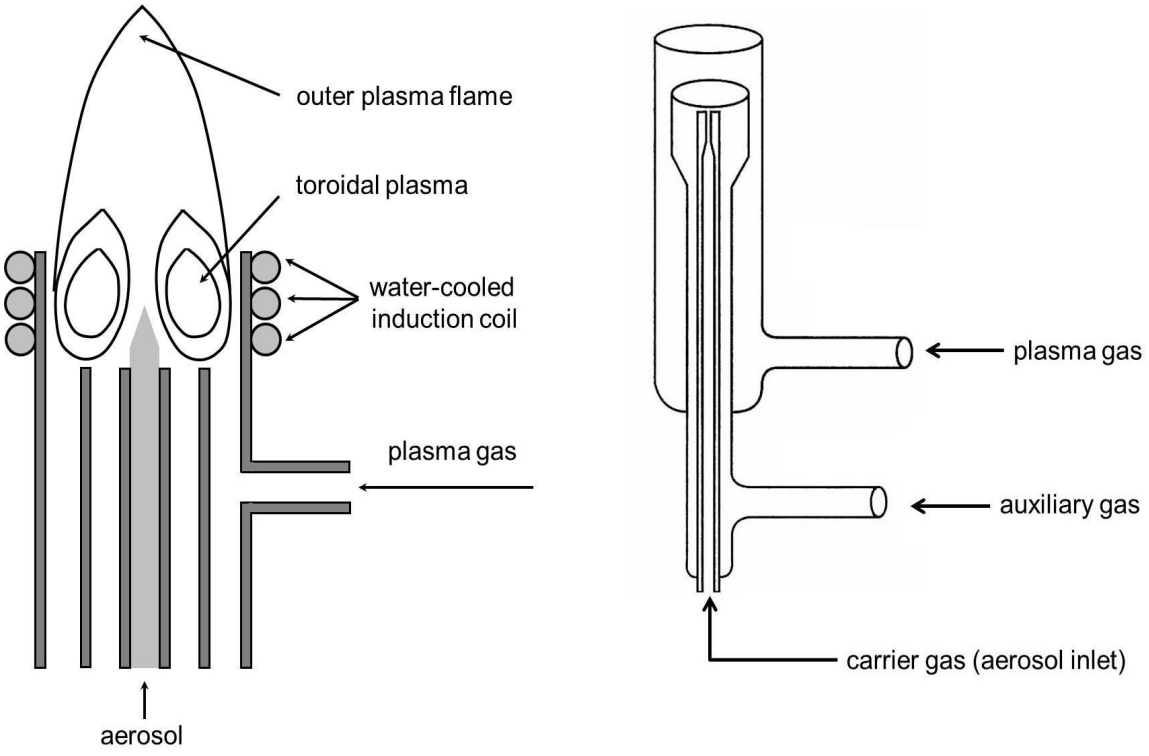

Fig. 61: Schematic design of a Fassel-type torch and the plasma (figures used with courtesy of [redacted], University of Cologne, Germany)

Sampling interface and ion optics

The sampling interface is designed to extract an ion beam from the plasma cloud, which can then be directed through the mass separator to the detector (Fig. 62). It consists of a water cooled sampling cone and a skimmer cone made of copper, nickel, or platinum.

Behind the cones, the ion optics can be found, a set of metal plates subjected to different voltages, which serve to separate all neutral species (UV photons, unionised atoms et cetera) from the desired ion beam. Most companies producing ICP-MS have special designs for the single components of the ion optics to shape and direct the ion beam.

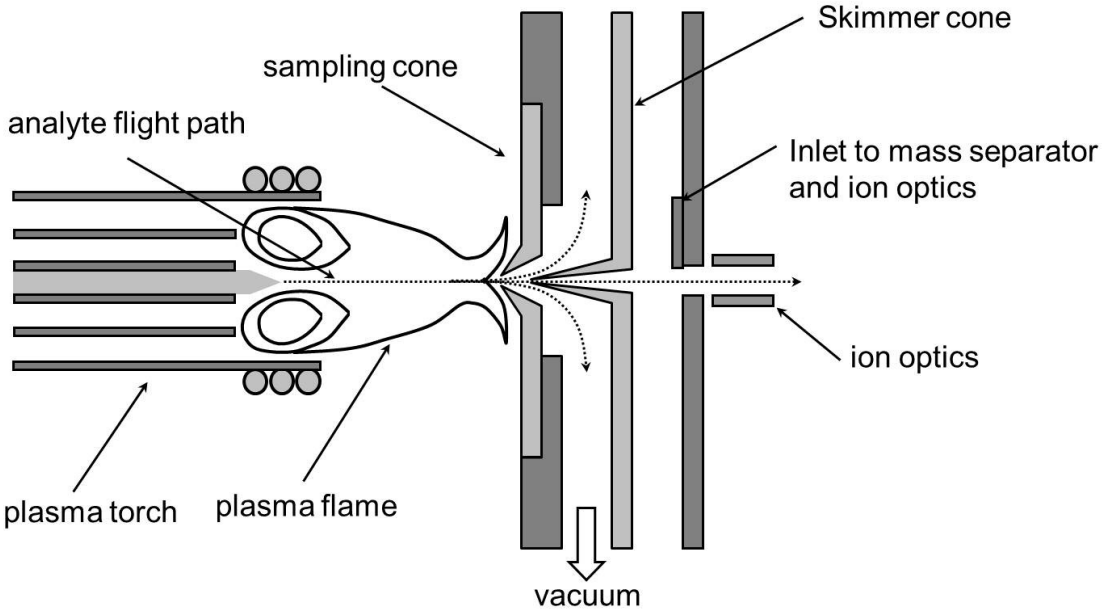

Fig. 62: Schematic design of the the ICP-MS interface assembly (figure used with courtesy of [redacted], University of Cologne, Germany)

Mass separation and ion detection

The most frequently found types of mass separators are magnetic sector analysers (appearing also in combination with an electrostatic sector as double-focusing mass analysers) and quadrupoles. Double-focusing sector instruments use the two fields to disperse ions with respect to their translational energy and momentum. Such instruments are characterised by their vastly higher resolution

compared to quadrupole instruments, but also by their cost and complexity in operation. Figure 63 shows the schematic design of a quadrupole mass separator.
A quadrupole consists of two pairs of electrically conducting rods. Two opposing rods make up one pair. Both pairs are supplied with a direct current voltage, one positive, the other negative. Additionally, both pairs are supplied with a radiofrequency field, thus creating an oscillating field between the rods. Ions passing through the rods are forced on a spiral flight path. The voltages can now be adjusted in a way that ions either pass through the quadrupole and reach the detector or that they collide with the rods and loose their charge.
As detectors, Faraday cups and electron multipliers (mostly different types of dynodes) are used.

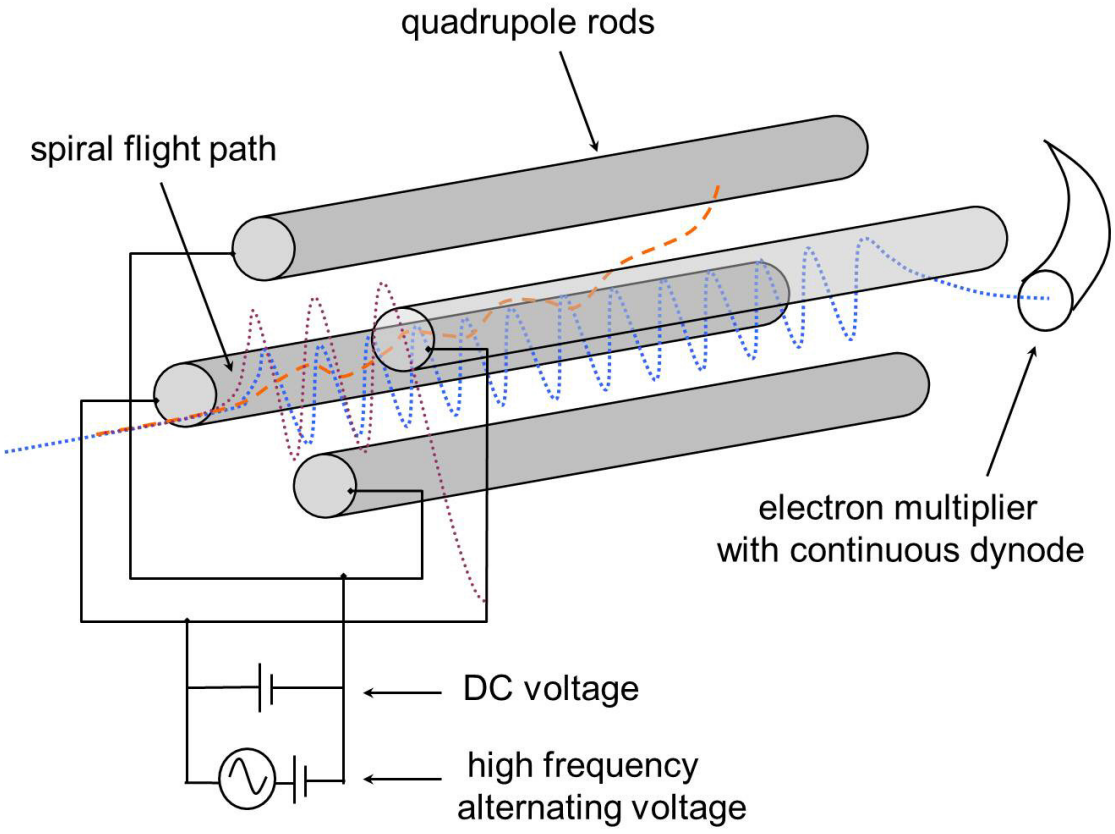

Fig. 63: Schematic design of a quadrupole mass filter (figure used with courtesy from [redacted], University of Cologne, Germany)

3.4.2 Boron determination by ICP-MS and ICP-OES particularly in BNCT

Both ICP-MS and ICP-OES are very often used for boron determination, for all kinds of sample matrices. Naturally, in BNCT research, boron determination in biological samples is a key issue and both methods are used by a number of groups. They show little difference in measurement performance when it comes to measuring samples equally prepared following the same protocol [164, 173].
Though both methods are only able to provide the integral boron concentration of a given sample, which is not a problem when analysing *in vitro* and blood samples. They have also been used for all kinds of tissue samples as well. Such analysis is usually combined with morphological or histological analysis to categorise tissue samples (mostly as “tumour tissue” or “healthy tissue”) before measurement. In a few cases, boron determination was carried out alongside immuno-histochemical staining or together with biological markers [88, 129, 248].

Apart from boron determination in clinical research projects, rapid and reliable boron determination is required during clinical application of BNCT for monitoring of the blood boron concentration or the boron concentration in tissue of a patient, which is decisive for dose calculation and for determination of the optimum point in time for neutron irradiation. This analysis must be quickly performed, in order to be able to adapt treatment planning as precisely as possible. Also, it may be necessary to choose a method with a high throughput of samples. While PGAA combines both abilities of being quick and therefore being able to theoretically analyse a large number of samples within a short time, it is not accessible to all groups, because it requires a very strong neutron source with a specially tailored neutron spectrum. As a result, alternatives like ICP-MS and ICP-OES are of interest.

When comparing analytical protocols published so far, it becomes clear that there is no standardised procedure for boron analysis in either of the methods. Most groups use individually created protocols for sample preparation, calibration, internal standardisation, and rinsing between samples. As stated above, especially for monitoring quick sample preparation is of great interest. Different groups have reported to perform boron analysis in blood samples within minutes by

DCP/ICP-OES and PGAA [25, 27, 43, 249–251] (among others) mostly relying on sample dilution to save time.
As it will be laid out in the following sections, different approaches for sample preparation and boron determination published in literature were tried and finally not considered to be suitable for the task, until a reliable protocol for routine analyis by ICP-MS was established.

3.4.3 Sample preparation

ICP-MS and ICP-OES are both methods requiring injection of liquid samples, if laser ablation or electrothermal evaporisation are not available for sample introduction. Though it is possible to inject organic solvents, it is far more common to use aqueous solutions. For boron determination in biological samples, usually complete decomposition of the samples is required, however, also mere dilution of whole blood or blood plasma has been reported for sample preparation [175, 252]. The most commonly applied were already presented in section 1.6.2: wet open vessel digestion by mineralic acids [153–155] or under basic conditions [156], dry ashing [153], wet ashing [118], fusion [157], combustion in oxygen atmosphere [158], liquid extraction with hot water [159] or nitric acid [160] and, favoured as a very reliable technique, microwave digestion [153, 159, 161–163].

When starting the work on biological samples, no possibility for combustion or microwave digestion was accessible for the size and quantity of the samples obtained during the clinical study.

Wet open vessel digestion

Therefore, wet open vessel digestion with basic and acid solutions was tried to enable the analyst to use ICP-MS as analytical technique. All tests with tissue samples were carried out with bovine liver purchased from a local butcher, whole blood was obtained from the blood bank of the University Hospital. All chemical

compounds used for sample preparation were checked for their boron content by ICP-MS measurement. This was first done for purified water, which was used as solvent for subsequent analysis of solid chemicals.

For acid sample decomposition, a combination of 65 % (w) HNO_3 and 35 % (w) H_2O_2 in a ratio of 2 : 1 was used for the liver samples weighed 400 to 900 mg in PTFE vessels. The vessels were closed between adding HNO_3 and H_2O_2 with a cap. When left at room temperature for an entire day, no more than “bleaching” of the sample surface was achieved. Therefore, the solution was kept at 70°C, while acid and peroxide were constantly added and evaporated. A mean amount of 88.8 ml ± 14.9 ml of HNO_3 and 43.8 ml ± 8.8 ml H_2O_2 were needed to reach sufficient sample decomposition. Acid and peroxide were added in 2 ml and 4 ml steps over 4 – 12 h. When left overnight, several of the samples showed larger solid particle formation the next morning.
Blood samples treated the same way never yielded fully decomposed samples. Although clear solutions were obtained, in almost each case large white particle clusters were floating in the solution, which were most probably acid induced protein formations, which were partly still insoluble when half-concentrated $HClO_4$ was added.
As a result, wet open vessel digestion for either blood or tissue samples was discarded as a technique too unreliable.

For basic sample decomposition, 10 % tetramethylammonium hydroxide (TMAH) was used. For each mg of sample 5 µl TMAH solution were added. First experiments with larger liver samples (up to 500 mg) heated at 70°C for two hours yielded brown solutions with large amounts of floating solid particles. When left without heating for up to 24 h, clear solutions were obtained, though partly larger chunks of residue of the original sample were floating in the solution and required the same amount of TMAH added for complete dissolution. The same approach carried out with the same amount of tissue cut to smaller parts of 40 – 60 mg each yielded clear solutions without visible solid particle formation after 1 - 24 h.

Though basic decomposition proved to be effective for samples of higher granularity, the time needed for sample decomposition was partly very long.

Another simple option for liquid sample preparation is dilution of whole blood or serum was tried as well, the outcome will be presented in section 3.4.4.2.

Microwave assisted sample digestion (wet-ashing)

After some time, fortunately together with the Department of Inorganic and Analytical Chemistry, the use of a laboratory microwave (Milestone ETHOSplus2, Shelton, CT, USA), enabling the user to perform digestions in ten separate vessels simultaneously, was made possible.
Sample digestion in a microwave comes with a number of practical advantages for the analyst. As the sample decomposition takes place in closed vessels, no external contamination or loss of sample material is possible. Furthermore, the digestion process takes place at high temperatures (up to 200 °C) and high pressures (up to 20 bar), which helps to completely decompose the sample material. However, this also prevents the analyst from immediately continuing sample preparation after microwave digestion, because a certain cool-down time is required before opening the vessels again.

For all works concerning sample preparation, the use of glassware was avoided. Laboratory glassware is usually made of borosilicate glass. As in contact with either acid or basic solutions, leaching of boron of no negligible amounts is to be expected, such glassware is obviously not fit for use in boron analysis. Hence, for the works described in this thesis, all solutions were stored in PTFE or perfluoroalkoxy (PFA) vessels. For routine laboratory works, also polyethylene (PE) vessels were used. The only pieces of glassware in direct contact with either solutions used for digestion or sample workup were nebuliser, spray chamber, transition tube and plasma torch.
For microwave sample digestion, PTFE vessels were used exclusively. PTFE is often used for microwave vessels, because the material is fit to resist the aforementioned high temperatures and pressures. Between digestions, all vessels were cleaned by HNO_3 vapour in a subboiling vessel cleaner. Before using the vessels for analysis for the first time, the vessels were used for the digestion of purified water (18.2 MΩ), followed by cleaning in the subboiling vessel cleaner.

This cycle was repeated until the background signal for lithium, boron, beryllium, magnesium, scandium, titanium, manganese, cobalt, copper, cadmium, rhodium, tin, and uranium, monitored by ICP-MS measurements, reached a constant minimum level for each element.
The vessels were additionally covered with caps containing a spring which would allow the release of the reaction gases, if the pressure inside the vessels surpasses 20 bar.

For the decomposition of 500 mg of organic material (blood or tissue), concentrated HNO_3 (4 ml) and H_2O_2 (2 ml) in combination with water (4 ml) were added to absorb the nitrogen oxide gases produced during digestion. For reaction safety and control of the digestion process, the microwave is equipped with a sensor to detect leaking reaction gases and with a temperature sensor in the principal reaction vessel. Consequently, the digestion was monitored by the temperature sensor. Heating eventually involved a four-step protocol, the microwave power was adjusted automatically between a range of 0 and 1000 W to match the previously set course of temperature: First, the vessels were heated for 2 min to a temperature of 75 °C, followed by 5.5 min heating to reach a temperature of 130 °C. After a period of 4 min heating to reach 200 °C, the temperature was kept stable at this temperature for additional 12 min. After a total heating time of 25.5 min, the microwave was ventilated for 30 min to facilitate cooling and pressure reduction inside the reaction vessels.
After digestion, the liquefied samples were transferred to PE-tubes. The PTFE vessels were rinsed with purified water, which was also further added to the PE tubes to reach a volume of 25 ml. The obtained solution was diluted tenfold for ICP-MS measurement with a solution containing 2 % Butanol, 1 % NH_3, 0.05 % EDTA and 0.05 % Triton-X 100 (all percentages are weight percentages).
The decision to use this solution emerged from a series of experiments assessing the difficulties of rinsing boron from the ICP-MS. This will be further looked at in the following section.

3.4.4 Development of the analytical protocol for ICP-MS measurements

Though ICP-MS is a versatile analytical method, there are elements whose analysis can be very demanding. Major factors to be considered are elemental composition of the sample matrix, the range of concentration in which the analyte is to be detected, the desired limit of quantification et cetera.
Boron is one of the elements with the characteristics of creating a particular challenge for the analyst. In this section, experiments undertaken ultimately leading to the creation of a verified analytical protocol for boron measurements by ICP-MS will be presented.

3.4.4.1 Optimisation of sample introduction assembly and rinsing protocols

Sample introduction

Sample introduction is one of the key steps when performing analysis of any kind with ICP-MS. The properties of all surfaces have to be taken into account, as the analyte is in direct contact with a variety of tubes and parts before it is injected as aerosol into the plasma. The standard sample introduction array of an Agilent 7500ce ICP-MS consists completely of glassware, i.e., quartz glass. As spray chamber, a Scott-type double pass spray chamber is the standard equipment (Fig. 60).
Several nebulisers made of quartz glass (all Micro Mist ®, with sample uptake rates of 50, 100, and 200 µl / min, respectively) were accessible and were tested with respect to the combination of signal intensity, signal stability, and relative standard deviation of the signal. After working with all of them, the nebuliser with the best performance proved to be the one with an uptake rate of 200 µl / min).

For the work with liquids containing boron, quartz glass is the logical choice when compared to borosilicate glass. However, there are still adsorption and resorption effects to be expected. Unfortunately, these effects do not follow a fixed rule, i.e.,

the exact influence on the boron signal occurs randomly and is hardly predictable. As a result, the best solution to avoid this problem is to exclude such effects as far as possible. To do that, two countermeasures are at hand: The optimisation of the rinsing solution, which clears out the boron from the sample introduction array, and the use of material for the array with lesser tendency to let adsorption and resorption happen on its surface.

Entire sample inert-kits consisting almost completely of PFA, with exception of the torch, which has to be made of quartz, are commercially available. Since such an inert-kit could not be purchased for the works presented, it was tried to work with some parts of the sample introduction array, which were separable and could be exchanged.

This included (A) a Scott type single-pass spray chamber, (lacking the central tube normally, compared to a double-pass spray chamber), i.e., the aerosol drops have to pass around only one corner instead of two. made of PFA, which was kindly provided by the group of Prof. Dr. Nicolas Bings, Department of Inorganic and Analytical Chemistry and (B) a Mira Mist ® nebuliser made of PFA with a liquid uptake rate of 20 µl / min, which was available at the Institute for Nuclear Chemistry.

In initial tests, it became obvious that the Micro Mist nebuliser produced far too few aerosol to create a signal with appropriate count rates for neither of the two spray chambers available. Consequently, the tests to determine the performance of the spray chambers were continued with the 200 µl / min quartz glass nebuliser.

Rinsing

First tests revealed that the pH of the solution containing boron could influence the rinsing behaviour, therefore, rinsing of boron from both basic and acid solutions was tested. At first, five optional rinsing solutions were considered, i.e., purified water (W) and two acid (A1/A2) and basic (B1/B2) solutions each:

- 1.25 % HNO_3 (A1)
- 1.25 % HNO_3 (obtained from subboiled distillation) (A2)

- A solution consisting of 3 % NH_3 + 0.25 % mannitol (B1)
- A solution consisting of 2,5 % butanol + 1 % NH_3 + 0,05 % EDTA + 0,05 % Triton X-100 (B2)

All chemicals were purchased from Merck, Darmstadt, Germany. The most common standard rinsing solution when performing analysis with ICP-MS, is low concentrated HNO_3, although most analysis with ICP-MS is carried out for the detection of transition metals. Fresh, subboiled HNO_3 is of higher purity than commercially available p.a. grade HNO_3 and was therefore considered as rinsing solution producing a lower background. Subboiled distillation was carried out in a quartz glas apparatus at the Department of Inorganic and Analytical Chemistry.
Both basic solutions were tried, because they were recommended in different publications [89, 253, 254] to minimise memory effects and to optimise the general rinsing of boron. Solution B1 offers the potential to rinse boron by complexation with mannitol. In solution B2, butanol was added to achieve a stable background for ^{11}B (more about this issue can be found in section 3.4.4.2), Triton-X 100 was added because of its ability to act as detergent and EDTA was added because of its chelating properties helping to complexate boron and to keep other elements in solution. Ammonia was added to both solutions as it was reported as well to assist elimination of memory effects when measuring boron [255].
For all rinsing experiments, a 160 ppb boron solution was prepared. The boron standard was diluted from a 1000 ppm boric acid solution purchased from High Purity Standards, Charleston, SC, USA, for dilution 1.25 % subboiled HNO_3 was used. Only the decrease of the ^{10}B signal was considered to evaluate the performance of the different rinsing solutions, because the ^{11}B is constantly influenced by the ^{12}C peak.

Rinsing from acid boron solutions

First, the rinsing experiments were carried out using the quartz glass double-pass Scott-type spray chamber (SC1). Rinsing from an acid boron solution was tried, as in most publications, boron analysis was performed after acid sample dissolution

or digestion. The results are shown in Figure 64. The percental decrease of the total boron signal is shown over time.

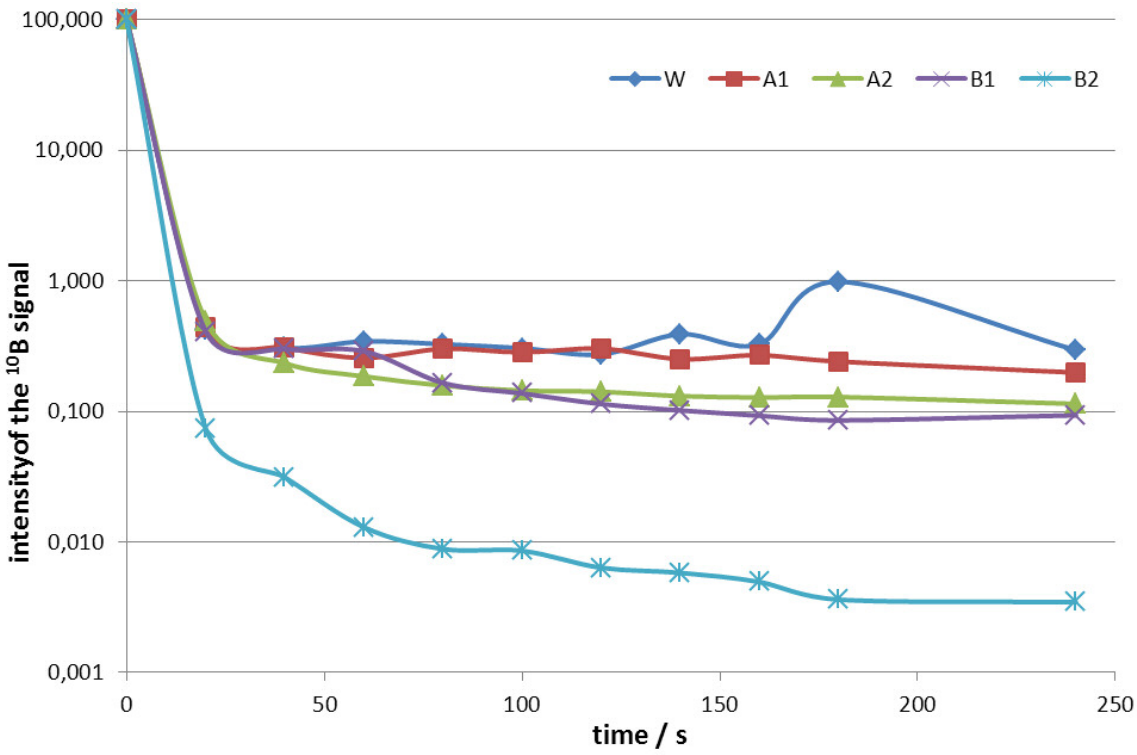

Fig. 64: Decrease of the boron signal while rinsing from an acid solution with five different rinsing solutions (sample injection setup SC1)

The rinsing performance of water and solutions A1, A2, and B1 are roughly comparable, whereas water showed the worst performance as expected. Though in all cases the signal fell steeply within the first 60 seconds, the final background signals were different. A2 rinsed better than A1, however, the difference was so small that for all future experiments only A1 (1.25 % HNO_3) was used, as the production of fresh subboiled HNO_3 was very time consuming. With both basic rising solutions better background signals were reached, especially B2 proved to be very effective.

The same experiment carried out for the sample injection setup using the PTFE spray chamber (SC2) yielded similar results (Fig. 65): basic rinsing solutions were more effective than acid solutions, B2 was the most effective of all solutions, though HNO_3 did not seem to be more effective for rinsing than water. The background values reached for boron were comparable to those reached when using sample injection setup SC1.

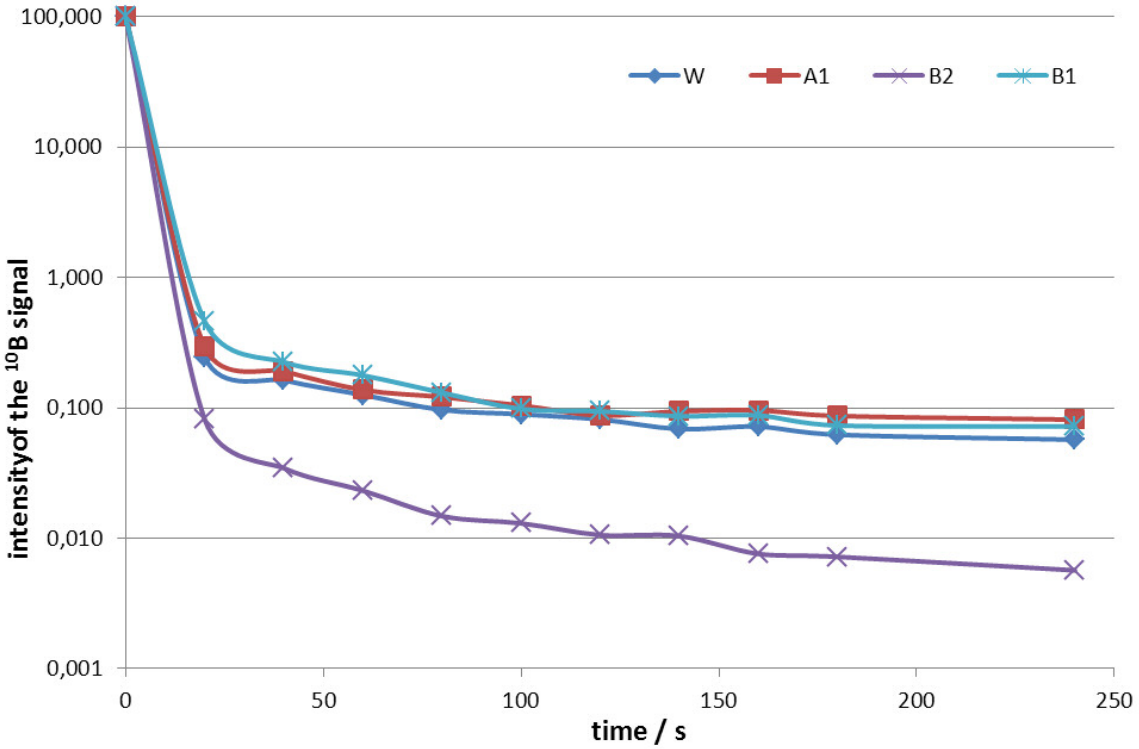

Fig. 65: Decrease of the boron signal while rinsing from an acid solution with four different rinsing solutions (sample injection setup SC2)

Rinsing from basic solutions

After that, rinsing was tried from a basic solution containing boron. The results are shown in Figures 66 (SC1) and 67 (SC2). As B2 had proved to be much more effective than B1 in all tests so far, for these experiments the use of B1 was not considered any longer an option. Again, B2 is the most effective rinsing solution. When rinsing with A1 in both cases, there is a sudden increase of the boron signal after 40 s. This is possibly due to the changing solubility when switching between pH greater than 7 to a pH below 7.

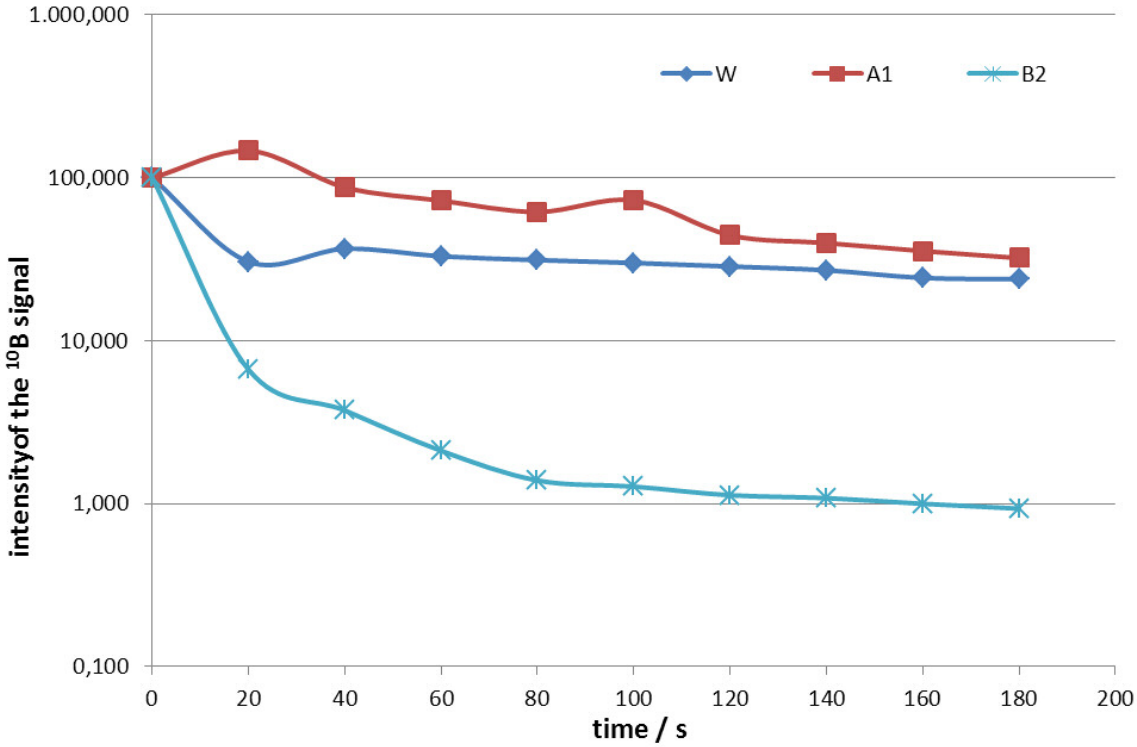

Fig. 66: Decrease of the boron signal while rinsing from a basic solution witht three different rinsing solutions (sample injection setup SC1)

The two experiments with basic boron solutions showed moreover that the use of the PFA-spray chamber has advantages in the general rinsing behaviour.
As a result, for all future experiments, it was decided to use rinsing solution B2, consisting of 2.5 % butanol, 1 % NH_3, 0.05 % EDTA, and 0.05 % Triton X-100. For all experiments described in the following sections, rinsing time between samples was fixed at 210 s.

Though rinsing and obtained background signals were more favourable in the spray chamber made of PFA, it was eventually decided not to use it.
When comparing the absolute signal intensity obtained from this spray chamber to the spray chamber made of quartz glass, the intensity was only about half as high. The signal loss was most probably due to the large volume of the spray chamber, which caused a larger part of the aerosol to get lost after injection.
However, it could be shown that only the replacement of the spray chamber would improve the quality of boron measurements. Therefore, future use of an inert-kit for sample introduction would be a valuable option.

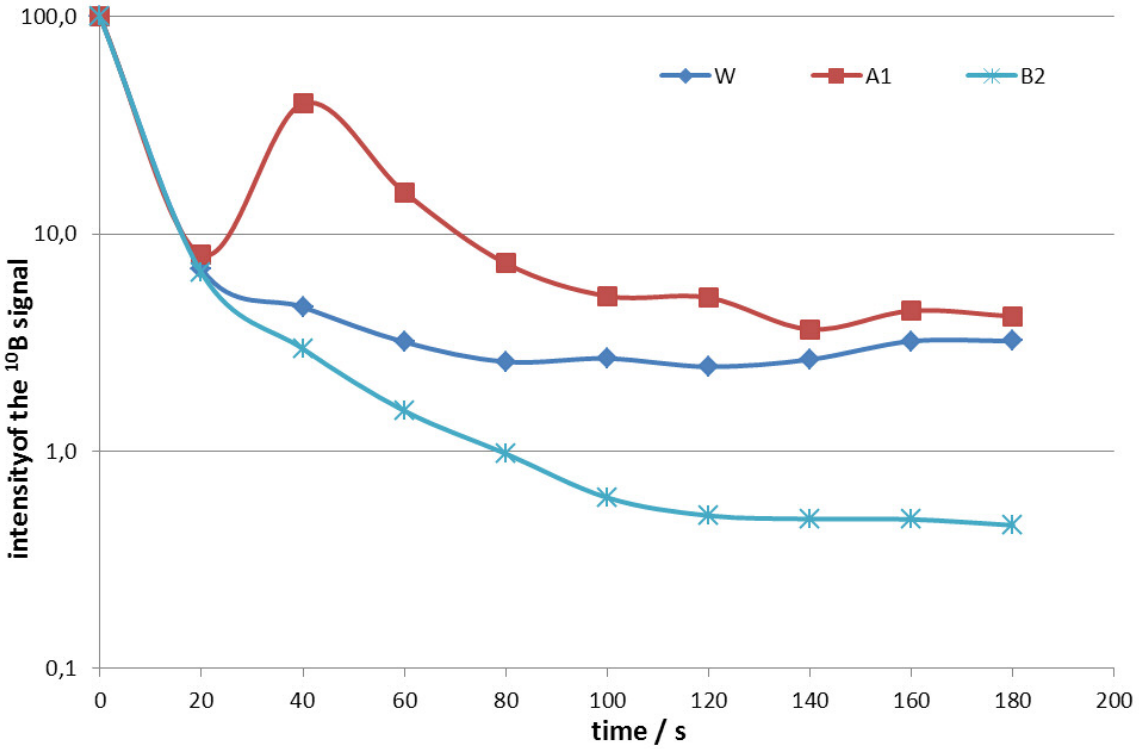

Fig. 67: Decrease of the boron signal while rinsing from a basic solution with three different rinsing solutions (sample injection setup SC2)

3.4.4.2 Matrix matched calibration

Boron determination by ICP-MS is a challenging task already due to the variety and complexity of elemental influences. Certain elements strongly influence the measured intensity of the boron signal, but could also be opposed to each other, i.e., while one (single) element caused signal depression, another element seemed to increase the signal.

After a number of initial experiments, it was obvious that calibration with an aqueous boric acid solution would not account correctly for such influences on the boron signal. Several tests showed that exact determination of elemental influences was too complex and time-consuming for the initial aims of this thesis. An example illustrating such elemental influence is shown in Figure 68.

However, it still remained the need to use ICP-MS for boron analysis of tissue and blood samples. As solution for this problem, matrix matched calibration was considered.

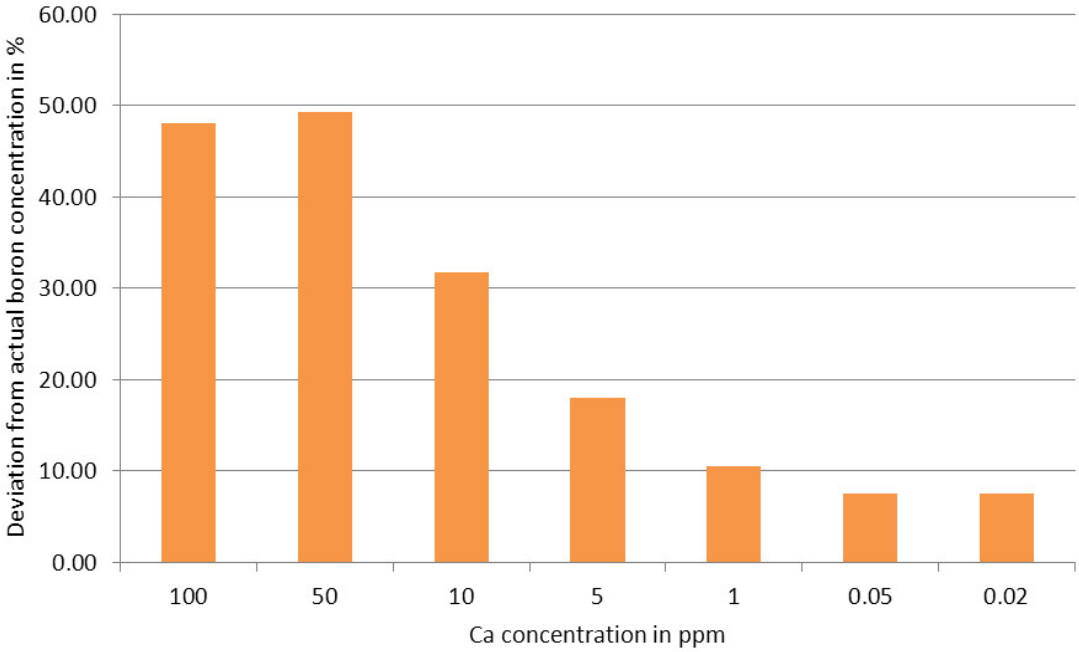

Fig. 68: Influence of calcium in different concentrations (0.02 – 100 ppm) on the boron signal recorded during ICP-MS measurement of an aqueous solution containing 5 ppm (from boric acid). Apart from Ca and B only Be was present in the solution (for internal standardisation)

In this section, preparative experiments will be presented highlighting the importance of considering parameters like date of production of calibration standards and samples, dilution of the sample matrix and the pH gradient between rinsing solution and samples or calibration standards. For the experiments, a set of 10 calibration samples with a certain matrix was prepared from 1000 ppm boric acid solution (High Purity Standards, Charleston, SC, USA), and additionally a number of samples with the same or a different matrix as well.

Rinsing solution as sample matrix

The initial sample matrix chosen was the rinsing solution B2 for both samples and calibration standards. By using the same solution for rinsing and sample dilution, no change of the chemical environment occurs between measuring boron and clearing it from the sample introduction system. For example, changes of viscosity, surface tension, vapour pressure and density of the liquid, which are key

parameters for the production of the aerosol, could eventually lead to greater changes of the boron signal when recording the signal of analyte liquid and rinsing solution. This way, memory effects could be feigned, on the contrary, could not appear even though they occur.

Samples were prepared with total boron concentrations of 5, 10, 25, 50, 100, and 200 ppb, sample preparation and measurement took place within 24 h. The measurement was repeated once to check reproducibility. In Figure 69, the percental recovery of the boron during the measurements is given.

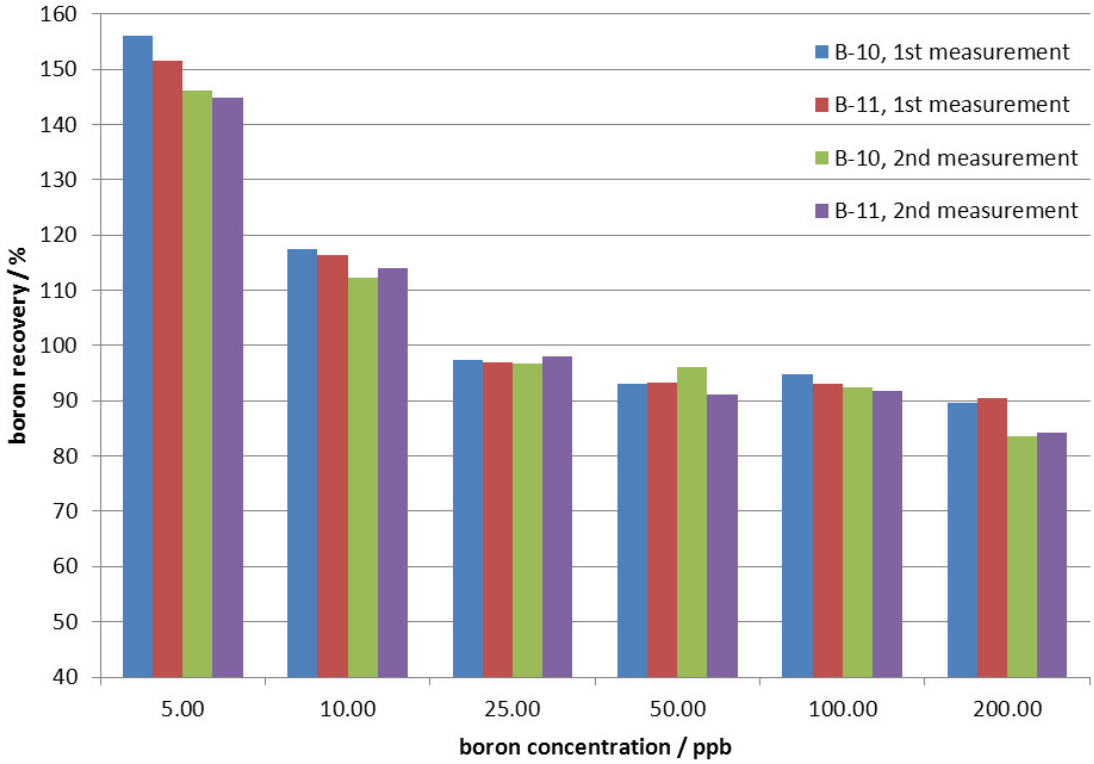

Fig. 69: Recovery of boron when measured in rinsing solution as sample matrix.

The values for recovered boron (both isotopes) exceed 100 % by far in case of 5 ppb total boron. The contribution to the background signal of ^{11}B introduced by ^{12}C can be corrected numerically, as it simply appears in a higher offset when calculating the regression curve. The contribution was constant, as by the use of butanol in the rinsing solution, there was always a stable ^{12}C signal to be expected. Due to its presence in air as CO_2, there is always a very strong ^{12}C signal when operating the instrument, which becomes more prominent if carbon in the sample matrix is measured. The influence on the ^{11}B signal is probably the

broad tailing of the ^{12}C peak, but also charge transfer between dissolved carbon matrix species and boron (or beryllium) have been proposed [256].

However, in all measurements a considerable boron background was observed no matter what rinsing solution used for whatever time. It appears that there is a sort of “intrinsic” high boron background, which is probably caused by the glassware of the ICP-MS, which retain and release boron constantly. This boron background is so significant that boron concentrations < 10 ppb cannot be quantified with utmost certainty.
While boron recovery is above 100 % for 5 and 10 ppb, it decreases to a minimum value of 90 % for the higher boron concentrations. Mean recovery (not considering measurements at 5 ppb) was 97.1 ± 9.7 % for both isotopes, whereas recovery was slightly better for ^{10}B. The control measurement revealed good reproducibility.

Blood equivalent solution as sample matrix

In order to determine boron from solutions with a sample matrix equivalent to blood, whole blood was obtained from the blood bank of the University Hospital. The blood was digested and further diluted following the protocol given at the end of section 3.4.3. Five samples with concentrations of 5, 25, 50, 100, and 150 ppb total boron were prepared. Sample preparation and measurement took place within 24 h.

The importance of equal dilution was checked in an additional experiment: Calibration standards and samples were prepared using the same blood equivalent matrix solution, but calibration standards were diluted twice as much as the samples. The resulting mean recovery was only 55.8 ± 9.7 %.
Similar results as presented for the experiments with rinsing solution as sample matrix were observed. However, the measurement was repeated three times to check reproducibility. The measurement of the 5 ppb yielded very unreliable recoveries, far above and below 100 %. In this experiment, the recovery of ^{11}B was usually higher (about 5 %) than the recovery of ^{10}B, which is probably due to the increased carbon content caused by the cellular fraction of the blood. Mean

recovery (not considering measurements at 5 ppb) was 100.6 ± 7.0 % for both isotopes and for all measurements (Fig. 70).

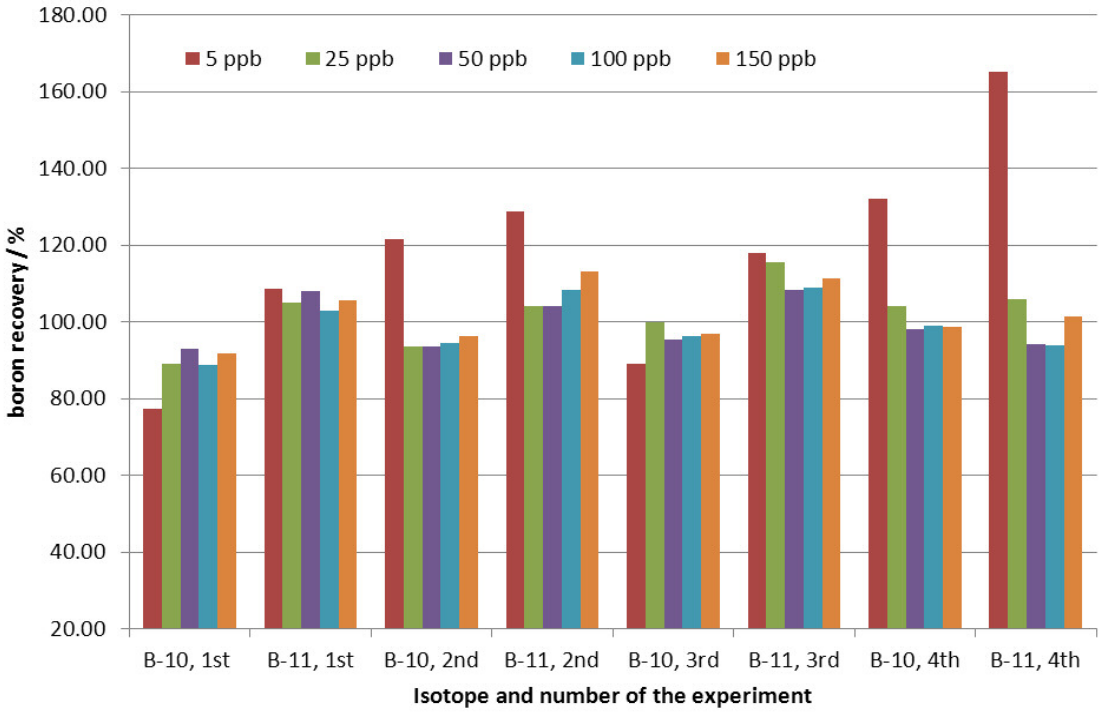

Fig. 70: Boron recovery when measured in blood equivalent solution as sample matrix.

The conclusion drawn from the preparative experiments presented in this section was that a boron recovery of around 95 %, with a standard deviation of up to 8 % could be expected, which means that correct boron determination in blood samples was achievable, including a particular measurement uncertainty (of around 8%) and probably also a considerable standard deviation.

Sample dilution for sample preparation combined with matrix equivalent calibration

In a series of experiments, it was eventually also tried to combine matrix matched calibration standards for merely diluted blood samples. First tests had been carried out with whole blood samples before the development of the aforementioned rinsing protocol, the samples were diluted with purified water. The tests yielded very inconsistent and not reproducible results regarding the boron recovery. Also, it was found that 50fold or 100fold dilution yields solutions with salt concentrations

too high that it caused problems with the sample introduction assembly, e.g., precipitation of salts inside the nebuliser capillary impairing aerosol production.
After establishing the sample preparation and rinsing protocol with the above mentioned basic rinsing solution B2, the tests were repeated by diluting whole blood samples with the rinsing solution 200fold and 400fold to work at reduced salt levels. Calibration samples were prepared accordingly with the same dilutions.
This time, boron recovery was more uniform for blood samples for all boron concentrations, though ultimately not satisfying. However, at the time of writing work on this issue had not been completed, yet.

3.4.5 Results of tissue and blood samples

After carrying out the analysis via PGAA, tissue and blood samples from the clinical study were analysed by ICP-MS. Sample digestion and preparation was done as described in section 3.4.3.

Reliability of the boron measurements with ICP-MS

The boron recovery achieved indicated that the chosen protocols for sample preparation (including possible digestion of blood), rinsing and the use of matrix equivalent calibration standards would allow reliable and reproducible boron determination with respect to certain error for the resulting concentration values.
For determination of the total uncertainty, several parameters have to be taken into account: weighing errors, pipetting errors (when either preparing calibration standards or when diluting solution to their appropriate concentration levels), relative standard deviation of the boron signal intensity measured by the ICP-MS and correctness of the calibration curves.
Determination of the propagation of uncertainty by the Gaussian formula (see section 1.7) was carried out according to the following relation:

$\frac{c_{B,smpl} \cdot D_{smpl}}{r_{B,smpl}} = \frac{c_{B,Std} \cdot D_{std}}{r_{B,std}}$, with c_B as boron concentration, D as dilution factor and r_B as count rate of the boron signal recorded by the ICP-MS of the sample (*smpl*) or the calibration standard (*std*).

Uncertainty of D_{smpl} is obtained from linear propagation of uncertainty considering the uncertainties of every weighing and pipetting step during sample preparation with respect to the intrinsic uncertainty of each pipette and balance used. Total uncertainty was 1.95 %.
Likewise the uncertainty of D_{std} was calculated. Since several standards had to be produced (in order to be able to create a calibration curve), for Gaussian propagation of uncertainty ultimately the standard produced with the highest uncertainty (3.45 %) was chosen.
Good linearity was found for the range of calibration and very little difference in RSD of the count rates of all standards used for linear regression analysis, which is why for the uncertainty of the count rate, a uniform value was chosen. Uncertainty of the count rates for both samples and calibration standard was obtained from the RSD of the boron signal recorded by the detector. Measurements of both were carried out with a RSD of 2 – 4 %, varying from day to day, but hardly within one day. For propagation of uncertainty, the more conservative value (4%) was chosen.
The total uncertainty calculated by Gaussian propagation of error was 6.91 %.

Results of blood samples

At first, for boron determination measurements by ICP-OES, which was possible at the Technical University of Graz, Austria, was considered. Thirteen blood samples of patients 1 - 3 were digested and used for test measurements, however these measurements revealed strong matrix interferences making boron determination far more complicated than anticipated, though similar sample preparation was carried out as described in literature [250]. Therefore, not for each time interval of the infusions, five samples were available for ICP-MS measurement. Therefore,

the values are mean values of four samples, including the standard deviation among them.

In case of patient 4 all samples were available; hence five samples were measured for each point in time. Mean values and standard deviation are reported accordingly. In total, 91 blood samples were measured. The blood-boron curves are given in Figure 71. The resemblance to the curves depicted in Figures 54 and 55 is obvious.

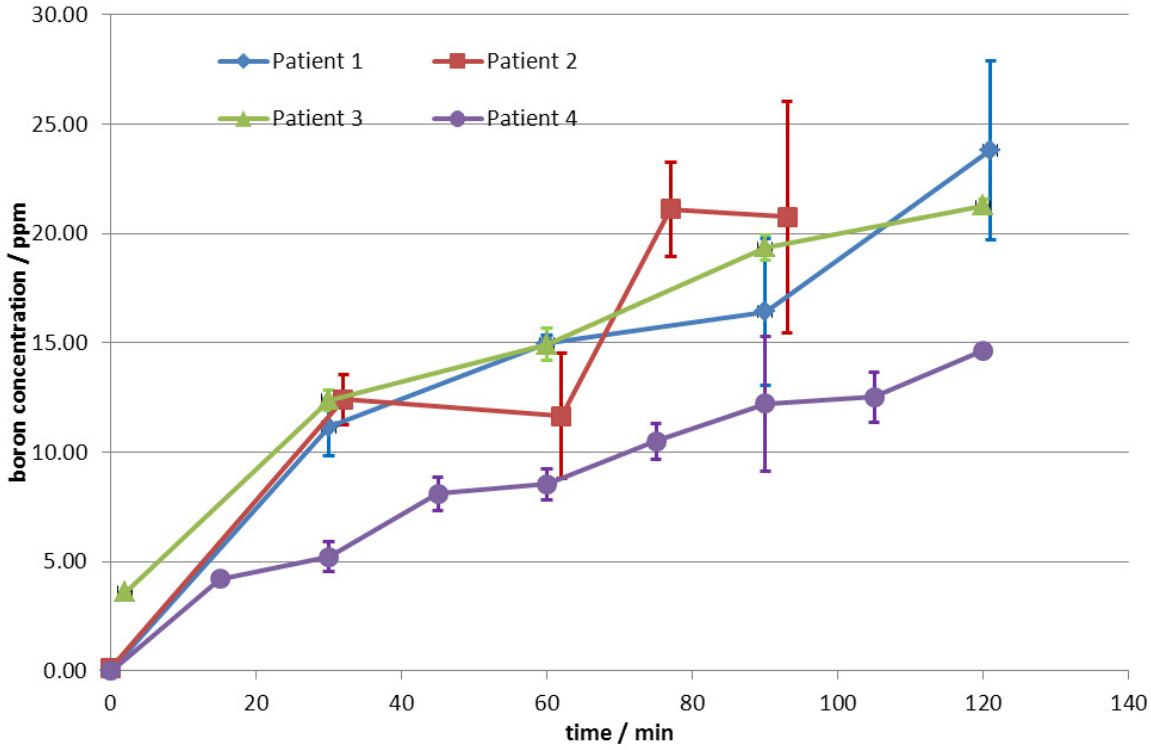

Fig. 71: Time-dependent boron concentration (including standard deviation) measured by ICP-MS in the blood of all patients

Apart from patient 3, the blood samples taken at the beginning of surgery should contain only the “natural” boron quantity, which is 20 – 50 ppb [257]. Due to the high dilution factor caused by samples preparation for analysis by ICP-MS, the boron concentration in the analyte liquid would be far too low to be correctly quantified. Several samples measured nevertheless revealed that indeed only the background signal was recorded. As a result, these samples were not considered to be useful for comparison. All measurements carried out by ICP-MS yielded values that were reproducible and consistent for each subset taken after every time interval during the BPA-infusion.

As it can be seen in Figure 71, for the majority of the measurements, relative standard deviation was relatively low (0.3 - 1.2 ppm), though in case of patients 1 and 2 for the latest sampling intervals, and for the seventh sampling interval of patient 4, much higher relative deviation of the values were determined. It could not be clarified, why there was a so different behaviour found for the respective groups of samples.

The maximum boron concentration reached in blood for each patient is given in Table 7. Maximum values for patients 1 - 3 were between 20.6 and 23.8 ppm, for patient 4 a maximum value of 14.7 ppm was reached.

Tab. 7: Results of the ICP-MS measurements (including standard deviation) of tissue and blood samples of all four patients. Concentrations are given in ppm

Patient	Petten ^{10}B-tissue conc.	Max. ^{10}B-blood conc.	blood : tissue ratio
1	9.3	23.8 ± 4.0	2.6 ± 0.4
2	12.8	20.6 ± 5.3	1.6 ± 0.4
3	11.1 ± 1.7	21.3 ± 0.3	1.9 ± 0.4
4	7.0 ± 1.6	14.7 ± 0.2	2.1 ± 0.5

Results of tissue samples

The boron concentration in tumour free tissue is reported for every patient. Standard deviation is reported only for patients 3 and 4, as for these patients, 5, respectively 6, samples could be measured. For patients 1 and 2, only 2, respectively 3, samples were available for ICP-MS measurement. As a result for patient 1 – 4, boron concentrations of 9.3, 12.8, 11.1 (± 1.7) and 7.0 (± 1.6) ppm were found. The mean boron concentration in tumour free tissue of all patients is 9.8 ppm. The resulting blood to tumour free tissue ratios are between 1.6 and 2.6. (Tab. 7). The values are very similar to those obtained by PGAA and will be further compared and discussed in section 3.5.

Also the samples taken before and after perfusion with preservation solution were measured, as it was the case for PGAA, only samples obtained from patients 1

and 4 were available. Results are shown in Figure 72, a comparison to the values obtained by PGAA can be found in section 3.5.

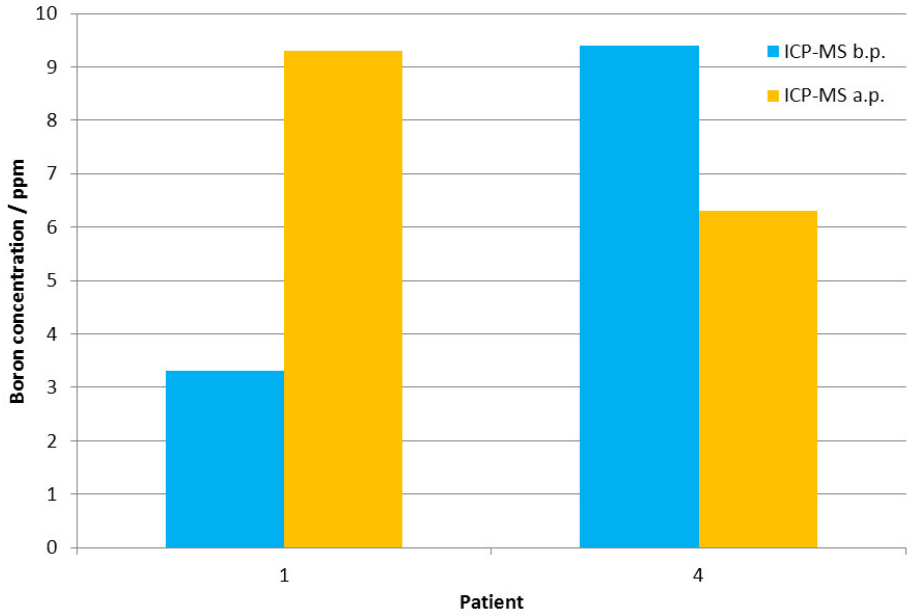

Fig. 72: Boron concentration found in tumour free tissue taken before perfusion (b.p.) with HTK solution and after perfusion (a.p.)

While the values for the boron concentration after perfusion for both patients and for the boron concentration before perfusion for patient 4 agree with those measured by PGAA, the measurement of the sample obtained from patient 1 before perfusion yielded an usually low boron concentration. This could not be explained, also because signal intensity and quality during the measurement did not indicate any error. Additional control measurements reproduced the initial result within a margin of 3%.

Neither did any other biopsy measured by any of the analytical techniques yield a comparable boron concentration, nor did the result agree in any way with the corresponding value obtained from both PGAA measurements (15.6 ppm in Petten and 12.5 ppm in Munich), therefore this value was excluded from clinical evaluation of the data. Apparent boron loss determined for patient 4 was 33.0 %.

Results of blood reference samples used for the production of standard calibration samples for QNCR

In Figure 73, the ^{10}B-recovery for the series of blood samples is shown, which was used for the production of standard calibration samples for QNCR, and which had already been measured by PGAA. No result is given for the sample originally prepared with 380 ppb boron, as after digestion and dilution, the boron signal was too similar to the background signal and very unstable, therefore, no reliable quantification was possible. Also caused by the high background signal, the sample prepared with 911 ppb showed a high RSD of 10 %.

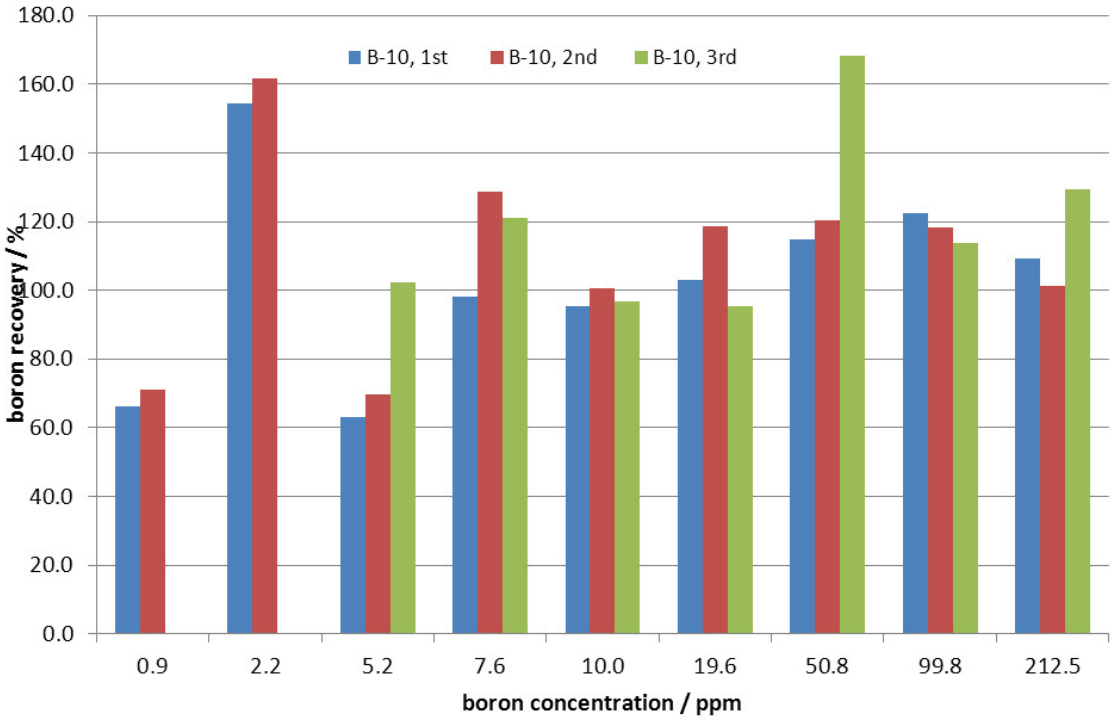

Fig. 73: Results of the three measurements carried out to determine the boron content in the blood samples used for the production of QNCR reference samples.

The measurement was carried out three times to ensure reliability. The mean recovery is between 100 and 120 % for measurements of samples with an initial boron content of 7.6 ppm and higher, for samples with lower boron contents it lies between 60 and 160 %. While the second measurement seemed to confirm the values of the first measurement, the third series is only partly consistent with the preceding measurements. More measurements were not possible, as no sample

material was left for analysis (as this was already the case for the samples containing 911 and 2210 ppb boron when preparing the third measurement).

Therefore, the mean recovery and relative standard deviation of the recovery for all three measurements is given. The mean recovery was 109.1 % ± 26.5 % and therefore far too high and with a too large standard deviation.
It was not possible to explain why only in this series of boron determinations the values were neither properly reproducible, nor show a distinct tendency or trend, as is was the case in for other samples, e.g., as presented in Figure 69.
The so determined results in 9 samples were a strong contrast to the 90 blood samples of the clinical study, which were reproducible and consistent for the respective time intervals when compared to each other. Nevertheless, due to the much greater number of samples, the author does not consider the correctness of boron determination by ICP-MS in blood samples to be compromised, because the boron content obtained for the blood samples are very much in agreement with the boron content obtained for the same samples by PGAA, as will be presented in the next section.

3.5 Intercomparison and validation of QCNR, ICP-MS and PGAA

The usual approach to validate analytical methods in direct comparison is to carry out measurements with all of the methods of a suitable standard reference material. A very common practice in Analytical Chemistry is the realisation of a so-called “Robin-Round trial”: One or several standard reference materials are measured by one or several analytical methods by a number of laboratories. The values have then to be collected and evaluated statistically to determine the conformity of each method against the others. Ideally, only the person collecting the data from each laboratory knows the content of the analyte to ensure the quality of such a trial. Such trials eventually yield individual information about the analytical quality of each participating laboratory, but they may also reveal, if there is a systematic error in boron determination by one specific method (provided that such errors can be surely traced back to the method alone and not to sample preparation, the analyst, or the laboratory).

For each of the analytical methods used in the work presented in this thesis, there are a number of publications available either proclaiming the correctness of the respective method or pointing out directly the difficulties arising during boron analysis. To ensure the correctness (and, thus, their relevance for future research) of the data gathered from the samples taken during the clinical study, it was decided that the analytical methods used in this work had to be validated.

For the analytical methods chosen, described, and used in this project, there was no suitable standard reference material commercially available. This was particularly difficult, since QNCR allows only the measurement of solid samples, whereas ICP-MS can only process liquid or liquefied samples. Also, not only the mere boron determination, but especially the boron determination in a tissue matrix (all three methods) or blood matrix (ICP-MS and PGAA) had to be carried out correctly. It was therefore decided to prepare an individual standard reference material for QNCR, which would later be measured by ICP-MS and QNCR. After that, all samples from the clinical study would then be measured with the matching analytical method.

Eventually for calibration of QNCR, standard reference samples of BPA in whole blood were prepared (described in detail in section 3.2.5). The known boron concentration in these samples was measured by ICP-MS and PGAA to check both methods.
All samples obtained during the clinical study were measured with at least one of the aforementioned methods:

- For tumour samples, only QNCR was chosen, as it was the only method capable of performing locally selective boron determination.

- For blood samples, first analysis by PGAA was performed, after which the same samples were used for subsequent analysis by ICP-MS.

- The only samples which were measured by all three methods were the biopsies from tumour free tissue. First, cryosections for QNCR were prepared from the original piece of tissue taken after surgery. The remainder of the piece was then sent to Petten and Munich and measured by PGAA. After that, these samples were analysed by ICP-MS.

In Figure 74 a schematic is shown illustrating the connections between measurements and samples, as well as the blood reference samples.
Unfortunately, it was not possible to perform the sequence of analysis for all samples of tumour free tissue. Several biopsies were used up completely for preparation of the cryosections. Therefore, in order to increase statistics for the measurements with PGAA and ICP-MS, the smallest samples were used for PGAA analysis first. Since they had to be measured at room temperature, thawing made these samples completely ineligible for analysis by QNCR, so only analysis by ICP-MS was performed afterwards.

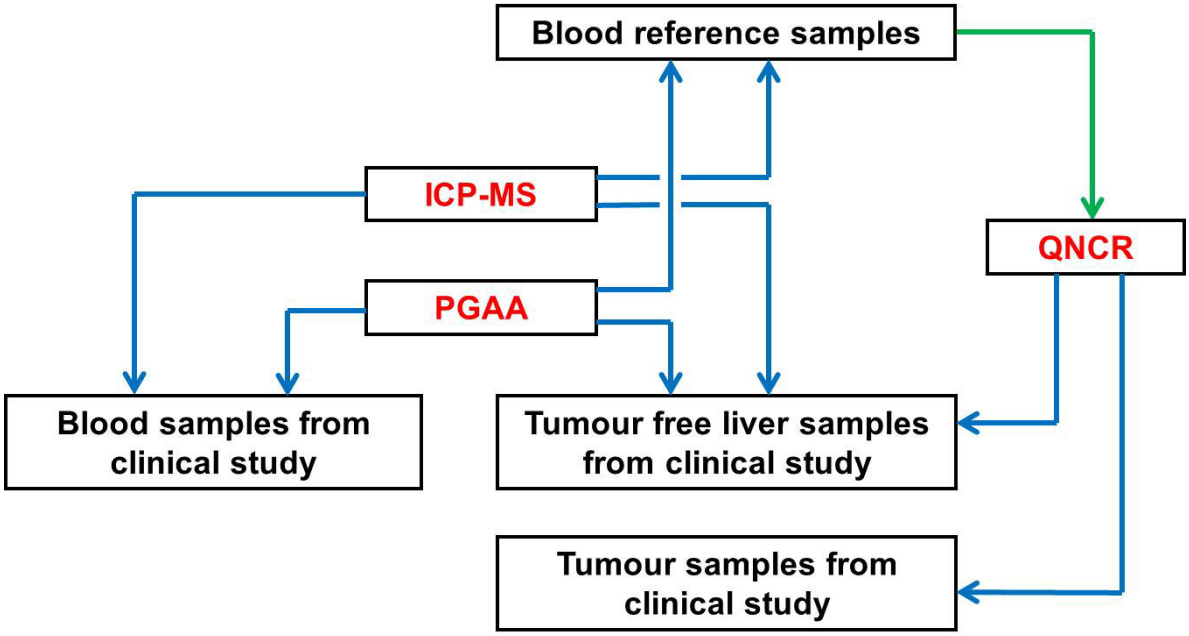

Fig. 74: Connection between QNCR, PGAA and ICP-MS as methods for boron determination, the samples obtained during the clinical study and the blood reference samples used for calibration during analysis with QNCR. Blue arrows indicate measurements of samples by a specific method, the green arrow indicates that one set of samples was used for production of reference samples for QNCR

Comparison of the measurements concerning the blood reference samples

The measurements related to the comparison of PGAA and ICP-MS were already presented in the preceding sections (3.2 – 3.4).

The overall boron recovery found evaluating the measurements of the blood reference by PGAA in Petten met the expectations. A recovery of 100.1 ± 6.9 % was confirmed by a control measurement (96.0 ± 8.7 %).

The measurement of the same samples by ICP-MS yielded problematic results. Though overall recovery was similar, the standard deviation of the recovery was very high (109.1 % ± 26.5 %). Moreover, not all results were reproducible in a satisfactory way.

A direct comparison of both methods for each sample of a given boron concentration hinted at first a trend that boron concentrations determined by ICP-MS (Fig. 75) would be too high. However, if the three highest concentrations are omitted, the values appeared to be in very good agreement, though from six

values it is hardly possible to gain appropriate information about the validity of the two methods in this case.

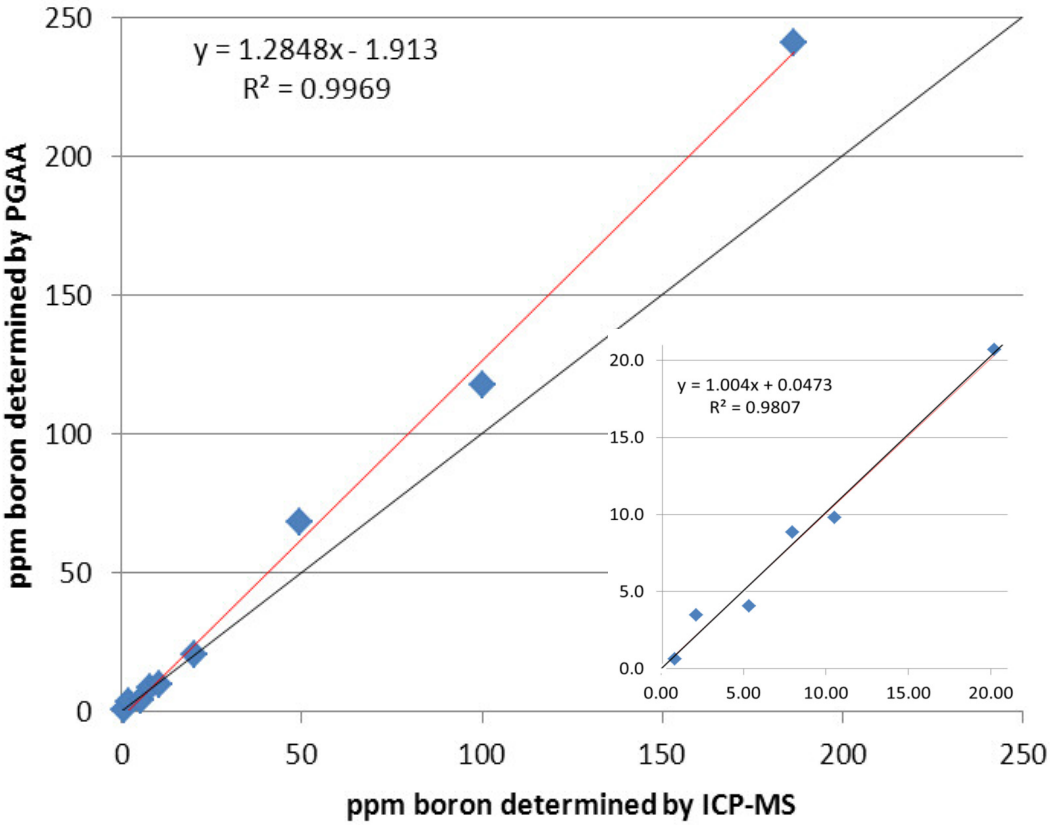

Fig. 75: Comparison of the boron concentration determined in the blood reference samples by ICP-MS and PGAA measured in Petten. In the smaller graph only the six lower concentrations are considered.

Therefore, from this comparison no conclusive validation of both methods against each other could be deduced. While PGAA seems to yield reliable results, ICP-MS appears to be less favourable. Nevertheless, boron determination for blood and tissue samples from the clinical study was carried out, because in all preparatory experiments with ICP-MS preceding the measurement of the reference samples consistent and reproducible results were obtained.

Comparison of the measurements concerning the blood samples from the clinical study

The PGAA measurements in Petten and Munich yielded very similar results with deviations for each sample between 1 and 5 %. Therefore, for a direct comparison to ICP-MS, the mean value for each sample obtained in both facilities was used. The direct comparison of both methods for each sample of a given boron concentration is shown in Figure 76.

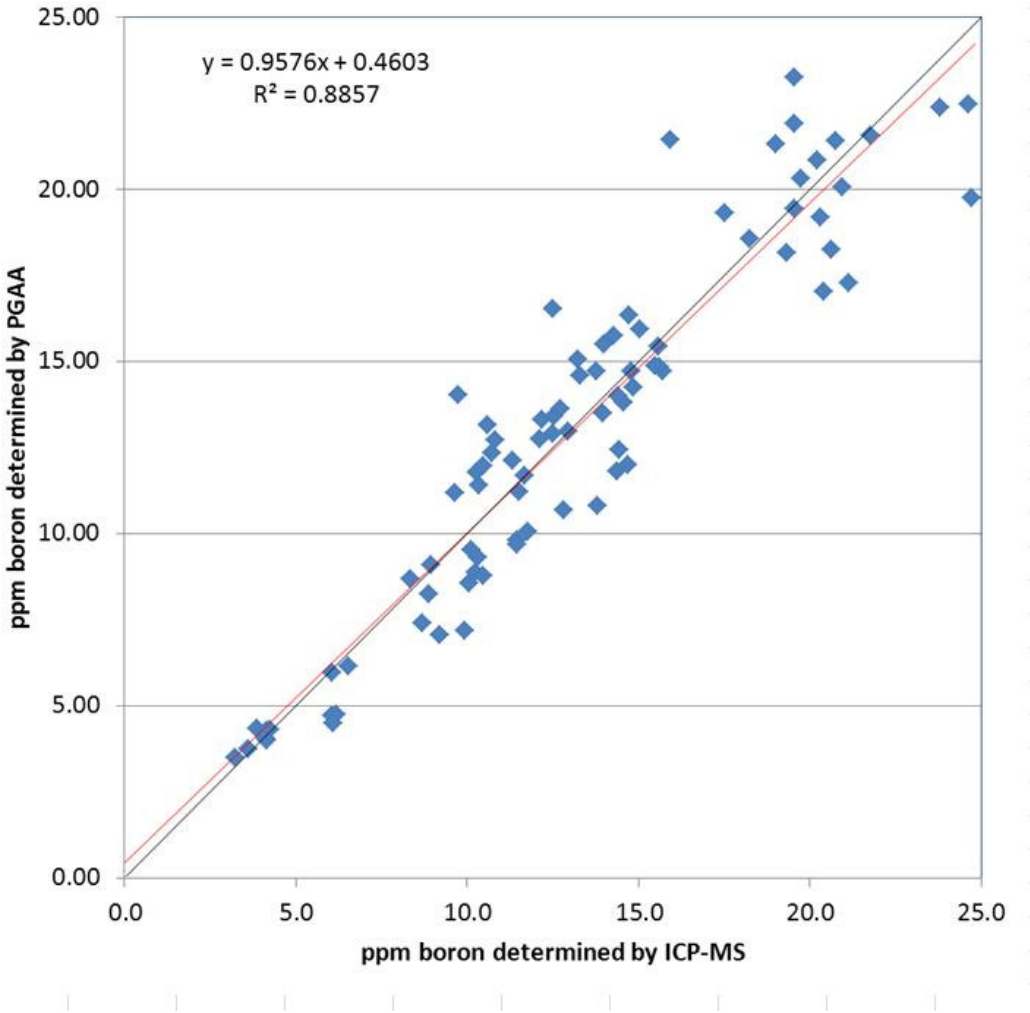

Fig. 76: Comparison of the boron concentration determined in the blood samples obtained during the clinical study by ICP-MS and PGAA

Overall 91 of 107 blood samples are compared by ICP-MS and PGAA in Mainz, Munich and Petten, samples taken at the start of the infusion were not considered (see section 3.4.5).

Compared to the blood reference samples, no trend was found for a specific relation between the outcome of ICP-MS and PGAA measurements. Though the coefficient of determination is a little higher than desired, the values are in good agreement. The deviation between the two methods is further illustrated in Figure 77.

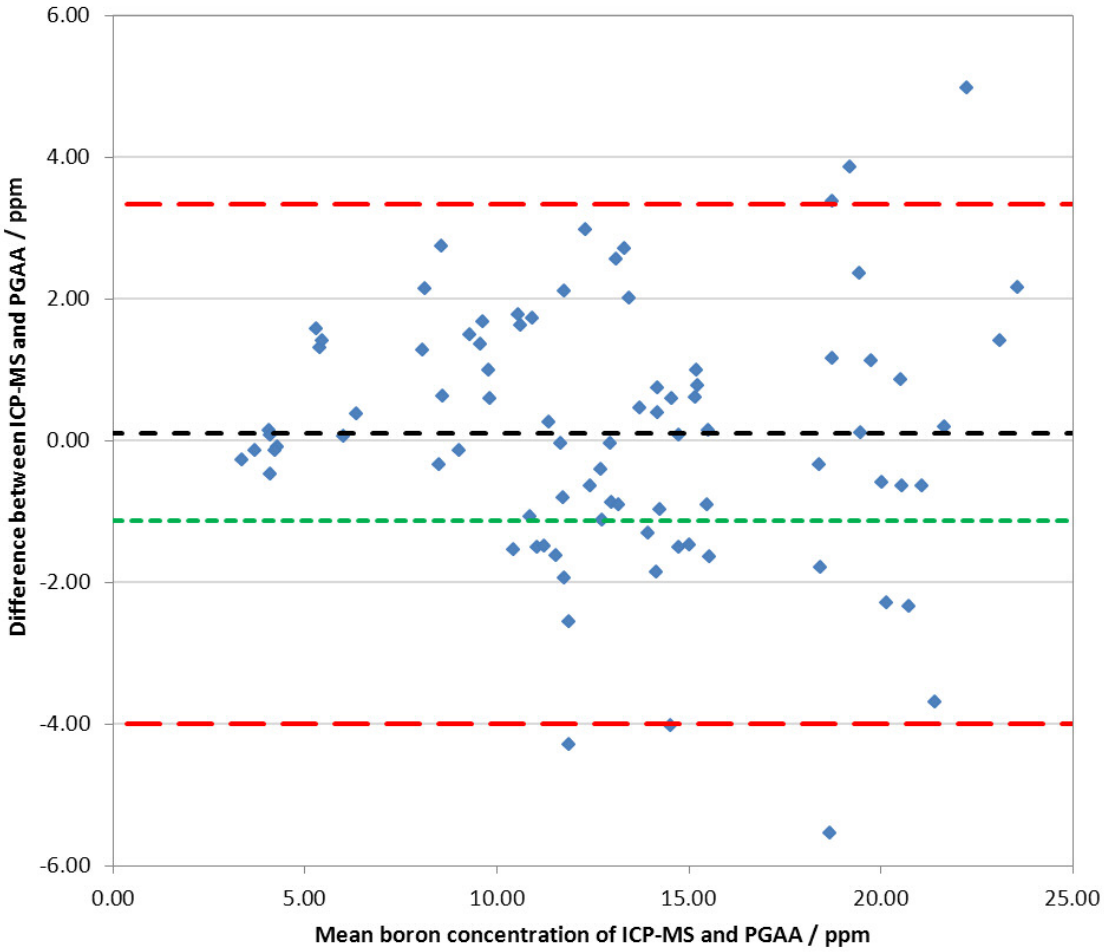

Fig. 77: Difference of the boron concentration determined by ICP-MS and PGAA. The upper and lower boundaries of the 95 % confidence limit are shown in red, arithmetic mean in black and geometric mean in green.

It may appear that samples of lower boron concentrations show less differences for both methods, however when regarding relative deviation between ICP-MS and PGAA, it becomes clear that there is no specific difference for samples of higher or lower boron content. Deviation of the values is assessed by the upper and lower confidence limit (= the 0.05 quantile of the data distribution, i.e., the upper and lower limit separating 5 % of the values at the edges of the distribution of all results).

The bias between both methods is expressed via arithmetic and geometric mean. Comparison reveals that they are not identical (AM = 0.10; GM = - 1.13), therefore the values are slightly unbalanced towards ICP-MS. However, no similar trend for samples of higher concentrations as in Figure 75 was found. Since statistically in this case, far more samples could be evaluated than for the comparison of the blood reference samples, one might assume that the three highest values shown in Figure 75 did not reveal a trend, but were rather random deviations from the desired results. However, it must be pointed out that no sample of these blood samples came close in concentration to the three highest values shown in Figure 75.
If setting the mean PGAA values as reference for the calculation of the boron recovery achieved by ICP-MS, overall recovery is 100.5 ± 9.5 %.

The curves for the blood boron kinetics presented in section 3.3.4 (PGAA) and section 3.4.5 (ICP-MS) were created from the (arithmetic) mean of the boron concentrations of each set of samples taken after certain time intervals during BPA infusion. When measuring these sets of samples with either of the two methods, a certain deviation within each set could be observed. Therefore, mean values of the sets measured with PGAA and ICP-MS were compared in the same way as carried out for the single measurements in Figures 76 and 77 (shown in Figures 78 and 79).

Comparison of the mean values reveals that this evaluation reveals a better accordance than evaluating only the single measurements. Arithmetic and geometric mean are almost identical (AM = - 0.09; GM = - 0.16), and upper and lower limit of the confidence limit (again, with a confidence interval of 95 %) are lower than in Figure 77. Since comparison of the mean values respects the (in most measurements occurring) normal distribution, it is more favourable to split up blood samples taken in clinical trials in different aliquots and measure them separately (and repeatedly, if possible).

In conclusion, comparison to the blood reference samples, did not show any trend revealing a specific relation between the outcome of ICP-MS and PGAA measurements. The values are in good accordance, this also agrees with data

published earlier in literature on the comparison of boron determination at the PGAA facility of the HFR Petten versus boron determination by ICP-OES [186].

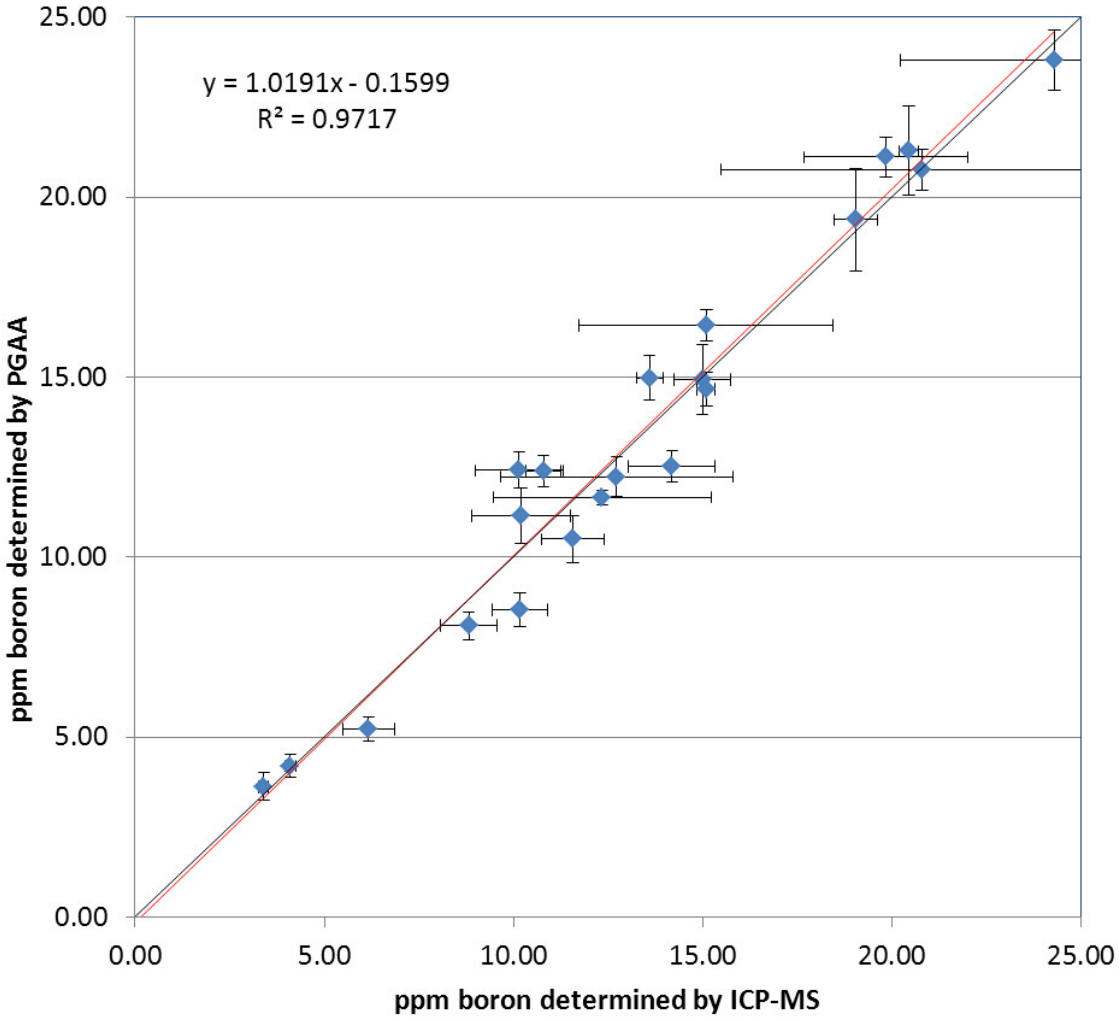

Fig. 78: Comparison of the mean boron concentration determined by ICP-MS and PGAA in blood after each time interval, including standard deviation of both methods

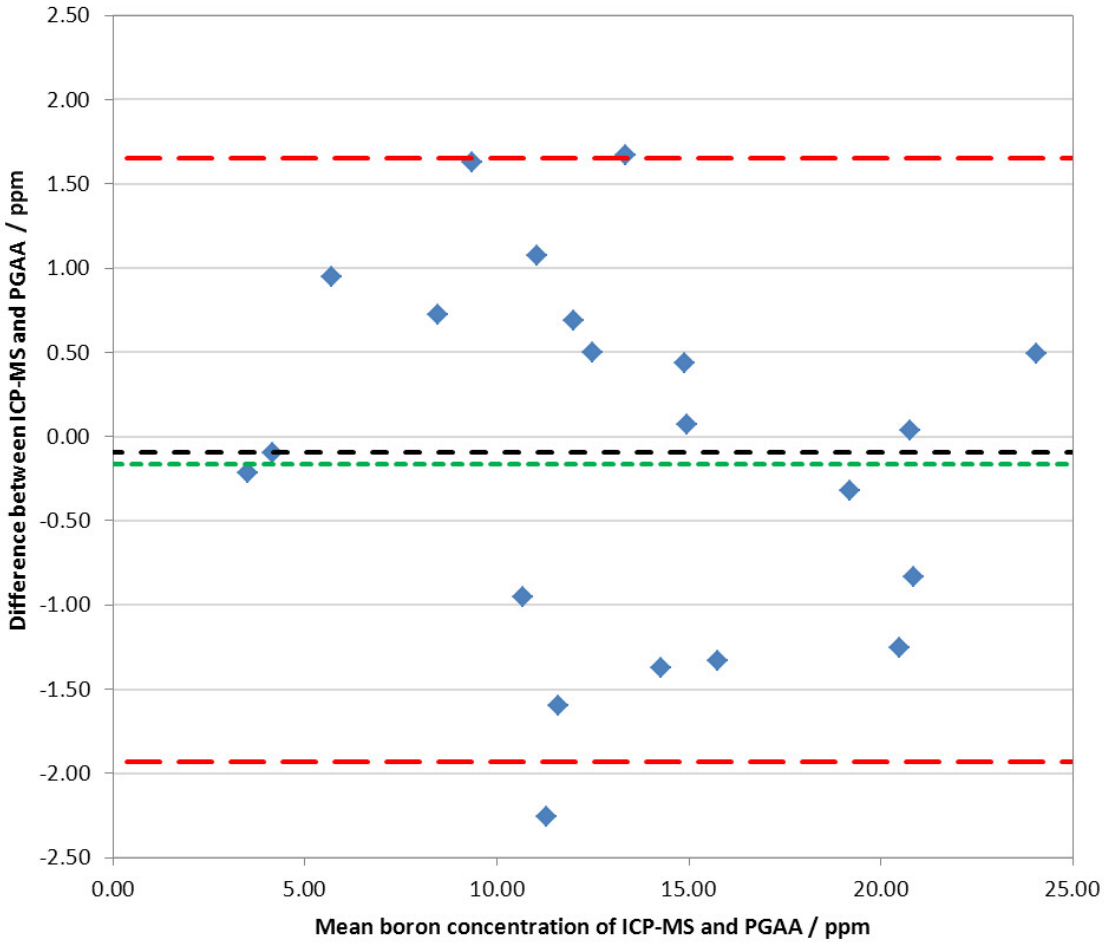

Fig. 79: Difference of the boron concentration determined by ICP-MS and PGAA. The upper and lower boundaries of the 95 % confidence limit are shown in red, arithmetic mean in black and geometric mean in green.

Comparison of the measurements concerning the tumour free tissue samples from the clinical study

The biopsies of tumour free tissue were the only type of samples which could be measured by PGAA, ICP-MS, and QNCR, but, as stated further above, this could not be carried out for each of the samples retrieved during the study. Therefore, only samples eventually measured with at least two different methods at three different institutions, for every sample all values are given (Fig. 80) including uncertainty in boron determination for each method.

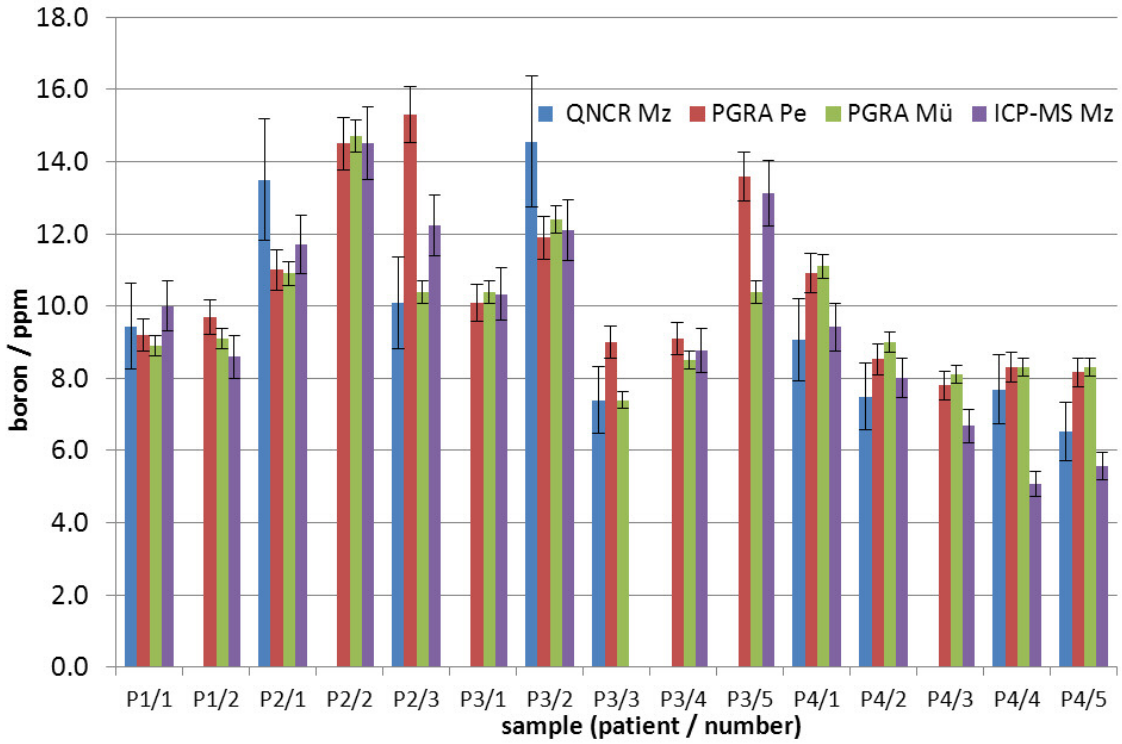

Fig. 80: Comparison of the boron concentration determined in tumour free tissue samples obtained during the clinical study by QNCR, ICP-MS and PGAA. The error bars denote the uncertainty of the respective method

Conformity of the values was assessed applying a criterion from Bayesian statistics (see section 1.7). The results are presented in Figure 81, reproducing partly Figure 80: Conformity was assessed for each value against the other values determined for the respective sample. Values in conformity with three (two) other values are given dark green, values in conformity with two (one) other value are given light green, values in conformity with one or no other value are given in orange (the criteria in parenthesis account for samples measured at three instead of four institutions).

In eight samples, good conformity for all or the majority of the values was found. In five samples conformity of all but one value was found and for two samples conformity was poor.

For better statistics and a more comprehensive assessment of the boron concentration in tumour free tissue samples, also samples which had not been measured with more than one method were included. The mean values derived from the results of all samples measured by PGAA, ICP-MS and QNCR, are compared in Figure 82. As it was done for the values presented in Figure 83, conformity of the methods for each patient was assessed, too.

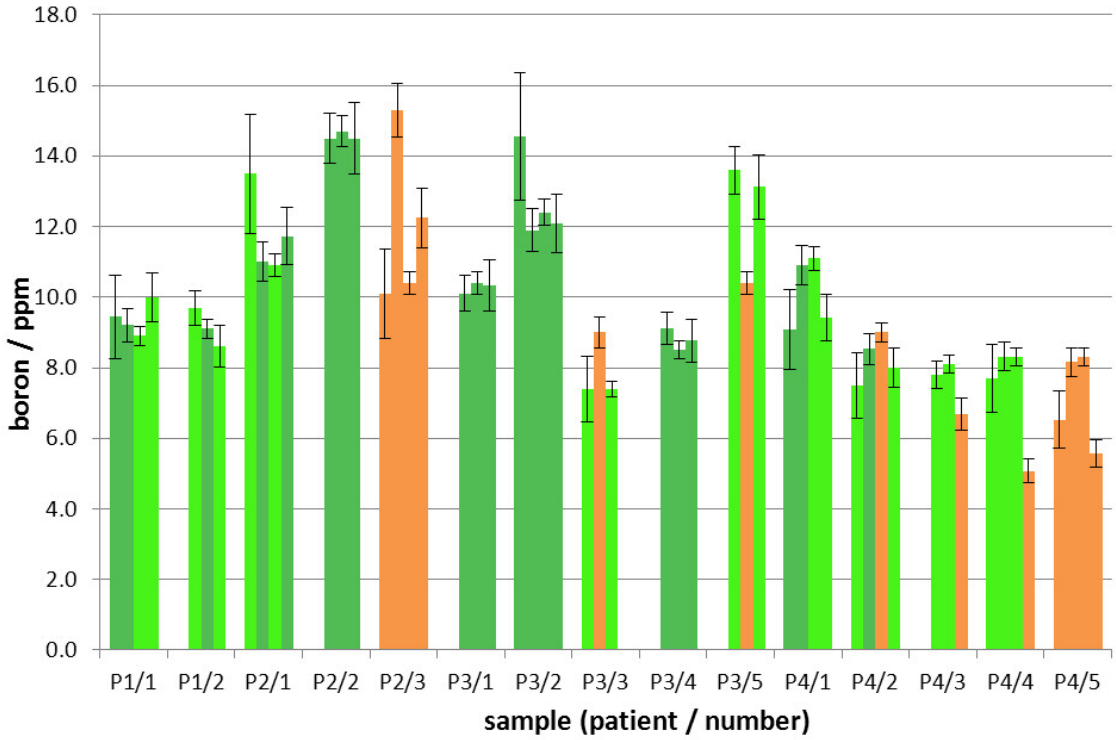

Fig. 81: Conformity of the boron concentration determined in tumour free tissue samples obtained during the clinical study by QNCR, ICP-MS and PGAA. The error bars denote the uncertainty of the respective method.

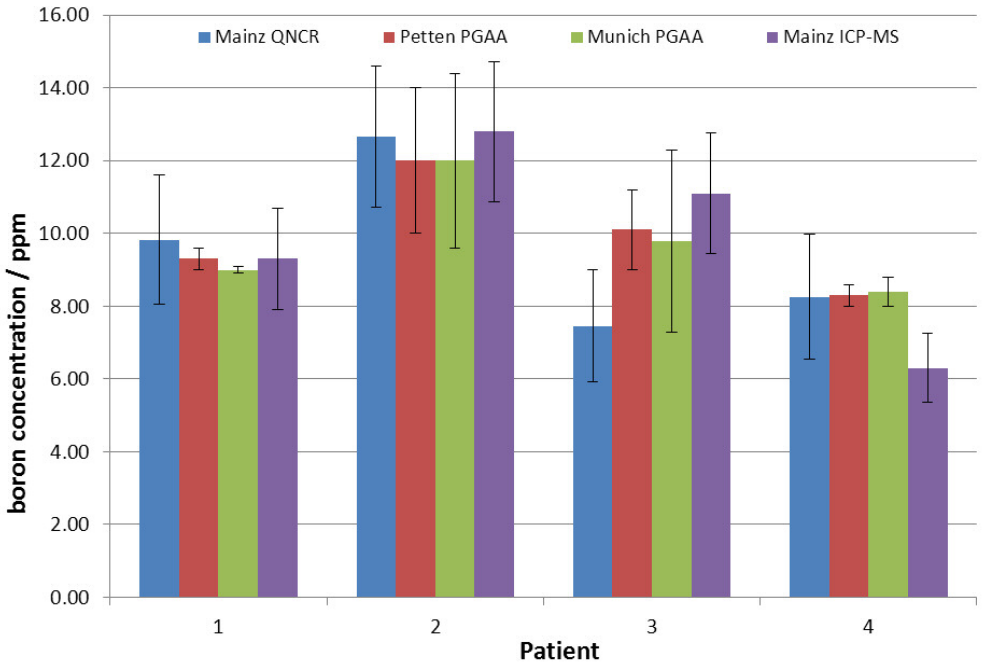

Fig. 82: Comparison of the mean boron concentration determined in tumour free tissue samples obtained during the clinical study by ICP-MS, QNCR and PGAA. Error bars denote the standard deviation in the boron concentration for each patient.

The plot reveals good conformity of the values, which is overall better with respect to the conformity of the measurement of single samples. The only problematic value appears to be the boron concentration determined in tumour free tissue of patient 4 by ICP-MS, though this is also due to the small standard deviation of the boron concentration found by PGAA.

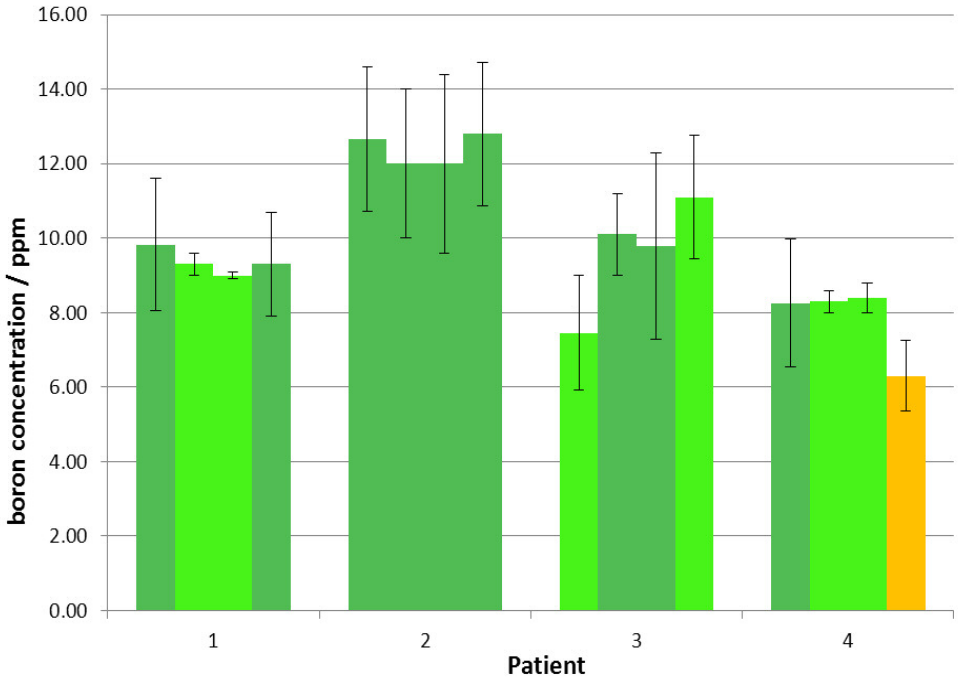

Fig. 83: Conformity of the mean boron concentration determined in tumour free tissue samples obtained during the clinical study by ICP-MS, QNCR and PGAA. Error bars denote the standard deviation in the boron concentration for each patient.

Conformity is obviously strongly dependent on the sharpness of the conformity criterion (for which $\sqrt{2}$ was chosen) and on the uncertainties (or standard deviations) of the involved methods.

Higher uncertainties will inevitably lead to higher conformity, therefore good conformity does not automatically mean that an ensemble of methods agrees well for a specific analytical task. Conformity rather serves to identify a method, which would be in contradiction to the others. In this particular comparison of ICP-MS, QNCR, and PGAA (carried out at two different facilities) no method could be identified as being inconsistent in its outcome, though obviously the deviations found suggest that further improvements for ICP-MS and QNCR in particular should be pursued.

Unfortunately, one parameter creating a possible deviation between boron concentrations determined with the three analytical techniques still remains and could not be clarified: In section 3.2.8 boron determination in steatotic hepatocytes was reported for two patients. Since they take up much less boron than other tumour free liver tissue, apparently dependent on the spatial extent and dimension of clusters of steatotic cells, integral boron determination only reflects the true situation in such samples, if they are taken from liver tissue completely free of steatosis. If steatosis occurs, the higher the percentage of steatotic cells compared to the rest of the analysed cells, the wronger the boron determination will eventually be, yielding a mean boron value for the whole tissue, which is lower than the actual boron concentration in the non-steatotic hepatocytes. The boron concentration determined in tumour free liver in case of patient 3 and 4 by ICP-MS and PGAA is therefore too low. It could however not determined to what extent the values would change, since steatosis in both patients did not occur uniformly, i.e., it was not possible to determine a fixed percentage of steatosis for the organ as a whole. This issue should be included in future analysis of tumour free liver tissue.

Nonetheless, it can be concluded that with respect for uncertainties and standard deviation for each method and patient, all three methods applied for boron determination are in good accordance.

Upper and lower limit of quantification of all methods presented

Analytical methods which would in principle enable the user to carry out a required analysis may not be suitable for the task, if upper and lower limit of quantification do not match the boron content in the sample which is to be analysed. Naturally, both limits depend not only on technical parameters, but also on sample preparation and the analyst himself.
As stated numerous times before, boron analysis in blood and tissue samples is of major interest in BNCT. From literature, for both types of sample can be derived that mostly boron concentrations between 0 and 40 ppm will be found during analysis. Few groups reported considerably higher boron values, often during *in vitro* studies or animal trials.

Though the three different methods used during the preparation of this thesis have been of course used with respect to their individual limitations, it was found that with all of them, boron analysis in the desired range of measurement is possible (Fig. 84). No sample was encountered, which would have had a boron concentration that could not be determined with the selected method.

ICP-MS is the method presently least limited. The lower limit of quantification when performing analysis of liquid samples was usually around 10 ppb total boron, or 2 ppb and 8 ppb for both isotopes (^{10}B and ^{11}B), respectively. No upper limit of quantification was found. With respect to an average dilution factor of 250 - 270 when preparing blood or tissue samples for measurement, the minimum detectable boron concentration in either types of sample was therefore 2.5 - 2.7 ppm (or 0.50 - 0.54 ppm for ^{10}B and 2.00 - 2.16 ppm for ^{11}B). Theoretically, the analyte signal should behave linearly during linear increase of the boron concentration up to higher concentration (several 100 ppm, though this can be isotope dependent). During the measurements carried out for this thesis, measurements were performed up to a boron concentration of maximum 2 ppm (undiluted). No change in the linear behaviour could be observed.

The limits of quantification for boron analysis by PGAA have to be discussed for both facilities in Petten and Munich separately. For the FRM II in Munich so far only the lower limit (1.8 ppm) has been reported [244]. The lower detection limit of the PGAA facility at the HFR in Petten is 1.5 ppm [186]. The upper limit of detection has been extended for boron measurements of samples containing up to 1972 ppm and checked by MCNP simulations [258].

Due to the use of a sigmoidal fit function for QNCR, the precise mathematical determination of the limit of quantification was very difficult. Furthermore, calibration curves behaved very differently between the single measurements, thus the limit of quantification would have to be calculated for each measurement, which is not practicable. The values are therefore given with respect to the experience of several hundred of calibration curves produced during this thesis. While a definite recognition of boron tracks was possible for boron concentrations of 0.2 – 0.5 ppm, their track area was too small to be distinctly altering the count of the total track area. In other words, naturally occurring α-tracks and proton tracks (produced by protons emerging from the tissue) generated a high “track area background”. As a result, certain quantification of ^{10}B was not possible for

concentrations below 2 ppm. This is much higher than reported in other publications concerning quantitative boron determination by radiographic methods [68]. The upper limit of quantification is 50 ppm, as somewhere between 50 ppm and 100 ppm the saturation of the track area proved to be too problematic for certain data evaluation.

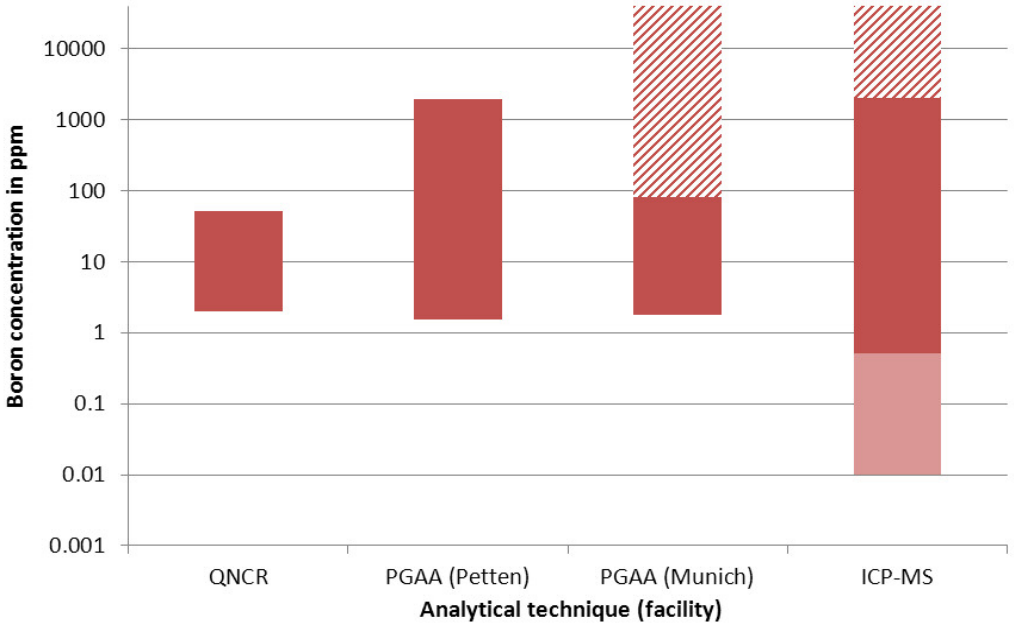

Fig. 84: Range of concentration where (with respect to presently followed analytical protocols) boron (for QNCR and PGAA: ^{10}B, for ICP-MS: both isotopes) quantification is possible with each of the analytical methods presented in this thesis. The hachured parts of the bars indicate that the exact upper limit of quantification of the respective method is unknown. The light red bar indicates the extension of the limit of quantification of ICP-MS if dilution of a sample would not have to be respected

While measurement uncertainties can partly be improved, standard deviation of the boron concentration may be patient or tissue specific and, therefore, will always occur. This should be taken into account when comparing performance of different analytical techniques. Where it was possible, repeated measurement of the same sample and measurement of different aliquots of the same sample were analysed during this thesis to minimise standard deviation. Of course, also optimisation of all methods involved will eventually lead later to a greater accordance between measurements. This issue will be further addressed in the next section.

4. Discussion

In this chapter, intercomparison of ICP-MS, QNCR, and PGAA will be discussed. Since the issues from two very different fields will be addressed, the discussion is split in two parts: one concerning clinical and the other one analytical implications following the work carried out for this thesis.

4.1 Comparison of analytical techniques used for boron analysis

In section 1.5.2, the importance of boron determination for BNCT was discussed. It is not only of utmost importance during clinical trials when boron concentrations in blood and tissue have to be examined, but also in pre-clinical research which ultimately provides all data for the design of clinical trials. Incorrect boron determination can lead to false conclusions in a way that, e.g., a certain boron compound contrary to its true properties does not appear as a suitable boron carrier, a tumour model during in vivo trial seems to not to match the expectations, boron uptake between different types of tissue appears to be higher than thought before and so on.

It remains the choice of the analyst what analytical method for boron determination for a given task (very often defined by a clinician) will be selected. The brief overview in section 1.6.3 over methods for boron analysis demonstrates that there is a wide range of methods with very different advantages and drawbacks. The choice of the right method for a specific research issue is as important as subsequent boron analysis itself – every method can generate values for the boron content in a given sample.

But even though an appropriate method may have been selected for a specific task, this does not necessarily mean that the data yielded by boron analysis are automatically correct, since for every method there are sources of interference (starting at the moment of sample retrieval, over sample preparation, until the measurement itself) possibly causing an incorrect result. Therefore, every analytical method for boron determination should be checked and controlled by other, well characterised methods to ensure analytical quality when generating data.

On the issue of boron analysis, only a few publications are available with respect to validation or comparison of results of different laboratories in multi-centre trials or Round-Robin trials. The analytical methods chosen in these trials are mostly ICP/DCP-MS and ICP/DCP-OES. The trials included also boron determination in other matrices (geological samples and plants) than tissue or blood [164, 259, 260]. To the authors knowledge only Probst et al. [164] presented data obtained by QNCR in direct comparison to other methods (ICP-MS and ICP-OES) for *in vivo* samples. While the two spectroscopic methods were in agreement, results obtained from QNCR varied considerably. This was believed to be caused by the heterogeneity of several of the tissues examined which eventually made direct comparison difficult, as QNCR was carried out for several selected areas in the samples. Though the different kinds of tissue were identified, no further morphological or histological correlation was drawn to the boron distribution.

One of the primary aims of the work presented in this thesis was to ensure analytical quality of the boron analysis carried out with ICP-MS, PGAA, and QNCR. Especially analysis by QNCR was very valuable for the clinical study carried out in Mainz, as it was the only method capable of performing locally selective tissue analysis. Since these data were to be the base for further research on the issue of designing a treatment protocol for liver malignancies, special attention had to be paid.

As illustrated in various sections, no certified, commercially available reference material existed to compare all three methods. A somewhat circular experiment (illustrated in Fig. 74) was designed to create reference samples for one method (QNCR), whose boron content were confirmed by the other methods (PGAA and ICP-MS), which eventually lead to the determination of the (unknown!) boron content in one set of samples obtained during the clinical study (tumour free liver tissue). The measurements of the boron concentration agreed well, however there are still issues to be addressed regarding the performance of each method individually.

QNCR

For a better understanding of tumours as biological entities in BNCT research, it is important to be aware of their morpholological and histological heterogeneity and complexity. Since tumours consist of an individual assortment of different cell types, an analysis of tumour biopsies planned to retrieve relevant data for the planning of future clinical trials, will not lead to conclusive answers to most questions if integral boron determination is carried out. Moreover, also analysis of tumour free tissue may demand local discrimination between cells of different uptake behaviour for a given boron compound.

QNCR has proven to be a very powerful tool to deal with these issues when it comes to boron analysis in tissue biopsies. The protocol presented in this thesis enables the analyst to carry out repeated analysis of the same cryosections of tissue (if stored correctly). After characterisation of a sample by a pathologist, the boron determination in different morphological areas can be determined. The present protocol is limited to a spatial resolution of about 500 µm. The reasons for that are two decisive factors:

Firstly, due to characteristics of the camera and the microscope, the dimensions of the digital images taken at maximum magnification were 410 x 325 µm². Secondly, the areas chosen for analysis on the etched SSNTD film had to be surely correlated to the corresponding areas in the HE-stained images. Though this was done using imaging programmes, some uncertainty has to be considered for this process. This uncertainty arises from the difficulty created by the fact that the cryosection used for histological comparison and the adjacent one used for radiography, though being cut consecutively, were slightly different in dimension.

A possibility to perform high-resolution radiography is a technique very closely related to QNCR called high-resolution alpha-track autoradiography (HRQAR) [205–207], which enables the analyst to perform histological staining and radiography of the same sample. This is achieved by carrying out a sequence of steps including coating the cryosection with two different polymers, staining, and irradiation. Ultimately a resolution of 1 – 2 µm can be reached, which enables the analyst to examine boron concentrations at a subcellular level. Since the analytical protocol which has to be followed is a very complex and time consuming

technique, it does not appear to be suited for a high throughput of samples. It should also be noted that HRQAR is an entirely qualitative, though very powerful, method for boron analysis.
Since it also relies on the revelation of fission fragments by polycarbonate films, several practical aspects, like staining and irradiation of the same cryosection, could be adapted to QNCR to increase spatial resolution. Also, the tracks analysed in this method are much smaller in diameter. The tracks produced in the images analysed for QNCR have a diameter of up to 5 µm, which automatically limits spatial resolution to certain extent and which also produces “saturated” images at higher boron concentrations. Improved image analysis would therefore lead to a higher resolution and consequently to a lower *and* higher limit of quantification.

The existing analytical protocol for QNCR presented in this thesis relies on the irradiation of one set of calibration samples with one cryosection on the same SSNTD, followed by development of the film. This is a very time consuming protocol, because for calibration, digital images of the reference standard have to be taken. Considering that for each concentration at least 5 images should be taken to ensure quality of the measurement, and bearing in mind that per cryosection usually 5 – 10 characteristic areas are selected for analysis, a calibration curve with 8 – 10 concentration steps requires 80 – 90 % of the time needed for taking images and their computed processing of a cryosection. This could be avoided by relying on only one common reference standard for analysis of all cryosections.
Though work on this matter (see section 3.2.4) was not successful, Portu et al. recently published an intriguing approach on establishing a general reference standard for quantitative radiography [261]. Most parameters (etching solution, etching times, SSNTD films, computed image evaluation) differed from the protocol presented in this thesis, but it could be demonstrated that two approaches, one relying on small Lexan cases filled with ^{10}B-enriched boric acid, the other one relying on boric acid enriched agarose gels, both can serve for general standardisation for quantitative radiography. Thus, a high throughput of samples in shorter time is possible. By variation of the etching parameters and the

etching solution, the protocol for QNCR presented in this thesis could possibly be further improved and a general standard for radiographic analysis be established.
Regarding particularly problems arising during the measurements carried out in Mainz, special attention should be paid to production and storage of the cryosections; they should be cut with the same thickness as the standard reference samples and should by all means be stored cooled and sealed to avoid fading of the boron content.

One feature that all protocols for quantitative radiographic boron analysis published in literature have in common, is their inability of performing rapid boron analysis, which would be of interest for monitoring purposes during clinical application of BNCT to a patient. Irradiation, etching, and image analysis require up to several hours, which is too long for shorter infusion times of boron compounds like BPA (1 – 6 h, for further information see also sections 1.3 and 1.5).

PGAA

Determination of the boron concentration in blood is an issue in clinical trials including both treatment of patients by BNCT and studies of clinically relevant parameters, as carried out in the study presented in this thesis. Also during animal trials, blood analysis might be a task.
Whole blood consists of a cellular (hematocrite) and a liquid component (plasma). While the analyst may choose to examine both components separately by PGAA, especially for monitoring of the boron concentration during clinical application of BNCT, rapid analysis of whole blood samples is required, therefore integral analytical techniques can be applied to accomplish such a task and no separation of both components is performed.
Since during analysis by PGAA, a *prompt* spectrum is recorded, the limiting factors for rapid boron determination are:

- transport of the sample to the PGAA facility

- insertion of the sample into the irradiation field

- recording of the spectrum and recording and calculation of the boron concentration

With proper planning (short distances between treatment facility and irradiation facility provided), all these steps can be carried out within minutes, though it might be required to record gamma spectra over longer time intervals to improve statistics of the measurement. Applicability and precision of PGAA has eventually lead to its routine use in BNCT [27, 33, 251, 262].
PGAA has also found frequent use for the analysis of tissue samples [127, 248, 263]. In this work, it could be shown that, while from a technical point of view this is a feasible task, it must be carefully decided what kind of tissue samples are to be measured and what information can be derived from the data.
A very important advantage for boron determination in any kind of sample is that PGAA enables the analyst to carry out repeated analysis of the same sample without interfering with the sample composition and integrity and, therefore, offering the possibility to analyse the sample also with other methods.

Though spectrum quality is better in Munich, measurements in both facilities yielded very similar results for the blood samples, which were reproducible and in accordance with results obtained by QNCR and ICP-MS. Therefore, experience during the study reported in this thesis at both facilities in Munich and Petten confirmed the effectiveness of PGAA for boron determination. Improvements of the limit of detection are highly subjected to the individual technical parameters of the irradiation facility and, unlike other methods, less to the skill of the analyst. Progress in enhancement of a PGAA facility is therefore also automatically limited by the original construction of the whole reactor or accelerator facility.
The only real drawback for the project in Mainz is obviously the geographical distance to both facilities, which renders their use for rapid boron determination in a clinical trial impossible. The implementation of a PGAA measurement assembly at the TRIGA Mainz research reactor is theoretically possible, neutron flux and field can be used at selected positions for PGAA. However, this would require larger reconstruction of the reactor facility, most notably of the involved irradiation tube, which is why such plans are presently not pursued.

ICP-MS

Much that has been said in the preceding paragraph about the application of PGAA accounts as well for ICP-MS: Boron can be determined integrally in both tissue and blood samples (analysed as whole blood or plasma and hematocrite analysed separately), though ICP-MS requires major alteration of the sample matrix to enable the measurement, e.g., dilution for blood samples or extraction / digestion for tissue samples

In direct comparison, both ICP-MS and ICP-OES appear to be equally suitable for blood and tissue analysis, however, for rapid boron analysis in clinical BNCT trials, ICP-OES has found more widespread use [25, 27, 43, 249, 250] (see also section 3.4.2), since it is a more robust method, tolerating particularly higher salt concentrations in the analyte liquid. With respect to limit of detection and analytical precision, ICP-MS would be the better choice, though this advantage hardly comes into effect regarding the range of concentration in which boron determination has to be usually carried out for BNCT (assuming 1 – 40 ppm boron in blood or tissue samples). Dilution requirements are very different for ICP-MS and ICP-OES because of their different abilities to tolerate salt concentrations in analyte liquid.

Though much literature is available on boron analysis in biological materials by ICP-MS, it took some time to establish a routinely useful and reliable analytical protocol to obtain the results presented in this thesis, because several procedures for sample preparation and rinsing of the instrument tried did not lead to the desired outcome.

The final protocol includes wet ashing, which by many analysts is considered the most thorough and suitable method for preparation of biological samples. Unfortunately, this automatically renders the protocol to be unfit for rapid boron analysis in blood, which is required during clinical application of BNCT. This could be overcome by establishing a protocol relying on simple dilution of blood samples. First tests have been carried out unsuccessfully, though this approach surely merits future efforts.

Despite having minimised memory effects with the present protocol, there is still the possibility for optimisation. This would include replacement of the whole quartz

glass based sample introduction assembly by a more inert assembly on polymer basis, e.g., PTFE or PFA. Another option to minimise memory effects could be to replace the entire sample introduction assembly consisting of nebuliser, spray chamber, and torch by a direct injection nebulisation assembly (DIN), though this is a very sensitive matter and requires great attention in use. In works concerning the use for boron determination and for other applications very favourable improvements regarding for example the limit of detection have been reported [264, 265]. Another option would be the use of LA-ICP-MS, which provides also the possibility to carry out locally selective boron analysis and would yield data comparable to QNCR. This would widen the present range of application to include also analysis of samples from tumour tissue. However, also the use of LA-ICP-MS is not a trivial issue, for many elements matrix effects have to be taken into account [266] and analysis has to be carried out accordingly.

The limit of quantification is presently relatively high, especially with respect to the original boron concentration in samples before dilution for sample preparation. The relatively high dilution factor (250 – 270) was chosen to avoid collateral problems caused by salts in the solution. If reduction of the dilution factor could be achieved without compromising quality of the measurement, automatically a lower limit of detection could be reached.

Apart from that, reduction of the boron background during the measurements could be achieved by isotope dilution analysis [267]. The presently available Agilent 7500ce instrument at the Institute for Nuclear Chemistry is not ideally suited for this task due to its quadrupole mass separator. For such work, sector field equipped ICP-MS instruments are the better choice [267].

Eventually, influences on the measurement by the sample matrix (both blood and tissue) could be ruled out by matrix matched calibration. Though orientational works have been published on this issue [164], the exact effects remain largely unknown. More research on this certainly very complex matter could prove very useful for optimisation of boron determination in biological samples.

Synopsis of the three methods

While general accordance of the three methods is given, data evaluation has shown that especially QNCR may need further improvement. Even though consistent values are produced, standard deviation (already when analysing different areas of only one cryosection) could be reduced by better statistics, i.e., analysis of more images per cryosection and more cryosections per tissue biopsy. This could be made possible by creation of method of general calibration to avoid the present time-comsuming analysis of the standard reference sample together with each cryosection.
Also, improved precision of ICP-MS measurements would possibly lead to smaller deviations when comparing values to other methods and therefore would increase agreement with the other methods. The measurements with PGAA have demonstrated precision and correctness of values obtained at both facilities in Munich and Petten. As stated above, improvement of the method is in case of PGAA particularly dependent on the parameters of the "instrumental hardware", e.g., especially regarding neutron spectrum and flux at the irradiation position of the sample or detector efficiency, which is why they are "out of reach" for the analyst who merely uses the equipment at a facility.

It can be ultimately concluded that, with respect to statistical data evaluation, the curves for the blood boron kinetics determined for the patients enrolled in the study have been determined correctly by both PGAA and ICP-MS, though further improvements of both method could obviously be achieved.

With respect to the present analytical protocol, QNCR appears to be the method with most limitations concerning the limits of boron quantification. However, it should be noted that this is the method where changes in the analytical protocol can possibly be easiest achieved, since several parameters (etching times, concentration of the etchant, and neutron fluence for irradiation) can be modified in very small intervals, which offers a great potential for further optimisation.

4.2 Clinical importance of the results gathered during the clinical study

Boron determination in BNCT is always linked to the clinical impact of the respective research project, be it indirect, in pre-clinical and basic research, or direct, as in clinical trials. All data presented in chapter 3 were retrieved in a study hopefully leading to the development of a treatment protocol for patients suffering from neoplastic diseases of the liver. Moreover, several findings are also of importance to investigate the applicability of BNCT to other tumour entities.

Blood and tissue samples were taken from all patients following the same procedure (see also section 3.1): At the beginning of surgery the BPA-infusion was started. During infusion after time intervals of 30 (in case of patient 4: 15 min) blood samples were retrieved. After completing surgery, from the resected liver specimen two tissue samples were taken: one from tumour tissue and one from tumour-free tissue. Then the specimen was perfused with preservation solution and more tissue biopsies were retrieved from the cancerous lesions and from different sites of the tumour-free parts of the specimen

The data for pharmacokinetic behaviour of BPA and the findings of the tissue biopsies will be addressed separately in this section.

Pharmacokinetics

The pharmacokinetic curves for each patient (depicted in sections 3.3.4 and 3.4.5) show common characteristics. Any differences are due to the respective course of surgery:

Patient 3 depicts a classical, monotonically increasing curve. Surgery was carried out as planned within 120 minutes. BPA was administered continuously over the whole period. The curve shows the characteristics of a saturation curve, and the boron concentration reaches its maximum at the end of the infusion time at approximately 20 ppm. This was the only patient where an “ideal” pharmacokinetic uptake curve was found (with respect to data known from literature).

Patient 1 shows minor changes compared to patient 3 which is obviously due to an occluded filter used for the BPA infusion. Consequently, less BPA was administered so that the BPA flow had to be accelerated to cope with the loss of time due to the malfunction of the infusomate. These effects are apparent in the respective figures, where the curve of patient 1 shows a sudden increase towards the end of infusion. With the blocked filter, the BPA concentration increased more slowly than with patient 3, but then increased more quickly when the infusion was accelerated.

Patient 2 shows some changes, too. Firstly, surgery was completed quicker than scheduled, so that the specimens had to be taken at different times and the infusion rate had again to be increased (doubled from minute 60 onwards). Secondly, severe bleeding half an hour after starting the BPA infusion occurred. Due to the subsequent blood transfusion, the boron concentration in the blood was diluted significantly. The effects can be clearly seen in the curves.

Patient 4 continuously lost considerable amounts of blood during surgery. Therefore blood transfusions were required during the same period of time as the BPA infusion. As a result, an expected saturation of at least 20 ppm could not be reached during the infusion time. From minute 45 to the end, the curve shows an almost linear course.

It can be concluded that all curves reflect the course of surgery very well. Every change of the boron level in blood can be traced back to direct influences from surgery.
Also in comparison to other groups reporting uptake curves of BPA for similar infusion times (intravenous administration), the values gathered so far are well within range of expectation. Ryynänen et al. reported data from 10 patients in a study at the Brookhaven National Laboratory, which had a maximum concentration average of 25.4 ppm in blood after receiving a 2 hour infusion of BPA, delivered at 290 mg / kg body weight [110, 268]. During a clinical trial at Harvard – MIT, reported by Kiger III et al. [105], studies were carried out on 24 patients, who were administered BPA using different administration protocols. For 1 hour infusions of 250 mg / kg body weight, typical peak concentrations of boron of about 27 ppm

were found. For infusions of 350 mg / kg body weight over 90 minutes, maximum concentrations of about 32 ppm were achieved. Liberman et al. reported data of 5 patients in an Argentinian trial: peak concentrations of 5.5 ppm and 9.8 ppm were obtained, respectively, after receiving a 60 to 90 minutes infusion of 100 mg / kg body weight and 22.1 to 25.4 ppm after an infusion of 300 mg / kg body weight over the same time [250]. The values show that the measured maximum blood concentrations in the work presented here are within the expected range.

However, the data gathered so far are not sufficient for the creation of a pharmacokinetic model. In order to achieve this, more patients have to be included in the study.

Boron concentration in tumour free liver tissue – comparison to other clinical trials

For tumour-free tissue samples gathered during the clinical study in Mainz, an average boron concentration of 9.74 ppm ± 0.14 ppm was achieved for all patients (mean value and standard deviation given for all methods used).
From all patients tumour free tissue samples were retrieved from different positions of the liver specimen. Therefore, it was possible to examine if there are three-dimensional shifts within the boron concentration: No significant differences were found for any of the four patients within the uncertainties of the analytical methods used for boron analysis.
During the application of BNCT for colorectal liver metastases in Pavia, concentrations of 8.0 ppm ^{10}B were found after an infusion of 300 mg / kg body weight for both patients [121, 134]. The infusion lasted for two hours. The samples were taken one hour and two hours after the start of perfusion. [126] observed mean concentrations of 4.8 ppm and 13.4 ppm after BPA infusions of 100 mg / kg body weight and 300 mg / kg body weight, respectively. The samples were retrieved 75 to 220 min after the end of infusion. In a clinical trial conducted by [127], which explored the uptake behaviour of BPA in liver tissue, a mean concentration in tumour-free tissue of 8.49 ppm was found after an infusion of 100 mg BPA per kg body weight for one hour; sampling was carried out two hours after the end of infusion.

Direct comparison of the four trials is difficult, as in each trial, different study protocols and infusion parameters were chosen. Additionally, the samples were analyzed using different analytical procedures. However, when normalized to a concentration of 100 mg / kg body weight, a comparison of each study reveals significant differences (Table 8).

Tab. 8: Comparison of results published for four clinical trials on intrahepatic boron distribution after administration of BPA. Concentrations are given in ppm

Trial	**Pavia, Italy**	**Buenos Aires, Argentina**	**Mainz, Germany**	**Essen, Germany**
Reference	**[134]**	**[250]**	**[216], this thesis**	**[127]**
Infusion time (min)	120	80-90	120	60
Infusion pathway	colic vein	intravenously	intravenously	intravenously
Sampling time after stop of infusion (min)	-60*; 0	75-220	0	120
Perfusion carried out	No	Yes	Yes	No
BPA Infusion: 300	8.0	13.5		
Concentration in mg / kg body weight 200			9.8 / 9.6† / 9.9	
100		4.7		8.5
Mean values normalized to 100 mg / kg body weight	2.7	4.3	4.9 / 4.8† / 5.0	8.5
Boron concentration determined by	α-spectrometry	ICP-OES	PGAA / QNCR / ICP-MS	PGAA

*one sampling was carried out one hour before the end of infusion, the other one at the end of infusion

† *in [216] and [217] different values for QNCR were reported, because the correction of values for the standard reference samples made of BPA in whole blood had not been carried out yet (see also sections 3.2.5 and 3.2.7)*

Effects of perfusion in tumour free tissue

It is even more difficult to compare data about perfusion effects. Only in the Argentinian trial, perfusion was carried out, however, each liver specimen was perfused differently [126].

In the study presented in this thesis, each perfusion was carried out via the hepatic artery and the portal vein. A “washout” of boron in tumour-free tissue could be

expected, since due to perfusion, any remaining blood, which has a higher boron concentration than tissue, is rinsed out of the liver specimen (Fig. 85).

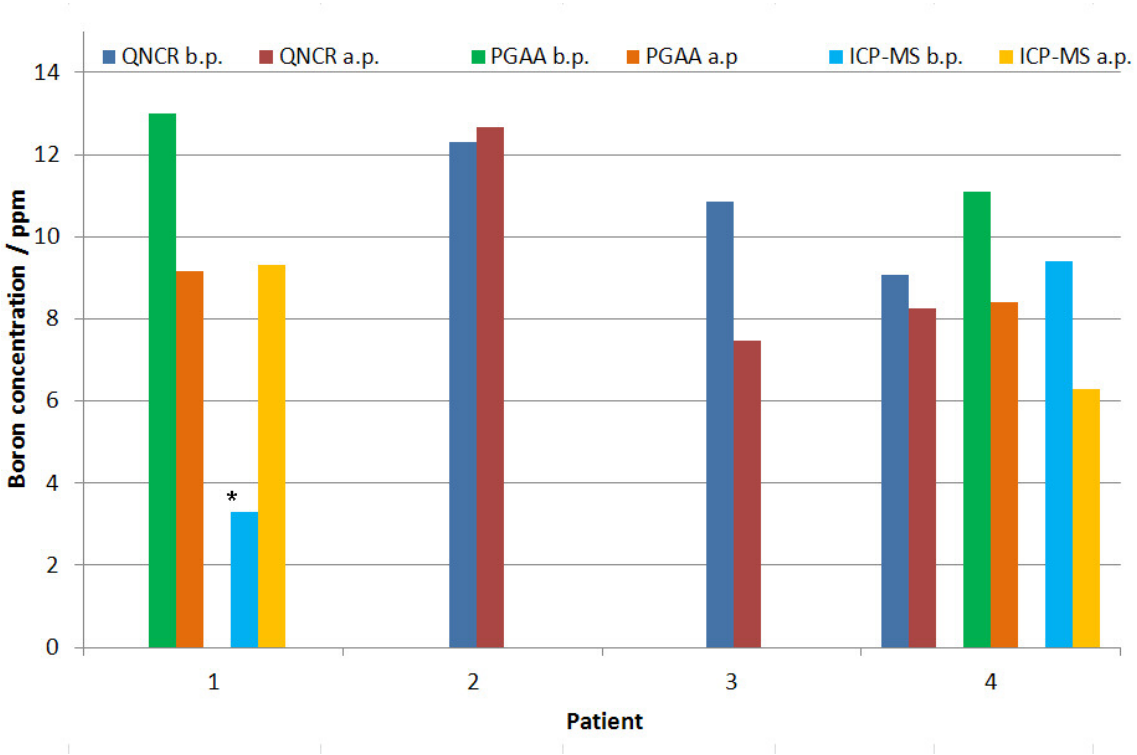

Fig. 85: Comparison of the boron concentration determined in tumour free tissue samples before (b.p.) and after (a.p.) perfusion by PGAA (mean values), QNCR and ICP-MS for all patients. (* value was not considered for clinical evaluation of the patient)

Unfortunately, only the biopsy of patient 4 before perfusion could be examined with QNCR, ICP-MS, and PGAA, for the biopsies of patients 1 – 3 this was not possible: In case of patient 1, the biopsy was taken with a needle and too small to prepare cryosections for QNCR and the result obtained by ICP-MS was considered not to be comparable (see section 3.4.5). In case of patients 2 and 3, the biopsy taken before perfusion was so small that it was completely used up for the preparation of cryosections.

After all, no clear conclusion can be drawn from the values obtained by PGAA, ICP-MS, and QNCR. While in case of patient 2, it appears that no washout took place (determined by QNCR), results for patients 1, 3, and 4 indicated that perfusion of the liver specimen indeed influenced the boron concentration in tumour free liver tissue.

Though the data gathered are consistent with respect to the respective uncertainties of the boron determination, no precise value for the relative boron

loss can be surely calculated. The mean boron loss (calculated for all analytical techniques) is 25.4 %.

Calculation of blood to tissue ratios

Most pharmacokinetic models rely entirely on the monitoring of the boron concentration in blood during treatment with BNCT. It is usually not possible (and not desired) to take tissue biopsies during surgery to deduce boron uptake directly. The determination of the boron concentration, therefore, is carried out indirectly via the blood-to-tissue ratio, which is calculated from the maximum blood concentration and the average tissue concentration.

With respect to the course of surgery, the result for the blood-to-tissue ratio for patient 1 is questionable, because of the sudden increase of the boron concentration towards the end of infusion, which was obviously triggered by the bolus-like administration of the remaining BPA after the forced stop of the infusion.

For patient 1, a second maximum blood concentration and also a second blood-to-tissue ratio were calculated for an expected saturation curve if no sudden increase had occurred at the end. For curves both determined by ICP-MS and PGAA, the resulting ratio would be 2.0.

The second maximum boron concentration was estimated using the first four data points only. These points have been fitted and a new maximum blood concentration has been calculated, whose value is the expected value without the increase at the end. This new ratio is similar to the other ones, indicating that shorter variations of the boron concentration in blood do not influence significantly the uptake behaviour in tumour-free tissue. Nevertheless, patient 1 is omitted for determination of the mean blood-to-tissue ratio.

Ratios determined relying on the results (patients 2 - 4) obtained from ICP-MS are between 1.6 and 2.1, those obtained by PGAA are more constant between 1.7 and 2.0. Since measurement uncertainty was higher for ICP-MS, also the error of the ratios is significantly higher than those calculated for PGAA (see Tables 6 and 7). The mean blood-to-tissue ratio is 1.9, though the determination of such a crucial parameter from data from only three patients is problematic.

The difference in the ratio between the patients is possibly a result of different metabolic cell activity, due to, for example, a fatty liver disease. Metabolic alterations of steatotic cells may influence BPA uptake, although for such a conclusive evaluation, more data are evidently needed. Also, it should be noted that, as of today, there is no proof that from blood-to-tumour ratios cellular uptake in different tumour tissues can be deduced.

As it was the case for boron concentration in tumour free tissue, comparison of the blood-to-tissue concentration ratio reported in other studies is problematic due to varying administration protocols for the BPA infusion. In the trial carried out in Mainz, the determined blood-to-tissue ratio is comparable to those observed by Wittig et al., where maximum blood concentrations around 12 to 13 ppm and about 8.5 ppm in tumour-free liver tissue were observed [127]. Cardoso et al. collected analogous data during their liver cancer trial for five patients [126]. However, no peak blood boron concentrations were reported. The observed blood data were gained from samples collected about one hour after the end of infusion. The BPA blood concentrations decrease quickly after the end of the infusion, as demonstrated in different studies and models on the pharmacokinetics of BPA [105, 110, 111] among others, see also section 1.5), so that the observed ratios with a value of about 1 are much smaller than those shown here.
Comparison with the data presented in this thesis is in this case again difficult, since no samples were taken after the infusion. The boron in the blood at that time did not affect the boron concentration in the liver anymore, because the blood vessels to the liver had been clamped. Furthermore, the decrease in the blood concentration would differ from the regular behaviour since the tumour and parts of the liver are no longer inside the body.

Boron concentration in tumour tissue – comparison to other clinical trials

Tumours have a very different vascularisation, i.e., the rim of a tumour is better supplied than inner parts, thus any perfusion effects would have a lesser effect than in tumour free liver tissue with a more dense and homogeneous vascularisation. The data gained from two patients did not indicate any loss of

boron by the perfusion. However, from such few data it is problematic to draw a consistent conclusion. Eventually, it will be necessary to examine biopsies from more patients to assess the effects of the perfusion of a resected liver specimen by hemihepatectomy.

In this thesis, the two-dimensional uptake and distribution of boron in cancer tissue and non-neoplastic liver is presented with respect to the morphological characteristics of such tissue; the respective measurements were carried out with QNCR. By comparing radiographic and histological cryosections, it could be shown that tumour cells and desmoplastic stromal cells had a high boron uptake, followed by tumour free liver tissue and steatotic hepatocytes. The lowest boron concentrations were found in necrotic tumour tissue.
The findings indicate that the biological characteristics of exposed tissue may be a decisive factor controlling the boron uptake. Regarding the potential clinical implications, the spatial boron distribution in different tissue compartments such as tumour cells, connective tissue, vessels, or necrotic areas has to be taken into account. Not only the overall BPA uptake into the tumour, but rather the uptake into the separate cell types in tumour tissue needs to be addressed, which was performed in the present study.
Analysis is still limited by the spatial resolution of the images taken by the digital camera. This means that it was possible to distinguish areas of different cell types, which enabled the determination the ^{10}B concentration in tissue in a much more differentiated way than in bulk analysis procedures.

The results obtained during the study presented in this thesis confirm the need for locally differentiating analysis for the assessment of tumour samples. As steatotic hepatocytes contain less boron than normal hepatocytes, steatotic regions must be excluded during analysis, when the aim is to determine the true concentration in tumour-free tissue to correctly calculate the radiation dose administered to healthy tissue during a clinical trial.

In cancerous tissue, the uptake behaviour varies greatly between different tumour areas. Necrotic areas usually show a very low uptake of BPA. However, as shown in patient 2, this also depends on the extent and the dimension of a necrotic area.

In larger necrotic areas, much lower concentrations were found in the centre. This is possibly due to the poorer vascular supply in such areas. Desmoplastic stromal cells showed an uptake comparable to that of tumour cells.

With respect to other clinical trials, comparison of the boron concentration found in vital tumour tissue, from the respective trials, is difficult as well. Although in other studies, tumour tissue identity was confirmed histologically, boron determination was not carried out in direct correlation to distinct cell types.
Cardoso et al. [126] and Wittig et al. [127] investigated the uptake of BPA in human liver tissue according to a similar protocol as applied in Pavia [131, 134, 135]. Both groups indicated the need for a correlation of histological analyses with the analysis of the boron concentration, as different areas within the same tumour had different uptake behaviour depending on biological tumour characteristics. Moreover, in these studies, partly bulk analysis methods for boron determination were chosen. To remedy the problem posed by the heterogeneity of the tissue, Coderre et al. [129] presented an approach to standardise cancer tissue analysis in BNCT, by taking into account the number of viable tumour cells in a certain tissue area (introduction of a “cellularity index”). This way values obtained from bulk analysis could later be calculated via a correction factor.
This idea was also applied by Wittig et al. for the evaluation of their liver biopsies, although the determination of “viable cells” poses the question of how this is to be defined within a complex and heterogenic morphological system, e.g., fibrotic tissue consists also of viable cells, however such cells are not primarily decisive for the prediction of the therapeutic outcome of BNCT.

As laid out in more detail in section 1.5, the amino acid transporter responsible for the uptake of BPA in numerous cells belongs to the L-system (LAT-1). The expression of LAT-1 is cell and tumour specific. This strengthens the assumption, which is fully supported by the results presented in this thesis, that discrimination between different cell types is a key factor to investigate the uptake of BPA, independent of whether cancerous or tumour-free tissue is regarded. Other groups reported side effects after clinical applications of BNCT, e.g., for oral cancer, and primary or metastatic brain tumours. Aihara et al. observed side effects such as acute reactions in the mucosal lining of the oral cavity and the oropharynx after application of BNCT for recurrent submandibular gland cancer [22], indicating that

tissue such as the mucosa may have a high LAT-1 expression, even though no neoplasia in this tissue was reported. Similar effects have been reported by Busse et al. [27] and by Coderre et al. [129] after the irradiation of patients with brain tumours after an infusion of BPA-F. This can be explained by findings about increased LAT-1 expression in the basal layers of healthy human mucosa [269, 270].

In colon cancer cells, the LAT-1 expression is much higher than in normal liver tissue, which appears to be one reason for the higher BPA uptake in viable cancer cells of colorectal liver metastases than in tumour free liver tissue [91]. In this respect, an interesting finding is that desmoplastic stromal cells showed an uptake comparable to tumour cells, yet the author could not find any reported values for LAT-1 expression in such cells.

In steatotic hepatocytes, metabolic disarrangement but also the solubility of BPA may be the reason for low concentrations. This issue could be addressed by experimental cell culture studies.

5. Conclusions and suggestions for future research

In this work, two major issues were addressed: The validity and comparability of three different analytical techniques (QNCR, PGAA, and ICP-MS) for boron determination in biological samples and application of these methods for examination of blood and tissue samples from a clinical study on boron uptake in blood, liver tissue, and neoplastic tissue, after infusion of BPA, of patients suffering from colorectal liver metastases.

The data of all methods and their comparison revealed that it is possible to obtain matching results from all three methods from a specific type of sample. In this case, this was tumour free liver tissue characterised by very homogeneous uptake of BPA, consequently, also analytical techniques for integral boron determination yield the consistent results in comparison to a locally selective method. Further validation was carried out using specially prepared reference samples of whole blood.
To the author's knowledge, this is the first work to:

- compare three analytical methods for boron determination with completely different principles of detecting boron (1.) directly via detection of boron ions by mass spectrometry, (2.) indirectly by recording the prompt γ-spectrum emitted after neutron capture of the isotope ^{10}B, and again (3.) indirectly by analysis of the fission fragments emerging from the nuclear reaction induced by neutron capture of ^{10}B,

- compare a locally selective method (QNCR) with two integral methods (PGAA and ICP-MS) to yield results in good agreement for the same tissue samples containing boron of a confirmed morphology,

- report results of a clinical study on the boron uptake by colorectal liver metastases with a study protocol closely resembling liver transplantation and assessing the possible consequences for the boron distribution due to perfusion of the resected liver specimen. Each resected specimen was perfused via the same blood vessels.

Boron determination has been carried out for all samples obtained during the ongoing clinical study. All pharmacokinetic data have been in agreement with results previously published by other groups. Furthermore, the course of surgery and administration of the BPA infusion is reflected very well in the curves of all patients participating in the study.

Regarding the biopsies from tumour and tumour free tissue, it was possible to demonstrate that a heterogeneous boron uptake in tissue areas of different morphology took place. Highest uptake was found for vital tumour cells, followed by desmoplastic cells, non-steatotic hepatocytes, and steatotic hepatocytes. The uptake in necrotic clusters largely depends on the dimensions of such cell clusters. Not only the heterogeneity of tumour tissue, i.e., regions of necrosis, fibrosis, or tumour cells, seems to be decisive for the varying uptake of tumours but it seems also important to consider inter-individual metabolic variations of cells regardless of the compartment. This statement is corroborated by differences in boron concentration of tumour cells and desmoplastic cells occurring in four patients enrolled in the study so far. Therefore, it appears not to be satisfactory to differentiate between “healthy” or “normal” and “tumourous” tissue, if a more specific characterisation is not available.

The results, therefore, demonstrate the need for differentiating analysis of tissue samples. For the ongoing clinical study, a combination of computed QNCR with histological analysis was established as a suitable method to correlate the morphology of tissue and the boron concentration. The conclusion must be that bulk sample analysis is not suitable to determine and to image the ^{10}B concentration in tumour tissue, especially if characterisation of the uptake behaviour of BPA for future clinical application of BNCT is required.

Also, higher resolution of the radiographic images would enable analysis of smaller cellular areas, possibly even for single cells. This way it would be possible to correlate boron uptake behaviour to individual cell characteristics, which might not only be assessed by mere morphological analysis, but rather by immuno-histochemical analysis of the examined tissue. Most works lack the correlation of the boron distribution and concentration to biomarker analysis for cell proliferation, grading of neoplasms, amino acid transport, epidermal growth factor expression et

cetera. First works addressing this issue have been started in cooperation with the Institute of Pathology of the University of Mainz.

Additionally, requests have been filed to the responsible ethics committee to enlarge the ongoing study on colorectal liver metastasis to investigation on hepatocellular carcinoma and intrahepatic cholangiocarcinoma. The revised protocol foresees furthermore administration of intra-arterial infusion, as different works indicate this might induce more favourable uptake behaviour of BPA-fructose.

Future comparison of clinically relevant data could furthermore be largely improved, if similar protocols for surgery, administration of the boron compound, and sample analysis could be established for all groups working on the application of BNCT for neoplastic diseases of the liver.

Clinical application of BNCT to *ex vivo* irradiated organs is very complicated, which makes the selection of patients for such a therapy crucial. Our results showed great variation in the uptake of BPA between different patients, which poses the question of diagnostic possibilities to select suitable patients for this kind of treatment. By finding a link between a biological parameter, which could be measured pre-operatively and which would allow a direct prediction of the boron distribution in different cell types of tumour tissue, diagnostics could be used to improve treatment planning.

6. List of references

1. Herrmann T (2006) *Klinische Strahlenbiologie*. *Kurz und bündig*. Thomas Herrmann, Michael Baumann und Wolfgang Dörr, 4th edn. Elsevier Urban und Fischer, München, Jena
2. Jones DTL, Wambersie A (2007) *Radiation therapy with fast neutrons: A review*. *Proceedings of the 10th International Symposium on Radiation Physics - ISRP 10.* Nuclear Instruments and Methods in Physics Research Section A: Accelerators, Spectrometers, Detectors and Associated Equipment 580(1):522–525
3. Terasawa T, Dvorak T, Ip S, Raman G, Lau J, Trikalinos TA (2009) *Systematic Review: Charged-Particle Radiation Therapy for Cancer.* Annals of Internal Medicine 151(8):556–565
4. Kraft G (2000) *Tumor therapy with heavy charged particles.* Progress in Particle and Nuclear Physics 45(Supplement 2):473–544
5. Muacevic A, Wowra B, Siefert A, Tonn J, Steiger H, Kreth F (2008) *Microsurgery plus whole brain irradiation versus Gamma Knife surgery alone for treatment of single metastases to the brain: a randomized controlled multicentre phase III trial.* Journal of Neuro-Oncology 87(3):299–307
6. Nag S, Beyer D, Friedland J, Grimm P, Nath R (1999) *American brachytherapy society (ABS) recommendations for transperineal permanent brachytherapy of prostate cancer.* International Journal of Radiation Oncology*Biology*Physics 44(4):789–799
7. Koukourakis G, Kelekis N, Armonis V, Kouloulias V (2009) *Brachytherapy for Prostate Cancer: A Systematic Review.* Advances in Urology Article ID 327945
8. Wieners G, Mohnike K, Peters N, Bischoff J, Kleine-Tebbe A, Seidensticker R, Seidensticker M, Gademann G, Wust P, Pech M, Ricke J (2011) *Treatment of hepatic metastases of breast cancer with CT-guided interstitial brachytherapy - A phase II-study.* Radiotherapy and Oncology 100(2):314–319
9. Buchegger F, Antonescu C, Helg C, Kosinski M, Prior JO, Bischof Delaloye A, Press OW, Ketterer N (2011) *Six of 12 Relapsed or Refractory Indolent Lymphoma Patients Treated 10 Years Ago with 131I-Tositumomab Remain in Complete Remission.* Journal of Nuclear Medicine 52(6):896–900
10. Witzig TE, Gordon LI, Cabanillas F, Czuczman MS, Emmanouilides C, Joyce R, Pohlman BL, Bartlett NL, Wiseman GA, Padre N, Grillo-López AJ, Multani P, White CA (2002) *Randomized Controlled Trial of Yttrium-90 Labeled Ibritumomab Tiuxetan Radioimmunotherapy Versus Rituximab Immunotherapy for Patients With Relapsed or Refractory Low-Grade, Follicular, or Transformed B-Cell Non-Hodgkin's Lymphoma.* Journal of Clinical Oncology 20(10):2453–2463
11. Hoffmann RT, Jakobs TF, Kubisch CH, Stemmler HJ, Trumm C, Tatsch K, Helmberger TK, Reiser MF (2010) *Radiofrequency ablation after selective internal radiation therapy with Yttrium90 microspheres in metastatic liver disease--Is it feasible? Emergency Radiology.* European Journal of Radiology 74(1):199–205
12. Lam MGEH, Klerk JMH, Rijk PP (2008) *186Re-HEDP for Metastatic Bone Pain in Breast Cancer Patients*. In: Bombardieri E, Gianni L, Bonadonna G (eds) Breast Cancer. Springer Berlin Heidelberg, pp 257–269

13. Luster M, Clarke S, Dietlein M, Lassmann M, Lind P, Oyen W, Tennvall J, Bombardieri E (2008) *Guidelines for radioiodine therapy of differentiated thyroid cancer.* European Journal of Nuclear Medicine and Molecular Imaging 35(10):1941–1959
14. Zalutsky MR *Radionuclide Therapy*. In: Handbook of Nuclear Chemistry, Vèrtes, A.; Nagy, S.; Klencsàr, Z.; Lovas, R. G.; Rösch, F. (eds.), vol. 4, pp 2180–2203
15. Kampen WU, Voth M, Pinkert J, Krause A (2007) *Therapeutic status of radiosynoviorthesis of the knee with yttrium [90Y] colloid in rheumatoid arthritis and related indications.* Rheumatology 46(1):16–24
16. Mulford DA, Scheinberg DA, Jurcic JG (2005) *The Promise of Targeted alpha-particle Therapy.* Journal of Nuclear Medicine 46(supplement 1):199–204
17. International Atomic Energy Agency IAEA (2001) *Current Status of Neutron Capture Therapy*. *IAEA-TECDOC-1223,* Vienna
18. Locher G (1936) *Biological effects and therapeutic possibilities of neutrons.* Am. J. Roentgenol. 36:1–13
19. Farr LE, Sweet WHRJS, Foster CG, Locksley HB, Sutherland DL, Mendelsohn ML, Stickley EE (1954) *Neutron capture therapy with boron in the treatment of glioblastoma multiforme.* Am. J. Roentgenol. 71(2):279–293
20. Barth RF, Coderre JA, Vicente MGH, Blue TE (2005) *Boron Neutron Capture Therapy of Cancer: Current Status and Future Prospects.* Clin Cancer Res 11(11):3987–4002
21. Imahori Y, Ueda S, Ohmori Y, Kusuki T, Ono K, Fujii R, Ido T (1998) *Fluorine-18-Labeled Fluoroboronophenylalanine PET in Patients with Glioma.* J Nucl Med 39(2):325–333
22. Aihara T, Hiratsuka J, Morita N, Uno M, Sakurai Y, Maruhashi A, Ono K, Harada T (2006) *First clinical case of boron neutron capture therapy for head and neck malignancies using 18F-BPA PET.* Head Neck 28(9):850–855
23. Koivunoro H, Kumada H, Seppälä T, Kotiluoto P, Auterinen I, Kankaanranta L, Savolainen S (2009) *Comparative study of dose calculations with SERA and JCDS treatment planning systems*. *13th International Congress on Neutron Capture Therapy BNCT: a new option against cancer.* Applied Radiation and Isotopes 67(7-8, Supplement 1):126–129
24. Joensuu H, Kankaanranta L, Seppälä T, Auterinen I, Kallio M, Kulvik M, Laakso J, Vähätalo J, Kortesniemi M, Kotiluoto P, Serén T, Karila J, Brander A, Järviluoma E, Ryynänen P, Paetau A, Ruokonen I, Minn H, Tenhunen M, Jääskeläinen J, Färkkilä M, Savolainen S (2003) *Boron Neutron Capture Therapy of Brain Tumors: Clinical Trials at the Finnish Facility Using Boronophenylalanine.* Journal of Neuro-Oncology 62(1):123–134
25. Kankaanranta L, Seppälä T, Koivunoro H, Välimäki P, Beule A, Collan J, Kortesniemi M, Uusi-Simola J, Kotiluoto P, Auterinen I, Serèn T, Paetau A, Saarilahti K, Savolainen S, Joensuu H (2011) *l-Boronophenylalanine-mediated Boron Neutron Capture Therapy for Malignant Glioma Progressing After External Beam Radiation Therapy: A Phase I Study.* International Journal of Radiation Oncology*Biology*Physics 80(2):369–376
26. Diaz AZ (2003) *Assessment of the results from the phase I/II boron neutron capture therapy trials at the Brookhaven National Laboratory from a clinician's point of view.* Journal of Neuro-Oncology 62(1):101–109
27. Busse P, Harling O, Palmer M, Kiger W, Kaplan J, Kaplan I, Chuang C, Goorley J, Riley K, Newton T, Santa Cruz GA, Lu X-, Zamenhof R (2003) *A critical examination of the results from the Harvard-MIT NCT program phase I*

clinical trial of neutron capture therapy for intracranial disease. Journal of Neuro-Oncology 62(1):111–121
28. Henriksson R, Capala J, Michanek A, Lindahl S-, Salford LG, Franzén L, Blomquist E, Westlin J-, Bergenheim AT (2008) *Boron neutron capture therapy (BNCT) for glioblastoma multiforme: A phase II study evaluating a prolonged high-dose of boronophenylalanine (BPA).* Radiotherapy and Oncology 88(2):183–191
29. Sköld K, H-Stenstam B, Diaz AZ, Giusti V, Pellettieri L, Hopewell JW (2010) *Boron Neutron Capture Therapy for glioblastoma multiforme: advantage of prolonged infusion of BPA-f.* Acta Neurologica Scandinavica 122(58-62)
30. Nakagawa Y, Pooh K, Kobayashi T, Kageji T, Uyama S, Matsumura A, Kumada H (2003) *Clinical Review of the Japanese Experience with Boron Neutron Capture Therapy and A Proposed Strategy Using Epithermal Neutron Beams.* Journal of Neuro-Oncology 62(1):87–99
31. Miyatake, S. - I., Kawabata S, Kajimoto Y, Aoki A, Yokoyama K., Yamada M., Kuroiwa T, Tsuji M, Imahori Y, Kirihata M, Sakurai Y, Masunaga S, Nagata K, Maruhashi A, Ono K (2005) *Modified boron neutron capture therapy for malignant gliomas performed using epithermal neutron and two boron compounds with different accumulation mechanisms: an efficacy study based on findings on neuroimages.* J Neurosurg 103:1000–1009
32. Yamamoto T, Nakai K, Tsurubuchi T, Matsuda M, Shirakawa M, Zaboronok A, Endo K, Matsumura A (2009) *Boron neutron capture therapy for newly diagnosed glioblastoma: A pilot study in Tsukuba*. *13th International Congress on Neutron Capture Therapy BNCT: a new option against cancer.* Applied Radiation and Isotopes 67(7-8, Supplement 1):25–26
33. Matsuda M, Yamamoto T, Kumada H, Nakai K, Shirakawa M, Tsurubuchi T, Matsumura A (2009) *Dose distribution and clinical response of glioblastoma treated with boron neutron capture therapy*. *13th International Congress on Neutron Capture Therapy BNCT: a new option against cancer.* Applied Radiation and Isotopes 67(7-8, Supplement 1):19–21
34. Miyatake, S. - I., Kawa, Yokoyama K., Kuroiwa T, Michiue H, Sakurai Y, Kumada H, Suzuki M, Maruhashi A, Kirihata M, Ono K (2009) *Survival benefit of Boron neutron capture therapy for recurrent malignant gliomas.* Journal of Neuro-Oncology 91(2):199–206
35. Kawabata S, Nonoguchi N, Hiramatsu R, Iida K, Miyata S, Yokoyama K., Doi A, Kuroda Y, Kuroiwa T, Michiue H, Kumada H, Kirihata M, Imahori Y, Maruhashi A, Sakurai Y, Suzuki M, Masunaga S, Ono K (2009) *Survival benefit from boron neutron capture therapy for the newly diagnosed glioblastoma patients*. *13th International Congress on Neutron Capture Therapy BNCT: a new option against cancer.* Applied Radiation and Isotopes 67(7-8, Supplement 1):15–18
36. Kageji T, Mizobuchi Y, Nagahiro S, Nakagawa Y, Kumada H (2011) *Long-survivors of glioblatoma treated with boron neutron capture therapy (BNCT).* Applied Radiation and Isotopes 69(12):1800–1802
37. Kawabata S, Miyatake S-, Koroiwa T, Yokoyama K., Doi A, Iida K, Miyata S, Nonoguchi N, Michiue H, Takahashi M, Inomata T, Imahori Y, Kirihata M, Sakurai Y, Maruhashi A, Kumada H, Ono K (2009) *Boron Neutron Capture Therapy for Newly Diagnosed Glioblastoma.* Radiation Research 50(1):51–60
38. Hopewell JW, Gorlia T, Pellettieri L, Giusti V, H-Stenstam B, Sköld K (2011) *Boron neutron capture therapy for newly diagnosed glioblastoma multiforme:*

An assessment of clinical potential. Applied Radiation and Isotopes 69(12):1737–1740
39. Sköld K, Gorlia T, Pellettieri L, Giusti V, H-Stenstam B, Hopewell JW (2010) *Boron neutron capture therapy for newly diagnosed glioblastoma multiforme: an assessment of clinical potential.* Br J Radiol 83(991):596–603
40. Cox DR (1972) *Regression Models and Life-Tables.* Journal of the Royal Statistical Society. Series B (Methodological) 34(2):187–220
41. Breiman L (1984) *Classification and regression trees.* Chapman & Hall/CRC
42. Gaspar LE, Scott C, Murray K, Curran W (2000) *Validation of the RTOG recursive partitioning analysis (RPA) classification for brain metastases.* International Journal of Radiation Oncology*Biology*Physics 47(4):1001–1006
43. Fukuda H, Hiratsuka J, Kobayashi T, Sakurai Y, Yoshino K, Karashima H, Turu K, Araki K, Mishima Y, Ichihashi M (2003) *Boron neutron capture therapy (BNCT) for malignant melanoma with special reference to absorbed doses to the normal skin and tumor.* Australasian Physical and Engineering Science in Medicine 26(3):97–103
44. Menéndez PR, Roth BMC, Pereira MD, Casal MR, González SJ, Feld DB, Santa Cruz GA, Kessler J, Longhino J, Blaumann H, Jiménez Rebagliati R, Calzetta Larrieu OA, Fernández C, Nievas SI, Liberman SJ (2009) *BNCT for skin melanoma in extremities: Updated Argentine clinical results*. *13th International Congress on Neutron Capture Therapy BNCT: a new option against cancer.* Applied Radiation and Isotopes 67(7-8, Supplement 1):50–53
45. Kankaanranta L, Seppälä T, Koivunoro H, Saarilahti K, Atula T, Collan J, Salli E, Kortesniemi M, Uusi-Simola J, Mäkitie A, Seppänen M, Minn H, Kotiluoto P, Auterinen I, Savolainen S, Kouri M, Joensuu H (2007) *Boron Neutron Capture Therapy in the Treatment of Locally Recurred Head and Neck Cancer.* International Journal of Radiation Oncology*Biology*Physics 69(2):475–482
46. Kankaanranta L, Seppälä T, Koivunoro H, Saarilahti K, Atula T, Collan J, Salli E, Kortesniemi M, Uusi-Simola J, Välimäki P, Mäkitie A, Seppänen M, Minn H, Revitzer H, Kouri M, Kotiluoto P, Seren T, Auterinen I, Savolainen S, Joensuu H (2011) *Boron Neutron Capture Therapy in the Treatment of Locally Recurred Head-and-Neck Cancer: Final Analysis of a Phase I/II Trial.* International Journal of Radiation Oncology*Biology*Physics 82(1):67–75
47. Kimura Y, Ariyoshi Y, Shimahara M, Miyatake S, Kawabata S, Ono K, Suzuki M, Maruhashi A (2009) *Boron neutron capture therapy for recurrent oral cancer and metastasis of cervical lymph node*. *13th International Congress on Neutron Capture Therapy BNCT: a new option against cancer.* Applied Radiation and Isotopes 67(7-8, Supplement 1):47–49
48. Kato I, Fujita Y, Maruhashi A, Kumada H, Ohmae M, Kirihata M, Imahori Y, Suzuki M, Sakrai Y, Sumi T, Iwai S, Nakazawa M, Murata I, Miyamaru H, Ono K (2009) *Effectiveness of boron neutron capture therapy for recurrent head and neck malignancies*. *13th International Congress on Neutron Capture Therapy BNCT: a new option against cancer.* Applied Radiation and Isotopes 67(7-8, Supplement 1):37–42
49. Morita N, Hiratsuka J, Kuwabara C, Aihara T, Ono K, Fukuda H, Kumada H, Harada T, Imajo Y (2006) *Successful BNCT for Patients with Cutaneous and Mucosal Melanomas: Report of 4 Cases*. In: International Society for Neutron Capture Therapy (ed) 12th International Congress on Neutron Capture Therapy. “From the Past to the Future”. Neutrino OSAKA Inc., Osaka, pp 18–20

50. Auterinen I, Kankaanranta L *The FiR 1 BNCT Facility - Improving and Continuing the Patient Treatment Service into the 2020's*. In: Proceedings of 14th International Congress on Neutron Capture Therapy, pp 395–397
51. Karnofsky DA (1949) *The clinical evaluation of chemotherapeutic agents in cancer,. In: Evaluation of Chemotherapeutic Agents (MacLeod CM ed),.* Columbia University Press, New York.
52. WHO (2011) *World Health Organisation*. *Cancer fact sheets. Fact Sheet N°297*. http://www.who.int/mediacentre/factsheets/fs297/en/index.html. Accessed August 21st
53. Olnes MJ, Erlich R (2004) *A Review and Update on Cholangiocarcinoma.* Oncology 66(3):167–179
54. Livraghi T, Meloni F, Di Stasi M, Rolle E, Solbiati L, Tinelli C, Rossi S (2008) *Sustained complete response and complications rates after radiofrequency ablation of very early hepatocellular carcinoma in cirrhosis: Is resection still the treatment of choice?* Hepatology 47(1):82–89
55. Lencioni R, Crocetti L (2007) *Radiofrequency Ablation of Liver Cancer*. *Interventional Oncology - Part 1: Hepatic Interventions.* Techniques in Vascular and Interventional Radiology 10(1):38–46
56. Jaeck D, Pessaux P (2008) *Bilobar Colorectal Liver Metastases: Treatment Options*. *Progress in Surgical Oncology: A European Perspective.* Surgical Oncology Clinics of North America 17(3):553–568
57. Adam R, Wicherts DA, Haas RJ de, Ciacio OLF, Paule B, Ducreux M, Azoulay D, Bismuth H, Castaing D (2009) *Patients With Initially Unresectable Colorectal Liver Metastases: Is There a Possibility of Cure?* Journal of Clinical Oncology 27(11):1829–1835
58. Berber E, Pelley R, Siperstein AE (2005) *Predictors of Survival After Radiofrequency Thermal Ablation of Colorectal Cancer Metastases to the Liver: A Prospective Study.* Journal of Clinical Oncology 23(7):1358–1364
59. Kemeny N, Fata F (1999) *Arterial, portal, or systemic chemotherapy for patients with hepatic metastasis of colorectal carcinoma.* Journal of Hepato-Biliary-Pancreatic Surgery 6(1):39–49
60. Kemeny N, Huang Y, Cohen AM, Shi W, Conti JA, Brennan MF, Bertino JR, Turnbull A, Sullivan D, Stockman J, Blumgart LHFY (1999) *Hepatic Arterial Infusion of Chemotherapy after Resection of Hepatic Metastases from Colorectal Cancer.* New England Journal of Medicine 341(27):2039–2048
61. Tse RV, Hawkins M, Lockwood G, Kim JJ, Cummings B, Knox J, Sherman M, Dawson LA (2008) *Phase I Study of Individualized Stereotactic Body Radiotherapy for Hepatocellular Carcinoma and Intrahepatic Cholangiocarcinoma.* Journal of Clinical Oncology 26(4):657–664
62. Fukumitsu N, Sugahara S, Nakayama H, Fukuda K, Mizumoto M, Abei M, Shoda Ji, Thono E, Tsuboi K, Tokuuye K (2009) *A Prospective Study of Hypofractionated Proton Beam Therapy for Patients With Hepatocellular Carcinoma.* International Journal of Radiation Oncology*Biology*Physics 74(3):831–836
63. Hata M, Tokuuye K, Sugahara S, Fukumitsu N, Hashimoto T, Ohnishi K, Nemoto K, Ohara K, Matsuzaki Y, Akine Y (2006) *Proton beam therapy for hepatocellular carcinoma with limited treatment options.* Cancer 107(3):591–598
64. Lee MT, Kim JJ, Dinniwell R, Brierley J, Lockwood G, Wong R, Cummings B, Ringash J, Tse RV, Knox JJ, Dawson LA (2009) *Phase I Study of*

Individualized Stereotactic Body Radiotherapy of Liver Metastases. Journal of Clinical Oncology 27(10):1585–1591
65. Kennedy AS, McNeillie P, Dezarn WA, Nutting C, Sangro B, Wertman D, Garafalo M, Liu D, Coldwell D, Savin M, Jakobs T, Rose S, Warner R, Carter D, Sapareto S, Nag S, Calkins A, Gates VL, Salem R (2009) *Treatment Parameters and Outcome in 680 Treatments of Internal Radiation With Resin 90Y-Microspheres for Unresectable Hepatic Tumors.* International Journal of Radiation Oncology*Biology*Physics 74(5):1494–1500
66. Smits MLJ, Nijsen JFW, van den Bosch MAAJ, Lam MGEH, Vente MAD, Huijbregts J. E., van het Schip AD, Elschot M, Bult W, Jong HWAM de, Meulenhoff PCW, Zonnenberg BA
67. Mazzaferro V, Chun Y, Poon R, Schwartz M, Yao F, Marsh J, Bhoori S, Lee S- (2008) *Liver Transplantation for Hepatocellular Carcinoma.* Annals of Surgical Oncology 15(4):1001–1007
68. Probst TU (1999) *Methods for boron analysis in boron neutron capture therapy (BNCT). A review.* Fresenius' Journal of Analytical Chemistry 364(5):391–403
69. Hatanaka H (1986) *Chapter I. Introduction*. *Boron Neutron Capture Therapy for Tumors. Niigata, Nishimura*
70. Coderre JA, Glass JD, Fairchild RG, Micca PL, Fand I, Joel DD (1990) *Selective Delivery of Boron by the Melanin Precursor Analogue p-Boronophenylalanine to Tumors Other than Melanoma.* Cancer Research 50(1):138–141
71. Yang W, Barth RF, Rotaru JH, Moeschberger ML, Joel DD, Nawrocky M, Goodman JH (1997) *Enhanced survival of glioma bearing rats following boron neutron capture therapy with blood-brain barrier disruption and intracarotid injection of boronophenylalanine.* Journal of Neuro-Oncology 33:59–70
72. Mikado S, Yanagie H, Yasuda N, Higashi S, Ikushima I, Mizumachi R, Murata Y, Morishita Y, Nishimura R, Shinohara A, Ogura K, Sugiyama H, Iikura H, Ando H, Ishimoto M, Takamoto S, Eriguchi M, Takahashi H, Kimura M (2009) *Application of neutron capture autoradiography to Boron Delivery seeking techniques for selective accumulation of boron compounds to tumor with intra-arterial administration of boron entrapped water-in-oil-in-water emulsion*. *ITMNR 08 - Proceedings of the sixth Topical Meeting on Neutron Radiography.* Nuclear Instruments and Methods in Physics Research Section A: Accelerators, Spectrometers, Detectors and Associated Equipment 605(1-2):171–174
73. Cruickshank GS, Ngoga D, Detta A, Green S, James ND, Wojnecki C, Doran J, Hardie J, Chester M, Graham N, Ghani Z, Halbert G, Elliot M, Ford S, Braithwaite R, Sheehan TMT, Vickerman J, Lockyer N, Steinfeldt H, Croswell G, Chopra A, Sugar R, Boddy A (2009) *A cancer research UK pharmacokinetic study of BPA-mannitol in patients with high grade glioma to optimise uptake parameters for clinical trials of BNCT*. *13th International Congress on Neutron Capture Therapy BNCT: a new option against cancer.* Applied Radiation and Isotopes 67(7-8, Supplement 1):31–33
74. Kageji T, Nakagawa Y, Kitamura K, Matsumoto K, Hatanaka H (1997) *Pharmacokinetics and boron uptake of BSH (Na2B12H11SH) in patients with intracranial tumors.* Journal of Neuro-Oncology 33(1):117–130
75. Yamamoto T, Nakai K, Kageji T, Kumada H, Endo K, Matsuda M, Shibata Y, Matsumura A (2009) *Boron neutron capture therapy for newly diagnosed glioblastoma.* Radiotherapy and Oncology 91(1):80–84

76. Yokoyama K., Miyatake, S. - I., Kajimoto Y, Kawabata S, Doi A, Yoshida T, Asano T, Kirihata M, Ono K, Kuroiwa T (2006) *Pharmacokinetic study of BSH and BPA in simultaneous use for BNCT.* Journal of Neuro-Oncology 78(3):227–232
77. Horn V, Pharm D, Slánský J, Janku I, Strouf O, Sourek K, Tovarys F (1998) *Disposition and tissue distribution of boron after infusion of borocaptate sodium in patients with malignant brain tumors.* International Journal of Radiation Oncology*Biology*Physics 41(3):631–638
78. Gabel D, Preusse D, Haritz D, Grochulla F, Haselsberger K, Fankhauser H, Ceberg C, Peters H-, Klotz U (1997) *Pharmacokinetics of Na12H2B12SH (BSH) in patients with malignant brain tumours as prerequisite for a phase I clinical trial of boron neutron capture.* Acta Neurochirurgica 139(7):606–612
79. Kageji T, Nagahiro S, Kitamura K, Nakagawa Y, Hatanaka H, Haritz D, Grochulla F, Haselsberger K, Gabel D (2001) *Optimal timing of neutron irradiation for boron neutron capture therapy after intravenous infusion of sodium borocaptate in patients with glioblastoma.* International Journal of Radiation Oncology*Biology*Physics 51(1):120–130
80. Chanana AD, Capala J, Chadha M, Coderre JA, Diaz AZ, Elowitz EH, Iwai J, Joel DD, Liu HB, Ma R, Pendzick N, Peress NS, Shady MS, Slatkin DN, Tyson GW, Wielopolski L (1999) *Boron Neutron Capture Therapy for Glioblastoma Multiforme: Interim Results from the Phase I/II Dose-Escalation Studies.* Neurosurgery 44(6):1182–1192
81. Bortolussi S, Bakeine JG, Ballarini F, Bruschi P, Gadan MA, Protti N, Stella S, Clerici A, Ferrari C, Cansolino L, Zonta C, Zonta A, Nano R, Altieri S (2011) *Boron uptake measurements in a rat model for Boron Neutron Capture Therapy of lung tumours.* Applied Radiation and Isotopes 69(2):394–398
82. Neumann M, Kunz U, Lehmann H, Gabel D (2002) *Determination of the Subcellular Distribution of Mercaptoundecahydro-icloso/i-dodecaborate (BSH) in Human Glioblastoma Multiforme by Electron Microscopy.* Journal of Neuro-Oncology 57:97-104
83. Ceberg C, Persson A, Brun A, Huiskamp R, Fyhr A-, Persson, B. R. R., Salford L (1995) *Performance of sulfhydryl boron hydride in patients with grade III and IV astrocytoma: a basis for boron neutron capture therapy.* J Neurosurg 83:79–85
84. Otersen B, Haritz D, Grochulla F, Bergmann M, Sierralta W, Gabel D (1997) *Binding and distribution of Na2B12H11SH on cellular and subcellular level in tumor tissue of glioma patients in boron neutron capture therapy.* Journal of Neuro-Oncology 33(1):131–139
85. Verrey F (2003) *System L: heteromeric exchangers of large, neutral amino acids involved in directional transport.* Pflügers Archiv European Journal of Physiology 445(5):529–533
86. Babu E, Kanai Y, Chairoungdua A, Kim DK, Iribe Y, Tangtrongsup S, Jutabha P, Li Y, Nesar A, Sakamoto S, Anzai N, Nagamori S, Endou H (2003) *Identification of a Novel System L Amino Acid Transporter Structurally Distinct from Heterodimeric Amino Acid Transporters.* Journal of Biological Chemistry 278(44):43838–43845
87. Bodoy S, Martín L, Zorzano A, Palacín M, Estévez R, Bertran J (2005) *Identification of LAT4, a Novel Amino Acid Transporter with System L Activity.* Journal of Biological Chemistry 280(12):12002–12011

88. Wittig A, Sauerwein WA, Coderre JA, Coderre JA (2000) *Mechanisms of Transport of p-Borono-Phenylalanine through the Cell Membrane In Vitro.* Radiation Research 153(2):173–180
89. Detta A, Cruickshank GS (2009) *L-Amino Acid Transporter-1 and Boronophenylalanine-Based Boron Neutron Capture Therapy of Human Brain Tumors.* Cancer Res 69(5):2126–2132
90. Campbell WA, Sah DE, Medina MM, Albina JE, Coleman WB, Thompson NL (2000) *TA1/LAT-1/CD98 Light Chain and System L Activity, but Not 4F2/CD98 Heavy Chain, Respond to Arginine Availability in Rat Hepatic Cells.* Journal of Biological Chemistry 275(8):5347–5354
91. Kaira K, Oriuchi N, Imai H, Shimizu K, Yanagitani N, Sunaga N, Hisada T, Tanaka S, Ishizuka T, Kanai Y, Endou H, Nakajima T, Mori M (2008) *L-type amino acid transporter 1 and CD98 expression in primary and metastatic sites of human neoplasms.* Cancer Science 99(12):2380–2386
92. Kaira K, Oriuchi N, Imai H, Shimizu K, Yanagitani N, Sunaga N, Hisada T, Tanaka S, Ishizuka T, Kanai Y, Endou H, Nakajima T, Mori M (2008) *Prognostic significance of L-type amino acid transporter 1 expression in resectable stage I-III nonsmall cell lung cancer.* Br J Cancer 98(4):742–748
93. Ohkame H, Masuda, H. Ishii, Y., Kanai Y (2001) *Expression of L-type amino acid transporter 1 (LAT1) and 4F2 heavy chain (4F2hc) in liver tumor lesions of rat models.* J. Surg. Oncol. 78(4):265–272
94. Fuchs BC, Bode BP (2005) *Amino acid transporters ASCT2 and LAT1 in cancer: Partners in crime? Tumor Metabolome.* Seminars in Cancer Biology 15(4):254–266
95. Sakata T, Ferdous G, Tsuruta T, Satoh T, Baba S, Muto T, Ueno A, Kanai Y, Endou H, Okayasu I (2009) *L-type amino-acid transporter 1 as a novel biomarker for high-grade malignancy in prostate cancer.* Pathology International 59(1):7–18
96. Haase C, Bergmann R, Fuechtner F, Hoepping A, Pietzsch J (2007) *L-Type Amino Acid Transporters LAT1 and LAT4 in Cancer: Uptake of 3-O-Methyl-6-18F-Fluoro-l-Dopa in Human Adenocarcinoma and Squamous Cell Carcinoma In Vitro and In Vivo.* Journal of Nuclear Medicine 48(12):2063–2071
97. Papaspyrou M, Feinendegen LE, Müller-Gärtner H- (1994) *Preloading with L-Tyrosine Increases the Uptake of Boronophenylalanine in Mouse Melanoma Cells.* Cancer Research 54(24):6311–6314
98. Capuani S, Gili T, Russo S, Porcari P, Cametti C, D'Amore E, Colasanti M, Venturini G, Maraviglia B, Lazzarino G, Pastore FS (2008) *L-DOPA Preloading Increases the Uptake of Borophenylalanine in C6 Glioma Rat Model: A New Strategy to Improve BNCT Efficacy.* International Journal of Radiation Oncology*Biology*Physics 72(2):562–567
99. Capuani S, Gili T, Bozzali M, Russo S, Porcari P, Cametti C, Muolo M, D'Amore E, Maraviglia B, Lazzarino G, Pastore FS (2009) *Boronophenylalanine uptake in C6 glioma model is dramatically increased by l-DOPA preloading. 13th International Congress on Neutron Capture Therapy BNCT: a new option against cancer.* Applied Radiation and Isotopes 67(7-8, Supplement 1):34–36
100. Hiratsuka J, Yoshino K, Kondoh H, Imajo Y, Mishima Y (2000) *Biodistribution of Boron Concentration on Melanoma-bearing Hamsters after Administration of ip-, m-, o/i-Boronophenylalanine.* Cancer Science 91(4):446–450

101. Smith DR, Chandra S, Coderre JA, Morrison GH (1996) *Ion Microscopy Imaging of 10B from p-Boronophenylalanine in a Brain Tumor Model for Boron Neutron Capture Therapy.* Cancer Research 56(19):4302–4306
102. Smith DR, Chandra S, Barth RF, Yang W, Joel DD, Coderre JA (2001) *Quantitative Imaging and Microlocalization of Boron-10 in Brain Tumors and Infiltrating Tumor Cells by SIMS Ion Microscopy.* Cancer Research 61(22):8179–8187
103. Chandra S, Lorey II DR (2007) *SIMS ion microscopy imaging of boronophenylalanine (BPA) and 13C15N-labeled phenylalanine in human glioblastoma cells: Relevance of subcellular scale observations to BPA-mediated boron neutron capture therapy of cancer*. *Imaging Mass Spectrometry Special Issue.* International Journal of Mass Spectrometry 260(2-3):90–101
104. Michel J, Sauerwein W, Wittig A, Balossier G, Zierold K (2003) *Subcellular localization of boron in cultured melanoma cells by electron energy-loss spectroscopy of freeze-dried cryosections.* Journal of Microscopy 210(1):25–34
105. Kiger WS, Palmer MR, Riley KJ, Zamenhof RG, Busse PM (2003) *Pharamacokinetic Modeling for Boronophenylalanine-fructose Mediated Neutron Capture Therapy; 10B Concentration Predictions and Dosimetric Consequences.* Journal of Neuro-Oncology 62(1):171–186
106. Bendel P, Wittig A, Basilico F, Mauri PL, Sauerwein W (2010) *Metabolism of borono-phenylalanine-fructose complex (BPA-fr) and borocaptate sodium (BSH) in cancer patients--Results from EORTC trial 11001.* Journal of Pharmaceutical and Biomedical Analysis 51(1):284–287
107. Gibson CR, Staubus AE, Barth RF, Yang W, Kleinholz NM, Jones RB, Green-Church K, Tjarks W, Soloway AH (2001) *Boron Neutron Capture Therapy of Brain Tumors: Investigation of Urinary Metabolites and Oxidation Products of Sodium Borocaptate by Electrospray Ionization Mass Spectrometry.* Drug Metabolism and Disposition 29(12):1588–1598
108. Nguyen T, Brownell GL, Holden SA, Kahl S, Miura M, Teicher BA (1993) *Subcellular Distribution of Various Boron Compounds and Implications for Their Efficacy in Boron Neutron Capture Therapy by Monte Carlo Simulations*. *Radiation Research.* Radiation Research 133(1):33–40
109. Elhanati G, Salomon Y, Bendel P (2001) *Significant differences in the retention of the borocaptate monomer (BSH) and dimer (BSSB) in malignant cells.* Cancer Letters 172(2):127–132
110. Ryynänen P, Kangasmaki A, Hiismaki P, Coderre JA, Diaz AZ, Kallio M, Laakso J, Kulvik M, Savolainen S (2002) *Non-linear model for the kinetics of 10B in blood after BPA-fructose complex infusion.* Physics in Medicine and Biology 47(5):737–745
111. Kortesniemi M, Seppälä T, Auterinen I, Savolainen S (2004) *Enhanced blood boron concentration estimation for BPA-F mediated BNCT*. *Topics in Neutron Capture Therapy: Proceedings of the Eleventh World Congress on Neutron Capture Therapy (ISNCT-11).* Applied Radiation and Isotopes 61(5):823–827
112. Gilman AG, Goodman IS, Rall TW, Murad F. (1985) *Goodman and Gilman's The Pharmacological Basis of Therapeutics,*. *7th edition,* 7th edn., p.1668 - 1733. Macmillan Publ Comp, New York

113. Scholz M (2003) *Effects of Ion Radiation on Cells and Tissues*. *In: Advances in polymer science: Radiation effects on polymers for biological use; Kausch, H.-H.; Anjum, N. (eds.),* 162, p.95-155. Springer, Berlin
114. Dagrosa M, Crivello M, Perona M, Thorp S, Santa Cruz GA, Pozzi E, Casal M, Thomasz L, Cabrini R, Kahl S, Juvenal GJ, Pisarev MA (2011) *First Evaluation of the Biologic Effectiveness Factors of Boron Neutron Capture Therapy (BNCT) in a Human Colon Carcinoma Cell Line.* International Journal of Radiation Oncology*Biology*Physics 79(1):262–268
115. Dale RG, Jones B, Cárabe-Fernández A (2009) *Why more needs to be known about RBE effects in modern radiotherapy*. *Proceedings of the first international conference on biomedical applications of high energy ion beams.* Applied Radiation and Isotopes 67(3):387–392
116. Hsu FY, Hsiao HW, Tung C-, Liu HM, Chou FI (2009) *Microdosimetry study of THOR BNCT beam using tissue equivalent proportional counter*. *13th International Congress on Neutron Capture Therapy BNCT: a new option against cancer.* Applied Radiation and Isotopes 67(7-8, Supplement 1):175–178
117. Kiger JL, Kiger WS, Patel H, Binns PJ, Riley KJ, Hopewell JW, Harling OK, Coderre JA (2004) *Effects of boron neutron capture irradiation on the normal lung of rats*. *Topics in Neutron Capture Therapy: Proceedings of the Eleventh World Congress on Neutron Capture Therapy (ISNCT-11).* Applied Radiation and Isotopes 61(5):969–973
118. Laakso J, Kulvik M, Ruokonen I, Vahatalo J, Zilliacus R, Farkkila M, Kallio M (2001) *Atomic Emission Method for Total Boron in Blood during Neutron-Capture Therapy*. Clin Chem 47(10):1796–1803
119. Khelifi R, Nievaart VA, Bode P, Moss RL, Krijger GC (2009) *Toward prompt gamma spectrometry for monitoring boron distributions during extra corporal treatment of liver metastases by boron neutron capture therapy: A Monte Carlo simulation study*. *13th International Congress on Neutron Capture Therapy BNCT: a new option against cancer.* Applied Radiation and Isotopes 67(7-8, Supplement 1):359–361
120. Wang LW, Wang SJ, Chu PY, Ho CY, Jiang SH, Liu YWH, Liu YH, Liu HM, Peir JJ, Chou FI, Yen SH, Lee YL, Chang CW, Liu CS, Chen YW, Ono K (2011) *BNCT for locally recurrent head and neck cancer: Preliminary clinical experience from a phase I/II trial at Tsing Hua Open-Pool Reactor.* Applied Radiation and Isotopes 69(12):1803–1806
121. Roveda L, Prati U, Bakeine J, Trotta F, Marotta P, Valsecchi P, Zonta A, Nano R, Facoetti A, Chiari P, Barni S, Pinelli T, Altieri S, Braghieri A, Bruschi P, Fossati F, Pedroni P (2004) *How to Study Boron Biodistribution in Liver Metastases from Colorectal Cancer.* Journal of Chemotherapy 16(5):12–18
122. Fujimoto T, Andoh T, Sudo T, Fujita I, Imabori M, Moritake H, Sugimoto T, Sakuma Y, Takeuchi T, Sonobe H, Epstein AL, Akisue T, Kirihata M, Kurosaka M, Fukumori Y, Ichikawa H (2011) *Evaluation of BPA uptake in clear cell sarcoma (CCS) in vitro and development of an in vivo model of CCS for BNCT studies.* Applied Radiation and Isotopes 69(12):1713–1716
123. Garabalino M, Monti Hughes A, Molinari A, Heber E, Pozzi E, Cardoso J, Colombo L, Nievas S, Nigg D, Aromando R, Itoiz M, Trivillin V, Schwint A (2011) *Boron neutron capture therapy (BNCT) for the treatment of liver metastases: biodistribution studies of boron compounds in an experimental model.* Radiation and Environmental Biophysics 50(1):199–207

124. Ferrari C, Bakeine J, Ballarini F, Boninella A, Bortolussi S, Bruschi P, Cansolino L, Clerici AM, Coppola A, Di Liberto R, Dionigi P, Protti N, Stella S, Zonta A, Zonta C, Altieri S (2010) *In Vitro and In Vivo Studies of Boron Neutron Capture Therapy: Boron Uptake/Washout and Cell Death*. *Radiation Research.* Radiation Research 175(4):452–462
125. Pignol JP, Oudart H, Chauvel P, Sauerwein W, Gabel D, Prevot G (1998) *Selective delivery of 10B to soft tissue sarcoma using 10B-L-borophenylalanine for boron neutron capture therapy.* Br J Radiol 71(843):320–323
126. Cardoso J, Nievas S, Pereira M, Schwint A, Trivillin V, Pozzi E, Heber E, Monti Hughes A, Sanchez P, Bumaschny E, Itoiz M, Liberman S (2009) *Boron biodistribution study in colorectal liver metastases patients in Argentina*. *13th International Congress on Neutron Capture Therapy BNCT: a new option against cancer.* Applied Radiation and Isotopes 67(7-8, Supplement 1):76–79
127. Wittig A, Malago M, Collette L, Huiskamp R, Bührmann S, Nievaart VA, Kaiser GM, Jöckel K-, Schmid KW, Ortmann U, Sauerwein WA (2008) *Uptake of two 10B-compounds in liver metastases of colorectal adenocarcinoma for extracorporeal irradiation with boron neutron capture therapy (EORTC Trial 11001).* International Journal of Cancer 122(5):1164–1171
128. Hideghéty K, Sauerwein W, Wittig A, Götz C, Paquis P, Grochulla F, Haselsberger K, Wolbers J, Moss R, Huiskamp R, Fankhauser HrM de, Gabel D (2003) *Tissue Uptake of BSH in Patients with Glioblastoma in the EORTC 11961 Phase I BNCT Trial.* Journal of Neuro-Oncology 62(1):145–156
129. Coderre JA, Chanana AD, Joel DD, Elowitz EH, Micca PL, Nawrocky MM, Chadha. M., Gebbers JO, Shady M:PNS, Slatkin MM (1998) *Biodistribution of boronophenylalanine in patients with glioblastoma multiforme: boron concentration correlates with tumor cellularity.* Radiation Research 149:163–170
130. Lu X, Kiger WS (2009) *Application of a Novel Microdosimetry Analysis and its Radiobiological Implication for High-LET Radiation.* Radiation Research 171(6):646–656
131. Pinelli T, Zonta A, Altieri S, Barni S, Braghieri A, Pedroni P, Bruschi P, Chiari P, Ferrari C, Fossati F, Nano R, Ngnitejeu Tata S, Prati U, Ricevuti G, Roveda L, Zonta C *TAOrMINA: From the first idea to the application to the human liver*. In: Research and Development in Neutron Capture Therapy. Proceedings of the 10th International Congress on NCT in Essen, Germany, pp 1065–1072
132. Bortolussi S (2007) *Boron Neutron Capture Therapy of Disseminated Tumours*. *PhD thesis – University of Pavia, vol.* 1, Pavia
133. Bortolussi S, Altieri S (2007) *Thermal neutron irradiation field design for boron neutron capture therapy of human explanted liver.* Med. Phys. 12(34):4700–4706
134. Zonta A, Pinelli T, Prati U, Roveda L, Ferrari C, Clerici AM, Zonta C, Mazzini G, Dionigi P, Altieri S, Bortolussi S, Bruschi P, Fossati F (2009) *Extra-corporeal liver BNCT for the treatment of diffuse metastases: What was learned and what is still to be learned*. *13th International Congress on Neutron Capture Therapy BNCT: a new option against cancer.* Applied Radiation and Isotopes 67(7-8, Supplement 1):67–75
135. Zonta A, Prati U, Roveda L, Ferrari C, Zonta S, Clerici A, Zonta C, Pinelli T, Fossati F, Altieri S, Bortolussi S, Bruschi P, Nano R, Barni S, Chiari P, Mazzini

G (2006) *Clinical lessons from the first applications of BNCT on unresectable liver metastases.* Journal of Physics: Conference Series 41:484–495
136. Suzuki M, Sakurai Y, Hagiwara S, Masunaga S, Kinashi Y, Nagata K, Maruhashi A, Kudo M, Ono K (2007) *First Attempt of Boron Neutron Capture Therapy (BNCT) for Hepatocellular Carcinoma.* Jpn. J. Clin. Oncol. 37(5):376–381
137. Hampel G, Wortmann B, Blaickner M, Knorr J, Kratz JV, Lizón Aguilar A, Minouchehr S, Nagels S, Otto G, Schmidberger H, Schütz C, Vogtländer L (2009) *Irradiation facility at the TRIGA Mainz for treatment of liver metastases*. *13th International Congress on Neutron Capture Therapy BNCT: a new option against cancer.* Applied Radiation and Isotopes 67(7-8, Supplement 1):238–241
138. Nievaart VA, Moss RL, Kloosterman JL, van der Hagen THJJ, van Dam H, Wittig A, Malago M, Sauerwein W (2006) *Design of a Rotating Facility for Extracorporal Treatment of an Explanted Liver with Disseminated Metastases by Boron Neutron Capture Therapy with an Epithermal Neutron Beam.* Radiation Research 166(1):81–88
139. Blaickner M, Kratz JV, Lizón Aguilar A, Minouchehr S, Nagels S, Otto G, Schmidberger H, Schütz C, Vogtländer L, Wortmann B, Hampel G (2011) *Dosimetric feasibility study for an extracorporeal BNCT application on liver metastases at the TRIGA Mainz.* Applied Radiation and Isotopes:in press
140. Oganov AR, Chen J, Gatti C, Ma Y, Ma Y, Glass CW, Liu Z, Yu T, Kurakevych OO, Solozhenko VL (2009) *Ionic high-pressure form of elemental boron.* Nature
141. Riedel E, Janiak C (2002) *Anorganische Chemie,* 5th. de Gruyter, Berlin; New York
142. Sommer AL, Lipman CB (1926) *Evidence on the indispensable nature of zinc and boron for higher green plants.* Plant Physiology 1(3):231–249
143. Nielsen FH (1996) *Evidence for the nutritional essentiality of boron.* J. Trace Elem. Exp. Med. 9(4):215–229
144. Pawa S, Ali S (2006) *Boron ameliorates fulminant hepatic failure by counteracting the changes associated with the oxidative stress.* Chemico-Biological Interactions 160(2):89–98
145. Bregadze VI, Sivaev IB, Glazun SA (2006) *Polyhedral Boron Compounds as Potential Diagnostic and Therapeutic Antitumor Agents.* Anti-Cancer Agents in Medicinal Chemistry (Formerly Current Medicinal Chemistry - Anti-Cancer Agents) 6:75–109
146. Dotsika E, Poutoukis D, Michelot J, Kloppmann W (2006) *Stable Isotope and Chloride, Boron Study for Tracing Sources of Boron Contamination in Groundwater: Boron Contents in Fresh and Thermal Water in Different Areas in Greece.* Water, Air, & Soil Pollution 174(1):19–32
147. Yazbeck C, Kloppmann W, Cottier R, Sahuquillo J, Debotte G, Huel G (2005) *Health Impact Evaluation of Boron in Drinking Water: A Geographical Risk Assessment in Northern France.* Environmental Geochemistry and Health 27(5):419–427
148. Hertlein R, Umminger K, Kliem S, Prasser H, Höhne T, Weiss F (2003) *Experimental and numerical investigation of boron dilution transients in pressurized water reactors.* Nuclear technology 141:88–107
149. Wittig A, Michel J, Moss R, Stecher-Rasmussen F, Arlinghaus H, Bendel P, Mauri P, Altieri S, Hilger R, Salvadori P, Menichetti L, Zamenhof RG, Sauerwein WA (2008) *Boron analysis and boron imaging in biological*

materials for Boron Neutron Capture Therapy (BNCT). Critical Reviews in Oncology/Hematology 68(1):66–90
150. Moore DE (1990) *A review of techniques for the analysis of boron in the development of neutron capture therapy agents.* Journal of Pharmaceutical and Biomedical Analysis 8(7):547–553
151. Sah RN, Brown PH (1997) *Boron Determination — A Review of Analytical Methods.* Microchemical Journal(56):285–304
152. Downing R, Strong P, Hovanec B, Northington J (1998) *Considerations in the determination of boron at low concentrations.* Biological Trace Element Research 66(1):3–21
153. Nyomora AMS, Sah RN, Brown PH, Miller RO (1997) *Boron determination in biological materials by inductively coupled plasma atomic emission and mass spectrometry: effects of sample dissolution methods.* Fresenius' Journal of Analytical Chemistry 357(8):1185–1191
154. Tamat SR, Moore DE, Allen BJ (1987) *Determination of boron in biological tissues by inductively coupled plasma atomic emission spectrometry.* Analytical Chemistry 59(17):2161–2164
155. Moreton JA, Delves TH (1999) *Measurement of total boron and 10B concentration and the detection and measurement of elevated 10B levels in biological samples by inductively coupled plasma mass spectrometry using the determination of 10B:11B ratios.* J. Anal. At. Spectrom 14(10):1545–1556
156. Barbosa Jr F, Palmer CD, Krug FJ, Parsons PJ (2004) *Determination of total mercury in whole blood by flow injection cold vapor atomic absorption spectrometry with room temperature digestion using tetramethylammonium hydroxide.* J. Anal. At. Spectrom. 19:1000–1005
157. Musashi M, Oi T, Ossaka T, Kakihana H (1990) *Extraction of boron from GSJ rock reference samples and determination of their boron isotopic ratios.* Analytica Chimica Acta 231:147–150
158. Magour S, Schramel P, Ovcar J, Mäser H (1982) *Uptake and distribution of boron in rats: Interaction with ethanol and hexobarbital in the brain.* Archives of Environmental Contamination and Toxicology 11(5):521–525
159. Krejcová A, Cernohorský T (2003) *The determination of boron in tea and coffee by ICP-AES method.* Food Chemistry 82(2):303–308
160. Al-Ammar A, Reitznerová E, Barnes R (2000) *Determination of Boron in Biological Samples.* Journal of Radioanalytical and Nuclear Chemistry 244(2):267–272
161. Kosanovic M, Hasan MY, Subramanian D, Al Ahbabi, A. A. F., Al Kathiri, O. A. A., Aleassa, E. M. A. A., Adem A (2007) *Influence of urbanization of the western coast of the United Arab Emirates on trace metal content in muscle and liver of wild Red-spot emperor (Lethrinus lentjan).* Food and Chemical Toxicology 45(11):2261–2266
162. Rudolph E, Hann S, Stingeder G, Reiter C (2005) *Ultra-trace analysis of platinum in human tissue samples.* Analytical and Bioanalytical Chemistry 382(7):1500–1506
163. Sun, D. - H., Waters KJ, Mawhinney TP (1997) *Microwave Digestion and Ultrasonic Nebulization for Determination of Boron in Animal Tissues by Inductively Coupled Plasma Atomic Emission Spectrometry With Internal Standardization and Addition of Mannitol.* J. Anal. At. Spectrom. 12(6):675–679
164. Probst TU, Berryman NG, Lemmen P, Weissfloch L, Auberger T, Gabel D, Carlsson J, Larsson B (1997) *Comparison of Inductively Coupled Plasma*

Atomic Emission Spectrometry and Inductively Coupled Plasma Mass Spectrometry With Quantitative Neutron Capture Radiography for the Determination of Boron in Biological Samples From Cancer Therapy. J. Anal. At. Spectrom.(12):1115–1122
165. Hill CJ, Lash RP *Ion chromatographic determination of boron as tetrafluoroborate.* Analytical Chemistry 52(1980):24–27
166. Kiss E (1988) *Ion-exchange separation and spectrophotometric determination of boron in geologic materials.* Analytica Chimica Acta 211:243–256
167. Carlson RM, Paul JL (1968) *Potentiometric Determination of Boron as Tetrafluoroborate.* Analytical Chemistry 40(8):1292–1295
168. Aggarwal JK, Palmer MR (1995) *Boron isotope analysis. A review.* Analyst 120(5):1301–1307
169. Elton-Bott RR (1976) *The determination of boron in plant tissue by atomic absorption spectrometry.* Analytica Chimica Acta 86:281–284
170. Fairchild RG, Gabel D, Laster BH, Greenberg D, Kiszenick W, Micca PL (1986) *Microanalytical techniques for boron analysis using the 10B(n,a)7Li reaction.* Med. Phys. 13(1):50–56
171. Barth RF, Adams DM, Soloway AH, Mechetner EB, Alam F, Anisuzzaman AKM (1991) *Determination of boron in tissues and cells using direct-current plasma atomic emission spectroscopy.* Analytical Chemistry 63(9):890–893
172. Pollmann D, Broekaert JAC, Leis F, Tschöpel P, Tölg G (1993) *Determination of boron in biological tissues by inductively coupled plasma optical emission spectrometry (ICP-OES).* Fresenius' Journal of Analytical Chemistry 346(4):441–445
173. Linko S, Revitzer H, Zilliacus R, Kortesniemi M, Kouri M, Savolainen S (2008) *Boron detection from blood samples by ICP-AES and ICP-MS during boron neutron capture therapy.* Scandinavian Journal of Clinical and Laboratory Investigation 68(8):696–702
174. Riley KJ (1997) *Improved boron 10 quantification via PGNAA and ICP-AES.* Massachusetts Institute of Technology, Boston
175. Barany E, Bergdahl I, Schütz A, Skerfving S, Oskarsson A (1997) *Inductively Coupled Plasma Mass Spectrometry for Direct Multi-element Analysis of Diluted Human Blood and Serum.* J. Anal. At. Spectrom. 12:1005–1009
176. Evans S, Krahenbühl U (1994) *Improved Boron Determination in Biological Material by Inductively Coupled Plasma Mass Spectrometry.* Journal of Analytical Atomic Spectrometry(9)
177. Goullé J-, Mahieu L, Castermant J, Neveu N, Bonneau L, Lainé G, Bouige D, Lacroix C (2005) *Metal and metalloid multi-elementary ICP-MS validation in whole blood, plasma, urine and hair: Reference values*. *2004 Joint Meeting of SOFT and TIAFT.* Forensic Science International 153(1):39–44
178. Vanhoe H, Dams R, Vandecasteele C, Versieck J (1993) *Determination of boron in human serum by inductively coupled plasma mass spectrometry after a simple dilution of the sample.* Analytica Chimica Acta 281:401-4 11
179. Vanderpool R, Hoff D, Johnson R (1994) *Use of inductively coupled plasma-mass spectrometry in boron-10 stable isotope experiments with plants, rats, and humans.* Environmental Health Perspectives 102:13–20
180. Pozebon D, Dressler VL, Curtius AJ (1998) *Determination of Mo, U and B in waters by electrothermal vaporization inductively coupled plasma mass spectrometry.* Talanta 47(4):849–859

181. Becker JS, Dietze H- (2000) *Precise and accurate isotope ratio measurements by ICP-MS.* Fresenius' Journal of Analytical Chemistry 368(1):23–30
182. Sinclair DJ, Kinsley, L. P. J., McCulloch MT (1998) *High resolution analysis of trace elements in corals by laser ablation ICP-MS.* Geochimica et Cosmochimica Acta 62(11):1889–1901
183. Tonarini S, Pennisi M, Leeman WP (1997) *Precise boron isotopic analysis of complex silicate (rock) samples using alkali carbonate fusion and ion-exchange separation.* Chemical Geology 142(1-2):129–137
184. Barth S (1997) *Boron isotopic analysis of natural fresh and saline waters by negative thermal ionization mass spectrometry.* Chemical Geology 143(3-4):255–261
185. Riley KJ, Harling OK (1998) *An improved prompt gamma neutron activation analysis facility using a focused diffracted neutron beam.* Nuclear Instruments and Methods in Physics Research Section B: Beam Interactions with Materials and Atoms 143(3):414–421
186. Raaijmakers CPJ, Konijnenberg MW, Dewit L, Haritz D, Huiskamp R, Philipp K, Siefert A, Stecher-Rasmussen F, Mijnheer B (1995) *Monitoring of Blood-10B Concentration for Boron Neutron Capture Therapy Using Prompt Gamma-Ray Analysis.* Acta Oncologica 34(4):517–523
187. Abdel-Haleem AS, Zohny EEM, Zaghloul RA (1994) *The use of neutron attenuation in borated materials as an indicator of their boron content.* Radiation Physics and Chemistry 44(1-2):233–235
188. Iyengar GV, Clarke WB, Downing RG (1990) *Determination of boron and lithium in diverse biological matrices using neutron activation-mass spectrometry (NA-MS).* Fresenius' Journal of Analytical Chemistry 338(4):562–566
189. Gabel D, Holstein H, Larsson B, Gille L, Ericson G, Sacker D, Som P, Fairchild RG (1987) *Quantitative Neutron Capture Radiography for Studying the Biodistribution of Tumor-seeking Boron-containing Compounds.* Cancer Res 47(20):5451–5454
190. Alfassi Z, Probst TU (1999) *On the calibration curve for determination of boron in tissue by quantitative neutron capture radiography.* Nuclear Instruments and Methods in Physics Research A:502–507
191. Larsson B, Gabel D, Borner HG (1984) *Boron-loaded macromolecules in experimental physiology: tracing by neutron capture radiography.* Physics in Medicine and Biology 29(4):361–370
192. Thellier M, Hennequin E, Heurteaux C, Martini F, Pettersson M, Fernandez T, Wissocq JC (1988) *Quantitative estimations in neutron capture radiography.* Nuclear Instruments and Methods in Physics Research Section B: Beam Interactions with Materials and Atoms 30(4):567–579
193. Stella S, Bortolussi S, Bruschi P, Portella C, Altieri S (2009) *Measurement of [alpha] particle energy loss in biological tissue below 2 MeV.* Nuclear Instruments and Methods in Physics Research Section B: Beam Interactions with Materials and Atoms 267(17):2938–2943
194. Nievaart VA, Daquino GG, Moss RL (2007) *Monte Carlo based treatment planning systems for Boron Neutron Capture Therapy in Petten, The Netherlands.* Journal of Physics: Conference Series 74:21012
195. Studenov A, Ding YS, Ferrieri R, Miura M, Coderre J, Fowler JS *Radiosynthesis and chiral separation of C11 labeled boronophenylalanine for*

BNCT studies with PET. In: Proceedings International symposium radiopharmaceutical chemistry, Interlaken (CH), 06/10/2001--06/15/2001
196. Kabalka GW, Smith GT, Dyke JP, Reid WS, Longford D, Roberts TG, Reddy NK, Buonocore E, Hübner KF (1997) *Evaluation of Fluorine-18-BPA-fructose for boron neutron capture treatment planning.* J Nucl Med 11(38):1762
197. Kabalka GW, Nichols TL, Smith GT, Miller LF, Khan MK, Busse PM (2003) *The Use of Positron Emission Tomography to Develop Boron Neutron Capture Therapy Treatment Plans for Metastatic Malignant Melanoma.* Journal of Neuro-Oncology 62(1):187–195
198. Nariai T, Ishiwata K, Kimura Y, Inaji M, Momose T, Yamamoto T, Matsumura A, Ishii K, Ohno K (2009) *PET pharmacokinetic analysis to estimate boron concentration in tumor and brain as a guide to plan BNCT for malignant cerebral glioma*. *13th International Congress on Neutron Capture Therapy BNCT: a new option against cancer.* Applied Radiation and Isotopes 67(7-8, Supplement 1):348–350
199. Menichetti L, Petroni D, Panetta D, Burchielli S, Bortolussi S, Matteucci M, Pascali G, Del Turco S, Del Guerra A, Altieri S, Salvadori PA (2011) *A micro-PET/CT approach using O-(2-[18F]fluoroethyl)-l-tyrosine in an experimental animal model of F98 glioma for BNCT.* Applied Radiation and Isotopes 69(12):1717–1720
200. Miura M, Micca LP, Nawrocky MM, Slatkin DN (1997) *Might iodomethyl-a-tyrosine be a surrogate for BPA in BNCT? In: Advances in Neutron Capture Therapy. Larsson, B.; Crawford J.; Weinreich, R. (eds);,* 302-307. Elsevier Science Inc., Amsterdam
201. Minsky DM, Valda AA, Kreiner AJ, Green S, Wojnecki C, Ghani Z (2011) *First tomographic image of neutron capture rate in a BNCT facility.* Applied Radiation and Isotopes 69(12):1858–1861
202. Wiehl N (2011) *Boron determination in Si-samples by PGAA at the HFR Petten, the Netherlands,* Mainz, personal communication
203. Coderre JA, Glass JD, Fairchild RG, Roy U, Cohen S, Fand I (1987) *Selective Targeting of Boronophenylalanine to Melanoma in BALB/c Mice for Neutron Capture Therapy.* Cancer Research 47(23):6377–6383
204. Bortolussi S, Pinto JM, Thorp SI, Farias RO, Soto MS, Sztejnberg M, Pozzi ECC, Gonzalez SJ, Gadan MA, Bellino AN, Quintana J, Altieri S, Miller M (2011) *Simulation of the neutron flux in the irradiation facility at RA-3 reactor.* Applied Radiation and Isotopes 69(12):1924–1927
205. Solares GR, Zamenhof RG (1995) *A Novel Approach to the Microdosimetry of Neutron Capture Therapy. Part I. High-Resolution Quantitative Autoradiography Applied to Microdosimetry in Neutron Capture Therapy.* Radiation Research 144:50–58
206. Kiger III, W. S., Micca LP, Morris MG, Coderre JA (2002) *Boron Microquantification in Oral Mucosa and Skin Following Administration of a Neutron Capture Therapy Agent.* Radiation Protection Dosimetry 99(1-4):409–412
207. Harris T (2006) *High resolution quantitative auto-radiography to determine microscopic distributions of B-10 in Neutron capture therapy*. Master Thesis, Massachussetts Institute of Technology
208. Bendel P (2005) *Biomedical applications of 10B and 11B NMR.* NMR Biomed 18(2):74–82

209. Bradshaw KM, Schweizer MP, Glover GH, Rock HJ, Tippets R, Tang P, Davis WL, Heilbrun PM, Johnson S, Ghanem T (1995) *BSH distributions in the canine head and a human patient using 11B MRI.* Magn. Reson. Med 34(1):48–56
210. Zuo CS, Prasad PV, Busse P, Tang L, Zamenhof R (1999) *Proton nuclear magnetic resonance measurement of p-boronophenylalanine (BPA): A therapeutic agent for boron neutron capture therapy.* Med. Phys. 26(7):1230–1237
211. Chandra S, Tjarks W, Lorey II DR, Barth RF (2008) *Quantitative subcellular imaging of boron compounds in individual mitotic and interphase human glioblastoma cells with imaging secondary ion mass spectrometry (SIMS).* Journal of Microscopy 229(1):92–103
212. Wittig A, Arlinghaus HF, Kriegeskotte C, Moss RL, Appelman K, Schmid KW, Sauerwein, W. A. G. (2008) *Laser postionization secondary neutral mass spectrometry in tissue: a powerful tool for elemental and molecular imaging in the development of targeted drugs.* Molecular Cancer Therapeutics 7(7):1763–1771
213. Arlinghaus HF, Spaar MT, Switzer RC, Kabalka GW (1997) *Imaging of Boron in Tissue at the Cellular Level for Boron Neutron Capture Therapy.* Analytical Chemistry 69(16):3169–3176
214. Weise K, Wöger W (1999) *Meßunsicherheit und Meßdatenauswertung.* Wiley-VCH, Weinheim
215. Schütz C (2008) *Borbestimmung in Gewebeproben im Rahmen der Entwicklung eines Behandlungsprotokolls für die Bor-Neutronen-Einfangtherapie an einer autotransplantierten Leber*. Diplomarbeit, Johannes Gutenberg-Universität Mainz
216. Schütz C, Brochhausen C, Bartholomew K, Altieri S, Bortolussi S, Enzmann F, Gabel D, Hampel G, Kirkpatrick CJ, Kratz JV, Minouchehr S, Schmidberger H, Otto G (2011) *Boron analysis in liver tissue by quantitative neutron capture radiography (QNCR) and histological methods for BNCT treatment planning at the TRIGA Mainz.* Radiation Research 176:388–396
217. Schmitz T, Appelman K, Kudejova P, Schütz C, Kratz JV, Moss R, Otto G, Hampel G (2011) *Determination of boron concentration in blood and tissue samples from patients with liver metastases of colorectal carcinoma using Prompt Gamma Ray Activation Analysis (PGAA).* Applied Radiation and Isotopes 69(7):936–941
218. Strasberg SM (2005) *Nomenclature of hepatic anatomy and resections: a review of the Brisbane 2000 system.* Journal of Hepato-Biliary-Pancreatic Surgery 12(5):351–355
219. Chadwick J (1932) *Possible Existence of a neutron.* Nature 129(3252):312
220. Khan HA, Qureshi IE (1999) *SSNTD applications in science and technology — a brief review*. *Proceedings of the 19th International Conference on Nuclear Tracks in Solids.* Radiation Measurements 31(1–6):25–36
221. Edwards LC (1956) *Autoradiography by neutron activation: The cellular distribution of B10 in transplanted mouse brain tumors.* Intern. J. Appl. Radiation Isotopes 1:184–190
222. Fairchild RG, Tonna EA, Seibold CT (1967) *Development of a Low-Background Neutron Autoradiographic Technique.* Radiation Research 30(4):774–787
223. Woollard JE, Blue TE, Curran JF, Mengers TF, Barth RF (1990) *An alpha autoradiographic technique for determination of 10B concentrations in blood*

and tissue. Nuclear Instruments and Methods in Physics Research Section A: Accelerators, Spectrometers, Detectors and Associated Equipment 299(1-3):600–605
224. Yanagie H, Ogura K, Matsumoto T, Eriguchi M, Kobayashi H (1999) *Neutron capture autoradiographic determination of 10B distributions and concentrations in biological samples for boron neutron capture therapy.* Nuclear Instruments and Methods in Physics Research Section A: Accelerators, Spectrometers, Detectors and Associated Equipment 424(1):122–128
225. Ogura K, Yamazaki A, Yanagie H, Eriguchi M, Lehmann EH, Küehne G, Bayon G, Maruyama K, Kobayashi H (2001) *Neutron capture autoradiography for a study on boron neutron capture therapy.* Radiation Measurements 34(1-6):555–558
226. Altieri S, Bortolussi S, Bruschi P, Chiari P, Fossati F, Stella S, Prati U, Roveda L, Zonta A, Zonta C, Ferrari C, Clerici A, Nano R, Pinelli T (2008) *Neutron autoradiography imaging of selective boron uptake in human metastatic tumours.* Applied Radiation and Isotopes 66(12):1850–1855
227. Abe M, Amano K, Kitamura K, Tateishi J, Hatanaka H (1986) *Boron Distribution Analysis by Alpha-Autoradiography.* J Nucl Med 27(5):677–684
228. Pettersson OA, Grusell E, Larsson B, Huiskamp R (1993) *Quantitative neutron capture radiography for boron in biological specimens.* Physics in Medicine and Biology 38(8):1089–1097
229. Ceballos C, Esposito J, Agosteo S, Colautti P, Conte V, Moro D, Pola A (2011) *Towards the final BSA modeling for the accelerator-driven BNCT facility at INFN LNL.* Applied Radiation and Isotopes 69(12):1660–1663
230. Green S, Phoenix B, Mill AJ, Hill M, Charles MW, Thompson J, Jones B, Ngoga D, Detta A, James ND, Doran J, Graham N, Ghani Z, Wojnecki C, Halbert G, Elliott M, Ford S, Sheehan TMT, Vickerman J, Lockyer N, Croswell G, Boddy A, King A, Cruickshank GS (2011) *The Birmingham Boron Neutron Capture Therapy (BNCT) Project: Developments towards Selective Internal Particle Therapy.* Clin Oncol (R Coll Radiol) 23(3):23–24
231. Wortmann B (2006) *Auslegung und Optimierung einer Bestrahlungseinrichtung für die Bor-Neutroneneinfangtherapie an autotransplantierten Organen*. Ph.D. Thesis, Technische Universität Dresden
232. Schmitz T, Blaickner M, Schütz C, Wiehl N, Kratz JV, Bassler N, Holzscheiter MH, Palmans H, Sharpe P, Otto G, Hampel G (2010) *Dose calculation in biological samples in a mixed neutron-gamma field at the TRIGA reactor of the University of Mainz.* Acta Oncol 49(7):1165–1169
233. Battistoni G, Muraro S, Sala P, Cerutti F, Ferrari A, Roesler F, Fasso A, Ranft J (2007) *The FLUKA code: Description and benchmarking*. *Proceedings of the Hadronic Shower Simulation Workshop 2006, Fermilab 6--8 September 2006.* AIP Conference Proceedings 896:31–49
234. Schmitz T, Blaickner M, Ziegner M, Bassler N, Grunewald C, Kratz JV, Schütz C, Langguth P, Sharpe P, Palmans H, Holzscheiter MH, Otto G, Hampel G (2011) *Dose determination using alanine detectors in a mixed neutron and gamma field for boron neutron capture therapy of liver malignancies.* Acta Oncologica 50(6):817–822
235. Ali A, Durrani SA (1977) *Etched-track kinetics in isotropic detectors.* Nuclear Track Detection 1:107–121
236. Somogyi G, Tóth-Szilágyi M, Hunyadi I, Hafez A (1986) *Effect of certain production parameters and post-production treatments on the etching*

characteristics of CR-39 sheets. *Special Volume Solid State Nuclear Track Detectors.* International Journal of Radiation Applications and Instrumentation. Part D. Nuclear Tracks and Radiation Measurements 12(1-6):97–100
237. Fromm M, Membrey F, Chambaudet A, Saouli R (1991) *Proton and alpha track profiles in CR39 during etching and their implications on track etching models.* International Journal of Radiation Applications and Instrumentation. Part D. Nuclear Tracks and Radiation Measurements 19(1-4):163–168
238. Fromm M, Meyer P, Chambaudet A (1996) *Ion track etching in isotropic polymers: etched track shape and detection efficiency*. *Swift Heavy Ions in Matter.* Nuclear Instruments and Methods in Physics Research Section B: Beam Interactions with Materials and Atoms 107(1-4):337–343
239. Phillips GW, Spann JE, Bogard JS, VoDinh T, Emfietzoglou D, Devine RT, Moscovitch M (2006) *Neutron spectrometry using CR-39 track etch detectors.* Radiat Prot Dosimetry 120(1-4):457–460
240. Altieri S, Bortolussi S, Bruschi P, Fossati F, Vittor K, Nano R, Facoetti A, Chiari P, Bakeine J, Clerici A, Ferrari C, Salvucci O (2006) *Boron absorption imaging in rat lung colon adenocarcinoma metastases.* Journal of Physics: Conference Series 41:123–126
241. Spath H (1985) *Cluster dissection and analysis: Theory, FORTRAN programs, examples*. *translated by J. Goldschmidt.* Halsted Press, New York
242. Patiris DL, Blekas K, Ioannides KG (2006) *TRIAC: A code for track measurements using image analysis tools.* Nuclear Instruments and Methods in Physics Research Section B: Beam Interactions with Materials and Atoms 244(2):392–396
243. Patiris DL, Blekas K, Ioannides KG (2007) *TRIAC II. A MatLab code for track measurements from SSNT detectors.* Computer Physics Communications 177(3):329–338
244. Canella L, Kudějová P, Schulze R, Türler A, Jolie J (2011) *Characterisation and optimisation of the new Prompt Gamma-ray Activation Analysis (PGAA) facility at FRM II.* Nuclear Instruments and Methods in Physics Research Section A: Accelerators, Spectrometers, Detectors and Associated Equipment 636(1):108–113
245. Molnár G, Révay Z, Paul R, Lindstrom R (1998) *Prompt-gamma activation analysis using the k0 approach.* Journal of Radioanalytical and Nuclear Chemistry 234(1):21–26
246. Schmitz T (2010) *Bestimmung und Simulation der Neutronen- und Gammadosis in der thermischen Säule des TRIGA Reaktors Mainz und Borbestimmung in Blut- und Gewebeproben mittels Prompt-Gamma-Aktivierungsanalyse im Rahmen der Bor-Neutronen-Einfangtherapie*. Diploma Thesis, Johannes Gutenberg-Universität Mainz
247. Schmitz T (2011) *Personal communication*
248. Wittig A, Sheu-Grabellus S-, Collette L, Moss R, Brualla L, Sauerwein W (2011) *BPA uptake does not correlate with LAT1 and Ki67 expressions in tumor samples (results of EORTC trial 11001).* Applied Radiation and Isotopes 69(12):1807–1812
249. Capala J, H.-Stenstam B, Sköld K, Rosenschöld P, Giusti V, Persson C, Wallin E, Brun A, Franzen L, Carlsson J, Salford L, Ceberg Cr, Persson Bl, Pellettieri L, Henriksson R (2003) *Boron neutron capture therapy for glioblastoma multiforme: clinical studies in Sweden.* Journal of Neuro-Oncology 62(1):135–144

250. Liberman SJ, Dagrosa A, Jiménez Rebagliati RA, Bonomi MR, Roth BM, Turjanski L, Castiglia SI, González SJ, Menéndez PR, Cabrini R, Roberti MJ, Batistoni DA (2004) *Biodistribution studies of boronophenylalanine-fructose in melanoma and brain tumor patients in Argentina*. *Topics in Neutron Capture Therapy: Proceedings of the Eleventh World Congress on Neutron Capture Therapy (ISNCT-11).* Applied Radiation and Isotopes 61(5):1095–1100
251. Kato I, Ono K, Sakurai Y, Ohmae M, Maruhashi A, Imahori Y, Kirihata M, Nakazawa M, Yura Y (2004) *Effectiveness of BNCT for recurrent head and neck malignancies. Topics in Neutron Capture Therapy: Proceedings of the Eleventh World Congress on Neutron Capture Therapy (ISNCT-11).* Applied Radiation and Isotopes 61(5):1069–1073
252. Sun, D. - H., Ma, R. - L., McLeod C, Wanga, X. - R., Cox A (2000) *Determination of boron in serum, plasma and urine by inductively coupled plasma mass spectrometry (ICP-MS). Use of mannitol-ammonia as diluent and for eliminating memory effect.* Journal of Analytical Atomic Spectrometry 15:257–261
253. Ishikawa T, Nakamura E (1990) *Suppression of boron volatilization from a hydrofluoric acid solution using a boron-mannitol complex*. *Analytical Chemistry.* Anal. Chem 62(23):2612–2616
254. Wright C, Fryer F, Woods G (2008) *Rinse solution for Boron Analysis and Boron Isotope Ratio.* Agilent ICP-MS Journal 33:4–5
255. Al-Ammar A, Gupta RK, Barnes RM (1999) *Elimination of boron memory effect in inductively coupled plasma-mass spectrometry by addition of ammonia.* Spectrochimica Acta Part B: Atomic Spectroscopy 54(7):1077–1084
256. Al-Ammar AS, Reitznerová E, Barnes RM (1999) *Feasibility of using beryllium as internal reference to reduce non-spectroscopic carbon species matrix effect in the inductively coupled plasma-mass spectrometry (ICP-MS) determination of boron in biological samples.* Spectrochimica Acta Part B: Atomic Spectroscopy 54(13):1813–1820
257. Iyengar GV (1997) *Reevaluation of the trace element content in reference man.* Radiation Physics and Chemistry 51(1):545–560
258. Nievaart S, Appelman K, Stecher-Rasmussen F, Sauerwein W, Wittig A, Moss R (2009) *Extension of the calibration curve for the PGRA facility in Petten*. *13th International Congress on Neutron Capture Therapy BNCT: a new option against cancer.* Applied Radiation and Isotopes 67(7-8, Supplement 1):362–364
259. Downing R, Strong P (1998) *A round-robin determination of boron in botanical and biological samples.* Biological Trace Element Research 66(1):23–37
260. Gonfiantini R, Tonarini S, Gröning M, Adorni-Braccesi A, Al-Ammar AS, Astner M, Bächler S, Barnes RM, Bassett RL, Cocherie A, Deyhle A, Dini A, Ferrara G, Gaillardet J, Grimm J, Guerrot C, Krähenbühl U, Layne G, Lemarchand D, Meixner A, Northington DJ, Pennisi M, Reitznerová E, Rodushkin I, Sugiura N, Surberg R, Tonn S, Wiedenbeck M, Wunderli S, Xiao Y, Zack T (2003) *Intercomparison of Boron Isotope and Concentration Measurements. Part II: Evaluation of Results.* Geostandards Newsletter 27(1):41–57
261. Portu A, Carpano M, Dagrosa A, Nievas S, Pozzi E, Thorp S, Cabrini R, Liberman S, Saint Martin G (2011) *Reference systems for the determination of 10B through autoradiography images: Application to a melanoma experimental model.* Applied Radiation and Isotopes 69(12):1698–1701

262. Yamamoto T, Matsumura A, Nakai K, Shibata Y, Endo K, Sakurai F, Kishi T, Kumada H, Yamamoto K, Torii Y (2004) *Current clinical results of the Tsukuba BNCT trial*. *Topics in Neutron Capture Therapy: Proceedings of the Eleventh World Congress on Neutron Capture Therapy (ISNCT-11).* Applied Radiation and Isotopes 61(5):1089–1093
263. Wittig A, Collette L, Appelman K, Bührmann S, Jäckel MC, Jöckel K-, Schmid KW, Ortmann U, Moss R, Sauerwein WA (2009) *EORTC trial 11001: distribution of two 10B-compounds in patients with squamous cell carcinoma of head and neck, a translational research/phase 1 trial.* Journal of Cellular and Molecular Medicine 13(8b):1653–1665
264. Goitom D, Bjorn E, Frech W, Loos-Vollebregt MTC de (2005) *Radial ICP characteristics for ICP-AES using direct injection or microconcentric nebulisation.* J. Anal. At. Spectrom 20(7):645–651
265. Smith FG, Wiederin DR, Houk RS, Egan CB, Serfass RE (1991) *Measurement of boron concentration and isotope ratios in biological samples by inductivey coupled plasma mass spectrometry with direct injection nebulization.* Analytica Chimica Acta 248(1):229–234
266. Scheid N (2011) *Elementanalytik und Isotopenverhältnisbestimmungen an humanbiologischen Materialien*. Ph.D thesis, Johannes Gutenberg-Universität Mainz
267. Hill S (2007) *Inductively Coupled Plasma Spectrometry and its Applications,* 2nd edn. Blackwell Publishing Ltd, Oxford
268. Ryynänen PM, Kortesniemi M, Coderre JA, Diaz AZ, Hiismäki P, Savolainen SE (2000) *Models for estimation of the 10B concentration after BPA-fructose complex infusion in patients during epithermal neutron irradiation in BNCT.* International Journal of Radiation Oncology*Biology*Physics 48(4):1145–1154
269. Yoon JH, Kim JI, Kim H, Kim H-, Jeong MJ, Ahn SG, Kim SA, Lee CH, Choi BK, Kim J-, Jung KY, Lee S, Kanai Y, Endou H, Kim DK (2005) *Amino acid transport system L is differently expressed in human normal oral keratinocytes and human oral cancer cells.* Cancer Letters 222(2):237–245
270. Kim DK, Ahn SG, Cheol PJ, Kanai Y, Endou H, Yoon JH (2004) *Expression of L-type Amino Acid Transporter 1 (LAT1) and 4F2 Heavy Chain (4F2hc) in Oral Squamous Cell Carcinoma and its Precusor Lesions.* Anticancer Research 24(3A):1671–1676

Appendix

A.: List of publications related to this thesis

First author:

Schütz, C.; Brochhausen, C.; Bartholomew, K.; Altieri, S.; Bortolussi, S.; Enzmann, F.; Gabel, D.; Hampel, G.; Kirkpatrick, C. J.; Kratz, J. V.; Minouchehr, S.; Schmidberger, H.; Otto, G.; *Boron determination in liver tissue by combining Quantitative Neutron Capture Radiography (QNCR) and histological analysis for BNCT treatment planning at the TRIGA Mainz.* Radiation Research, **(176)**, 2011, 388-396

Co-Author:

Hampel, G.; Wortmann, B.; Blaickner, M.; Knorr, J.; Kratz, J. V.; Lizón Aguilar, A.; Minouchehr, S.; Nagels, S.; Otto, G.; Schmidberger, H.; **Schütz, C.**; Vogtländer, L.; *Irradiation facility at the TRIGA Mainz for treatment of liver metastases,* Applied Radiation and Isotopes, (**67**), 2009, 7-8, 238-241

Nagels, S.; Hampel, G.; Kratz, J. V.; Aguilar, A. L.; Minouchehr, S.; Otto, G.; Schmidberger, H.; **Schütz, C.**; Vogtländer, L.; Wortmann, B.; *Determination of the irradiation field at the research reactor TRIGA Mainz for BNCT*, Applied Radiation and Isotopes, (**67**), 2009, 7-8, 242-246

Schmitz, T.; Blaickner, M.; **Schütz, C.**; Wiehl, N.; Kratz, J.V.; Bassler, N.; Holzscheiter, M.H.; Palmans, H.; Sharpe, P.; Otto, G.; Hampel, G.; *Dose calculation in biological samples in a mixed neutron-gamma field at the TRIGA reactor of the University of Mainz*, Acta Oncologica, **(49)**, 2010, 7, 1165-1169

Schmitz, T.; Appelman, K.; Kudejova, P.; **Schütz, C.**; Kratz, J. V.; Moss, R.; Otto, G.; Hampel., G.; *Determination of boron concentration in blood and tissue samples from patients with liver metastases of colorectal carcinoma using Prompt Gamma Ray Activation Analysis (PGAA)*. Applied Radiation and Isotopes, **(69)**, 2011, 7, 936-941

Schmitz, T.; Blaickner, M.; Ziegner, M.; Bassler, N.; Grunewald, C.; Kratz, J. V.; **Schütz, C**.; Langguth, P.; Sharpe, P.; Palmans, H.; Holzscheiter, M.H.; Otto, G.; Hampel., G.; *Dose determination using alanine detectors in a mixed neutron and gamma field for boron neutron capture therapy of liver malignancies,* Acta Oncologica, **(50)**, 2011, 6, 817-822

Blaickner, M.; Hampel, G.; Kratz, J. V.; Lizón Aguilar, A.; Minouchehr, S.; Nagels, S.; Otto, G.; Schmidberger, H.; **Schütz, C.;** Vogtländer, L.; Wortmann, B.; *MCNP simulations for treatment planning in the course of BNCT on liver metastases at the TRIGA Mainz,* Applied Radiation and Isotopes, **(70)**, 2012, 139-143